PROCESSES OF STRATIFICATION AND DESTRATIFICATION IN THE MEKONG ROFI

SEASONAL AND INTRASEASONAL VARIABILITY

DISSERTATION

ZUR ERLANGUNG DES DOKTORGRADES

DER NATURWISSENSCHAFTEN IM FACHBEREICH

GEOWISSENSCHAFTEN

DER UNIVERSITÄT HAMBURG

VORGELEGT VON

BIRTE HEIN

AUS

CELLE

HAMBURG

2013

Als Dissertation angenommen vom Fachbereich Geowissenschaften der Universität Hamburg

Auf Grund der Gutachten von PD. Dr. T. Pohlmann
und Prof. Dr. J. Sündermann

Hamburg, den 25.01.2013

Prof. Dr. Jürgen Oßenbrügge
Leiter des Fachbereichs Geowissenschaften

Hiermit erkläre ich an Eides statt, dass ich die vorliegende Dissertationsschrift selbst verfasst und keine anderen als die angegebenen Quellen und Hilfsmittel benutzt habe.

Koblenz, den

Birte Hein

CONTENTS

ABSTRACT

The Mekong River discharges a great amount of freshwater into the South China Sea annually. This freshwater supply has a considerable effect on the physical processes in this region, i.e., the Mekong Region Of Freshwater Influence (ROFI). These physical processes establish the level of stratification of the water column. Both sediment dynamics and dynamics of the marine ecosystem are strongly influenced by the governing physical processes and the resulting level of stratification of the water column.

The Mekong ROFI – situated in tropical latitudes – is subject to strong seasonal variability in terms of river runoff and monsoon winds, both of which force the physical processes in this area. Therefore in this study, the Mekong ROFI is taken as a representative example to analyze the seasonal differences in the physical processes of a tropical ROFI. Methodically, the following steps are performed for this analysis: a model study, in-situ measurements and the application of the three-dimensional dynamic equation for the potential energy anomaly on the model results.

The hydrodynamic HAMburg Shelf Ocean Model (HAMSOM) is applied to the Mekong ROFI to simulate the currents and density distribution during the low-flow season (NE monsoon) and during the high-flow season (SW monsoon). The model results are validated with both measured in-situ and altimeter data. It is shown that the regional circulation as well as the salinity and temperature distributions are represented reasonably well by the model. The hydrodynamic model results display that during the NE monsoon a plume which is constraint to the coast flows southwestward in the direction of Kelvin wave propagation. During the SW monsoon a broad plume heads northeastward against the direction of Kelvin wave propagation.

To get an overview of the governing physical processes acting during each monsoon phase in the Mekong ROFI, the three-dimensional dynamic equation for the potential energy anomaly is applied to the numeric model results. The equation has been presented by different authors as a good tool to study the processes contributing to stratification and destratification of a water column. In this study, for the first time by means of the Mekong ROFI, the seasonal differences of a ROFI in tropical latitudes are analyzed by the equation.

In the three-dimensional dynamic equation for the potential energy anomaly six processes are differentiated to investigate the processes acting on stratification and destratification of the water column: horizontal advection; mean straining; non-mean straining; shear dispersion; mixing; and vertical advection. A comparison is made between the main processes which are of importance on a seasonal time scale during the low-flow and during the high-flow season. Both seasons are also considered to draw comparisons on the relevant processes on the tidal time scale. These results provide the basis for discussing whether it is possible to transfer the results from the tidal time scale to the seasonal time scale.

On the seasonal time scale during both periods mean straining and mixing dominate nearly the whole Mekong ROFI. However, the mixing term shows some lower values at the boundary of the plume. Mean straining acts predominantly to stratify the water column and mixing acts as destratifying agent. A major difference between the two monsoon phases is that during the SW monsoon the other four physical processes are of importance as well, although usually locally restricted.

In detail, the horizontal advection term indicates that well-mixed estuarine water enters the Mekong ROFI during the high-flow season. The shear dispersion and the non-mean straining term show an inverse picture as stratifying and destratifying agents. Additionally the results show that during the high-flow season upwelling occurs in the plume region. Downwelling occurs mainly at the river plume front. Although the strength of the processes is generally lower during the low-flow season the results demonstrate that in the plume region again upwelling occurs. Downwelling occurs primarily at the river mouths and in the coastal regions. The horizontal advection term gives evidence of shelf water intrusion into the Mekong Estuary. The shear dispersion and the non-mean straining term are again counterparts.

Due to the pronounced seasonal differences, even on the tidal time scale the physical processes are considered independently for each monsoon phase. During the NE monsoon the mean straining and mixing term play a major role in the whole Mekong ROFI. Also the advection terms show high values. Horizontal advection acts predominantly in the plume area off the coastal area and vertical advection in the coastal area as well as in the adjacent region of the inner river plume. In contrast during the SW monsoon all processes are approximately of equal importance. Nevertheless, the strength of the individual processes is distributed spatially heterogeneous during this monsoon phase.

Comparing both time scales the most apparent difference is that vertical and horizontal advection are more important on the tidal rather than the seasonal time scale. The instantaneous advection of density structures by the tidal flow (tidal time scale) due to the forward and backward movement during the tidal cycle is stronger than the advection by the constant flow forced by wind stress, density variations, tidal residuals and remote currents (seasonal scale).

Altogether, the Mekong ROFI can be taken as a good proxy for analyzing the seasonal variability of physical processes in tropical latitudes. It is shown that not simply the flow

direction of the river plume changes during the seasons, but that also the physical processes change significantly. Especially the flow reversal during summer coincides with a complex and variable superposition of the investigated physical processes. Identifying the seasonality of the processes is the necessary base for applied regional studies of the impact of climate change, sediment management and ecology.

ZUSAMMENFASSUNG

Jedes Jahr fließen große Mengen an Frischwasser über den Mekong in das südchinesische Meer. Diese Frischwasserzufuhr hat einen entscheidenden Einfluss auf die physikalischen Prozesse in diesem Küstengewässer, das auch als Mekong ROFI (Region Of Freshwater Influence) bezeichnet wird. Die physikalischen Prozesse bestimmen maßgeblich den Schichtungsaufbau bzw. -abbau in einer Wassersäule und haben somit einen unmittelbaren Einfluss sowohl auf die Sedimentdynamik als auch auf die Dynamik des marinen Ökosystems.

Das Mekong ROFI liegt in den tropischen Breitengeraden und ist deshalb im Hinblick auf den Abfluss und die Monsunwinde einer ausgeprägten saisonalen Schwankung unterworfen. Diese beiden Randbedingungen mit ihrer Saisonalität bestimmen die physikalischen Prozesse in dieser Region maßgeblich. Deshalb wird in dieser Studie das Mekong ROFI als ein repräsentatives Beispiel herangezogen, um die saisonalen Unterschiede in den physikalischen Prozessen eines tropischen ROFIs zu analysieren. Methodisch werden folgende Punkte für diese Analyse bearbeitet: eine Modellstudie, in-situ Messungen und die Anwendung der dreidimensionalen dynamischen Gleichung für die potentielle Energieanomalie auf die Modellergebnisse.

Das hydrodynamische HAMburg Schelf-Ozean-Modell (HAMSOM) wird verwendet, um die Strömungen und die Dichteverteilung im Mekong ROFI während der Niedrigwasserperiode (NO Monsun) bzw. der Hochwasserperiode zu simulieren (SW Monsun). Die Modellergebnisse werden sowohl mit gemessenen in-situ Daten als auch mit Altimeterdaten validiert. Es wird gezeigt, dass sowohl die regionale Zirkulation als auch die Salz- und Temperaturverteilungen hinreichend gut mit dem Modell abgebildet werden können. Die hydrodynamischen Modellergebnisse zeigen, dass sich die Flussfahne während des NO Monsuns südwestwärts ausbreitet, d.h. in Ausbreitungsrichtung einer küstengebundenen Kelvinwelle. Die Flussfahne ist dabei auf einen schmalen Streifen entlang der Küste beschränkt. Während des SW Monsuns erstreckt sich eine ausgedehnte Flussfahne nach Nordosten, d.h. entgegen der Ausbreitungsrichtung einer küstengebundenen Kelvinwelle.

Die numerischen Modellergebnisse werden verwendet, um einen Überblick über die physikalischen Prozesse zu erlangen, die während der jeweiligen Monsunphase im Mekong

ROFI vorherrschen. Hierzu wird die dreidimensionale dynamische Gleichung für die potentielle Energieanomalie auf die Modellergebnisse angewandt. Verschiedene Autoren haben gezeigt, dass diese Gleichung ein gutes Werkzeug darstellt, um die physikalischen Prozesse zu beschreiben, die zu einem Schichtungsaufbau bzw. -abbau in der Wassersäule führen. In der vorliegenden Studie werden mit der Gleichung anhand des Mekong ROFIs zum ersten Mal die saisonalen Unterschiede der physikalischen Prozesse in einem ROFI der tropischen Breiten analysiert.

Um diejenigen Prozesse zu untersuchen, die zu einem Schichtungsaufbau bzw. -abbau in einer Wassersäule führen, kann mit der dreidimensionalen dynamischen Gleichung für die potentielle Energieanomalie zwischen sechs Prozessen unterschieden werden: die horizontale Advektion, die mittlere differentielle Advektion (sogenanntes „Straining“), die nichtlineare differentielle Advektion (nichtlineares Straining), die (Scherungs-) Dispersion, die vertikale Durchmischung und die vertikale Advektion. Auf saisonaler Ebene werden die vorherrschenden Prozesse während der Niedrigwasserperiode mit denen der Hochwasserperiode verglichen. Beide Perioden werden auch herangezogen, um die relevanten Prozesse auf der Ebene der Gezeitenperiode vergleichend zu betrachten. Die Ergebnisse liefern die Basis für die Diskussion, ob es möglich ist, Ergebnisse die auf der Ebene der Gezeitenperiode erzielt worden sind auf die saisonale Ebene zu übertragen.

Auf saisonaler Ebene dominieren während der beiden Zeiträume das Straining und die vertikale Durchmischung fast das gesamte Mekong ROFI. An der Flussfahnengrenze zeigt der Durchmischungsterm jedoch geringere Werte auf. Das Straining trägt hauptsächlich dazu bei, die Wassersäule zu schichten. Der Prozess der Durchmischung führt dahingegen zu einem Schichtungsabbau in der Wassersäule. Ein wesentlicher Unterschied zwischen den beiden Monsunphasen besteht darin, dass während des SW Monsuns die vier weiteren physikalischen Prozesse ebenfalls von Bedeutung sind. Diese Terme spielen jedoch gewöhnlich nur räumlich begrenzt eine Rolle.

Im Einzelnen betrachtet zeigt der horizontale Advektionsterm auf, dass aus dem Mekong während der Hochwasserperiode vertikal durchmischtes ästuarines Wasser in das Mekong ROFI hineintransportiert wird. Die Dispersion und das nichtlineare Straining ergänzen sich zu einem inversen Bild als Schichtungsaufbau- bzw. Schichtungsabbauterm. Zusätzlich zeigen die Ergebnisse, dass während der Hochwasserperiode in der Flussfahne der Auftrieb eine Rolle spielt. Downwelling findet dahingegen hauptsächlich an der Front der Flussfahne statt. Auch wenn die Größenordnung der Prozesse während der Niedrigwasserperiode im Allgemeinen geringer ist, so findet auch während dieses Zeitraumes Auftrieb innerhalb der Flussfahne statt. Downwelling findet hauptsächlich im Mündungs- und Küstenbereich statt. Der horizontale Advektionsterm gibt einen Hinweis darauf, dass Schelfwasser in das Mekongästuar eindringt. Der Dispersionsterm und der nichtlineare Strainingterm verhalten sich wieder gegensätzlich.

Aufgrund der ausgeprägten saisonalen Unterschiede werden die physikalischen Prozesse auch

auf der Ebene der Gezeitenperiode für jede Monsunphase einzeln betrachtet. Während des NO Monsuns spielen sowohl der Strainingterm als auch der Durchmischungsterm eine große Rolle im gesamten Mekong ROFI. Auch die beiden Advektionsterme nehmen hohe Werte an. Die horizontale Advektion dominiert hauptsächlich die Flussfahne außerhalb des Küstengebietes. Vertikale Advektion tritt hauptsächlich an der Küste und in dem direkt angrenzenden Bereich der Flussfahne auf. Im Unterschied zur NO Monsunphase sind während des SW Monsuns alle Prozesse im Mittel gleich gewichtet. Erst bei räumlich detaillierter Betrachtung zeigen die einzelnen Prozesse unterschiedlich hohe Werte auf.

Ein Vergleich beider Zeitskalen zeigt, dass die vertikalen und horizontalen Advektionsterme auf der Ebene der Gezeitenperiode wichtiger sind als auf der saisonalen Ebene. Die momentane Advektion einer Dichtestruktur durch den Gezeitenstrom auf den Bahnlinien der Gezeitenellipsen ist ausgeprägter als die Advektion durch die zeitlich konstante Strömung auf der saisonalen Ebene, die durch den Wind, die Dichteunterschiede, die Restströme und die großräumige Zirkulation hervorgerufen wird.

Zusammenfassend kann gesagt werden, dass das Mekong ROFI ein guter Proxy darstellt, um die saisonale Variabilität der physikalischen Prozesse in den tropischen Breiten zu analysieren. Es wird gezeigt, dass sich nicht nur die Strömungsrichtung der Flussfahne während der Monsunperioden, sondern auch die physikalischen Prozesse signifikant ändern. Vor allem die Strömungsumkehr während des Sommers geht mit einer komplexen und variablen Überlagerung der untersuchten physikalischen Prozesse einher. Eine direkte Übertagung der Ergebnisse von der Ebene der Gezeitenperiode auf die saisonale Ebene ist nicht möglich. Die zeitliche Variabilität der physikalischen Prozesse zu bestimmen, stellt eine wichtige Grundlage für angewandte regionale Studien über die Auswirkungen des Klimawandels, für das Sedimentmanagement und für die Ökologie dar.

CHAPTER 1

INTRODUCTION

Coastal oceans and estuaries are important areas where ecology and economy overlap. From an ecological point of view these areas are of particular interest as the coastal waters are biological highly productive. They are the nursery grounds for many ocean species. But it is also interesting from an economical point of view as in countries like Vietnam 80 % of households in the coastal communities get their income - or at least a part of their income - from fishery. In Vietnam about 4 million people are working in this sector (STREAM, 2000; POMEROY et al., 2009). Furthermore, coastal waters are important for shipping. Both the ecological and economical interests turn these areas into important research areas.

Many rivers discharge into the coastal ocean, thereby bringing freshwater into the system. The freshwater input has an effect on the flow regime in these areas and thus on the sediment dynamics as well as on the nutrient transport. The marine ecosystem depends on both the suspended sediment concentration in the water column and the availability of nutrients. Increased suspended sediment concentrations reduce the penetration of light into the water column which in turn causes a reduced primary production. The supply of nutrients also has an effect on the phytoplankton growth and thus on the subsequent species of the marine food web.

From an oceanographic point of view the input of freshwater causes processes of stratification and destratification in these coastal systems. Due to the stratification of a water column the vertical flux of water properties like heat, salt, momentum and of water substances like nutrients, sediments is significantly affected (SIMPSON et al., 1990). WISEMAN et al. (1997) stated that the hypoxia during summer in the Louisana coastal current – which forms part of the freshwater region of the Mississippi river system - is favored by the stratification of the water column which inhibits the transport of oxygen into lower layers. Thus, the investigation of physical processes in estuaries and the coastal ocean which determine stratification and destratification of the water column is a challenging as well as an important task.

1.1 MOTIVATION

DAI and TRENBERTH (2002) studied the annual mean freshwater discharge from the continents and considered the influence of latitudinal variations on the magnitude of river discharge. Based on different datasets, they stated that the main discharge into the global oceans occurs between 10° S and 20° N. Also SIMPSON (1997) postulates the need to investigate the extensive **R**egions **O**f **F**reshwater **I**nfluence (ROFIs) in tropical regions. A ROFI is a system which is influenced by a large input of buoyancy as freshwater. The tropical shelf seas to the east of Asia receive massive inputs of freshwater depending on the monsoonal cycle. To date, most studies of ROFIs have concentrated on temperate latitude. To counteract this deficiency, the focus in this study will be on the investigation of the Mekong ROFI as an example of a tropical ROFI.

The vertical structure of a water column can be seen as a result of the competition between the regime specific boundary conditions. In a ROFI, these boundary conditions are on the one hand the buoyancy input as river discharge which tends to induce haline stratification. On the other hand, stirring by tides and wind stress has an opposing effect on the vertical structure of the water column (SIMPSON, 1997).

In a tropical ROFI, like the Mekong ROFI, the river runoff and the monsoon winds display a strong seasonal variability. During the winter monsoon the Mekong has a flow comparable to that of the Rhine (SIMPSON, 1997). The monsoon winds blow from the northeast and the river plume flows southward into the Gulf of Thailand (HORDOIR et al., 2006). However, during the summer monsoon the flow reverses with the changing main wind direction (WOLANSKI et al., 1996). The discharge of the Mekong is increased by a factor of 20 (SIMPSON, 1997).

The seasonal variability of river discharge and monsoon winds has a large influence on the physical processes acting to stratify and/or destratify the water column in a tropical ROFI. Furthermore, the seasonal occurrence of stratification has an effect on the sediment dynamics and/or ecosystem processes. WOLANSKI et al. (1996) and WOLANSKI et al. (1998) show by means of measurements of vertical salinity profiles and suspended sediment concentrations that in the Mekong Estuary the position and extension of the Turbidity Maximum Zone is different depending on the seasons and on the stratification induced by the seasonal varying strength of the estuarine circulation. During the high-flow season the Turbidity Maximum Zone is limited to the toe of the salt wedge situated near the river mouths. During the low flow season according to the conceptual model in WOLANSKI et al. (1996) a more extended Turbidity Maximum Zone is located several kilometres upstream of the Mekong River mouth in accordance with the salinity intrusion limit. During the low-flow season WEI et al. (2007) stated the influence of stratification on the maintenance of summer hypoxia in the Changjiang Estuary which lies in the area of the East Asian Monsoon. Although it is not a tropical ROFI, WISEMAN et al. (1997) studied the variability in stratification within the Louisiana Coastal Current on the basis of ten years of survey cruise data. They observed a strong relationship between stratification and hypoxia during summer.

However, there exists not only a seasonal variability in the stratification cycle of a tropical ROFI but also an intra-seasonal variability on time scales of a tidal cycle. HORDOIR et al. (2006) stated that on a short time scale the vertical haline structure in the Mekong ROFI is strongly influenced by tidal mixing. They claimed that further work has to be done to determine how tidal mixing affects fluxes of salt and freshwater in the Mekong ROFI. Therefore, in this study not only the seasonal variability in stratification will be investigated but also the intra-seasonal variability.

In the Mekong ROFI primarily river discharge, wind stress, and tides force temporally and locally distinct physical processes that result in a change of the potential energy of a water column and thus in a change of stratification. As the buoyancy input as heat is almost spatially homogeneous, it plays only a secondary role for the physical processes in a ROFI (SIMPSON, 1997).

In this study, the physical processes contributing to increasing or decreasing stratification in the Mekong ROFI on the different time scales are determined based on the publications of BURCHARD and HOFMEISTER (2008) and DE BOER et al. (2008); the processes to be investigated are depth-mean straining, non-mean straining, horizontal advection, shear dispersion, up/downwelling and vertical mixing. In recent studies these processes have been examined only on a tidal time scale but not on a seasonal time scale. Although HOFMEISTER et al. (2009) applied the three-dimensional dynamic equation for the potential energy anomaly for one whole year to the Limfjord which is situated in the temperate latitudes, they did not study the seasonal variability.

This study is part of the German-Vietnamese joint research project ‘Land-Ocean-Atmosphere Interactions in the Coastal Zone of Southern Vietnam’ which is funded by the ‘Deutsche Forschungsgemeinschaft’.

1.2 AIMS

In this study, the Mekong ROFI is considered as an example of a tropical ROFI and the contribution of the different physical processes to stratify and/or destratify the water column is quantified. The following topics will be investigated:

1. the seasonal variability of the hydrodynamic conditions (currents, salinity and temperature distribution) due to changing boundary conditions (wind, river discharge)
2. the level of stratification on a seasonal as well as on a tidal time scale
3. the main physical processes tending to stratify and/or destratify the water column during the different monsoon phases on each time scale
4. comparison of the two time scales and deduction of the possibility to transfer the results of the tidal time scale to the seasonal time scale

1.3 OUTLINE

After formulating the motivation of this study (1.1) and defining the aims (1.2), in the next chapter (2) the terms 'Estuary' and 'ROFI' are outlined (2.1). General physical processes in a ROFI are sketched in section 2.2. In the following sections an overview of the Mekong ROFI and the adjacent waters is given to provide a background of the regional system.

As in this study the level of stratification is quantified by means of the potential energy of the water column, some basics about potential energy are outlined in section 3.1. In the next section (3.2) the theoretical background for the equation of the **P**otential **E**nergy **A**nomaly (PEA), which is used to determine the stability of the system, is pointed out. The derivation of PEA for the one-dimensional flow is summarized (φ_{1D}). The derivation of the tendency of PEA for the three-dimensional flow (φ_{t3D}), which is used to establish the main physical processes stratifying and/or destratifying the water column in the Mekong ROFI, is shown in section 3.3.

In the 4th chapter, the HAMburg Shelf Ocean Model is introduced. The pre-processing of the Mekong River discharge data, which is required as a fundamental boundary condition to model the seasonal variability in the Mekong ROFI, is presented. The numerical model results are validated with satellite and insitu data.

The two subsequent chapters depict the results and discuss them. In the 5th chapter the seasonal variability of the system in terms of the hydrodynamic conditions (currents, salinity and temperature distribution, section 5.1/5.2) and in terms of stratification ($\varphi_{1D}/\varphi_{t3D}$, section 5.3/5.4) is displayed. In section 6.1 the hydrodynamic processes of the Mekong ROFI are discussed and the particularities of the different seasons are revealed. In section 6.2 the temporal variability in the level of stratification is analyzed. In the next section (6.3) the main physical processes that strengthen or weaken the stratification of the water column on each time scale are determined. The temporal variability of the physical processes is analyzed as well. Subsequently, a synthesis of these results is given for each time scale. In the next section other studies in which the three-dimensional dynamic equation for the potential energy anomaly has been applied are summarized. The results are compared to the results of this study (6.4).

Conclusions are drawn in chapter 7. An outlook is given in chapter 8.

CHAPTER 2

THE MEKONG ROFI

2.1 DEFINITIONS: ESTUARY AND ROFI

The most widely used definition of an *estuary* is given by PRITCHARD (1967): "An estuary is a semi-enclosed coastal body of water which has a free connection with the open sea and within which sea water is measurably diluted with fresh water derived from land drainage". Thus, estuaries are the transition area from the river to the ocean. They are characterized by tidal motions originating in the ocean and by a gradient of salinity and density arising from the low density water of the river and the high density water of the ocean (HANSEN and RATTRAY, 1966).

SIMPSON (1997) defined a *ROFI* as the region between the estuary and the shelf sea which receives a significant amount of buoyancy as freshwater from discrete sources, i.e., rivers. In a ROFI the buoyancy input as freshwater from rivers is comparable with or even greater than the seasonal buoyancy input as heat like in the other parts of the shelf sea. Therefore in a ROFI the physical processes are quite different from those in the other parts of the shelf sea as both, estuarine processes and shelf sea processes overlap.

Altogether, a fundamental difference between an estuary and a ROFI is that a ROFI is not a semi-enclosed coastal body of water but is part of the shelf sea. Hence, the alongshore component plays a major role in a ROFI.

In this study, the term ROFI according to SIMPSON (1997) is used to refer to the freshwater influenced part of the Sunda shelf adjacent to the estuarine part of the Mekong River (Figure 1).

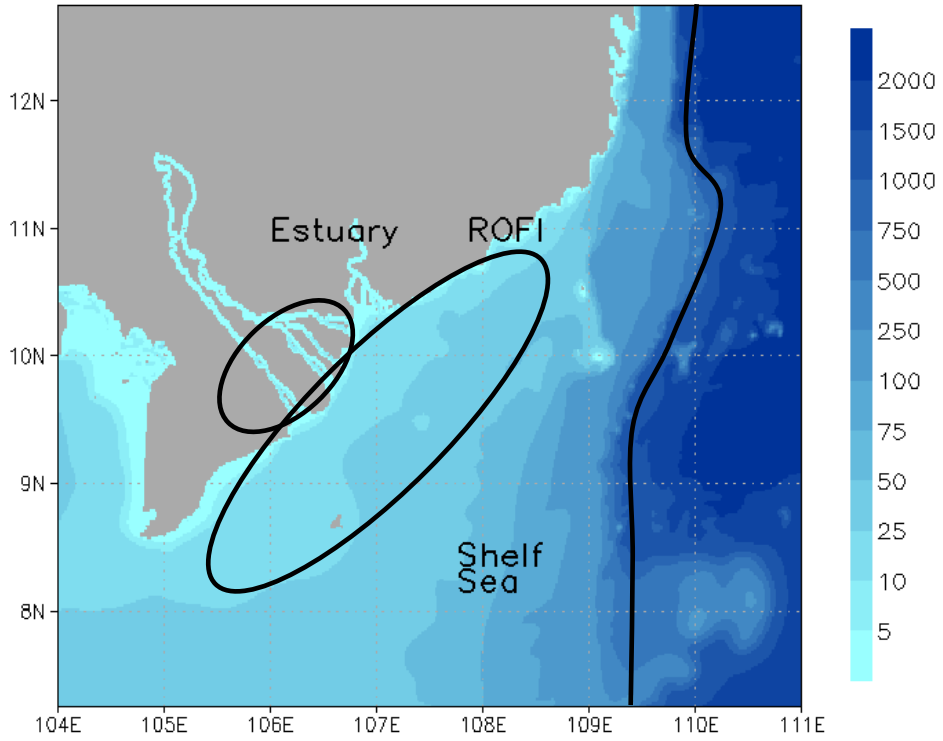

Figure 1: Schematic illustration of the Mekong River estuary, the Mekong ROFI and the adjacent shelf sea. The shelf edge is sketched by the black line. The Bathymetry [m] is based on the ETOPO2 (http://www.ngdc.noaa.gov/mgg/global/etopo2.html) and GEBCO (http://www.gebco.net/data_and_products/gridded_bathymetry_data) dataset.

2.2 PHYSICAL PROCESSES IN A ROFI: STRATIFICATION VERSUS MIXING

A broad overview of the physical processes in ROFIs is given by SIMPSON (1997). In his study he pointed out that two important characteristics of the ROFI system are:

1) The buoyancy input is spatially heterogeneous as freshwater enters at discrete sources.

2) The state of the water column can change between vertically mixed and stratified conditions on short time scales like a tidal cycle.

SIMPSON (1997) stated that seasonal buoyancy input as heat is spatially uniform and performs a regular pattern of seasonal stratification and mixing on long time scales.

Lateral input of buoyancy like freshwater input from river sources inevitably establishes horizontal density gradients. These gradients contribute to a horizontal pressure gradient which drives the density-driven circulation. SIMPSON (1987) conducted a lock exchange experiment in a tank to study the dynamics of a density-driven flow. He stated that under the influence of gravity, the salt water starts to collapse and to flow beneath the freshwater. The result is a two layer counterflow. Thus, stratification of the water column is induced. In order to minimize the

potential energy of the system, baroclinic density fields tend to pursue a state in which isopycnals are horizontal, i.e., a stratified water column.

However, the density-driven circulation changes because of mixing. SIMPSON (1987) and LINDEN and SIMPSON (1988) conducted a lock exchange experiment but additionally they controlled the turbulence by releasing air bubbles through holes in the base of the tank. By switching the bubbles periodically on and off, they were able to simulate the effects of turbulence generated by mechanical stirring through wind, waves and tides. The authors showed that vertical mixing damps the density-driven current and thus the development of stratification. It may develop a zone which is characterized by a region of horizontal density gradients, i.e., a region where isopycnals are vertical and the baroclinic circulation is weak. However, when the stirring ceases, the baroclinic circulation accelerates and the water column stratifies. The longer the period between switching bubbles on/off, the more pronounced is the density-driven flow, the stratification of the water column and the associated longitudinal transport of buoyancy.

When considering the influence of the Coriolis force on the density-driven current, the geostrophic flow adjustment process has to be taken into account. Hereby, the freshwater flow is deflected with the land on the right (left) in the Northern (Southern) hemisphere, i.e., in the direction of Kelvin wave propagation (e.g., SIMPSON, 1997; HILL, 1998). A characteristic S-shaped density profile is formed. The flow is confined to about one internal Rossby radius of deformation which is the length scale at which rotational effects become as important as buoyancy or gravity effects. The final two layer flow is in geostrophic equilibrium, i.e., the Coriolis force balances the horizontal cross-estuary pressure gradient (HILL, 1998).

However, the final steady two-layer flow is potentially unstable, since in geostrophic equilibrium the isopycnals are inclined, but not horizontal, i.e., the potential energy is not minimized (HILL, 1998). Instabilities have been observed in laboratory experiments by SIMPSON (1987) and GRIFFITHS and LINDEN (1982). The excess potential energy in the density field can convert into kinetic energy, which feeds growing instabilities in the baroclinic flow (PEDLOSKY, 1987). Thus, when the buoyancy forcing is dominant and stirring is weak, the density-driven flow can cause baroclinic instabilities, which leads to a meandering of the flow and to a formation of a complex frontal system. However, in many ROFIs frictional effects are important and the horizontal density field is maintained by mixing which stabilizes the density-driven flow and prevent baroclinic instabilities (SIMPSON, 1997).

Thus, in general, in a ROFI system a competition between the stratifying influence of the buoyancy input as freshwater and the stirring effect of wind, waves and tides takes place. The mean level of stratification of the water column is established by the competition between the density-driven flow, which underlies the influence of rotation, and the stirring effect of tides, wind stress and waves (SIMPSON, 1997).

During a tidal cycle semi-diurnal oscillations in stability occur when considering the Liverpool Bay and the Rhine ROFI. In the Liverpool Bay minimum (maximum) in stability occurs close to

the time of high (low) water. Here, the tides are dominated by a standing wave. During ebb (flood) tide due to a vertical velocity shear fresher surface water moves faster seaward (shoreward) than underlying saline water so that stratification (destratification) occurs; a maximum stability is reached close to/at low water. The process in which the tidal shear acts on the horizontal density gradients to stratify or destratify the water column is termed tidal straining. In the Rhine ROFI the tides are dominated by a progressive Kelvin wave and minimum (maximum) stratification is observed at low (high) water. Here, the tidal ellipses have to be accounted for. The form of the tidal ellipses changes during periods of stratification. Under conditions of strong wind and tidal stirring, the water column is mixed and the tidal ellipses are close to degenerate. There exists only a strong alongshore velocity component. However, reduced mixing yields the horizontal density gradient to relax under gravity so that stratification is induced and the tidal ellipses are modified. They become anticyclonic at the surface and cyclonic near the bottom. The resulting cross shore velocity component induces a strong straining in the cross-shore direction and thus a semi-diurnal oscillation in stratification (SIMPSON, 1997).

The spring-neap cycle imposes a 14.8 days variation on the stability of the water column in ROFIs. In the Liverpool Bay ROFI maximum stratification is observed 2–3 days after neap. At spring tide the water column is completely mixed (SHARPLES and SIMPSON, 1995). With additional wind stirring the spring-neap cycle in the stratification is less apparent (SIMPSON, 1997).

MÜNCHOW and GARVINE (1993) reported some observations of the Delaware Coastal Current. The current flows in the direction of Kelvin wave propagation. But during strong upwelling favourable wind a reversal of the buoyancy driven flow on the shelf is reported by the authors. However, these strong wind events are rare. Generally, the wind constitute only as a mixing agent for the buoyant discharge. In contrast to the Delaware Coastal Current, in the Mekong ROFI a reversal of flow is common during the summer monsoon (DIPPNER et al., 2007; HEIN, 2007; HORDOIR et al., 2006).

Overall, a ROFI is characterized by a complex and variable superposition of different physical processes. To identify the main processes in a ROFI, analyzing stratification and destratification is an essential task.

2.3 THE HYDROGRAPHY OF THE MEKONG ROFI AND THE ADJACENT WATERS

The Mekong ROFI is defined as the area between the Mekong Estuary and the region of the shelf sea, which is significantly influenced by freshwater (Figure 1). The physical processes in a ROFI are determined by both estuarine processes and shelf sea processes (SIMPSON, 1997). For convenience, before considering the hydrography of the Mekong ROFI, the hydrography of the Mekong Estuary as well as of the adjacent waters of the South China Sea is presented.

2.3.1 THE MEKONG RIVER AND ITS ESTUARY

The Mekong River is one of the largest rivers in the world with a length of approximately 4800 km and a mean annual discharge of 475 km³, which is approximately 15000 m³/s (mean annual discharge of the Rhine is 2200 m³/s (SOUZA and JAMES, 1996)). It originates on the Tibetan Plateau and disembogues into the South China Sea (SCS) flowing through six countries namely China, Myanmar, Lao PDR, Thailand, Cambodia and Vietnam. The Mekong River drains a catchment area of 795000 km² (MRC, 2005).

Phnom Penh marks the beginning of the delta system where the Mekong mainstream divides into its two main distributaries, the Mekong and the Bassac. Further downstream the Mekong then divides into six branches and the Bassac divides into three branches forming together a complex river network of nine branches altogether. The major branches of the Bassac are the Tranh De and the Din An. The Mekong consists of five major branches: Tieu, Dai, Ham Luong, Chien and Hau. The main delta covers an area of about 55000 km² (MRC, 2005). The Mekong River mouths are situated between 9.4° N and 10.4° N (Figure 2).

The Mekong Delta has developed mostly after the mid-Holocene sea level highstand, i.e., during the last 6000–7000 years. During the time of the highstand the sea level was recorded at around 4.5 m above the present sea level. The coastline had been situated around the Cambodian border and had prograded more than 200 km forming today the coastline of southern Vietnam (LAP NGUYEN et al., 2000). However, the delta progradation was not constant. The upper delta during the first 3000 years had been formed by tidal processes, the lower delta during the latter 3000 years by waves (TA et al., 2002a; TA et al., 2002b; TANABE et al., 2003). The Mekong Delta itself has the shape of a triangle which lies between Phnom Penh in Cambodia, the Saigon River inlet (Ho Chi Minh City) and the Ca Mau Cape to the south. MILLIMAN and MEI-E (1995) estimated the annual sediment discharge of the Mekong River at 160 million t. The annual suspended load of the Rhine River near the Dutch-German border is 3.4 million t (KEMPE and KRAHE, 2005).

Semi-diurnal tides prevail in the Mekong Estuary (WOLANSKI et al., 1998) with a dominant M2 tide (ZU et al., 2008). A strong seasonality exists due to the two monsoon seasons. The seasonal variability is reflected in both the river discharge and the wind stress (HORDOIR et al., 2006). The SW monsoon (May to September) and its transition period in October are accompanied by heavy rainfall, particularly from August to October. During the NE monsoon (November to March) and its transition period in April rainfall is decreased (MRC, 2005). The average peak flow of the Mekong is greater than 45000 m³/s (at Phnom Penh), whereupon the rising of the water level usually begins in May and is highest around September and October. Around November the flow declines and the lowest level is reached in March and April (1500 m³/s) (KITE, 2001). WOLANSKI et al. (1996) and WOLANSKI et al. (1998) carried out a study in the Mekong Estuary during a high-flow season (November) and a low-flow season (April), respectively. From measurements, WOLANSKI et al. (1998) deduced that during the low-flow

season the salinity intrusion length of the Mekong Estuary is about 50 km. Near the river mouth, depending on the tidal cycle, the salinity varies between 7 and 23 psu. Vertical stratification occurs around slack tidal currents. During the high-flow season WOLANSKI et al. (1996) discovered that a salt wedge forms near the river mouth. However, it does not penetrate more than a few kilometres upstream.

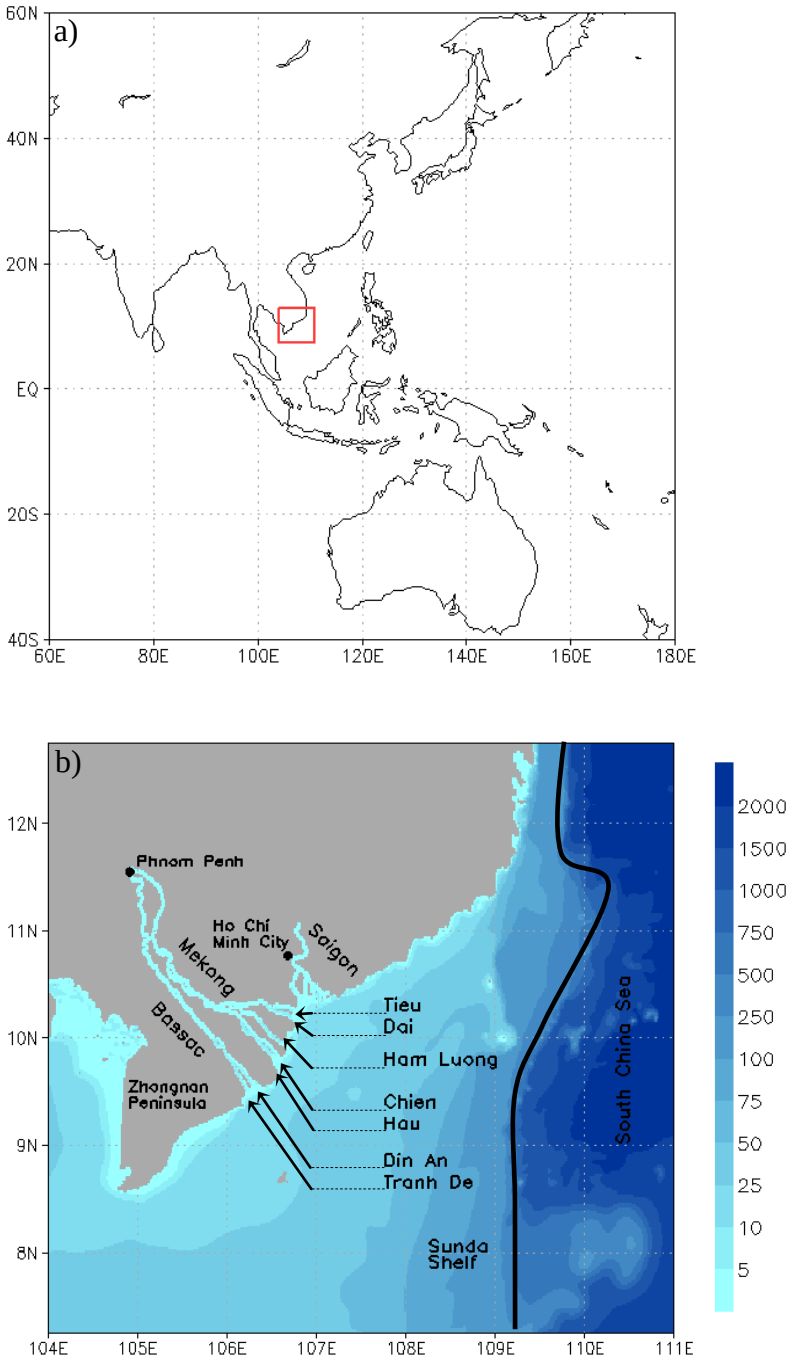

Figure 2: a) Geographical location of the investigation area (red rectangle): the Mekong ROFI and the adjacent South China Sea. b) Overview of the Mekong Delta with its river branches, the Sunda Shelf and the South China Sea. Bathymetry [m] is based on the ETOPO2 (http://www.ngdc.noaa.gov/mgg/global/etopo2.html) and GEBCO (http://www.gebco.net/data_and_products/gridded_bathymetry_data) dataset.

2.3.2 THE SUNDA SHELF SEA

The circulation of the Mekong ROFI is strongly linked with the circulation of the surrounding basin – the SCS. HU et al. (2000) give a review on the currents of the SCS. They stated that the seasonal circulation of the SCS is mainly driven by the monsoon winds.

The regional monsoon, the South China Sea Monsoon, is part of the Asian Monsoon System. Beside the Meiyu in central China, Baiu in Japan and Changma in Korea the SCS Monsoon forms a part of the East Asian Monsoon (LIM et al., 2002). In the west, the SCS Monsoon is connected to the Indian Monsoon. In the south, there are strong connections to the Australian Monsoon System. In general the summer (winter) monsoon in the SCS starts in May (November) and ends in September (March). In winter north-easterly winds with an averaged magnitude of 9 m/s prevail, whereas in summer south-westerly winds of about 6 m/s dominate the region of the southern SCS (DING et al., 2004; LIU and XIE, 1999).

During the transition period between the two monsoon seasons (April, October) the wind is calm. While the transition period during April is a smooth process, during October a more abrupt change takes place (LIU and XIE, 1999). It is related to a break-off of the SW monsoon and the arrival of the NE monsoon which is amplified by a cold surge. A cold surge is a typical regional pattern of the atmospheric circulation (DING and KRISHNAMURTI, 1987). In contrary to the monsoon seasons, the wind direction during the inter-monsoon periods is often variable and the wind speeds seldom exceed 4 m/s.

Early studies of the SCS give still an adequate view on the regional circulation in the adjacent coastal waters off the Mekong, whereby the work of WYRTKI (1961) is based on observations and the work of POHLMANN (1987) on simulations. More recent studies of the general circulation of the SCS show the same circulation in adjacent coastal waters of the Mekong as the former studies (e.g., SHAW and CHAO, 1994; METZGER and HURLBURT, 1996; WU et al., 1998; SHAW et al., 1999; ISOBE and NAMBA, 2001; GAN et al., 2006; HWANG and CHEN, 2000).

While the circulation in the northern and central SCS would be completely different if the wind stress curl were neglected, in the southern part the wind stress is a good indicator for the regional circulation (XIE et al., 2003; METZGER, 2003; XU et al., 2007). Based on wind direction, the circulation in the upper layer of the southern SCS is cyclonic during winter and anticyclonic during summer. A boundary current is forced whereby the core is located at the shelf edge. During winter the core is directed southward and flows along the Vietnamese coast, whereas during summer it is directed northward. In winter a cyclonic eddy is located near the western coast of Luzon Island (Philippines) and in the southeast of the Zhongnan Peninsula. In summer an anticyclonic eddy appears to the east of the Zhongnan Peninsula. East of the central Vietnamese coast a cyclonic eddy exists which may be induced by summer upwelling (HU et al., 2000). These findings by HU et al. (2000) are also represented by the model results of the Navy Coastal Ocean Model (Figure 3).

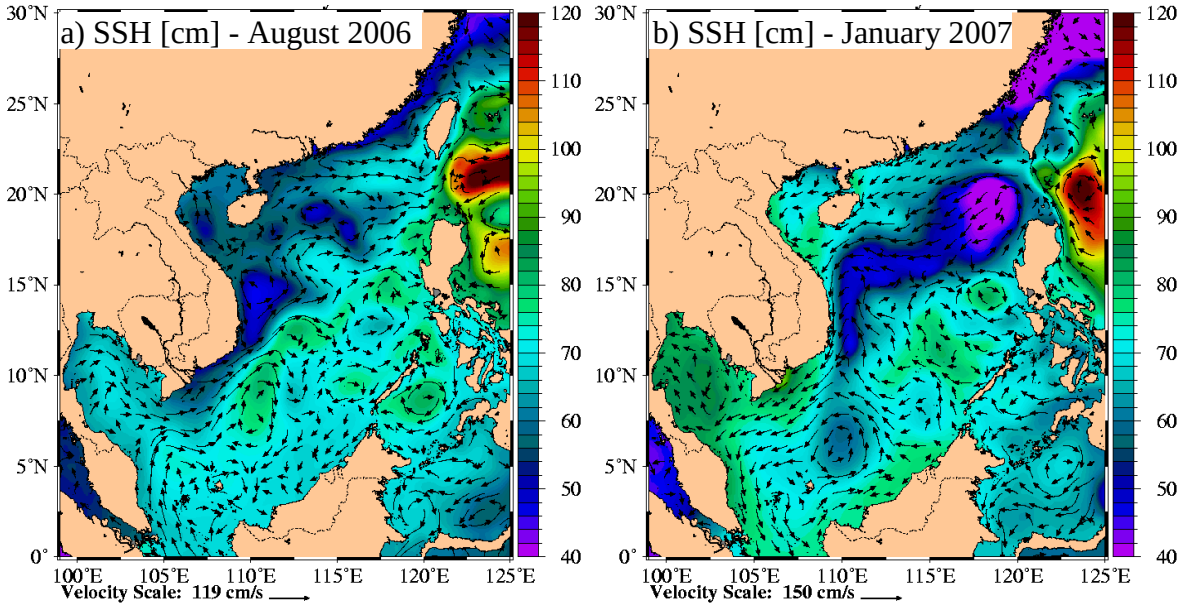

Figure 3: Surface currents [cm/s] over height [cm] in the SCS extracted from the Navy Coastal Ocean Model provided by the Naval Research Laboratory (http://www7320.nrlssc.navy.mil/global_ncom/glb8_3b/html/scs.html) a) during the summer monsoon (18/08/2006) and b) during the winter monsoon (18/01/2007).

The circulation in the coastal waters off South Vietnam follows the basin-wide circulation pattern, i.e., during winter a south-/southwestward current exists which flows in the direction of Kelvin wave propagation and during summer a north-/northeastward current exists in the direction opposite to Kelvin wave propagation (Figure 3). The reversal of the flow during summer has also been demonstrated in other studies. By means of ship experiments DIPPNER et al. (2007) showed the northward flow of the Mekong plume during summer up to 11° N. TANG et al. (2006) studied the seasonal variability of phytoplankton blooms in the SCS and the adjacent Gulf of Thailand and its coupling to monsoonal influences. Due to seasonal changes in the direction of the Mekong River discharge flow, which is correlated to the direction of the monsoon winds, phytoplankton blooms develop either in the Gulf of Thailand during the winter monsoon or in the SCS during the summer monsoon.

Due to a lack of resolution in recent simulations of the SCS, it is difficult to determine whether the basin-wide boundary current penetrates the Sunda Shelf and influences the regional circulation on the shelf or whether it just flows along the shelf edge. However, an intensification of the regional wind-driven circulation due to the boundary current can be suggested. In the figures of CHU et al. (1999) the boundary current especially during summer adjoins the coastal region of Zhongnan Peninsula.

Considering the sea surface salinity it is obvious that generally the salinity is higher in the Northern SCS than in the Southern SCS apart from coastal regions which are influenced by freshwater input from rivers (Figure 4b and d). Saline water from the Pacific Ocean enters the

Northern SCS through the Luzon Strait, which is the only salinity source for surface waters in the SCS (SHAW and CHAO, 1994). Regarding the temperature in summer (Figure 4a) there is no strong gradient throughout the SCS. Only the upwelling area along the coast off central Vietnam shows lower temperatures. During winter a temperature gradient exists with colder water in the Northern SCS and warmer water in the Southern SCS (Figure 4c). Also during winter the temperatures are decreased in the coastal region off central Vietnam. These water masses are advected southward by the western boundary current.

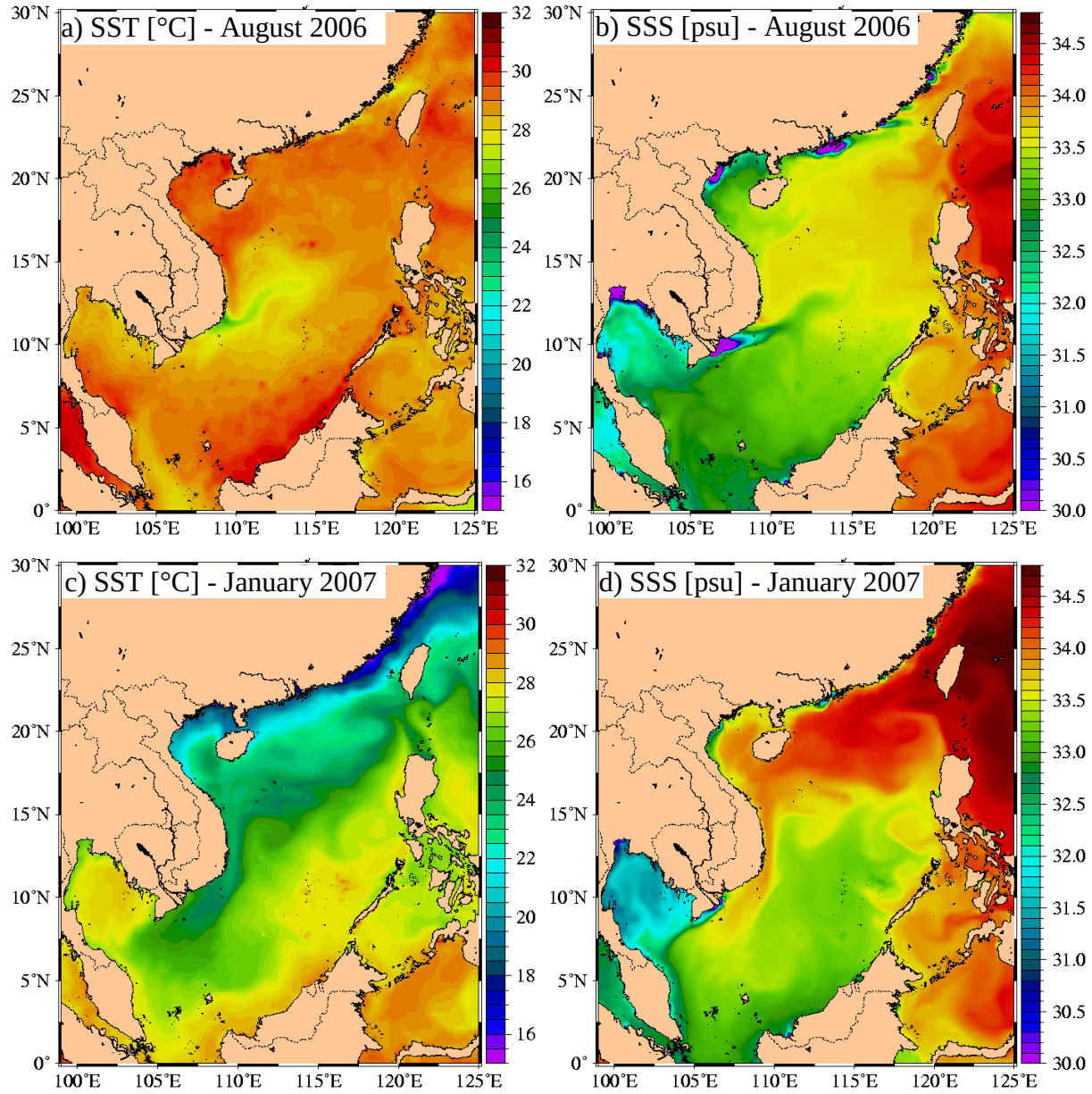

Figure 4: a) Sea surface temperature [°C] as well as b) sea surface salinity [psu] during the summer monsoon (18/08/2006) and c) sea surface temperature [°C] as well as d) sea surface salinity [psu] during the winter monsoon (18/01/2007) in the SCS extracted from the Navy Coastal Ocean Model provided by the Naval Research Laboratory (http://www7320.nrlssc.navy.mil/global_ncom/glb8_3b/html/scs.html).

2.3.3 THE MEKONG ROFI

The Mekong ROFI as a tropical ROFI is characterized by a high seasonal variability related to the monsoon winds and to the river flow (HORDOIR et al., 2006). It experiences high tidal ranges (WYRTKI, 1961). Another important feature of the Mekong ROFI is that the Coriolis parameter is small in comparison with the mid-latitude case (SIMPSON and SNIDVONGS, 1998).

While several publications deal with the lower Mekong (e.g., YOSHIMURA et al., 2009; PLATE, 2007; KITE, 2001) or the South China Sea (e.g., HU et al., 2000; GAN et al., 2006; POHLMANN, 1987), a comprehensive study of the Mekong ROFI has been made only by HORDOIR et al. (2006). Their overall purpose was the parameterization of freshwater runoff for global circulation models, whereby in their paper they focus on the identification and parameterization of the main processes that shape river plumes in tropical regions. As an example for testing their parameterizations they consider the Mekong River plume. Additionally, in the Cuu Long Project (HUNGSPREUGS et al., 1998) some rough investigations on the hydrodynamics of the Mekong Estuary and the adjacent coastal zone were made.

The findings of HORDOIR et al. (2006) will be summarized in the following. As the freshwater input of the Mekong River into the SCS is strongly seasonal, in the subsequent chapters it will be differentiated between a low-flow season (November to April) and a high-flow season (May to October). HORDOIR et al. (2006) studied the dynamics of the Mekong ROFI during both seasons (March and beginning as well as end of October). Generally, the high-flow season overlaps with the SW monsoon and the low-flow season with the NE monsoon. However, during the month of October river discharge is still increased but the monsoon starts to change. Thus, the time period at the end of October does not represent a typical situation of the high-flow season like the months of August and September. The time period from December until March is typical for the low-flow season as the river discharge is decreased and the NE monsoon is fully developed.

LOW-FLOW SEASON

During the dry season (NE monsoon) the freshwater input creates a density-current which is deflected under the influence of the Coriolis force to the right looking downstream. The river plume heads toward the SW. The wind tends to create an Ekman transport towards the coast. The plume is compressed against Zhongnan Peninsula (Figure 2) and downwelling occurs.

HORDOIR et al. (2006) stated that the flow is mainly created by the four lower branches of the Mekong River system (Tranh De, Din An, Hau and Chien). A cross section through the salinity distribution south to the Hau branch shows that during March the water column is strongly stratified (their figure 6). The upper branches of the Mekong River system discharge less water into the SCS and in that coastal area the baroclinic current is much weaker. The authors suggest that the weakness of the baroclinic flow is not only a result of the lower freshwater input by these branches but also of the shallow bottom extending far offshore in that coastal area.

Also the coastal region to the south of the Mekong River mouths is very shallow and the currents are weak. The authors suggest that in this area stratification is destroyed by vertical mixing. However, the main current stays off the shallow coastal area and is weakly stratified. It flows along the coast ending up in the Gulf of Thailand.

HORDOIR et al. (2006) summarize that the plume is strongly influenced by tidal mixing. Tidal motions induce a frictional velocity shear in the bottom boundary layer which generates vertical mixing of the water column (SIMPSON and HUNTER, 1974).

HIGH-FLOW SEASON

At the beginning of October, the decreasing SW monsoon tends to create an Ekman transport away from the coast that advects the plume offshore and upwelling occurs. The surface currents of the river plume are directed towards E/SE. The river plume is strongly stratified. Outside the river plume weak surface currents mainly follow the wind stress direction. At the end of October the situation changes as the wind reverses and a weak NE wind blows. A broad plume heading SW which is compressed against the coast can be observed. Altogether, in the high-flow season the plume is wider and stratification is higher than in March. The surface velocities of the baroclinic current are more than twice as large as in the low-flow season. Strong horizontal pressure gradients exist. Velocities remain low in the shallow coastal region to the south of the Mekong River mouths.

Altogether, the authors promote that the Mekong River plume is mostly geostrophic. Due to the strong interaction between the river plume and the bottom, vertical mixing has a strong impact on the vertical haline structure of the water column.

2.4 TIDES IN THE MEKONG ROFI AND THE ADJACENT WATERS

The tides in the Southeast Asian Waters are co-ocillating tides from the Pacific Ocean and the Indian Ocean. The SCS is dominated by tides from the Pacific (WYRTKI, 1961). Tidal waves enter the SCS mainly through the Luzon Strait (ZU et al., 2008; BEARDSLEY et al., 2004). The main tidal constituents are the M_2, K_1, O_1 and to a lesser extent S_2 (BEARDSLEY et al., 2004). Thus, basically the tides in the SCS have a mixed diurnal and semi-diurnal character (NGUYEN et al., 2007). However, on the Sunda Shelf they mainly have a diurnal characteristic (WYRTKI, 1961) and in the Mekong ROFI between Vung Tau and Tran De branch they are predominantly semi-diurnal (NGUYEN et al., 1998).

ZU et al. (2008) studied the tides and tidal dynamics in the SCS. In their figure 2 they show the cotidal charts and the tidal current ellipses of M_2. The figure demonstrates that the M_2 amplitude is small in the central part of the SCS but it is amplified in the coastal regions. Regarding the Mekong ROFI, the M_2 tide has an amplitude > 1 m. The tidal current ellipses show a similar pattern. In the central part of the SCS the currents are weak. However, in the coastal region

strong currents exist. Considering the Mekong ROFI, the tidal ellipses in the region off the Mekong River mouth are aligned and have a strong cross-shore component which may be related to a standing wave. However, the tidal ellipses in the coastal region to the south of the Mekong River mouth are broader and have an alongshore component. This shape rather corresponds to a progressive wave. The K_1 tide is shown in their figure 3. It can be deduced that the K_1 tide is amplified in the region of the Mekong River as well. The amplitude is about 0.75 m. In contrast to the tidal current ellipses of the M_2 tide, the ellipses of K_1 are aligned both in the region of the Mekong River and in the coastal region to the south of the Mekong River mouth. Regarding the amplitudes of the S_2 and O_1 tides (their figure 4), it can be concluded that the O_1 tide has an amplitude of about 0.5 m in the coastal region of the Mekong River whereas the S_2 tide is only of minor importance with an amplitude of about 0.25 m.

With regard to the Mekong Estuary, the main part is tidal with an amplitude from the SCS between 3 and 3.5 m (MRC, 2005). The tides move within the estuary as a progressive wave (WOLANSKI et al., 1996, 1998).

CHAPTER 3

ANALYSING STRATIFICATION AND MIXING IN A ROFI

To quantify the stability of a water column in an area under investigation, evaluation of the potential energy anomaly (one-dimensional potential energy anomaly, φ_{1D}) is an excellent method (SIMPSON et al., 1981). Recently, BURCHARD and HOFMEISTER (2008) and DE BOER et al. (2008) derived a dynamic equation for the potential energy anomaly which can be used for analyzing three-dimensional flows (three-dimensional dynamic potential energy anomaly, φ_{t3D}). Thus, by means of the dynamic equation for the potential energy anomaly three-dimensional numerical model results can be analyzed with regard to the main physical processes stratifying and/or destratifying the water column.

3.1 SOME BASICS ABOUT POTENTIAL ENERGY

For convenience before we start with the equation for the potential energy of a water column, the concept of centre of mass of a water column will be considered in order to get a basic understanding.

The centre of mass (R) of a water column [m] can be calculated by

$$R = \frac{\int_{-h}^{\eta} \rho z dV}{\int_{-h}^{\eta} \rho dV} \tag{3.1}$$

where V is the volume of the water column or of the different layers [m³], ρ is the density of the water column or of the layers [kg/m³], z is the vertical coordinate of the geometric centre of the water column or of the geometric centre of the individual layers [m], η is the free surface [m] and h the location of the bed [m].

Figure 5 illustrates two different water columns with their respective geometric centres (yellow lines) and their respective centre of masses (red lines).

In total there exist three different states:

1. If the water column is mixed, the centre of mass of a water column equals the geometric centre (Figure 5a). According to the second law of thermodynamics, this process is irreversible and stratification can only be reproduced by an additional energy input.
2. Under conditions of stable stratification the centre of mass of a water column lies below the geometric centre of that water column (Figure 5b). To mix the stably stratified fluid, kinetic energy is required to raise the centre of mass to the centre of mass of the mixed water column.
3. Under conditions of reversed (unstable) stratification the centre of mass lies above the geometric centre.

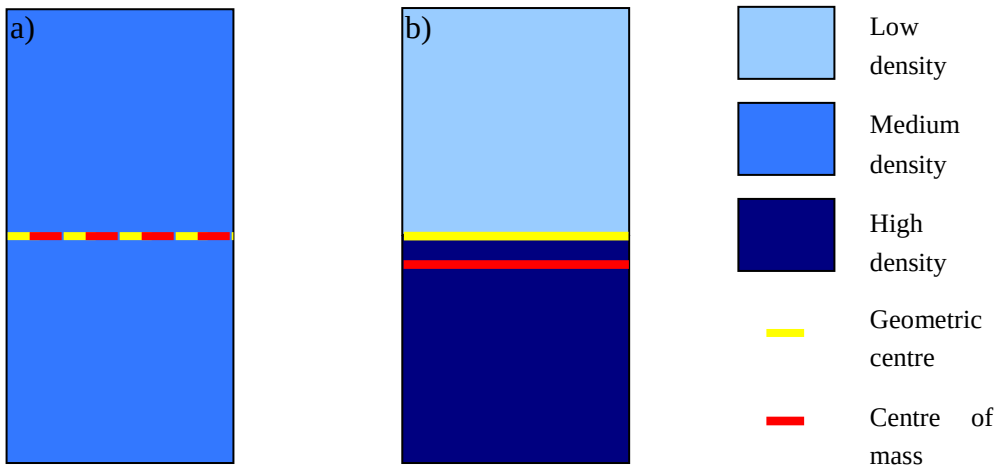

Figure 5: Schematic illustration of the concept of centre of mass of two water columns: a) mixed conditions and b) stratified conditions. The centre of mass of a stratified water column lies below the centre of mass of a mixed water column.

After having introduced the concept of the centre of mass, now we consider the potential energy PE [J] of such a system:

$$PE = \int_{-h}^{\eta} \rho g z \, dx \, dy \, dz \tag{3.2}$$

where ρ is the density [kg/m³], g is the gravitational acceleration [m/s²], x,y is the horizontal coordinate [m], z is the vertical coordinate [m], η is the free surface [m] and h the location of the bed [m]. For simplification, the potential energy is normalised to an area of 1 m².

The distance through which the centre of mass is raised after mixing is a measure of the work that has been done against gravity, and hence of the potential energy change of the water column.

It can be concluded that energy for mixing must be provided if the density of the lower layer is greater than the density of the upper layer. Typically energy for mixing would be provided by kinetic energy in the form of a velocity shear or turbulent kinetic energy (e. g., wind stress or wave stress at sea surface) (WILLIAMS, 2006). Otherwise, in case that the upper layer has a higher density than the lower layer, energy for mixing is available.

In addition to a changing water level, the potential energy of a water column also changes,

1) when the depth averaged water density is modified and/or
2) when the vertical gradient of density is transformed (i.e., the stratification of the water column is changed).

The dynamic processes, which cause changes of the vertical mean density and/or of the vertical density gradient, are horizontal advection, straining, mixing and up/downwelling, for instance. However, the process of vertical advection changes the elevation of the centre of mass without changing the vertical density gradient and thus the stratification of the water column. Nevertheless, due to conservation of mass vertical advection of a density structure is inevitably linked with horizontal advection, which may change not only the depth averaged density but also the vertical density gradient of the water column.

3.2 THE EQUATION FOR THE POTENTIAL ENERGY ANOMALY

The equation for the potential energy anomaly has been used in a large number of studies as a measure for stratification, e.g., LIN and KUO, 2001; FISHER et al., 2002; SIMPSON et al., 1990; SIGNORET et al., 2006. The term 'Potential Energy Anomaly' has been defined by SIMPSON et al. (1981) following the ideas of SIMPSON and HUNTER (1974) and SIMPSON et al. (1978). These authors consider the actual potential energy of a water column due to a given vertical density profile relative to the potential energy when this water column would be mixed instantaneously.

According to SIMPSON et al. (1981) the potential energy anomaly of a water column φ_{1D} [J/m³] is given by

$$\varphi_{1D} = \frac{g}{H}\int_{-h}^{\eta}(\bar{\rho}-\rho)z\,dz \tag{3.3}$$

where ρ is the vertical density profile [kg/m³] over the water column of depth H [m], $\bar{\rho}$ is the depth averaged density [kg/m³], g is the gravitational acceleration [m/s²], z is the vertical coordinate [m], η is the free surface [m] and h the location of the bed [m].

The PEA equation quantifies the work required to bring about complete vertical mixing. Equation 3.3 shows that φ_{1D} = 0 J/m³, when the water column is mixed (i.e., no work is required to mix the water column instantaneously). As shown in the last section (3.1), the centre of mass of that kind of water column lies at the geometric centre of the water column. If φ_{1D} > 0 J/m³, then the water column is stably stratified. The centre of mass lies in the lower half of the water

column, i.e., work is required to raise the centre of mass of the stratified water column to the height of the centre of mass of the mixed water column. In general, it can be noted that more work is required to mix a strongly stratified water column than to mix a slightly stratified water column. $\varphi_{1D} < 0$ J/m³, when the water column is unstably stratified. In this case the centre of mass lies in the upper half of the water column and energy for mixing is available.

The tendency of the PEA is defined as φ_{t1D} [W/m³]:

$$\varphi_{t1D} = \frac{\partial \varphi_{1D}}{\partial t} = \frac{g}{H} \int_{-h}^{\eta} \frac{\partial(\bar{\rho} - \rho)}{\partial t} z dz \tag{3.4}$$

where t is time [s], ρ is the vertical density profile [kg/m³] over the water column of depth H [m], $\bar{\rho}$ is the depth averaged density [kg/m³], g is the gravitational acceleration [m/s²], z is the vertical coordinate [m], η is the free surface [m] and h the location of the bed [m].

It can be deduced from this formulation:

1) If a system is stratified and becomes less stratified or even mixed, then the time rate change is negative.
2) If a system is stratified and becomes more stratified, then the time rate change is positive.
3) If a system is mixed and becomes stratified, then the time rate change is also positive.

To complete the formulation of SIMPSON et al. (1981) (equation 3.4), two additional, barotropic terms will be considered in the equation for the tendency of PEA:

$$\varphi_{t1D\_barotrop} = -\frac{\varphi_{1D}}{H} \frac{\partial H}{\partial t} - \left(\frac{g}{H} \right) \left[\tilde{\rho}_{\eta} \eta \frac{\partial \eta}{\partial t} \right] \tag{3.5}$$

Hence equation 3.4 becomes

$$\varphi_{t1D} = \frac{\partial \varphi_{1D}}{\partial t} = \frac{g}{H} \int_{-h}^{\eta} \frac{\partial(\bar{\rho} - \rho)}{\partial t} z dz - \frac{\varphi_{1D}}{H} \frac{\partial H}{\partial t} - \left(\frac{g}{H} \right) \left[\tilde{\rho}_{\eta} \eta \frac{\partial \eta}{\partial t} \right] \tag{3.6}$$

where $\tilde{\rho}_{\eta}$ is the perturbation density at the free surface [kg/m³]. The barotropic terms include the changes in the water depth and in the sea surface elevation, for example the rise and fall of a water column due to tidal forces.

If the formulas 3.3 and 3.4 are applied to a time series of data, it is possible to identify the mean level of stratification in an area under investigation and to quantify the time evolution of stratification and destratification of a water column throughout a given time period, e.g., a spring-neap cycle. However, using this approach it is not possible to determine the physical processes which contribute to increase and/or decrease the stratification. Moreover, especially in a ROFI horizontal exchange processes affecting the vertical density gradient are of importance, hence an equation for the PEA suitable for three-dimensional flows is necessary.

3.3 THE THREE-DIMENSIONAL DYNAMIC EQUATION FOR THE POTENTIAL ENERGY ANOMALY

DE BOER et al. (2008), BURCHARD and HOFMEISTER (2008) and HOFMEISTER et al. (2009) have shown that the three-dimensional dynamic PEA equation is a powerful tool to analyze the physical processes affecting stratification in a ROFI. DE BOER et al. (2008) used idealized numerical model results over a time period of 36 h for the Rhine ROFI. BURCHARD and HOFMEISTER (2008) utilized the model results of a one-dimensional tidal straining model over a tidal period (M2) as well as the results of a two-dimensional estuarine circulation model over three tidal periods. HOFMEISTER et al. (2009) applied the three-dimensional dynamic PEA equation to investigate processes of stratification and destratification by means of the result of a three-dimensional model study in the Limfjord (Denmark) for the year 2003.

In this study, the three-dimensional dynamic PEA equation is applied for the first time to analyze the mechanisms contributing to mixing and stratification in a tropical ROFI reflecting the seasonal differences. This ROFI is strongly influenced by monsoon winds and seasonal varying river discharge. Here, seasonal time scales may dominate over tidal or sub-tidal time scales.

The starting point for the three-dimensional dynamic PEA equation is the Reynolds averaged advection-diffusion equation for density $\frac{\partial \rho}{\partial t}$:

$$\frac{\partial \rho}{\partial t} + u\frac{\partial \rho}{\partial x} + v\frac{\partial \rho}{\partial y} + w\frac{\partial \rho}{\partial z} = \frac{\partial}{\partial x}\langle\ \rho' u'\ \rangle + \frac{\partial}{\partial y}\langle\ \rho' v'\ \rangle + \frac{\partial}{\partial z}\langle\ \rho' w'\ \rangle + Q(x,y,z,t) \tag{3.7}$$

where x and y are the horizontal coordinates [m], z is the vertical coordinate [m], ρ is the density [kg/m³], u and v are the horizontal velocities [m/s], w is the vertical velocity [m/s] and $\langle\ \rho' u'\ \rangle$, $\langle\ \rho' v'\ \rangle$, $\langle\ \rho' w'\ \rangle$ are the turbulent fluxes of mass in the x, y, z direction [kg/(m² s)] resulting from the Reynolds decomposition. Q(x,y,z,t) represents the modification of density due to sources and sinks of temperature and/or salinity. Density can be calculated from temperature, salinity and pressure using the equation of state for sea water (FOFONOFF and MILLARD, 1983).

The turbulent fluxes of mass $\langle\ \rho' u'\ \rangle$, $\langle\ \rho' v'\ \rangle$, $\langle\ \rho' w'\ \rangle$ of equation 3.7 are commonly not resolved numerically by a simulation. Therefore these terms are parameterized as a function of the mean density gradient which is a common way to solve the turbulent closure problem.

The expressions for the vertical and horizontal fluxes of mass are:

$$\langle\ \rho' w'\ \rangle = -K_z \frac{\partial \overline{\rho}}{\partial z} \tag{3.8}$$

$$\langle\ \rho' u'\ \rangle = -K_x \frac{\partial \overline{\rho}}{\partial x} \tag{3.9}$$

$$\langle\ \rho' v'\ \rangle = -K_y \frac{\partial \overline{\rho}}{\partial y} \tag{3.10}$$

where K_z is the vertical eddy diffusivity [m²/s] and $K_{x,y}$ are the horizontal eddy diffusivities [m²/s]. The negative sign on the right hand side of equation 3.8 to 3.10 implies that the density gradient decreases by the turbulent fluxes.

With this parameterization the turbulent diffusion terms are introduced and the density equation can be rewritten

$$\frac{\partial \rho}{\partial t} + u\frac{\partial \rho}{\partial x} + v\frac{\partial \rho}{\partial y} + w\frac{\partial \rho}{\partial z} = \frac{\partial}{\partial x}K_x\frac{\partial \rho}{\partial x} + \frac{\partial}{\partial y}K_y\frac{\partial \rho}{\partial y} + \frac{\partial}{\partial z}K_z\frac{\partial \rho}{\partial z} + Q(x,y,z,t) \tag{3.11}$$

The depth integrated density equation to calculate $\frac{\partial \bar{\rho}}{\partial t}$ is:

$$\frac{\partial \bar{\rho} H}{\partial t} + \frac{\partial \bar{u}\bar{\rho} H}{\partial x} + \frac{\partial \bar{v}\bar{\rho} H}{\partial y} = -\frac{\partial \overline{\tilde{u}\tilde{\rho}} H}{\partial x} - \frac{\partial \overline{\tilde{v}\tilde{\rho}} H}{\partial y} - \langle p'w' \rangle|_s + \langle p'w' \rangle|_b + \bar{Q} \tag{3.12}$$

where $\bar{\rho}$ is the depth averaged density [kg/m³], $\bar{u}$ and $\bar{v}$ are the depth averaged velocities [m/s], $\langle \rho'w' \rangle|_s$ and $\langle \rho'w' \rangle|_b$ are the surface and bottom density flux, $\bar{Q}$ is the depth integrated source and sink term. $\tilde{u} = u - \bar{u}$, $\tilde{v} = v - \bar{v}$ and $\tilde{\rho} = \rho - \bar{\rho}$ are the deviation from the depth mean values. The first and the second term on the right hand side are shear dispersion terms.

Now substituting the density equation (3.11) and the averaged-mean density equation (3.12) into the equation for the tendency of PEA (equation 3.6 and neglecting bottom and surface density fluxes for simplification, this yields the three-dimensional dynamic PEA equation φ_{t3D} [W/m³]:

$$\varphi_{t3D} = \frac{\partial \varphi_{3D}}{\partial t} =$$

$$\frac{g}{H}\int_{-h}^{\eta}\Bigg[\underbrace{\tilde{u}\frac{\partial \tilde{\rho}}{\partial x}}_{\mathbf{MS_X}} \underbrace{+\bar{u}\frac{\partial \tilde{\rho}}{\partial x}}_{\mathbf{ADV_X}} \underbrace{+\tilde{u}\frac{\partial \tilde{\rho}}{\partial x}}_{\mathbf{NS_X}} \underbrace{-\frac{1}{H}\frac{\partial \overline{\tilde{u}\tilde{\rho}} H}{\partial x}}_{\mathbf{DIS_X}} \underbrace{+w\frac{\partial \rho}{\partial z}}_{\mathbf{UD_Z}}$$

$$\underbrace{+\tilde{v}\frac{\partial \tilde{\rho}}{\partial y}}_{\mathbf{MS_Y}} \underbrace{+\bar{v}\frac{\partial \tilde{\rho}}{\partial y}}_{\mathbf{ADV_Y}} \underbrace{+\tilde{v}\frac{\partial \tilde{\rho}}{\partial y}}_{\mathbf{NS_Y}} \underbrace{-\frac{1}{H}\frac{\partial \overline{\tilde{v}\tilde{\rho}} H}{\partial y}}_{\mathbf{DIS_Y}} \underbrace{-\frac{\partial}{\partial z}K_z\frac{\partial \rho}{\partial z}}_{\mathbf{MIX_Z}}\Bigg] z\,dz$$

$$+\frac{g}{H}\int_{-h}^{\eta}\Bigg[\underbrace{\frac{\partial}{\partial x}K_x\frac{\partial \rho}{\partial x}}_{\mathbf{DIFF_X}} \underbrace{+\frac{\partial}{\partial y}K_y\frac{\partial \rho}{\partial y}}_{\mathbf{DIFF_Y}}\Bigg] z\,dz$$

$$\underbrace{-\frac{\varphi_{1D}}{H}\frac{\partial H}{\partial t}}_{\mathbf{BT_D}} \underbrace{-\left(\frac{g}{H}\right)\left[\tilde{\rho}_\eta \eta \frac{\partial \eta}{\partial t}\right]}_{\mathbf{BT_S}} \tag{3.13}$$

In this study, the first twelve terms on the right of equation 3.13 will be named baroclinic terms and the last two terms barotropic terms. The baroclinic terms quantify the density effects depending on temperature, salinity and pressure on φ_{t3D}. The barotropic terms represent

barotropic effects like the influence of depth (BT_D) and surface elevation change (BT_S) on φ_{t3D}. In this study, the baroclinic terms represented in the three-dimensional dynamic PEA equation (red and grey rectangles) are clustered to seven terms because no differentiation in the horizontal between the x and y direction will be made when analyzing the results.

As opposed to the rough SIMPSON et al. (1981) formulation (equation 3.3), using the three-dimensional dynamic PEA equation of BURCHARD and HOFMEISTER (2008) and DE BOER et al. (2008) allows distinguishing between horizontal and vertical exchange processes. Thereby, horizontal exchange processes are represented by the mean straining term (MS_X+MS_Y), the horizontal advection term (ADV_X+ADV_Y), the non-mean straining term (NS_X+NS_Y), the shear dispersion term (DIS_X+DIS_Y) and the horizontal diffusion term ($DIFF_X$+$DIFF_Y$). Because of an artificial numerical diffusion a physically based horizontal mass diffusion is commonly not considered in the equations of a hydrodynamic model. Thus, it is not reasonable to calculate the horizontal diffusion term.

Vertical exchange processes are determined by the vertical mixing term (MIX_Z) and by the vertical advection term (UD_Z). Hence, the three-dimensional dynamic PEA equation is a good tool to investigate the competing influence of processes that increase stratification and those that mix the water column.

In the following, the first ten baroclinic terms of the three-dimensional dynamic PEA equation will be explained in detail. Similar schematic illustrations can partly also be found in BURCHARD and HOFMEISTER (2008). Thereafter these terms will be quantified for the Mekong ROFI to analyze the physical mechanisms contributing to stratification and mixing in this region (chapter 5).

VERTICAL PROCESSES

VERTICAL ADVECTION (UD_Z)

The term represents the vertical advection of a vertical density structure. In a hydrostatic model vertical velocities are calculated diagnostically by use of the continuity equation. In general as mentioned above the vertical advection term does not cause a change in stratification. However, from an Eulerian point of view due to the model discretization a change in stratification can be induced by vertical advection. Up/downwelling can occur during a tidal cycle as well as on a seasonal scale due to changing monsoon winds.

In this study, if the vertical advection term has a negative value, upwelling occurs. If the term is positive, downwelling occurs.

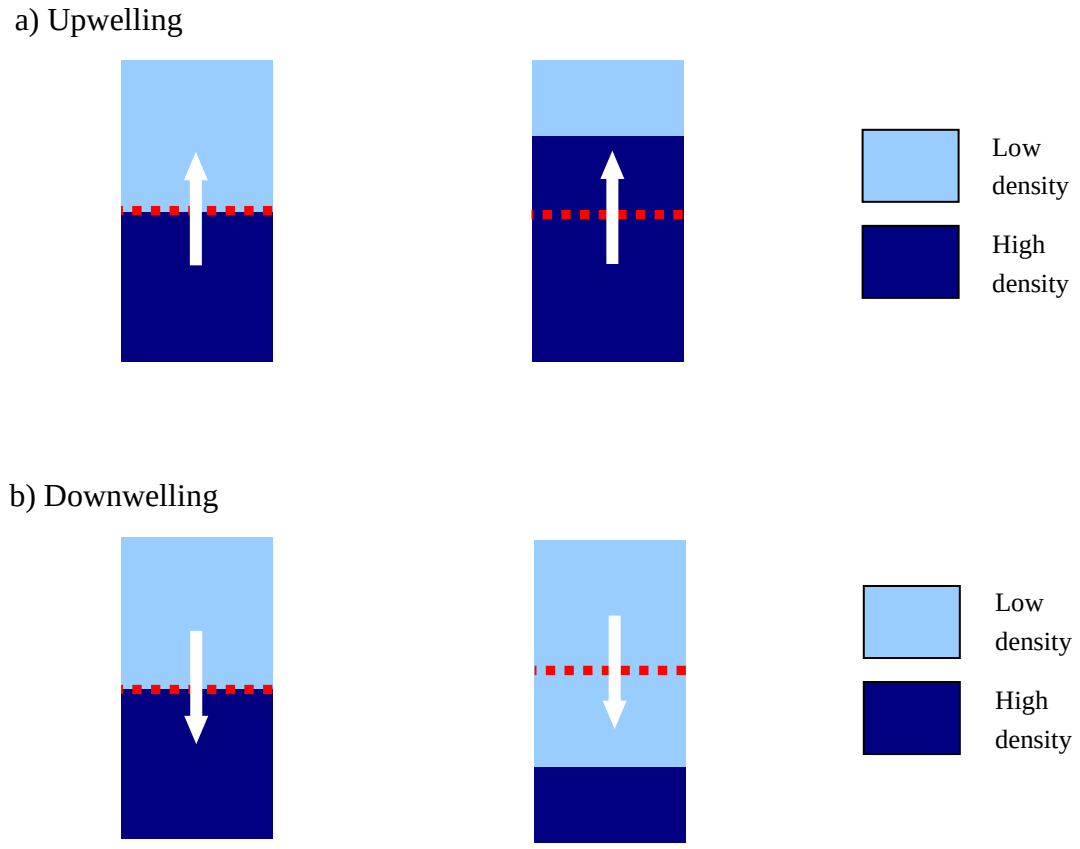

Figure 6: Schematic illustration of the vertical advection term from the three-dimensional dynamic PEA equation: a) upwelling and b) downwelling.

MIXING (MIX_Z)

The mixing term represents the effect of the vertical turbulent flux of mass on a density profile. Thereby, it cannot be distinguished between mixing by tides or wind when analyzing the hydrodynamic model results.

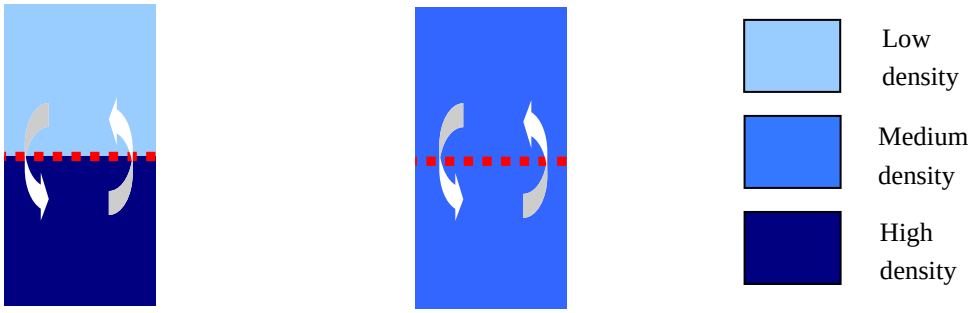

Figure 7: Schematic illustration of the mixing term from the three-dimensional dynamic PEA equation.

HORIZONTAL PROCESSES

HORIZONTAL ADVECTION ($ADV_X + ADV_Y$)

The horizontal advection term represents the transportation of a vertical density structure (deviation of mean density) by a depth mean current (mean velocity).

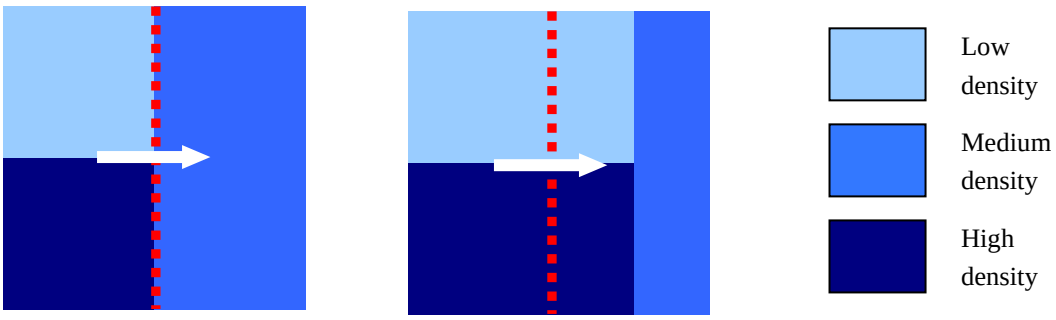

Figure 8: Schematic illustration of the advection term from the three-dimensional dynamic PEA equation.

MEAN STRAINING ($MS_X + MS_Y$)

The mean straining term represents a differential advection of mass by a vertical velocity shear. Straining induces stratification by deforming a horizontal density gradient (mean density) by a vertically sheared flow (deviation of mean velocity). Thereby, straining acts independently from a vertical density gradient. Even in the absence of mixing it can occur that stratification is decreased by a velocity shear.

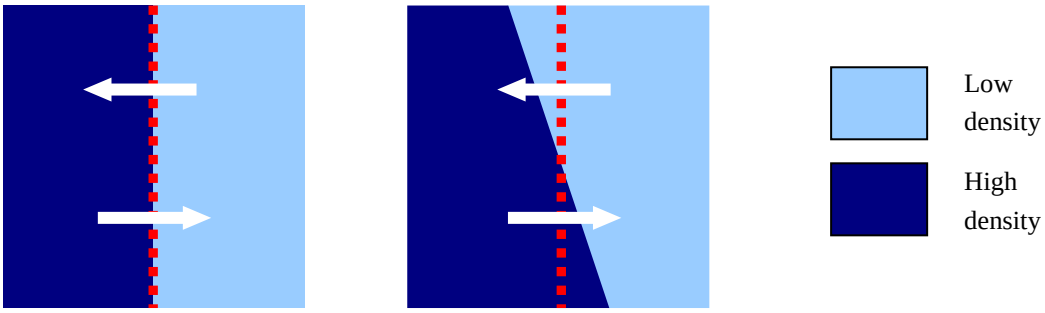

Figure 9: Schematic illustration of the mean straining term from the three-dimensional dynamic PEA equation.

NON-MEAN STRAINING ($NS_X + NS_Y$)

The non-mean straining terms represent the induction of stratification by deforming a horizontal density structure (deviation of mean density) by a velocity shear (deviation of mean velocity). Thus, even for a case where a mean horizontal density gradient does not exist (i.e., the depth averaged density is equal for two adjacent water columns, but the vertical density profiles are

different), the non-mean straining term can change the stratification.

If the velocity anomaly is in the direction of decreasing $\tilde{\rho}$, then $\tilde{u}\frac{\partial\tilde{\rho}}{\partial x}<0$ and the water column is stabilized ($\varphi_{t3D}>0$). If the velocity anomaly is in the direction of increasing $\tilde{\rho}$, then $\tilde{u}\frac{\partial\tilde{\rho}}{\partial x}>0$ and the water column is de-stabilized ($\varphi_{t3D}<0$).

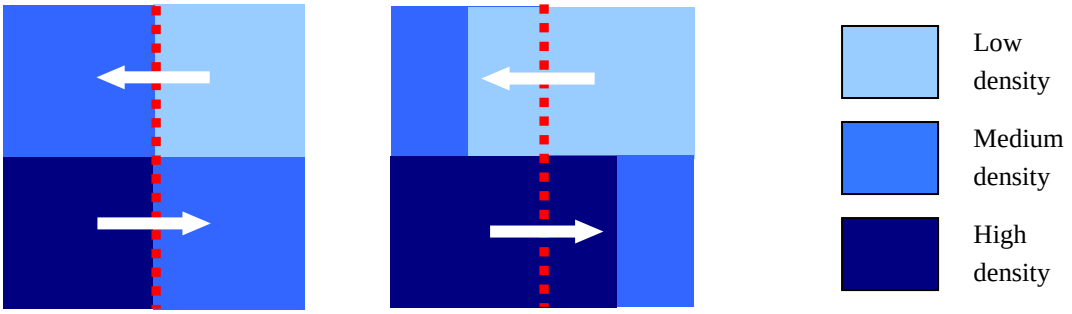

Figure 10: Schematic illustration of the non-mean straining term from the three-dimensional dynamic PEA equation.

SHEAR DISPERSION (DIS_X + DIS_Y)

The shear dispersion terms result from the depth-integrated advection-diffusion equation for density. These terms represent the horizontal dispersion due to a combined effect of a vertical velocity shear and vertical mixing.

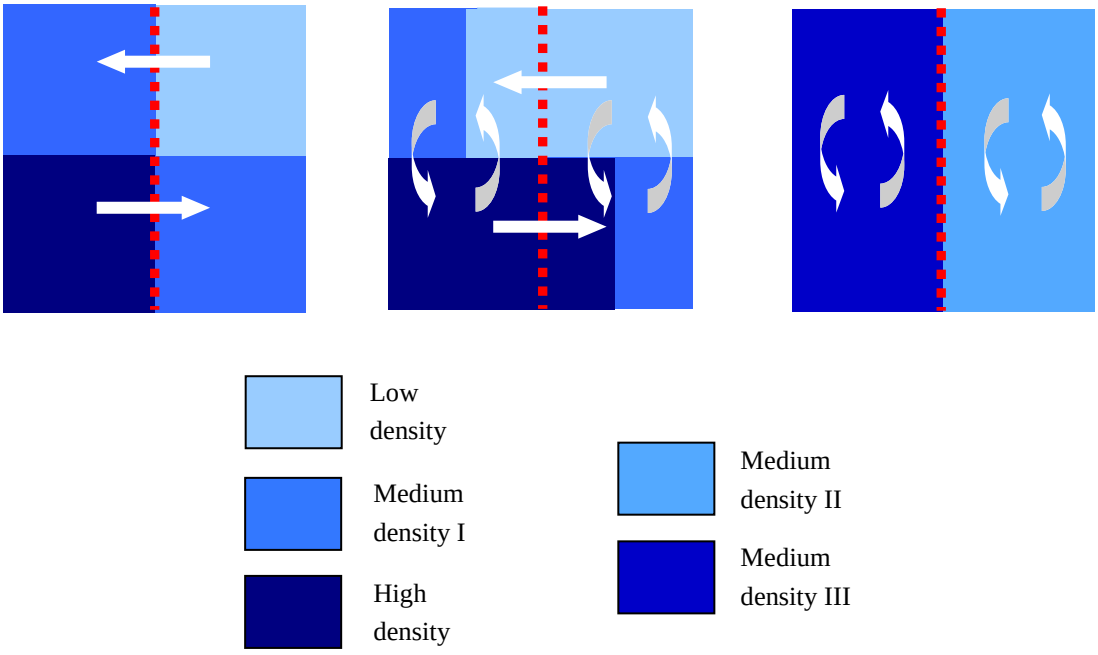

Figure 11: Schematic illustration of the processes which act simultaneously during shear dispersion. The process yields different horizontal densities (medium density II and III).

The result is a longitudinal spreading of a density structure, i.e., a spreading along the flow. The shear dispersion terms can be considered as the depth averaged counterparts of the non-mean straining terms. For the occurrence of a vertical velocity shear and a horizontal density gradient, the non-mean straining term represents the stratification that is induced by the differential advection of the horizontal density gradient. But the non-mean straining term excludes the transverse diffusion which yields the longitudinal spreading. This is included in the shear dispersion terms. Regarding equation 3.13 it is apparent that the effect of shear dispersion – like vertical mixing – decreases φ_{t3D}. This is because the horizontal density gradient is reduced by the longitudinal spreading.

CHAPTER 4

NUMERICAL MODELLING AND VALIDATION

A common and solid tool for hydrodynamic studies is given by models that are based on physical equations. In this study, the **HAM**burg **S**helf **O**cean **M**odel (HAMSOM) developed by BACKHAUS (1982, 1985) is used to specify both the influence of seasonal changes in river discharge as well as monsoonal wind and the influence of tidal forces on the temporal variability of the hydrodynamic conditions in the Mekong ROFI. HAMSOM has been widely used for modelling coastal and estuarine processes, e.g., POHLMANN, 2006; SCHRUM, 1997; HUANG et al., 1999; HARMS et al., 2003; HUYNH, 2002; LE SOUËF, 2006.

In general, it is also possible to represent main river dynamics with HAMSOM so that it can be used to model the hydrodynamics of the Mekong River downstream of the Phnom Penh region. Thus, it is not necessary to use a long-term mean value of discharge with a weighted distribution over the branches of the river mouths as was done in the study of HORDOIR et al. (2006).

4.1 BASICS OF THE HAMBURG SHELF OCEAN MODEL

GOVERNING EQUATIONS AND NUMERICAL SCHEME

The HAMburg Shelf Ocean model is a three-dimensional, baroclinic, primitive equation model with a free surface. It is defined in z-coordinates on an Arakawa C-Grid. The governing equations are the momentum equations in x, y and the hydrostatic assumption in z, the equation of continuity, the equation of state for sea water (FOFONOFF and MILLARD, 1983) and the transport equation for salinity and temperature. The equations are solved with finite differences. More details can be found in POHLMANN (1991, 1996a) and SCHRUM (1994).

The vertical sub-grid scale turbulence is parameterized by means of a second order turbulent closure approach proposed by KOCHERGIN (1987), and extended and implemented by POHLMANN (1991, 1996a, 1996b, 1996c, 1996d). The vertical eddy viscosity is dependent on the vertical velocity gradient and on the stability of the water column. The vertical eddy diffusivity is calculated from the turbulent eddy viscosity using the Prandtl number. Thereby, the Prandtl number is only a function of the Richardson number which relates vertical stability to vertical

shear according to MELLOR and DURBIN (1975) and MELLOR and YAMADA (1974). Details can be found in POHLMANN (1991) and POHLMANN (1996a). In this approach it is taken into account that vertically unstable conditions do not exist for long-term or steady state considerations. For the case of an unstably stratified water column the vertical turbulent exchange coefficient is set to a maximum value promoting vertical exchange. After several time steps the unstable stratification vanishes.

To parameterize horizontal turbulent sub-scale processes, i.e., the diffusion of horizontal momentum, the Smagorinsky-scheme is implemented (SMAGORINSKY, 1993). The scheme is used to obtain variable values of the horizontal turbulent exchange coefficient which depend on the horizontal velocity shear of the flow. The scheme has also been used by HEIN (2007). To date, in HAMSOM a horizontal diffusivity is only calculated for the momentum transport but not for the mass transport.

To conserve eddies and frontal structures on the shelf, the horizontal nonlinear terms in the equation of motion are solved by the Arakawa J7 algorithm (ARAKAWA and LAMB, 1977). This energy and enstrophy conserving scheme has been implemented in HAMSOM by SCHRUM (1994). It is applied for the upper layers. For reasons of numerical stability in the lower shelf sea layers ($\geq$ 200 m depths), a selective vector-upstream algorithm is used. To calculate the Coriolis term with a second order approximation in time, a rotational matrix is utilized according to BACKHAUS (1985).

An implicit numerical scheme is applied for the free surface and vertical shear stress terms in the equation of motion to avoid stability constraints for surface gravity waves as well as for vertical diffusion of both mass and momentum. The advective terms of the momentum equation and of the transport equation of salinity and temperature are solved explicitly.

The source and sink terms of salinity are represented by the river inflow at the lateral boundary and by evaporation and rainfall at the sea surface. The source and sink terms of temperature are represented by heat fluxes at the sea surface.

BOUNDARY CONDITIONS

At the sea surface the kinematic surface boundary condition and the wind stress boundary condition (quadratic stress law) is valid. Fluxes of momentum, heat and freshwater at the sea surface are determined by means of bulk formulae from meteorological parameters. For incoming solar radiation the bulk formula of the COHERENS model (COupled Hydrodynamical Ecological model for REgioNal Shelf seas) is adopted (LUYTEN et al., 1999). The outgoing long-wave radiation is calculated according to FUNG et al. (1984). The sensible and latent heat flux parameterisation are obtained from KONDO (1975). At the seabed the kinematic condition and bottom stress boundary condition (non-linear friction law) is used. At the lateral open boundaries the ocean temperature and salinity is given by a climatological monthly mean. Sea surface elevation is calculated as a result of the inverse barometric effect, tidal elevations, river

discharge effects and dynamical height. As inflow condition a relaxed climatological monthly mean value for temperature and salinity is prescribed. As outflow condition a Sommerfeld radiation condition is adopted (ORLANSKI, 1976). For the calculation of the transports a zero gradient condition is used. At closed lateral boundaries a semi-slip and zero flux condition is applied.

4.2 ADAPTATION OF HAMSOM TO THE MEKONG ROFI

MODEL FORCING

To force the model, various datasets have been pre-processed reproducing the atmospheric conditions, river discharge, tidal elevation, water temperature and salinity. The data for the atmospheric conditions (wind stress, sea level pressure, evaporation, precipitation, solar radiation, air temperature, cloud cover, relative humidity) were delivered by the NCEP/NCAR reanalysis project (http://www.cdc.noaa.gov/data/reanalysis/reanalysis.shtml) (KALNAY et al., 1996). The use of NCEP/NCAR reanalysis data as surface forcing is an established method (MAYER et al., 2010; PUTRI and POHLMANN, 2009; SIMIONATO et al., 2006). The climatological monthly mean for salinity and water temperature is extracted from the Levitus database (BOYER et al., 1998a; BOYER et al., 1998b; ANTONOV et al., 2006; LOCARNINI et al., 2006). The river discharge has been provided by the WaterGAP Global Hydrology Model (DÖLL et al., 2003) as a mean monthly value. The data has been bias-corrected as will be described in the next section (section 4.3). For the Saigon River the discharge data is also delivered by the WGHM.

The Oregon State University Tidal Inversion Software (OTIS) represents a tool to get the tidal inverse solution for different ocean regions. For this study the regional inverse tidal solution for the Indonesian Seas has been used. The spatial resolution of the Indonesian Seas Inverse Tidal Solution is 1/6°. A generalized inversion scheme for assimilation of TOPEX/POSEIDON altimeter data into different regional models has been developed by EGBERT et al. (1994) and EGBERT and EROFEEVA (2002). The Oregon State University Tidal Prediction Software (OTPS) can be used to extract tidal harmonic constants. This has been done to achieve the phases and amplitudes at the open boundaries of the model domain. Eight tidal constituents are accounted for in the Mekong ROFI (M2, S2, K1, O1, N2, P1, K2, Q1).

RESOLUTION AND BATHYMETRY

The Mekong ROFI is represented by a uniform grid spacing of 1/60° in spherical coordinates. The model domain ranges from 104° E to 111° E and from 7.25° N to 12.75° N. In the horizontal this results in 421 grid points in x-direction and 331 in y-direction, respectively. The model bathymetry that is used is shown in Figure 2b. The vertical grid spacing varies. In total, there are 26 vertical layers. The upper layers down to a depth of 30 m have a thickness of 3.0 m, except for the surface layer which has a thickness of 3.5 m and the second layer of 2.5 m. The

irregular thicker surface layer was chosen to account for large tidal amplitudes. Down to 100 m the layer thickness is 10 m, then down to 200 m the spacing is 25 m and between 200 m to 300 m the thickness is 50 m. Below this, the spacing increases from 200 m down to 1000 m. The deepest layer ends at about 3500 m. The bathymetry has been extracted from the ETOPO2 dataset available from the National Geophysical Data Center, National Oceanic and Atmospheric Administration, U.S. Department of Commerce (http://www.ngdc.noaa.gov/mgg/global/etopo2.html) and from the GEBCO dataset (General Bathymetric Chart of the Oceans, http://www.gebco.net/data_and_products/gridded_bathymetry_data/). A merged dataset has been used to optimize the representation of the bathymetry on the shelf.

The time step has been set to 2.5 minutes to get a high temporal resolution.

MODEL SET-UP AND RUN-TIME

The baroclinic-prognostic mode has been used. The spin up period has been set to one year so that the simulation is not influenced by the initial conditions. Model simulations have been conducted for the years 2004 to 2008.

4.3 MODIFICATION OF HAMSOM

Because of the spatial heterogeneous distribution of buoyancy in a ROFI, it is important that the hydrodynamic model HAMSOM is able to simulate the horizontal advection of freshwater through the region and related mixing processes sufficiently precise. Particularly, the gradients of the density field in the frontal zone have to be preserved during the modelling process. In an Eulerian model various advection schemes implicate different numerical diffusions which yield a greater or lesser artificial smoothing of the frontal zone. Thus, to preserve the gradients of the density field in an adequate accuracy, an advection scheme which attenuates the numerical diffusion in the simulation process has to be found. Since presently there is no general optimal advection scheme, recent authors deal with different solutions of this problem in the case of Eulerian advection, e.g., BORIS and BOOK, 1973; PEDERSEN and PRAHM, 1974; LEONARD, 1979, 1991.

Previously, a first-order, vector upstream advection scheme was implemented in HAMSOM. By means of a basic one-dimensional model it has been shown that a second order advection scheme (LAX and WENDROFF, 1960; LAX and WENDROFF, 1964) in combination with using a Superbee flux limiter (ROE, 1986) is able to simulate the interaction between the Mekong discharge and the coastal saline water more realistically, i.e., the diffusion and moreover the mixing processes in the model are controlled by physical processes (HEIN et al., 2007). Therefore, the above mentioned less diffusive higher-order advection scheme has been implemented in the model by HEIN et al. (submitted).

4.4 MEKONG RIVER DISCHARGE DATA

The Mekong River discharge data is provided by the WaterGAP Global Hydrology Model (WGHM) used by DÖLL et al. (2003). The WGHM is a global hydrological model which simulates surface runoff, groundwater recharge and river discharge. The main task of the WGHM is to support the sustainable use of water. Therefore, it assesses the long-term average water resources and water availability indicators which take the seasonal and interannual variability of runoff and discharge into account. The spatial resolution of the WGHM is 0.5°.

As this spatial resolution is too sparse to represent the nine branches of the Mekong River, the Mekong River downstream of Phnom Penh which marks the beginning of the delta system is resolved in the model domain of this study. The discharge data of the WGHM is used to force the hydrodynamic model at the open boundary which is represented by a river cross section near Phnom Penh. Discharge data for the Saigon River, which also may influence the dynamics in the Mekong ROFI, is also provided by the WGHM. This approach is different to that of HORDOIR et al. (2006), who also outlined a study of the Mekong ROFI, but did not include the river upstream of the Mekong River mouths.

Modelling the Mekong River downstream of Phnom Penh allows to represent the estuarine processes which interact with the physical processes of the Mekong ROFI. In their study NGUYEN et al. (2007) reported that the tidal influence is noted until My Thuan and Can Tho, which are located 95 km upstream of the Dai mouth and 80 km upstream of the Dinh An mouth, respectively. The maximum tidal amplitude in the Mekong Estuary is between 3 m and 3.5 m (MRC, 2005). In addition, during the low-flow season a salinity intrusion from the SCS has been observed by NGUYEN and SAVENIJE (2006) and NGUYEN et al. (2007).

In the following the Mekong River discharge data provided by the WGHM is compared with discharge data from observations. The observed river discharge data has been published by the Mekong River Commission in the Lower Mekong Hydrologic Yearbooks 2003/2004. The yearbooks contain basin-wide hydrological and meteorological data. For the Saigon River there is no reference data available.

For the year 2003 the observed river discharge is considered at Tan Chau station (Mekong River) and Chau Doc station (Bassac). By these stations the two main branches of the river are represented. However, due to the sparse resolution of the WGHM, in the model the river is represented by only one branch. The above mentioned stations are represented by a single grid cell with its centre at 105.25° E and 11.25° N. Therefore, to accomplish comparable datasets the data at Tau Chau station and Chau Doc station extracted from the Hydrologic Yearbook is summed (Figure 12).

Several differences can be observed when comparing the simulated data of 2003 of the WGHM with the observed data of the Mekong River Commission:

1) During the wet season the WGHM overestimates the river discharge. During the dry

season the WGHM underestimates the discharge.

2) The observed peak discharge is broader than the modelled peak discharge.

3) The total annual discharge for 2003 (345 km³/a) is overestimated by the calculated discharge (517 km³/a). The factor is about 1.5.

These differences arise as the WGHM is used to model the global hydrologic cycle and does not take into account all of the special local features of the Mekong River. On the one hand, the flow reversal of the Tonle Sap River towards or from the Tonle Sap Lake is an important factor for the magnitude of discharge during the seasons. This particularity is not reflected by the WGHM (Fiedler, pers. communication). On the other hand, the seasonal change in the extension of the Mekong floodplain has to be considered. Indeed, the WGHM takes into account floodplains that are represented as stretches of the river. However, the water level can rise or fall throughout a year (± 2 m), but the extension of the flooded area is considered to be constant (Fiedler, pers. communication). Thus, the complex flood system of the Mekong River with its broad extensions during the rainy season is not represented by the WGHM. Additionally, the varying seasonal extension of the Tonle Sap Lake is not considered in the WGHM because lakes are defined to have a constant surface area. However, the water level can change (± 5 m) as is the case for the floodplains (Fiedler, pers. communication).

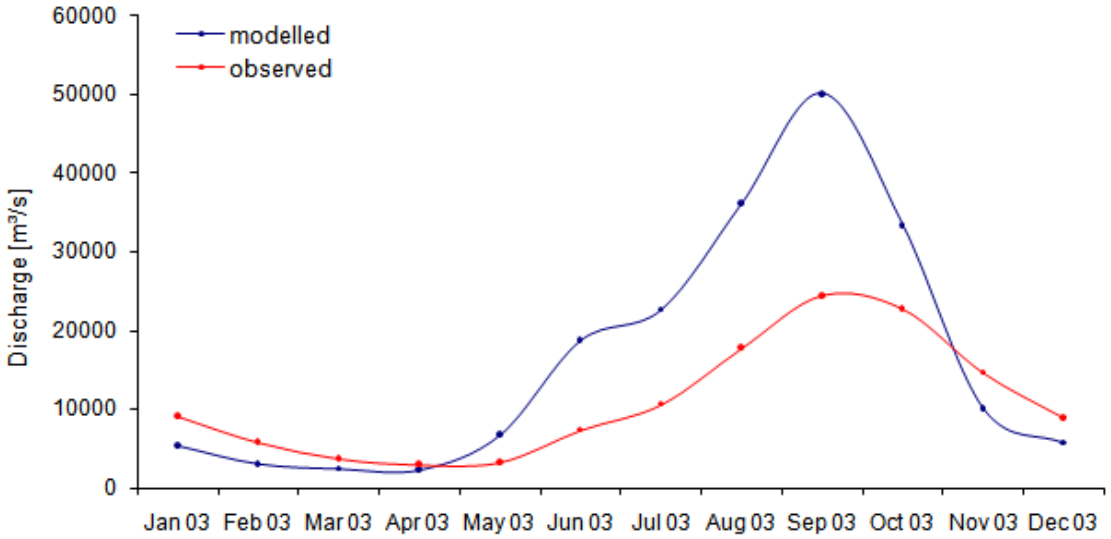

Figure 12: Observed Mekong River discharge [m³/s] in 2003 (sum of Tan Chau and Chau Doc station - red line) (MRC, 2004) and modelled Mekong River discharge [m³/s] at 105.25° E and 11.25° N in 2003 (blue line) provided by DÖLL et al. (2003).

In summary, the retention capacity of the floodplain, the retention capacity of the Tonle Sap Lake and the reversal of the flow in the rainy season towards the Tonle Sap Lake influence the peak discharge. As a consequence of these three factors the river discharge peak is broadened and retarded in nature. This yields an attenuation of the peak discharge which is overestimated

by the WGHM. Due to the differences in the river discharge data the calculated data has to be bias-corrected to approximate the observations.

The bias-correction is done as follows: In a first step the discharge of 2003 provided by the WGHM is averaged for each month over a period of two months (the previous month plus the actual month). In a second step to reduce the overestimation/underestimation in the discharge data during the different seasons and the annual overestimation of the amount, the two datasets are correlated and a linear regression analysis is conducted for the year 2003. A comparison between the bias-corrected river discharge and the observed discharge of the year 2003 shows a good agreement between the datasets (Figure 13**)**. Thus, this method is applied for the bias-correction of the discharge data for the simulation years 2004 to 2008. Considering the data of the year 2004 for validation, the bias-corrected river discharge agrees well with the observed river discharge (Figure 13**)** so that the bias-corrected values can be used to force the three-dimensional hydrodynamic model at the open boundary. Recently, river discharge data from observation is only available until the end of the year 2004.

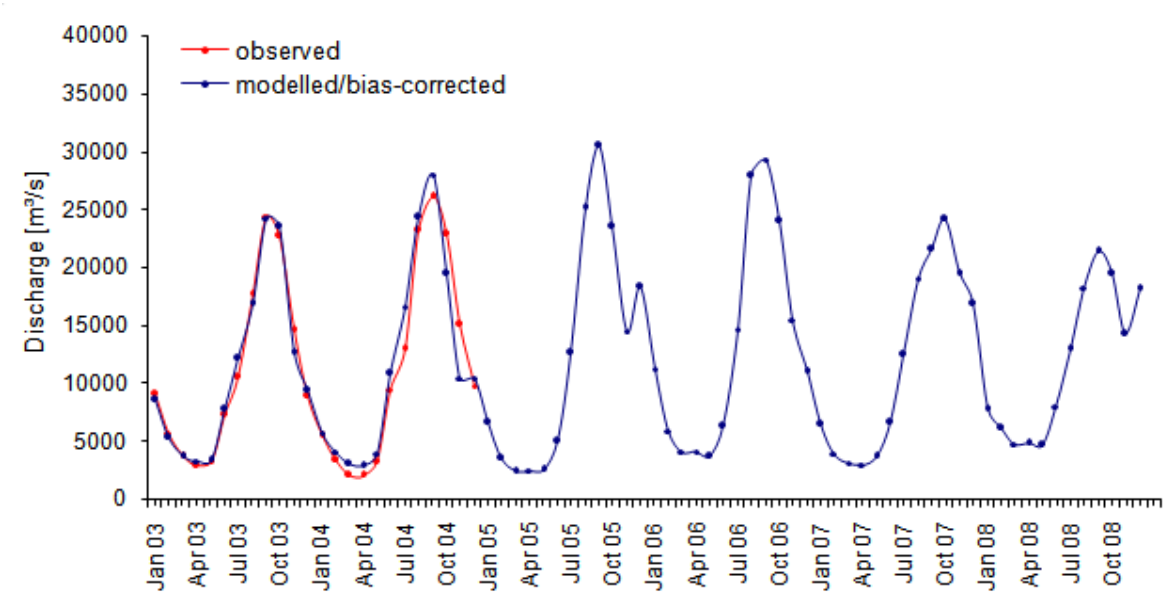

Figure 13: Observed Mekong River discharge [m³/s] from 2003 to 2005 (sum of Tan Chau and Chau Doc station - red line) (MRC, 2004) and bias-corrected Mekong River discharge [m³/s] at 105.25° E and 11.25° N from 2003 to 2008 (blue line) based on DÖLL et al. (2003).

4.5 VALIDATION OF HAMSOM

The overall goal of this study is to specify the main physical processes influencing stratification and destratification in the Mekong ROFI and their temporal and local variability. To accomplish this aim, it is a precondition that the circulation on the Sunda Shelf as driving mechanism for the Mekong River plume dispersion is reproduced well by the three-dimensional hydrodynamic model HAMSOM.

Different datasets are used to validate the modelled river discharge, sea surface heights, sea surface temperatures, salinities and tidal elevations:

For validating the river discharge (section 4.5.1), data were exacted from the lower Mekong hydrologic yearbooks 2003/3004 published by the Mekong River Commission. For the sea surface heights and the sea surface temperatures datasets which are based on satellite observations are used: on the one hand the absolute dynamic topography of Aviso France (http://las.aviso.oceanobs.com/las/getUI.do) (section 4.5.2) and on the other hand the sea surface temperature (SST) of the Modular Ocean Data Assimilation System (MODAS) (FOX et al., 2002; BARRON and KARA, 2006; KARA and BARRON, 2007) (section 4.5.3). In this way, it is possible to get a well-resolved picture of the whole model area.

As the main attention in this study is focused on the seasonal variation of the freshwater buoyancy input from the Mekong River and the related stratification and destratification processes, the key parameter that has to be analyzed is the salinity. At the moment no long-term dataset of salinity based on satellite observations is available. Therefore, the modelled salinity is validated with in-situ measurements conducted during two field studies, the first in April 2007 and the second in September 2008 (section 4.5.4). The in-situ measurements are only able to provide a very limited picture of the salinity distribution - locally and temporally. Nevertheless, unlike satellite observations it is a good bolt material that is able to show the salinity distribution over depth. In addition to the lateral buoyancy input, stirring and straining resulting from tidal currents are important processes in a ROFI.

Section (4.5.5) of this chapter presents a validation of the water level simulated by the hydrodynamic model. A time series of modelled sea surface elevations is compared with a time series of tidal elevations predicted by OTPS (http://volkov.oce.orst.edu/tides/region.html) to control the internal accuracy of the simulations with HAMSOM. These data have also been used to calculate the phases and amplitudes at the open boundaries. Secondly, as an independent dataset for the model validation, the times and heights of high and low waters determined from harmonic analysis of tidal observations are used. The data are provided by the software WXTide32 (http://www.wxtide32.com/index.html). As Vung Tau (10.333° N, 107.067° E) is a reference tide gauge in the vicinity of the Mekong River mouth, all three datasets were reproduced for this station.

4.5.1 VALIDATION – MEKONG RIVER DISCHARGE

HAMSOM is a hydrodynamic shelf-ocean model. Here, it is used to simulate not only the dynamical processes in the Mekong ROFI but also the hydrodynamics of the different Mekong River branches themselves.

Figure 14 shows a comparison between the observed Mekong River discharge, which had been provided by the Mekong River Commission, and the calculated river discharge by HAMSOM

for the year 2004 at Can Tho (Bassac) and My Thuan (Mekong River). For the year 2004, the data from observations illustrate that the discharge decreases from January until April. Then in April river discharge starts to increase and peak discharge is reached in September. From September until the end of the year the river discharge is declining again. The simulated discharge curve represents the seasonal cycle adequately. Nevertheless, during the period of low river discharge, the river discharge is slightly overestimated by the model. During the high discharge season, the declining of discharge is slightly overestimated by the model, i.e., the discharge is marginally underestimated. The discrepancy in discharge may be related to the fact that the retention capacity of the complex delta system is underestimated by the model like it has been mentioned in section 4.3.

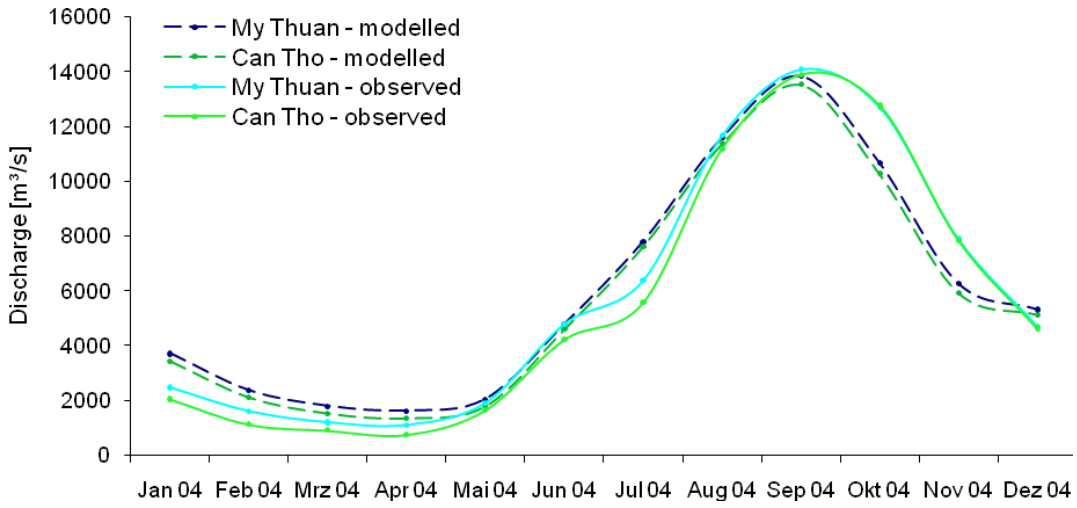

Figure 14: Modelled Mekong River discharge [m³/s] at My Thuan (dashed dark blue line) and Can Tho (dashed dark green line) for the year 2004 and observed Mekong River discharge [m³/s] at My Thuan (solid light blue line) and Can Tho (solid light green line) in 2004 provided by the Mekong River Commission.

Figure 15 depicts the discharge ratio between the Mekong River and the Bassac at My Thuan and Can Tho, respectively. The discharge ratio between the Mekong River and the Bassac based on the observations shows a slightly larger inequality during the months of low river discharge than during the months of high river discharge. During the months of high river discharge the ratio is nearly equalized (i.e., 50 %). The discharge ratios calculated from the simulation results are analogous to the discharge ratio based on observations.

The annual averaged discharge ratio from observations between the Mekong River and the Bassac lies at 53 % to 47 %, whereby the annual averaged simulated discharge ratio is 52 % to 48 %.

Together, these results verify that HAMSOM is able to simulate the river discharge in the estuary and that further investigations based on the freshwater buoyancy input from the Mekong

River can be made.

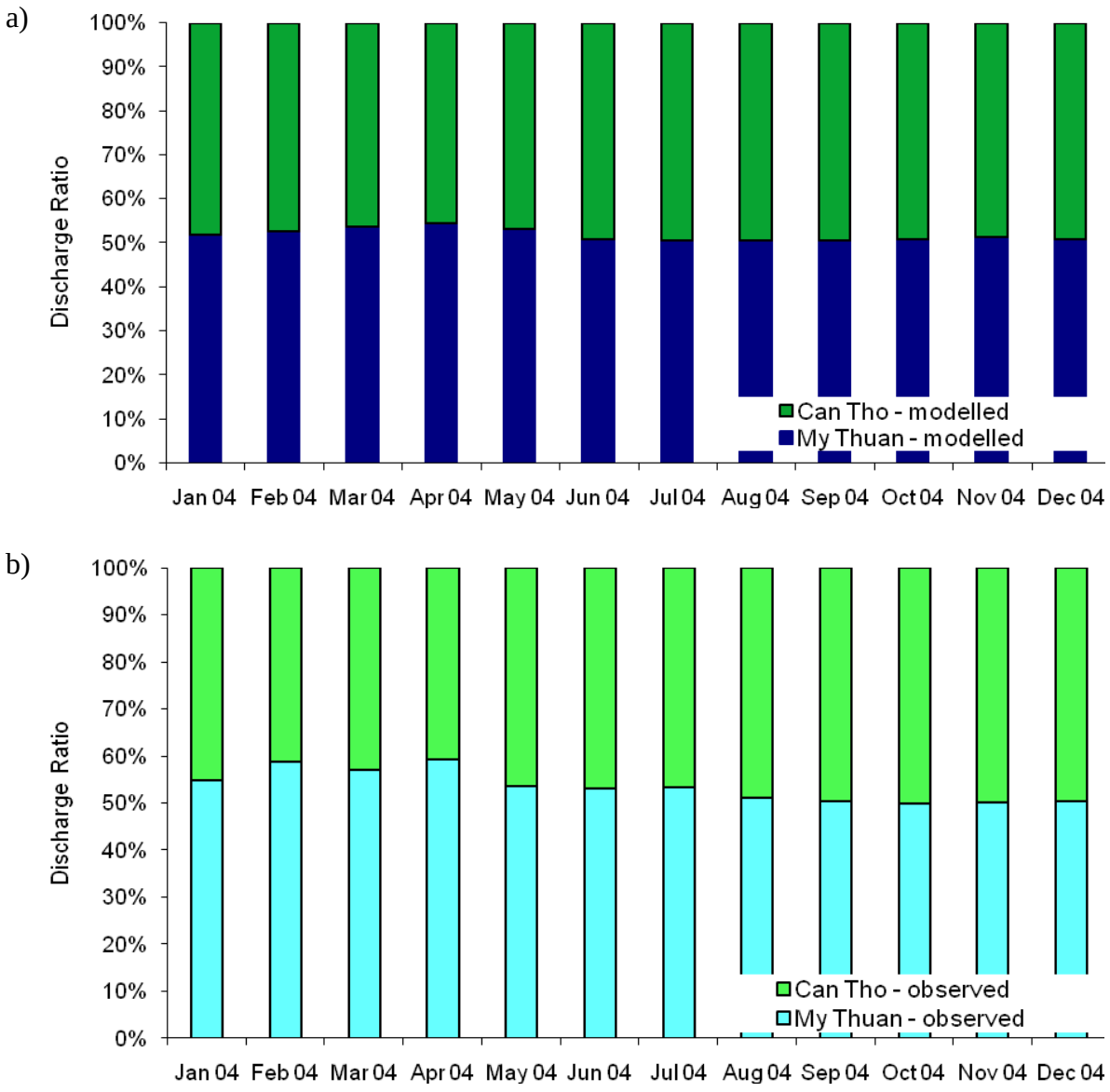

Figure 15: a) Modelled discharge ratio [%] of My Thuan (dark blue) to Can Tho (dark green) for the year 2004 and b) observed discharge ratio [%] of My Thuan (light blue) to Can Tho (light green) in 2004 based on the data provided by the Mekong River Commission.

4.5.2 VALIDATION – DYNAMIC TOPOGRAPHY

The altimeter products used here were produced by SSALTO/DUACS (Segment Sol multimissions d'ALTimétrie, d'Orbitographie et de localisation précise/Data Unification and Altimeter Combination System) and distributed by AVISO (Archiving, Validation and Interpretation of Satellite Oceanographic data), with support from CNES (Centre National d'Etudes Spatiales). The satellite altimetry data are derived from Topex/Poseidon, Jason-1,

ERS-1/2, GFO and EnviSat. This dataset has been widely used to study the general circulation of the oceans (e.g., LIHAN et al., 2008; WU and CHIANG, 2007; RONG et al., 2007). The spatial resolution of the dataset is 1/3° and the temporal resolution is seven days.

The absolute dynamic topography is a result of the mean dynamic topography, i.e., the mean sea surface height, plus the sea level anomaly, i.e., the variation of the sea surface height. Altogether they represent the ocean sea surface heights (SSHs). More detailed information on the dataset can be found in the user handbook of SSALTO/DUACS (DIBARBOURE et al., 2008).

In the following the altimeter data is compared with SSHs calculated by HAMSOM. Firstly, a time series from 01/2004 until 12/2008 at four different stations in the Mekong ROFI is presented. Secondly, the whole model area for a period during August 2006 (SW monsoon) and for a period during January 2007 (NE monsoon) is depicted. In the following, these two periods are utilized for further investigations on the seasonal and intra-seasonal variability of the physical processes in the Mekong ROFI.

Figure 16 shows a time series (01/2004–12/2008) of modelled SSHs and measured dynamic topography at different stations in the Mekong ROFI. The datasets were normalized with the time average. Overall, it can be noted that the datasets agree well for the simulation period. The intra-annual variability, i.e., the higher sea level in winter and the lower sea level in summer, is represented adequately by the hydrodynamic model. However, the annual amplitude of the sea surface heights is underestimated by HAMSOM.

A more sophisticated picture is given by comparing the comprehensive distribution of the sea surface heights. The SSHs are shown as an average over one month during high river discharge (August) in 2006 (Figure 17) and low river discharge (January) in 2007 (Figure 18). The datasets were normalized with the area average.

In general there is good agreement between the pattern of the modelled and measured sea surface heights. The general seasonal characteristics of the area are represented well by HAMSOM:

The picture of the measured SSHs of August 2006 (Figure 17b) shows a typical situation for the upwelling favourable summer monsoon. The sea surface heights at the coast are decreased. In direction to the SE in the open sea the sea surface heights are raised. These two characteristics indicate the anticyclonic circulation which is typical during the SW monsoon in the southern SCS (HU et al., 2000). These features can also be denoted in the figure of the modelled sea surface heights (Figure 17a). However, the anticyclonic eddy in the SE and the cyclonic eddy in the NE of the area are represented stronger by the model results. Another difference in the SSHs can be observed in the Gulf of Thailand. There, the modelled SSHs overestimate the measured SSHs. The monsoon related wind surge does not occur in the altimeter data.

In January 2007, the situation is different compared to the situation of August 2006: the sea surface in the Mekong ROFI is observed to be elevated, whereas the sea surface heights in direction to the eastern open boundary are decreased (Figure 18b). The modelled SSHs represent

these characteristics indicating a typical cyclonic winter circulation in the southern SCS which is also mentioned by HU et al. (2000). Both simulations and observations show two cyclonic eddies off the shelf break (Figure 18a and b). Nevertheless, the simulated SSHs depict a stronger cyclonic eddy in the SE of the region than the satellite data. In between these two cyclonic eddies the modelled SSHs are elevated compared to the SSHs from satellite data. Furthermore again, there is a difference in the Gulf of Thailand between the modelled and measured SSHs. However, in this region the decreased values in HAMSOM seem reasonable taking into account the offshore drift current at the sea surface due to the north-easterly winds during the winter monsoon.

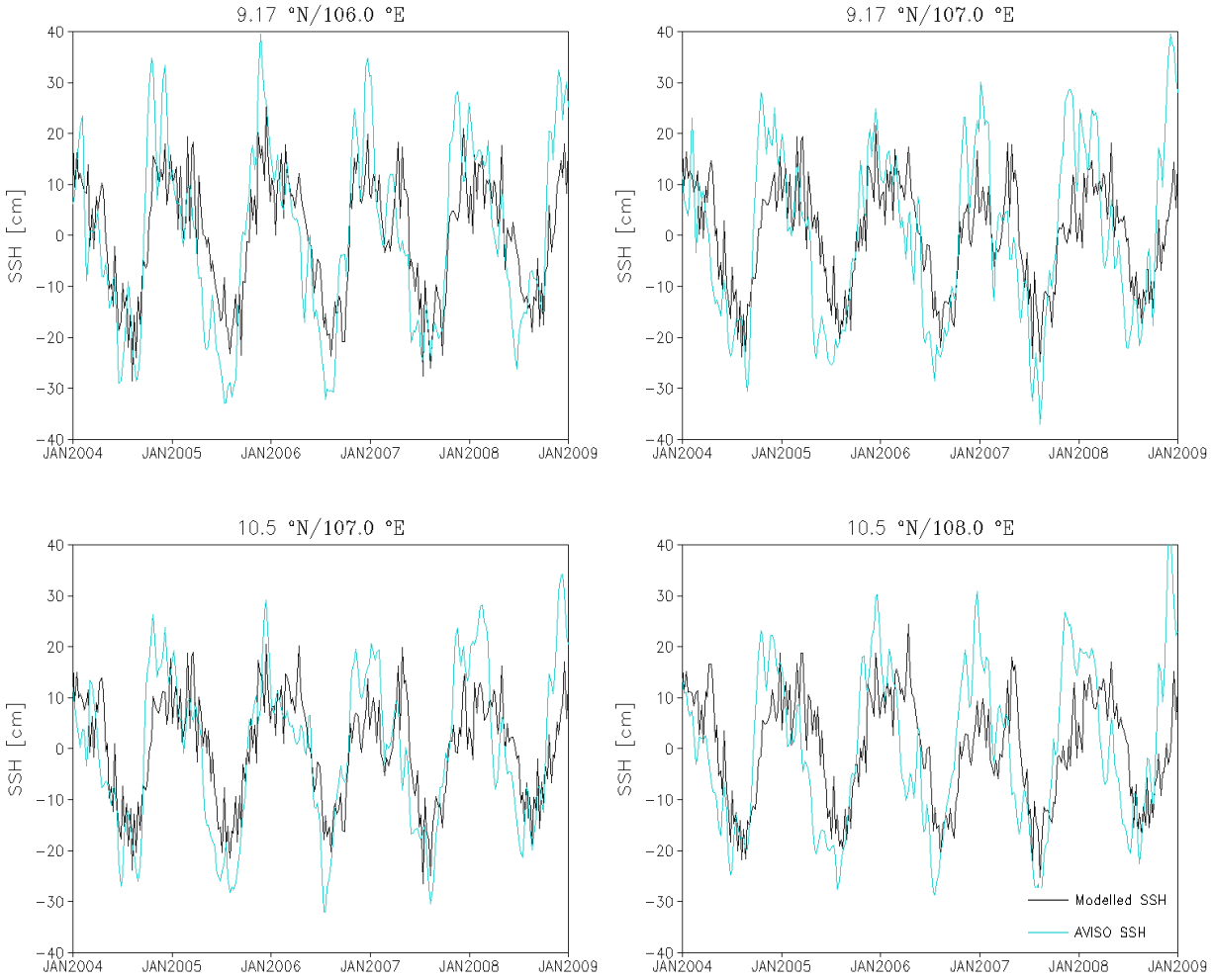

Figure 16: Time series (07/01/2004–24/12/2008) of modelled SSHs [cm] normalized with the time average (black line) and of the Absolute Dynamic Topography [cm] distributed by AVISO (light blue line) also normalized with the time average at four different stations in the Mekong ROFI.

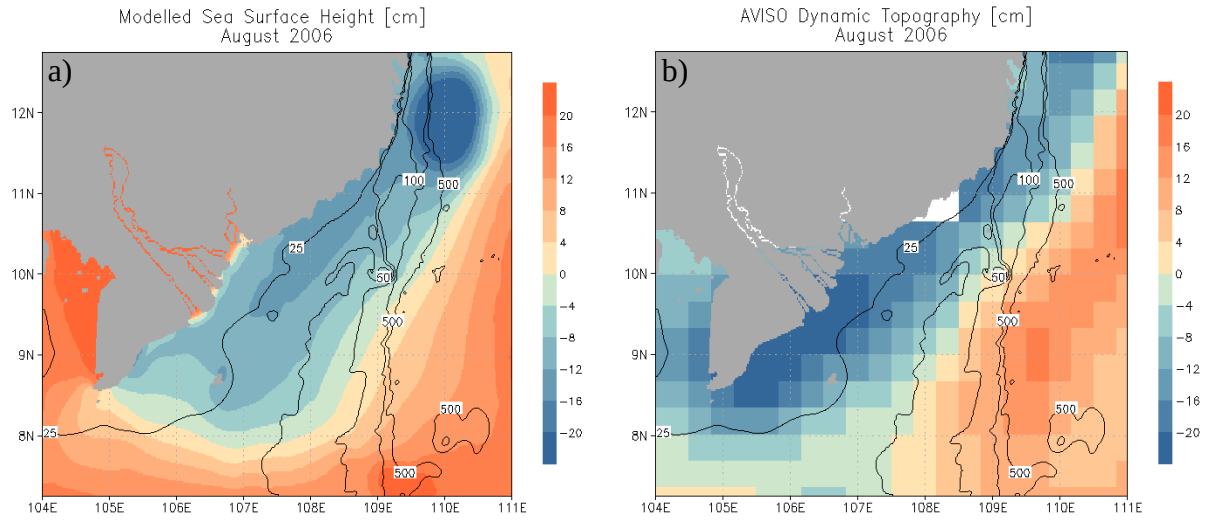

Figure 17: a) Modelled Sea Surface Heights (time average between 06/08/2006 and 11/08/2006) [cm] normalized with the area average and b) Absolute Dynamic Topography [cm] on 09/08/2006 distributed by AVISO also normalized with the area average.

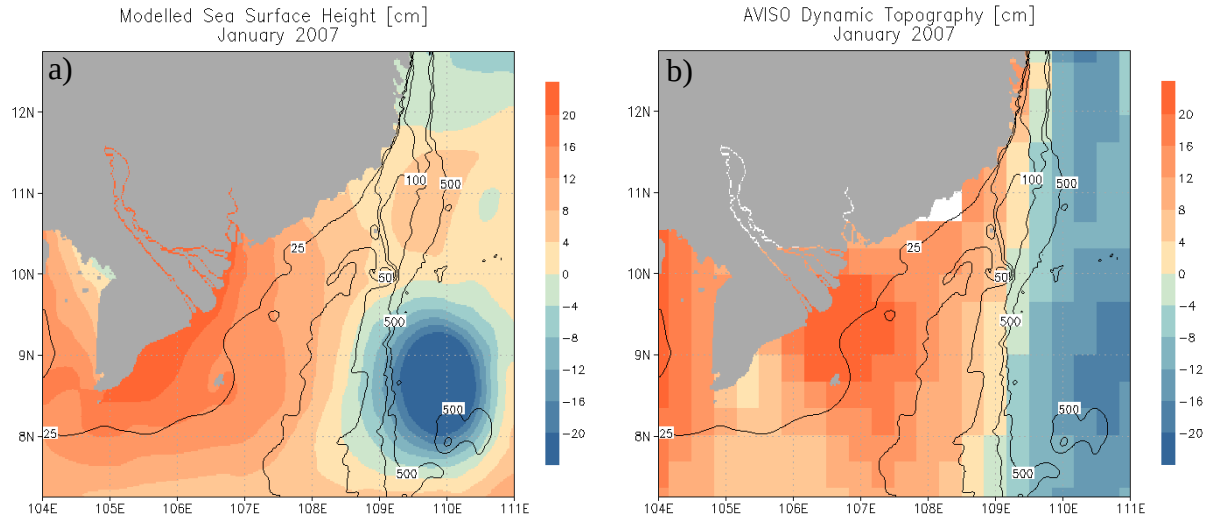

Figure 18: a) Modelled Sea Surface Heights (time average between 07/01/2007 and 12/01/2007) [cm] normalized with the area average and b) Absolute Dynamic Topography [cm] on 10/01/2007 distributed by AVISO also normalized with the area average.

Together, regarding Figure 16 to Figure 18 three differences between the model results and the satellite data have been detected:

1) the underestimation of the annual amplitude of the sea surface heights (Figure 16)
2) the differences in the SSHs in the Gulf of Thailand (Figure 17 and Figure 18)
3) the difference in the SSHs in between the two cyclonic eddies during the winter monsoon (Figure 18)

A possible explanation for the underestimation of the annual amplitude of the modelled sea surface heights is the low resolution of the forcing data which yields a smoothing of the extreme values. On the one hand, for determining the baroclinic component of the SSH, data of water temperature and salinity with low temporal resolution (climatological monthly means) have been applied at the open boundaries. On the other hand, the NCEP/NCAR reanalysis data which are used to calculate the heat fluxes and particularly the wind stresses in the investigation area have a rather low spatial resolution. Another possible explanation is that in the nearshore region (25–50 km) there exist no reliable estimates of SSH from altimeter data which is on the one hand due to the difficulties in the correction of the nearshore data (e.g., wet tropospheric component, tidal corrections). On the other hand, only a marginal resolution to represent the complex structures of the coastal region is provided due to the interpolation of the along-track data collected by the satellite. Mostly, in the gridded AVISO field the problem in the nearshore region is dealt with extrapolation of the data to the coast (SARACENO et al., 2008). The latter could also be an explanation for the difference in the SSHs in the Gulf of Thailand like it is visible on Figure 17b and Figure 18b. In contrast, the difference in the SSHs in between the two cyclonic eddies during the winter monsoon (Figure 18) might be explained by the interpolation of the along-track data collected by the satellite.

Although some model deficiencies could be detected, during both seasons the fundamental SSH pattern is reproduced adequately by the model. The gradient of the modelled SSH throughout the model area fits well with the gradient of the observed SSH. Hence, the seasonal signal of the geostrophic current is represented correctly by the model.

4.5.3 VALIDATION – TEMPERATURE

Global fields of sea surface temperature (SST) are produced by the Modular Ocean Data Assimilation System (MODAS) developed by the Naval Research Laboratory. Spatial resolution of MODAS SST is 1/8°, temporal resolution is one day. Conditions in the upper few meters of the ocean are represented by the dataset.

MODAS SST is produced on the basis of Advanced Very-High Resolution Radiometer (AVHRR) nonlinear SST observations. A combination of optimal interpolation and climatologically corrected persistence is used to transform the observations in a regular gridded product and to adjust the irregular and cloud obscured AVHRR SST data. The base data is achieved by the NOAA TIROS-N series satellites, from NOAA-11 to NOAA-18. More detailed information can be found by FOX et al. (2002), BARRON and KARA (2006) and KARA and BARRON (2007).

In the following the MODAS SST is related to the water temperature in the surface layer calculated by HAMSOM. Throughout this study to simplify matters, the modelled water temperature of the surface layer is named SST. On the one hand, time series from 01/2004 until 12/2008 for different stations in the Mekong ROFI are presented (Figure 19). On the other hand,

the five-year averages of the monthly mean temperature fields of August and of January are illustrated (Figure 21 and Figure 22).

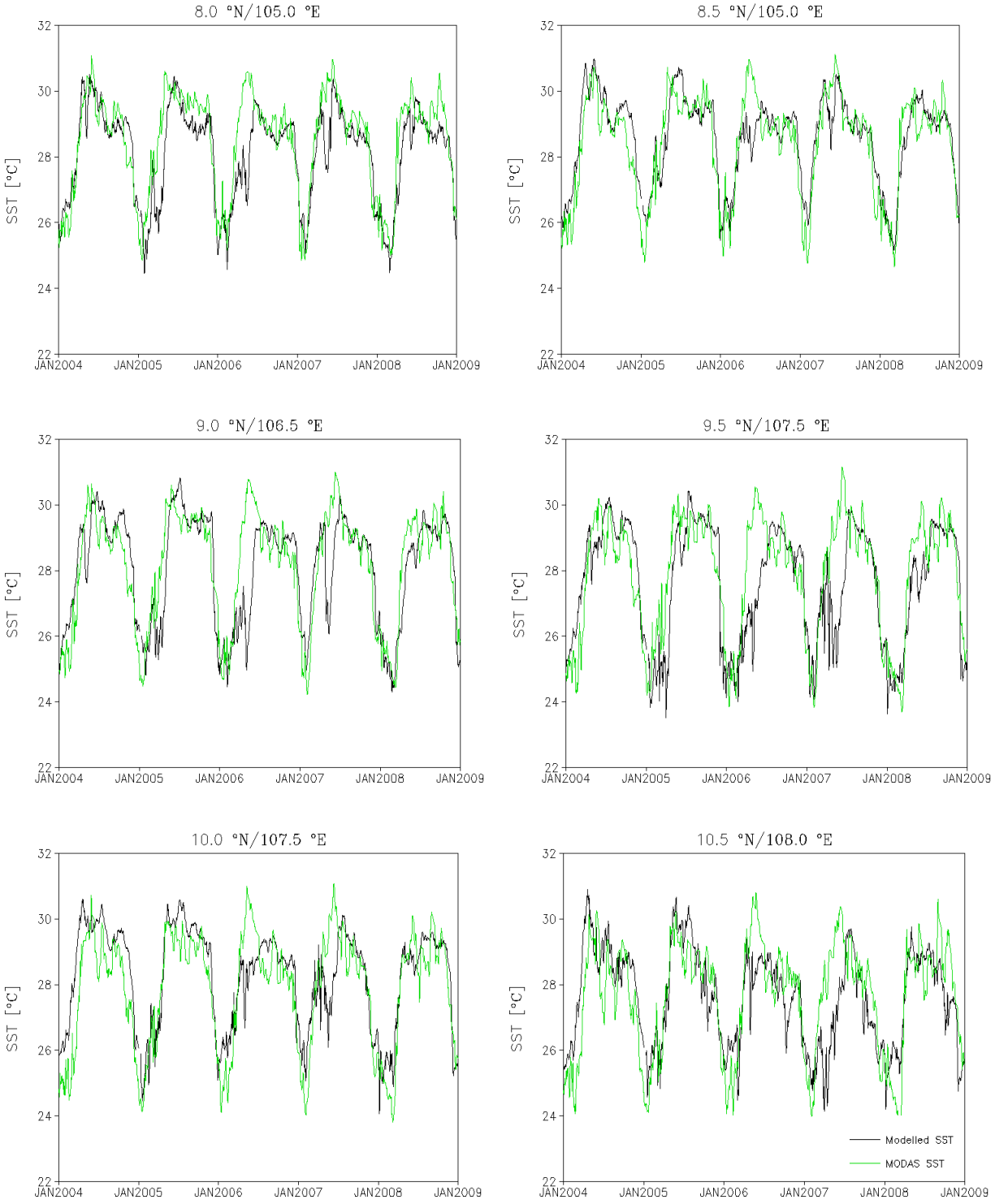

Figure 19: Time series (01/01/2004–31/12/2008) of modelled SSTs [°C] (black line) and MODAS SSTs [°C] (green line) at six different stations in the Mekong ROFI.

Referring to Figure 19 the surface water temperature calculated by HAMSOM for the years 2004 to 2008 shows a good agreement with the observed SSTs. The general seasonal variability of the SSTs can be depicted in both datasets. However, there is a difference between modelled and observed SSTs in spring when a warming of the SCS takes place (CHU and CHANG, 1997). The difference is rather high for the spring season of the years 2006 and 2007. In the other years the warming is reproduced well by the model. Although a sea surface heating of the SCS is represented in the modelled surface temperatures for the years 2006 and 2007, compared to the observed SSTs the modelled values are too low during spring. During the warming period in the modelled SSTs a strong decrease of the values can be observed. In summer the SSTs show comparable values.

An explanation can be found in CHU et al. (1997). They used the SST data of the US Navy's Master Oceanographic Observation Data Set (MOODS) to investigate the cooling and warming phases of the SCS. To represent the different phases they established an ensemble mean SST field (1963–1984) and an averaged SST anomaly field. From April to May they detected a warm pool in the central SCS (116–118° E, 16–18° N). According to the authors the existence of the warm pool might be explained by the bowl-type bottom topography and an anticyclonic wind stress curl over the central SCS. This forces a warm-core anticyclonic eddy with downwelling occurring in the central part and upwelling at the boundaries of the anticyclone.

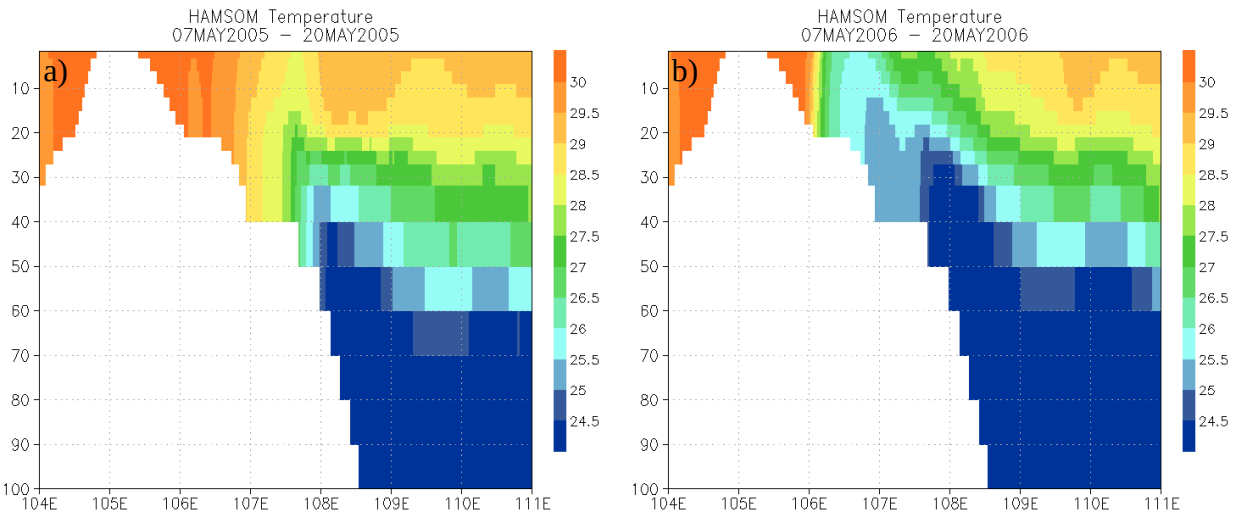

Figure 20: Cross-section of modelled temperature [°C] at 9° N a) averaged from 07/05/2005 to 20/05/2005 and b) averaged from 07/05/2006 to 20/05/2006.

All stations presented in Figure 19 are situated at the western boundary of the bowl where the boundary current forces upwelling at the shelf edge in April and May. This upwelling has been documented by ship experiments during April 2006 (e.g., WIESNER and PARTICIPANTS, 2006). When regarding a cross-section of a 14-days averaged modelled temperature distribution at 9° N for the years 2005 and 2006 (Figure 20), it is obvious that the isotherms show the typical

structure for upwelling at the shelf edge. In the region of the above shown station (9.0° N/106.5° E) during both years the water column is mixed. However, the temperature of the water column is strongly decreased in 2006.

These characteristics suggest that the upwelled water reaches the sea surface and counteracts the surface warming of the SCS. The mechanism is obviously stronger in 2006 compared to 2005. This explains the higher difference in temperature in spring 2006 that is apparent in Figure 19. The reason why the modelled upwelling is stronger in 2006 than in 2005 lies behind the scope of this study. Considering the MODAS SST of the different stations in Figure 19 cold water is not detectable at the sea surface.

In general, taking the ship experiments by WIESNER and PARTICIPANTS (2006) into account, the fact that upwelling occurs is represented well by the model results but it is developed too strong. As the subsequent model studies are performed before and after the warming phase of the SCS, there is no need for further investigations on this feature. With the exception of the warming phase, modelled surface temperatures and satellite SSTs agree well.

To get a more comprehensive picture, the SST distribution of the whole model area is illustrated in Figure 21 and Figure 22. These figures show the five-year average (2004–2008) of the temperature distribution in August (high river discharge) and in January (low river discharge).

Comparing the modelled temperature of the first layer with the MODAS SST, the general pattern is reflected reasonably well by the model (Figure 21). However, in comparison with the observed SSTs the modelled SSTs are colder in the NE of the model domain. As mentioned before, upwelling in this region may influence model SSTs. WANG and WANG (2006) and XIE et al. (2003) described a decrease in SSTs for the Southern SCS as a consequence of coastal upwelling off the Vietnamese coast after the onset of SW monsoon. Also CHAO et al. (1996b) and CHAO et al. (1996a) reported upwelling NE of Vietnam in the Southern SCS in summer. Upwelling detected in AVHRR data in this region is presented by KUO et al. (2000, 2004). Again, upwelling seems to be too strong in the simulation results, but in accordance with the above mentioned studies also an underestimation of the SSTs in the MODAS dataset may be possible.

Also Figure 22, which illustrates the averaged modelled and observed SSTs in January, shows that the large scale pattern of both datasets are in a good agreement. However, the modelled SSTs underestimate the observed SSTs in the SE of the model region. In the shallow water region the modelled SSTs overestimate the observed SSTs.

The extension of the area where the modelled SSTs underestimate the observed SSTs agree well with the extension of the measured cyclonic eddies shown in Figure 18b. CHAO et al. (1996b) and CHAO et al. (1996a) documented upwelling SE of Vietnam in winter at the edge of the Sunda Shelf break.

The other feature that is represented by the simulation results of HAMSOM but not by the observed SSTs is the process of differential heating around Zhongnan Peninsula, i.e., water in

shallow regions heats more rapidly than that in deeper regions. It should be noted that the satellite data used here close to the coast and in cloudy regions have an explainable greater uncertainty. However, it cannot be excluded that the assignment of values to the model parameters for calculating the surface heat fluxes results in a too strong warming in the shallow water.

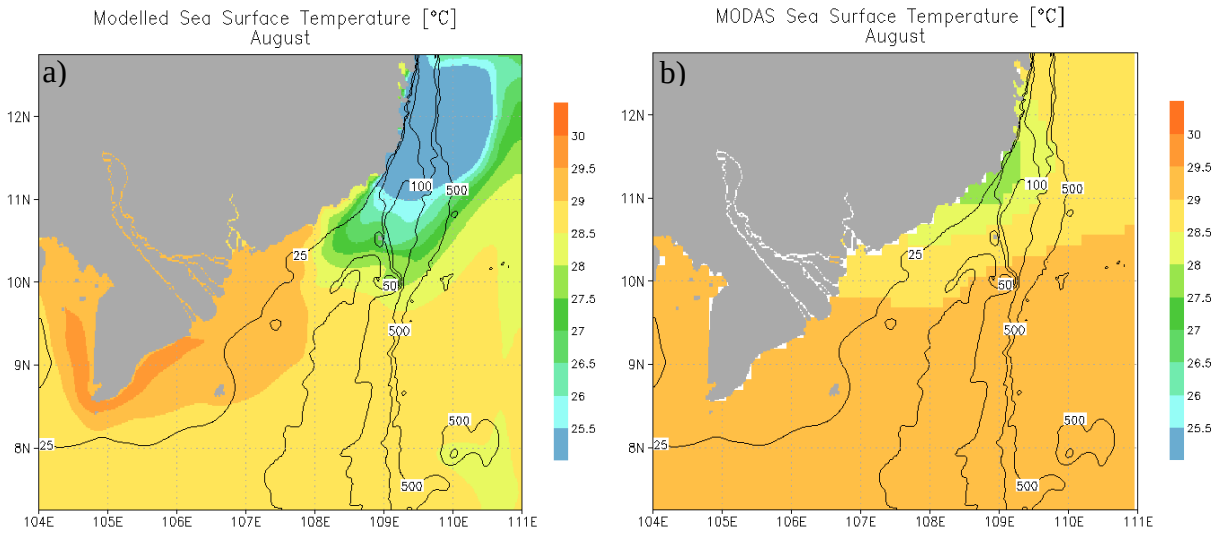

Figure 21: A five-year average of the temperature fields in August (2004–2008) a) modelled SSTs [°C] and b) MODAS SSTs [°C].

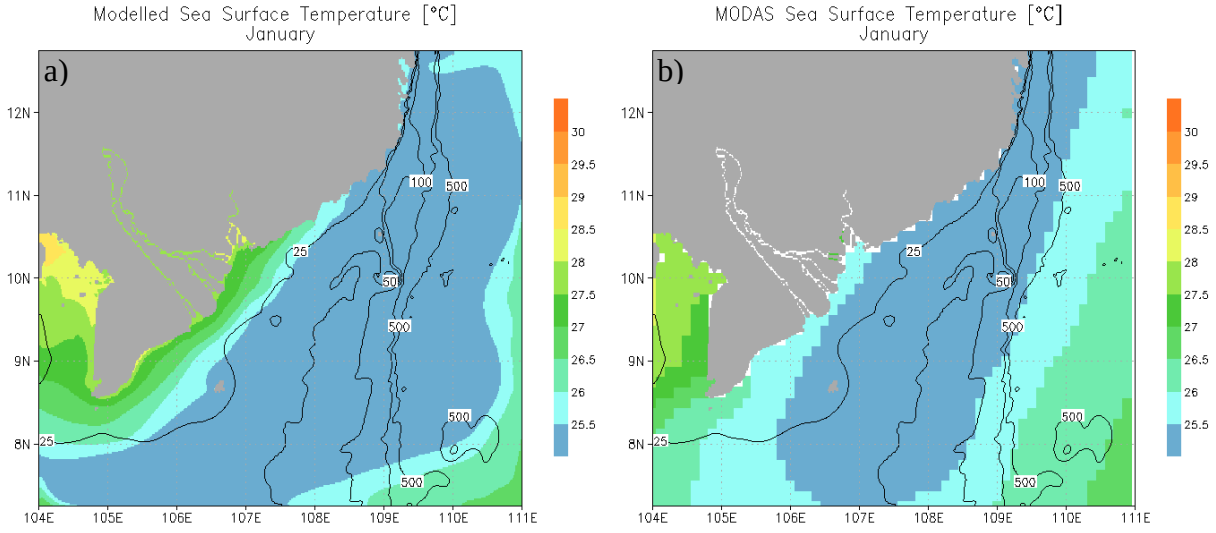

Figure 22: A five-year average of the temperature fields in January (2004–2008) a) modelled SSTs [°C] and b) MODAS SSTs [°C].

An enduring challenge is the rather sparse resolution of the forcing and boundary data which inevitably lead to inaccuracies in the model results. At the open boundaries climatological

monthly means of water temperature (and salinity) have been used. Moreover, the spatial resolution of the NCEP/NCAR reanalysis data which is used to calculate the heat fluxes and the wind stresses in the investigation area is rather low.

The pattern of the modelled temperature fits quite well with the pattern of the MODAS data. Although upwelling seems to be overestimated by the model, there exists an excellent long-term stability of the surface temperature over several years.

4.5.4 VALIDATION – SALINITY

A primary aim of this study is to focus on the seasonal variability of buoyancy input from the Mekong River and the related baroclinic circulation in the Mekong ROFI. Thus, the key parameter to be analyzed is the salinity distribution in the area. In the following, salinity profiles accomplished during various research cruises are used to validate the modelled salinity.

To represent the different meteorological conditions and the varying hydrological situation of the Mekong River, two field studies with ship experiments were conducted in different seasons. The first field study took place during the period of minimum river discharge in April 2007. The second field trip was carried out in the period of maximum river discharge in September 2008. The circulation during the cruises is representative of the characteristic circulation during winter and summer, respectively.

A binational research team consisting of various scientists from the Institute of Oceanography, Nha Trang, Vietnam, and from the Institute of Oceanography, Hamburg, Germany, collected CTD (SBE19+) profiles of salinity, temperature and turbidity in the Mekong ROFI and the adjacent SCS. Current velocity profiles were measured with an ADCP (Workhorse Sentinel). Additionally, during both field studies suspended sediment concentrations were recorded by the LISST 100X (Sequoia) instrument. In-situ measurements of chlorophyll a concentration by the Seapoint Chlorophyll Fluorometer were realized only during the field study in September 2008. Overall, the hydrographic situation in the Mekong ROFI and the adjacent SCS has been recorded.

The first field study was conducted from 14/04/2007 until 20/04/2007. Three transects perpendicular to the coast and two mooring stations (one over a period of 25 h and the other over a period of 8 h) were accomplished. The measurements on the three transects were taken with a station distance of three minutes in the vicinity of the Mekong River and with a distance of five minutes in the shelf region (Figure 23). To represent the hydrographic situation in the Mekong ROFI throughout a complete tidal cycle, a 25 h mooring station was positioned at 09.26° N and 106.31° E. CTD measurements were carried out every hour and the ADCP was deployed over the whole time period. At the 8 h mooring station (10.2° N, 106.74° E) CTD measurements were acquired at a time span varying between one and two hours. The ADCP was lowered only for the first six hours.

The second field study took place from 17/09/2008 until 22/09/2008. Altogether, six transects representing the whole extension of the Mekong ROFI during the summer monsoon and a 25 h mooring station were performed. The station distance on each transect was about 3 to 5 minutes (Figure 23). The mooring station was located in the proximity of the mooring station of April 2007 (09.24° N and 106.31° E). During the day CTD measurements at the mooring station were carried out every hour in case that it was possible because of the rough weather. During the night because of the rough weather no CTD measurements were conducted. The ADCP was deployed over the whole time span for 25 h.

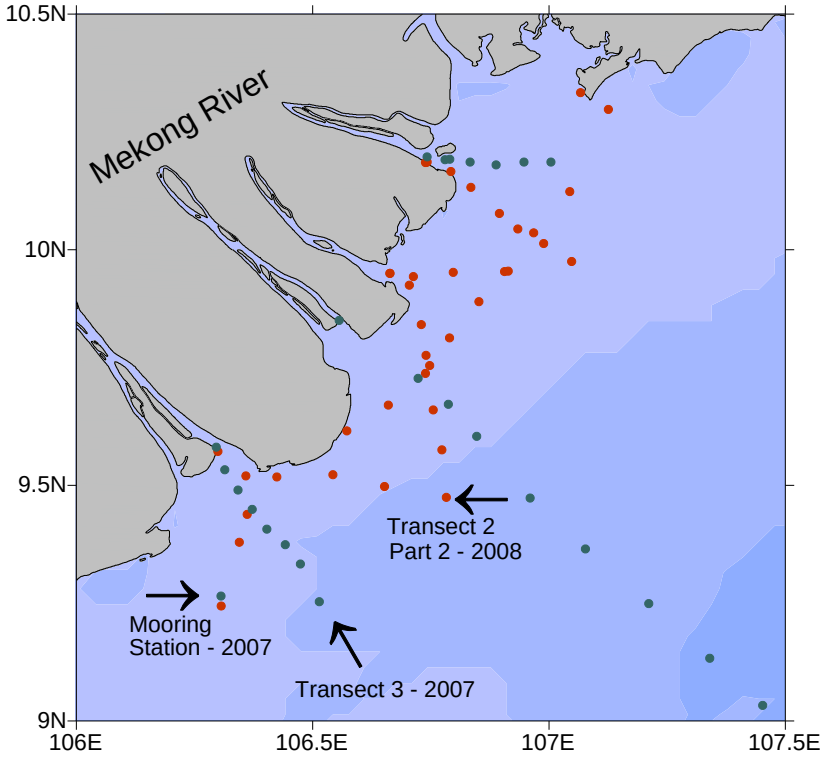

Figure 23: Stations of the field studies in the Mekong ROFI during April 2007 (green dots) and during September 2008 (red dots). The data of the marked transects and of the mooring station is shown in the following.

LOW-FLOW SEASON – APRIL 2007

In the following, the modelled salinity distribution is compared with the measured salinity profiles at transect three and with the measured salinity profiles of the moored station. In addition, a comprehensive picture over the whole investigation area of April 2007 is depicted.

Figure 24b shows the comprehensive picture of the measurements conducted during the cruise in April 2007. A horizontal salinity gradient is clearly visible in the figure. The extension of the river plume is restricted to the area close to the mouths of the Mekong River. The figure of the modelled salinity (Figure 24a) shows that HAMSOM is able to represent the horizontal salinity gradients.

Considering Figure 25b which represents a transect perpendicular to the coast, a horizontal gradient with low salinity water at the mouth of the Mekong River (< 15 psu) to high salinity water further offshore (> 32.5 psu) can be observed. At the station close to the mouth of the Mekong River, the water column is stratified. The adjacent shallow water stations are characterized by a horizontal change in salinity, which defines a frontal zone. The offshore stations illustrate the transition to high salinity Open Sea Water (ROJANA-ANAWAT et al., 2001). These characteristics can also be seen in Figure 25a, which shows the cross-section of the modelled salinity.

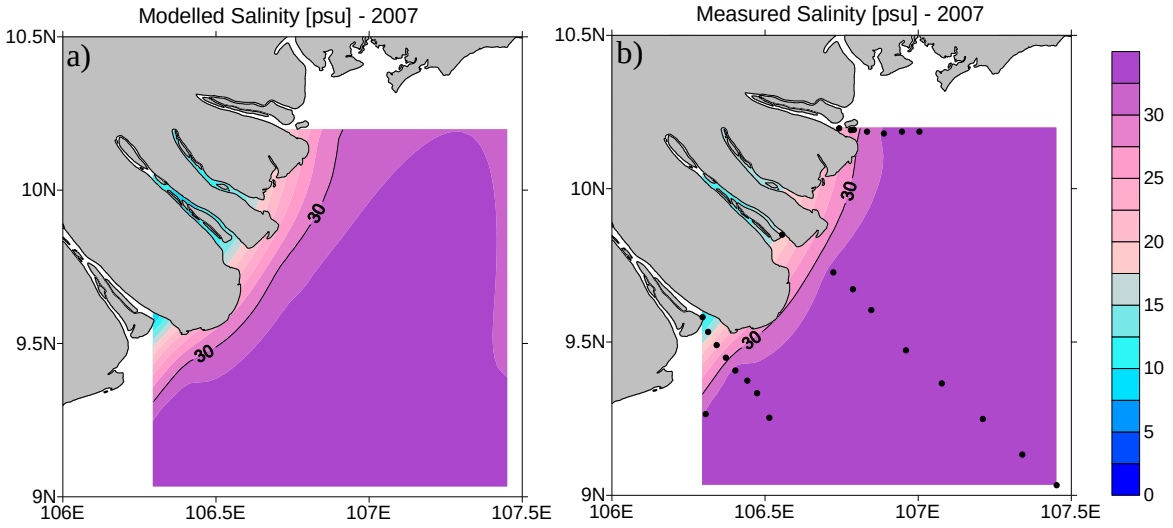

Figure 24: a) Averaged modelled salinity [psu] from 15/04/2007 00:00 to 21/04/2007 00:00 and b) comprehensive picture of measured salinity [psu] throughout the whole research area from 15/04/2007 10:00 to 20/04/2007 01:30. The 30 psu isohaline and the position of the stations are marked.

At the mooring station the measured salinity values range between 30 psu and 33.5 psu (Figure 26b). The highest salinity value is reached around high water at the bottom of the water column whereas the lowest salinity value is found at the surface two hours before second high water. Throughout the entire tidal cycle the salinity profile of the water column is highly variable, i.e., there is an oscillation in stratification. Thus, depending on the tidal cycle the water column is either stratified or entirely mixed.

At low water the salinity profile of the water column is almost homogenous, i.e., the water column is mixed. During flood tide processes that stratify the water column are dominant. At high water the water column is strongly stratified and is characterized by a steep vertical salinity gradient near the sea surface. After high water the destratification process starts and proceeds during ebb tide, so that at low water the water column is mixed again. During second flood tide a strongly stratified low salinity surface plume was observed.

From the observations it is impossible to determine if during the tidal cycle either local (de)stratification takes place or if just advective processes yield the change in stratification.

However, the single plume of low salinity during second flood tide is an effect of horizontal advective processes.

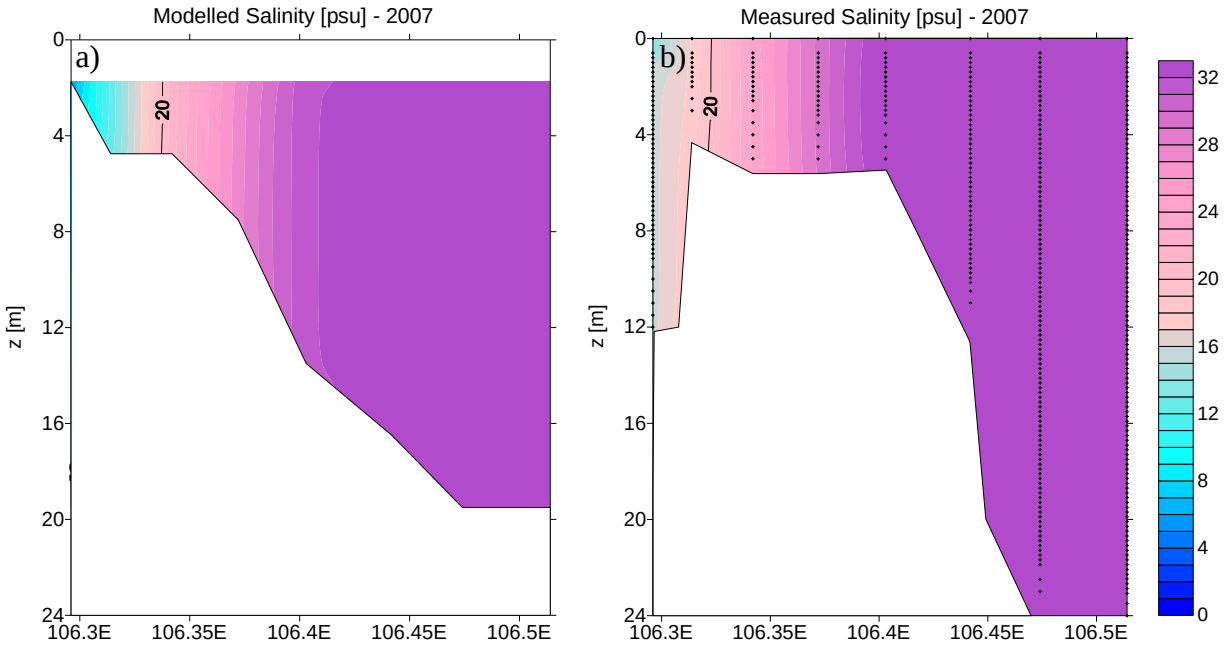

Figure 25: Cross section at transect 3 of a) averaged modelled salinity [psu] from 16/04/2007 00:00 to 17/04/2007 00:00 and b) measured salinity [psu] between 16/04/2007 04:00 and 16/04/2007 11:30. The 20 psu isohaline and the position of the CTD casts are marked.

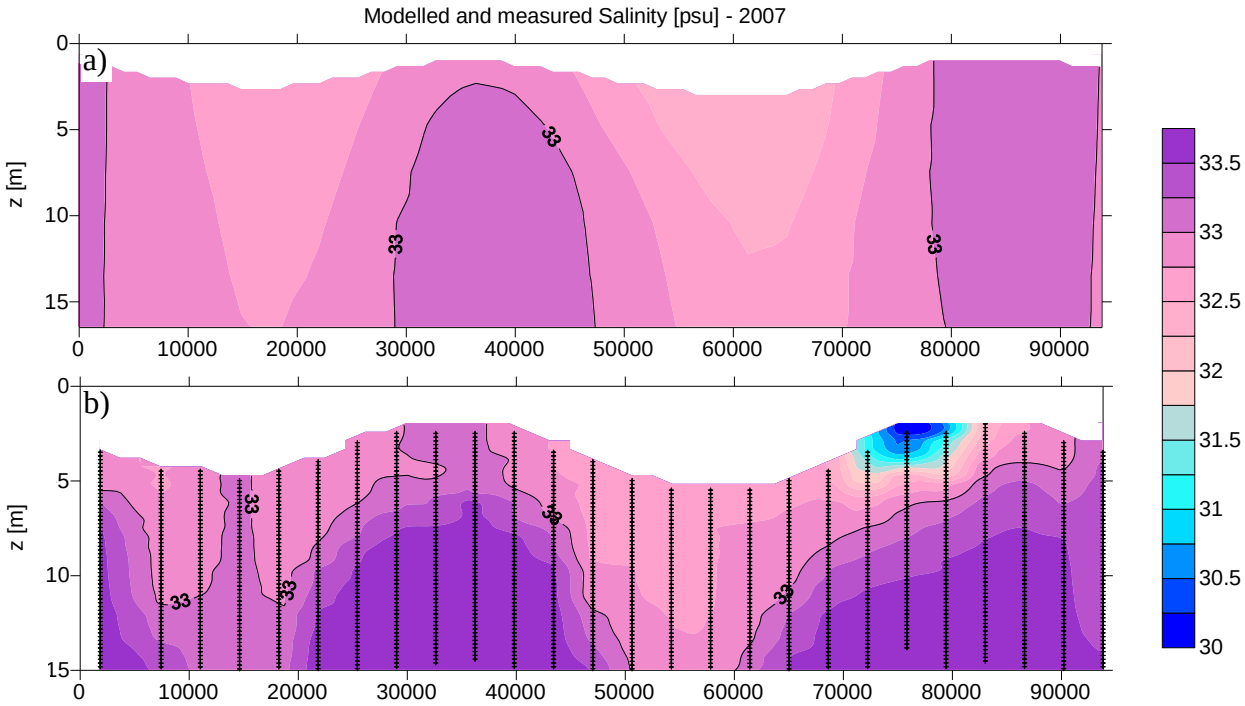

Figure 26: Time series between 17/04/2007 22:00 and 19/04/2007 00:00 [s] at 09.26° N and 106.31° E of a) modelled salinity [psu] and b) measured salinity [psu]. The position of the CTD casts is marked. Scale is different.

Regarding modelled salinity, the above described characteristics are well represented. The model is able to represent the (de)stratification of the water column throughout a tidal cycle. However, the very localized low salinity surface plume which has been observed during second flood tide cannot be found in the model results. As the resolution of the model is 1/60°, such small scale processes cannot be resolved explicitly. However, in HAMSOM sub-scale processes are treated as turbulence with a Smagorinsky scheme and the mean distributions can be represented well. Single processes are of chaotic nature and cannot be modelled deterministically

HIGH-FLOW SEASON – SEPTEMBER 2008

A comprehensive picture of the measurements conducted during the cruise in September 2008 is shown in Figure 27b. As opposed to Figure 24b, the individual plumes of the different river branches are more pronounced. The salinity in the vicinity of the Mekong River mouths is < 2.5 psu whereas in April the lowest salinity is around 15 psu. A horizontal salinity gradient is still apparent. The river plume in September extends further offshore than in April. The modelled salinity distribution (Figure 27a) shows that HAMSOM is able to represent the horizontal salinity gradients. However, the constraints of the model are sketched. Also, a less diffusive, second order advection scheme has been implemented into HAMSOM, artificial diffusion seems to be apparent. The result is a widening of the frontal zone as shown in Figure 27a. Furthermore, the measurements represent a random picture of a highly dynamic system in space and time. A hydrodynamic model is commonly not able to reproduce fluctuations of chaotic nature and small scale processes.

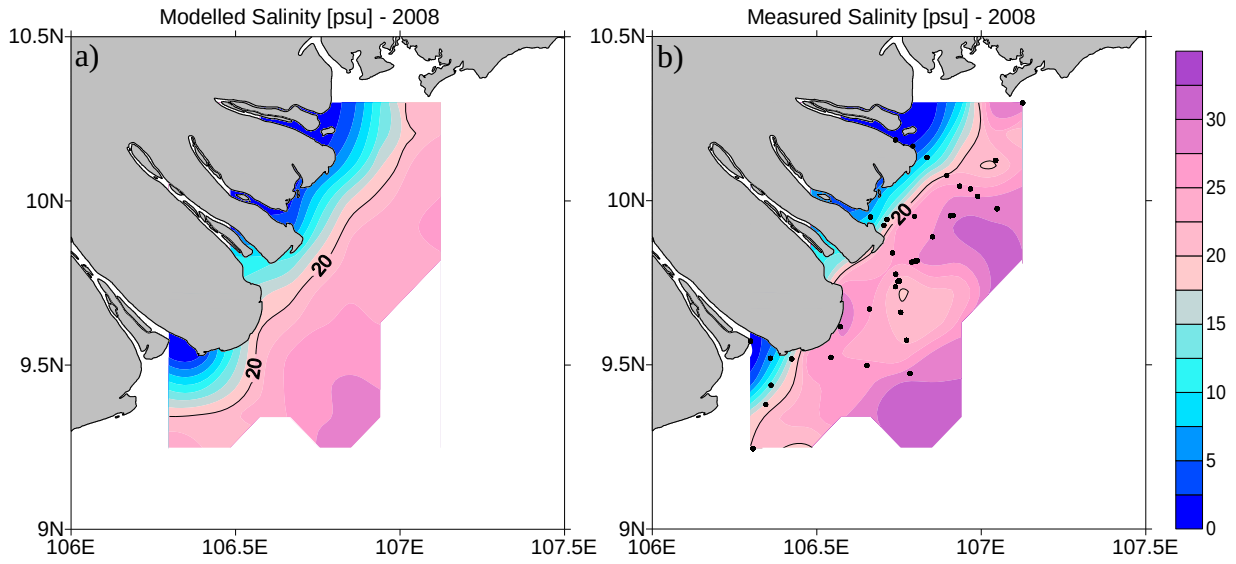

Figure 27: a) Averaged modelled salinity [psu] from 18/09/2008 00:00 to 23/09/2008 00:00 and b) comprehensive picture of measured salinity [psu] throughout the whole research area from 18/09/2008 00:00 to 22/09/2008 06:00. The position of the stations is marked.

Figure 28b represents a transect through the Mekong River plume during the cruise in September 2008. A salinity gradient which changes from low salinity water at the mouth of the Mekong River (< 2.5 psu) to high salinity water further offshore (> 30 psu) is clearly depicted. The water column in the vicinity of the Mekong River mouth is mixed. The region is characterized by a horizontal gradient of salinity. The adjacent deeper stations further offshore are weakly stratified with lower salinity water at the surface (25 to 27.5 psu) and higher salinity water (> 30 psu) at the bottom. Comparing the results with modelled salinity (Figure 28a) low salinity water (< 2.5 psu) is also illustrated in the vicinity of the Mekong River mouth. The measured horizontal gradient of salinity is also represented by the model. However, the modelled salinity gradient extends further offshore into the deeper shelf sea area. The salinity in the offshore region is about 27.5 to 30 psu. In this region the model results do not depict high salinity water (> 30 psu) at the bottom.

On the one hand, the difference between the measurements and the model results can be explained by the same fact as mentioned above. Numeric diffusion establishes an artificial widening of the frontal zone. Also vertical diffusion seems to be too strong in the model. On the other hand, observations show a random picture of the dynamic system like mentioned above. However, fluctuations and small scale processes are not represented in the model results.

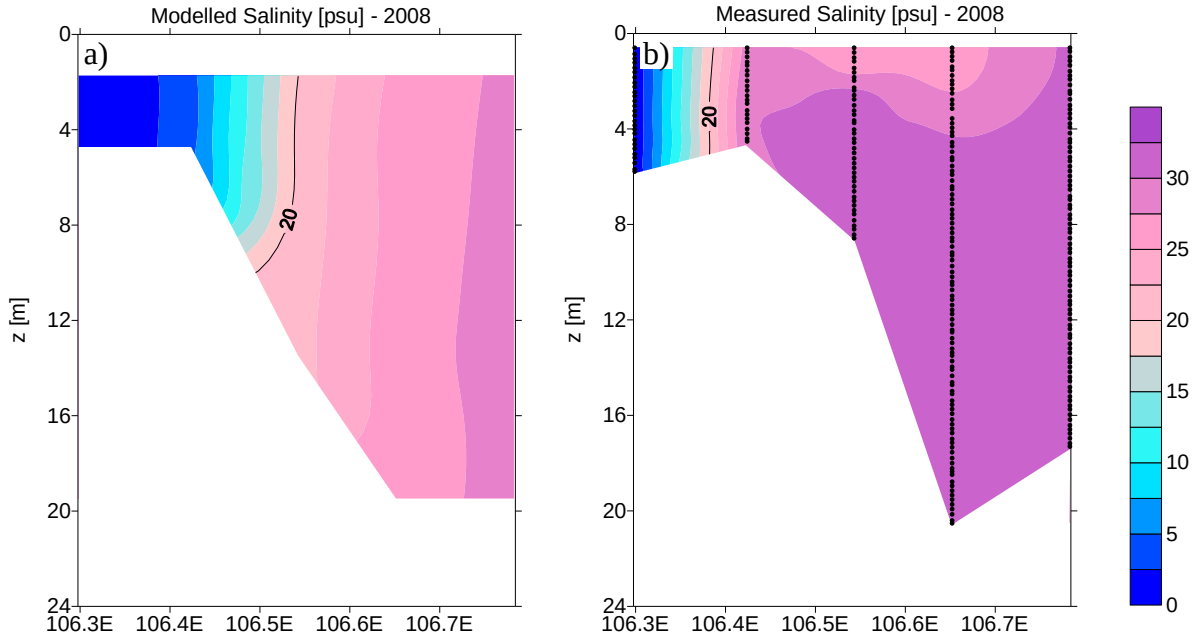

Figure 28: Cross section at transect 2 part 2 of a) averaged modelled salinity [psu] from 19/09/2008 00:00 to 20/09/2008 00:00 and b) measured salinity [psu] between 19/09/2008 06:00 and 11:00. The position of the CTD casts is marked.

In summary, the differences in the hydrographic situation between the low-flow and the high-flow season are well reproduced by HAMSOM. The stratification and destratification of the

water column within a tidal cycle is also represented adequately by HAMSOM. The constraints of the model are disclosed as well. Altogether, the model results can be used to analyze the seasonal variability of stratifying and destratifying processes in the Mekong ROFI.

4.5.5 VALIDATION – TIDES

The software WXTide32 (http://www.wxtide32.com/index.html) provides daily predictions of times and heights of low and high waters. A reference tide gauge situated in the Mekong ROFI is Vung Tau (10.333° N, 107.067° E). This dataset is used for comparison with fortnightly modelled sea surface heights between 09/04/07 and 22/04/07.

Additionally, tidal elevations can be predicted by OTPS (EGBERT et al., 1994; EGBERT and EROFEEVA, 2002). This dataset has also been used to extract tidal harmonic constants to achieve the phases and the amplitudes at the open boundaries for HAMSOM (section 4.2). Using OTPS, tidal elevations between 09/04/07 and 22/04/07 for Vung Tau are calculated.

Figure 29 shows a time series of the heights for the three different datasets: the sea surface height calculated by HAMSOM (dark blue line), the predicted tidal elevation using the Indonesian Seas Inverse Tidal Solution calculated by OTPS (light blue line) and the heights of high and low water provided by WXTide32 (red bars). In general, HAMSOM is able to simulate the tidal elevations in the model area reasonably well.

Differences between predicted tidal elevations using the Indonesian Seas Inverse Tidal Solution and modelled sea surface heights by HAMSOM can be attributed to the fact that on the one hand the sea surface elevation in HAMSOM is not only caused by tidal effects but also by wind and/or baroclinic effects. On the other hand, if the simulated phase velocity of the different tidal constituents is marginally inaccurate, at an arbitrary point in space the phases of the different tidal constituents are imprecisely superposed. Thus, the simulated tidal elevations of HAMSOM may deviate from the predicted tidal elevations of OTPS.

Considering the heights of high and low water provided by WXTide32, there exists a difference between the two datasets for the first four days and at the end of the depicted time period. Possible reasons have been mentioned above. However, in general the semidiurnal character is represented well by the model results. The tidal amplitude is mostly reproduced well and consequently the tidal energy which is introduced into the system. The fact that the results of HAMSOM fits better with the results of WXTide32 than with the OTPS solution which has been used to force the model at the open boundaries indicates that an optimum of a possible accuracy is attained.

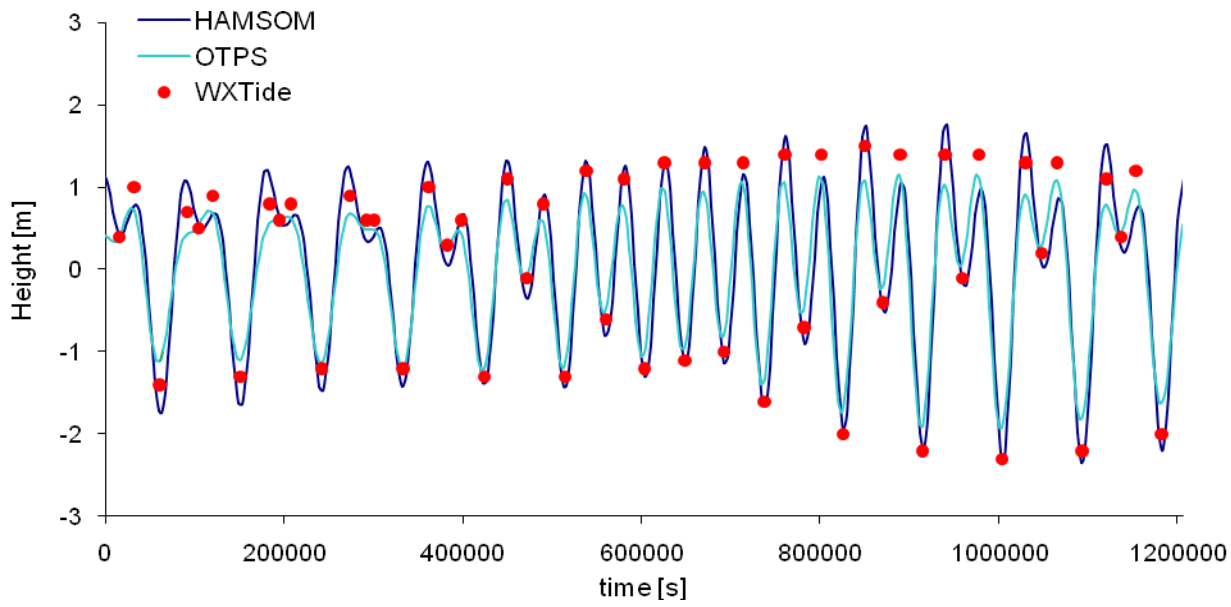

Figure 29: Modelled Sea Surface Heights [m] (dark blue line), heights of high and low water [m] with an offset of 2.3 m reproduced from WXTide (red dots) and predicted tidal elevations [m] using Indonesian Seas Inverse Tidal Solution (light blue line) at Vung Tau (10.333° N, 107.067° E) from 09/04/2007 to 22/04/2007 [s].

CHAPTER 5

RESULTS

To describe the hydrodynamic model results of the Mekong ROFI, the area is divided into two main regions, each with three sub-regions, i.e., a total of six regions (Figure 30). The first main region extends from the Saigon River to the south of the Tranh De branch. It is termed the Northern ROFI (NROFI). The second main region extends from south of the Tranh De branch to the southern tip of Zhongnan Peninsula. This region is called Southern ROFI (SROFI). The sub-regions are the coastal region, the Main Plume region (MPR) and the shelf region. The coastal region describes the coastal area with a depth < 10.5 m. The MPR is the adjacent region and is characterized by strong vertical and horizontal gradients of salinity. The extension of the MPR changes with the seasonal varying freshwater input from the Mekong River, i.e., the region does not have a static extension throughout the year. The region adjacent to the MPR extending further offshore is called shelf region. However, during the summer monsoon, the MPR exists only in the NROFI as the plume is advected to the NE. Thus, for this season the SROFI is only divided into coastal area and shelf region.

To investigate the seasonal variability in the region, in the following the model results will be shown as a temporal average over one spring-neap cycle during August 2006 (13^{th} to 29^{th}) and January 2007 (15^{th} to 31^{th}). For showing φ_{1D} and φ_{t3D} a time series during the two above mentioned periods is depicted as well.

In this study, ‘seasonal’ means a representative period over a spring-neap cycle in which the river discharge and the wind stress corresponds roughly to a typical seasonal pattern. The first period has been chosen to represent a typical high-flow situation, i.e., the SW monsoon is fully developed and the river discharge is strongly elevated. Therefore, in the following this period in August is termed “high-flow season” or “summer monsoon”. The second period represents a typical situation during the low-flow season, as the NE monsoon is fully developed and the river discharge is conspicuously decreased. This period in January is denoted as “low-flow season” or “winter monsoon”.

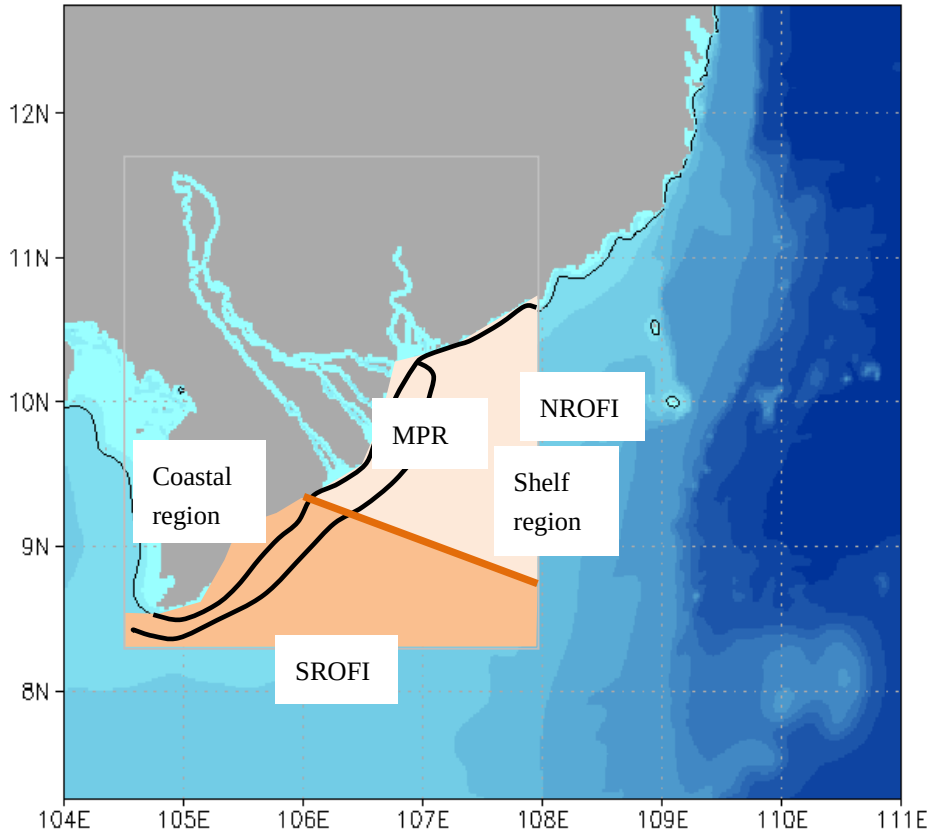

Figure 30: Main regions (NROFI and SROFI) and sub-regions (coastal region, Main Plume Region (MPR), shelf region) of the Mekong ROFI. The grey rectangle shows the investigation area of this study. The MPR changes with the seasonal varying freshwater input from the Mekong River. Here, a schematic overview of a representative situation during the low-flow season is given. The 10.5 m depth contour line is marked. Bathymetry [m] is based on the ETOPO2 (http://www.ngdc.noaa.gov/mgg/global/etopo2.html) and GEBCO (http://www.gebco.net/data_and_products/gridded_bathymetry_data) dataset.

5.1 HYDRODYNAMIC CONDITIONS IN THE MEKONG ROFI DURING THE LOW-FLOW SEASON

During the winter monsoon the residual surface currents are directed mainly to the SW (Figure 31a). However, in the coastal region in the vicinity of the upper five river mouths and the adjacent MPR the residual surface currents are dominantly directed to the south.

In the coastal area and in the MPR of the NROFI the residual surface velocities are weak (< 0.2 m/s, Figure 31c). The residual surface currents are also weak in the coastal region of the SROFI (< 0.2 m/s). However, in the MPR of the SROFI the residual surface velocities are elevated (up to 0.4 m/s) forming a pronounced baroclinic current. A surface convergence zone is formed where the currents of the shelf meet the baroclinic current (Figure 31a). The current sticks to the coast in the region around the southern tip of Zhongnan Peninsula and ends up in the Gulf of Thailand.

The residual bottom currents show a different picture (Figure 31b). In the coastal region and the MPR of the NROFI the residual bottom currents are directed to the NW, i.e., a baroclinic circulation is developed with surface currents showing an offshore component and bottom currents showing an onshore component. In the coastal region of the SROFI, the residual bottom currents are directed mainly to the SW and in the MPR of the SROFI to the W – hence more onshore.

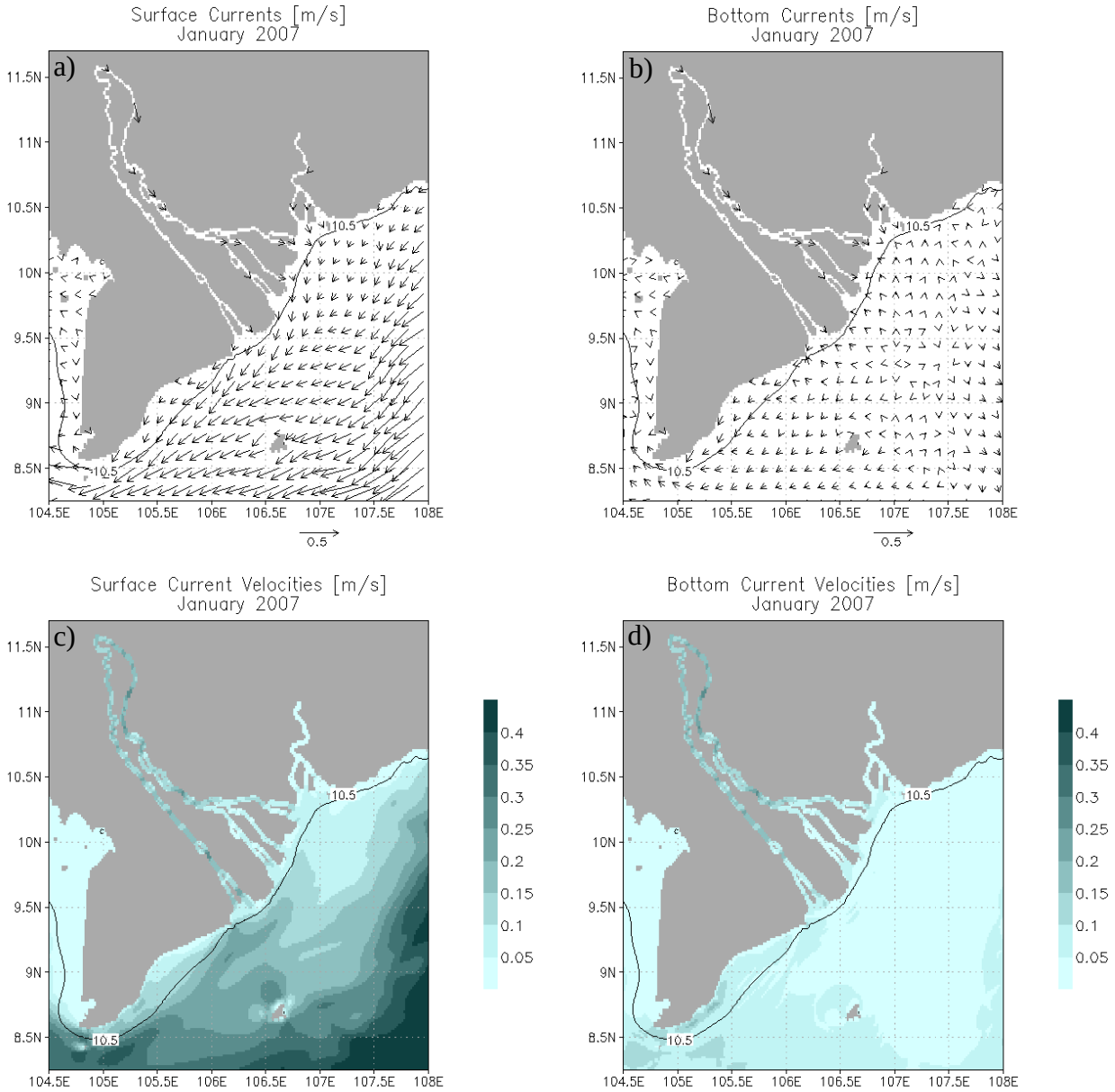

Figure 31: a) Modelled residual surface currents [m/s], b) modelled residual bottom currents [m/s], c) modelled residual surface velocities [m/s] and d) modelled residual bottom velocities [m/s] in the Mekong ROFI during the low-flow season (January 2007). The values show an average over one spring-neap cycle. In figure a and figure b every 8th arrow is depicted.

Throughout the whole model region, the residual bottom currents are mainly weak with velocities < 0.1 m/s (Figure 31d). The residual bottom currents are strongest in the coastal area of the SROFI (up to 0.2 m/s) near the southern tip of the Peninsula.

Figure 32 shows a temporal average of the surface salinity and temperature distribution during the winter monsoon in the Mekong ROFI. The Mekong River plume is constrained to the coast. The salinity changes within a narrow area from < 3 psu to 33 psu in the NROFI and from 21 psu to 33 psu in the SROFI.

The temperature distribution shows the influence of the basin-wide winter circulation. Both advection of cold water from the northern SCS and upwelling at the edge of the Sunda Shelf (CHAO et al., 1996a) result in relative cold temperatures for these latitudes. The cold water originating from the northern part of the SCS and the warm river water build a high gradient throughout the model area. The highest temperatures are about 28 °C in the Gulf of Thailand and the lowest about 23.5 °C in the SE of the model region. However, in the Mekong ROFI itself the temperature gradient is weak (1–1.5 °C).

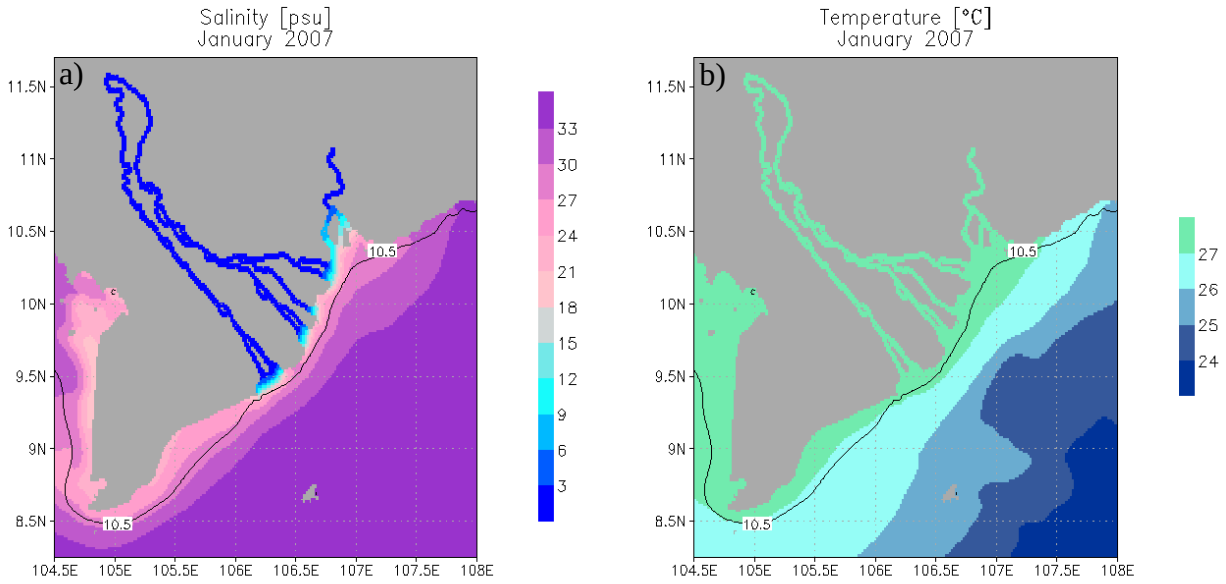

Figure 32: a) Modelled surface salinity [psu] and b) modelled surface temperature [°C] in the Mekong ROFI during the low-flow season (January 2007). The values show an average over one spring-neap cycle.

Figure 33a illustrates that the horizontal salinity gradient is highest at the Mekong River mouths. Values are about > 1.0 psu/km. The horizontal salinity gradient is also elevated in the area extending from the coastline to the eastern boundary of the MPR. The horizontal gradient is sustained as far as the Gulf of Thailand. In contrast, on the shelf the horizontal salinity gradient is low (< 0.025 psu/km).

Figure 33b shows the horizontal density gradient. Here, the same pattern as in Figure 33a is depicted, i.e., the horizontal gradients are due to differences in salinity and not in temperature.

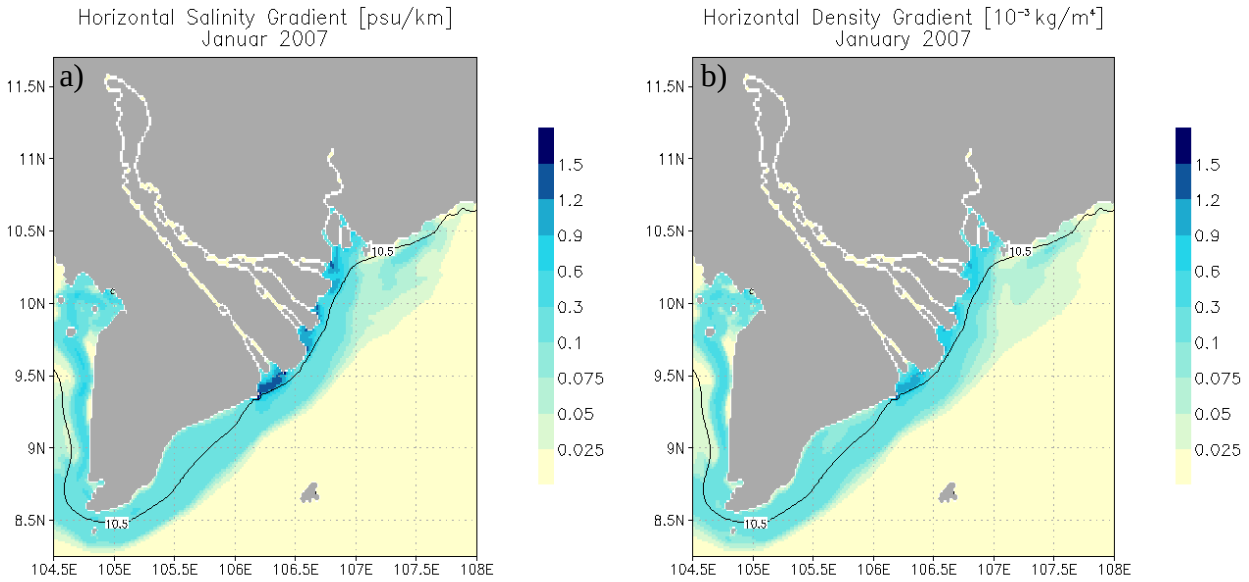

Figure 33: a) Modelled horizontal salinity gradient [psu/km] and b) modelled horizontal density gradient [10^{-3} kg/m^4] at the surface in the Mekong ROFI during the low-flow season (January 2007). The values show an average over one spring-neap cycle. In the blanked areas values could not be calculated due to the model discretization.

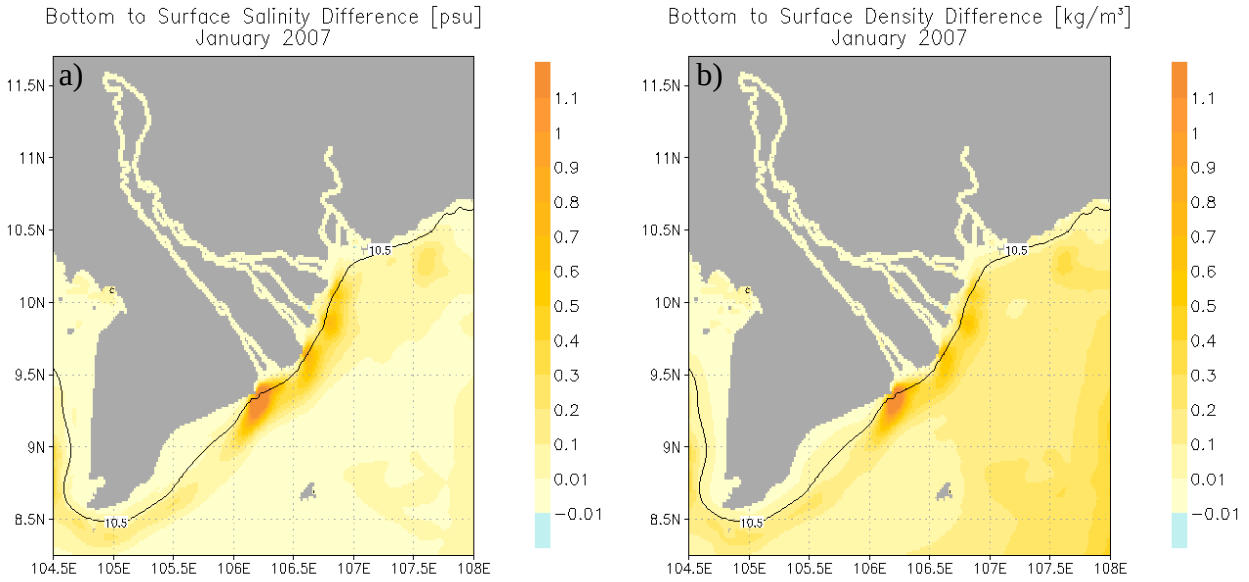

Figure 34: a) Modelled bottom to surface salinity difference [psu] and b) modelled bottom to surface density difference [kg/m³] in the Mekong ROFI during the low-flow season (January 2007). The values show an average over one spring-neap cycle. Positive values indicate a stably stratified water column and values around 0 a mixed water column.

Considering the vertical salinity difference, the most stable stratification (1.1 psu) can be found in the MPR to the south of the Tranh De branch (Figure 34). The positive values indicate that

the salinity at the surface is lower than the salinity at the bottom. Thus, the water column is stably stratified due to the salinity. In general, the vertical salinity difference is low in the coastal region, increases in the MPR, but decreases further offshore on the shelf. Hence, in the shallow coastal region the water column is mixed. When the water deepens in the MPR, the water column is stratified. On the shelf the water column is mixed in terms of salinity. However, due to the temperature gradient a weak stratification of the water column is developed on the shelf as can be concluded from Figure 34b. By comparing Figure 34a (bottom to surface salinity difference) and Figure 34b (bottom to surface density difference), it can be deduced that the stratification in the MPR is caused by the freshwater input from the river. Besides, it is obvious that the largest vertical salinity difference can be found in the direction of Kelvin wave propagation – which is in the Northern Hemisphere with the land on the right looking downcurrent – rather than directly at the Mekong River mouths.

5.2 HYDRODYNAMIC CONDITIONS IN THE MEKONG ROFI DURING THE HIGH-FLOW SEASON

Unlike the situation during the winter monsoon, on the shelf of the NROFI as well as of the SROFI the residual surface currents are mainly directed to NE (Figure 35a). A great part of the shelf region shows residual surface velocities greater than 0.3 m/s (Figure 35c). The influence of the basin-wide circulation on the local circulation is represented by a northeastward current parallel to the coast in the shelf region of the SROFI. South of the Bassac River this current builds a strong convergence zone with the baroclinic current formed by the Mekong River outflow. The influence of the boundary current on the Mekong ROFI is also indicated in the figures of CHU et al. (1999).

In the MPR of the NROFI the residual surface currents are directed to SE/E. In this area the highest residual surface velocity can be found in the region before the Bassac River mouth (> 0.3 m/s). The residual surface currents in the coastal area of the NROFI are directed to the SE with velocities up to 0.2 m/s in the region of the Bassac River mouths, whereas in the coastal area of the SROFI they are generally heterogeneously directed and weak (0.1 m/s).

The residual bottom currents are mainly weak during the summer monsoon with velocities < 0.15 m/s (Figure 35d). In the coastal area and in the MPR of the NROFI the residual bottom currents are directed to the N/NW (Figure 35b), i.e., also during the summer monsoon a baroclinic circulation is developed. On the shelf of the NROFI, the residual bottom currents are mainly directed to the N/NW as well. In contrast to the situation during the winter monsoon, in the coastal area of the SROFI the residual bottom currents are mainly weak and heterogeneously directed. There exists no area with elevated velocities. However, on the shelf of the SROFI the velocities are elevated compared to the situation during the winter monsoon. The residual bottom currents are mainly directed towards NE.

The residual bottom currents are strongest in the part of the MPR closest to the river mouths and

on the shelf (up to 0.2 m/s). A strong bottom convergence zone can be found at the river mouths. Here, a baroclinic onshore current converges with the river outflow.

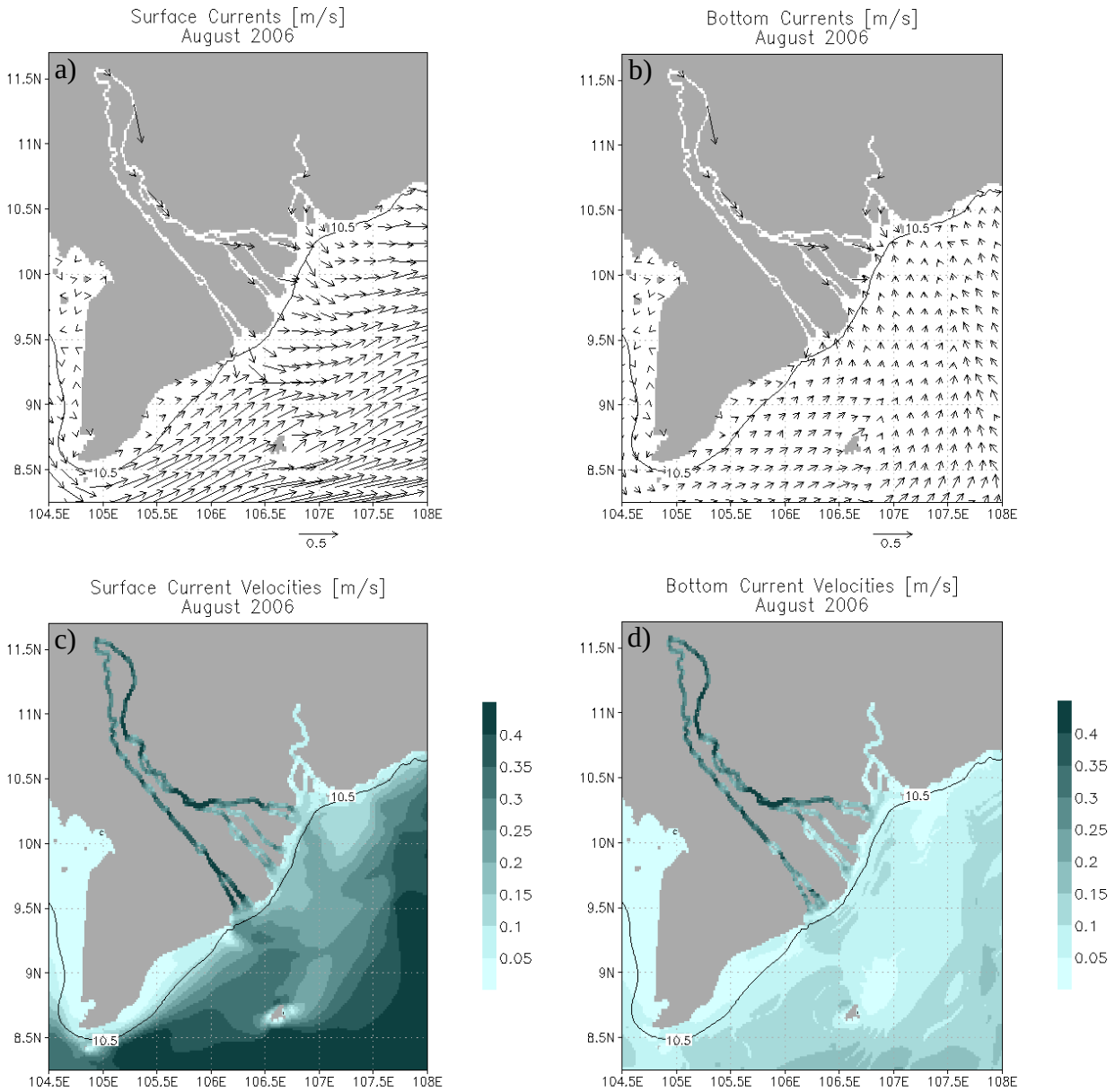

Figure 35: a) Modelled residual surface currents [m/s], b) modelled residual bottom currents [m/s], c) modelled residual surface velocities [m/s] and d) modelled residual bottom velocities [m/s] in the Mekong ROFI during the high-flow season (August 2006). The values show an average over one spring-neap cycle. In figure a and figure b every 8th arrow is depicted.

Unlike the situation during the winter monsoon, the river plume is directed towards NE (Figure 36a) against the direction of Kelvin wave propagation. The plume is not as constrained to the coast as it is in January. In the coastal area of the NROFI, salinities < 3 psu can be found. In the adjacent MPR the salinity ranges from 3 psu to 30 psu. The adjacent shelf water has salinities

about 30 psu. Regarding the SROFI, in all regions the water has salinities about 30 psu.

Compared to the situation in January, the temperature distribution shows a low gradient throughout the model area (Figure 36b). The highest temperatures in August are elevated to those of January, with values about 29 °C. They can be found mainly in the coastal region and the MPR of the NROFI. The lowest temperatures are about 28 °C in the E and S of the model region.

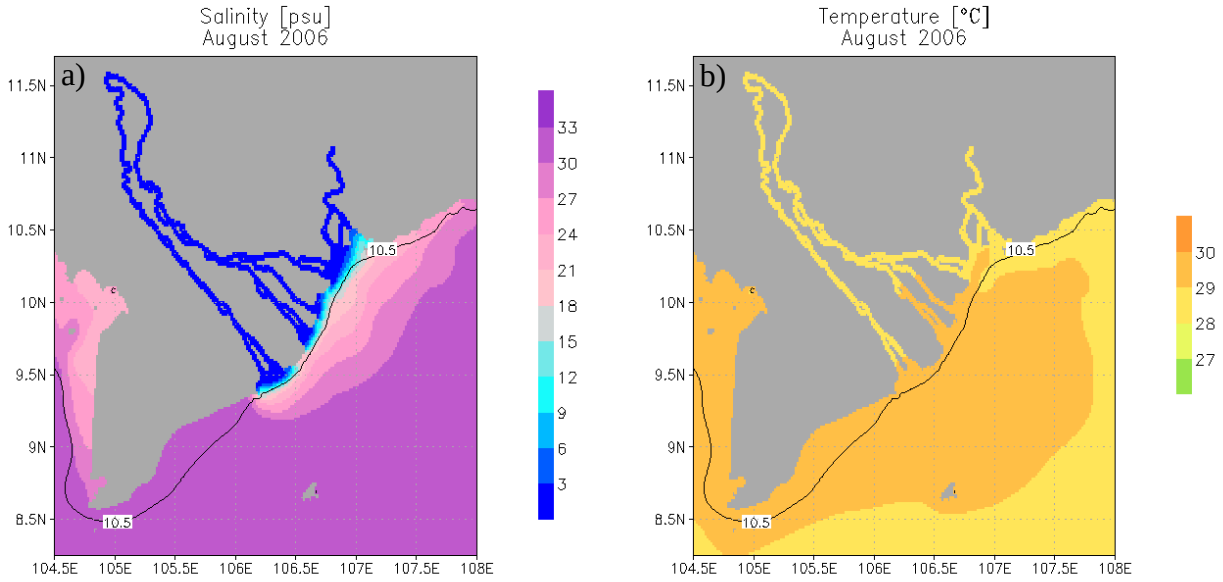

Figure 36: a) Modelled surface salinity [psu] and b) modelled surface temperature [°C] in the Mekong ROFI during the high-flow season (August 2006). The values show an average over one spring-neap cycle.

As specified in January, the strongest horizontal salinity gradient can be found in the coastal region of the NROFI where the fresh Mekong River water encounters the salinity water of the SCS (Figure 37a). But the extension of the region where a horizontal gradient exists spreads further offshore. Values are > 1.3 psu/km. Like in January, the MPR of the NROFI is dominated by a horizontal salinity gradient. There exists also a horizontal gradient in the Gulf of Thailand. However, the horizontal salinity gradient in the Gulf of Thailand is not directly linked to the Mekong River plume. In the region of the SROFI no horizontal salinity gradient is depicted in the figure (< 0.025 psu/km). These values can also be found on the shelf of the NROFI. Figure 37b shows the horizontal density gradient. From this figure it can be deduced that the horizontal gradients are due to differences in salinity and not in temperature. Thus, during both seasons temperature differences play a minor role.

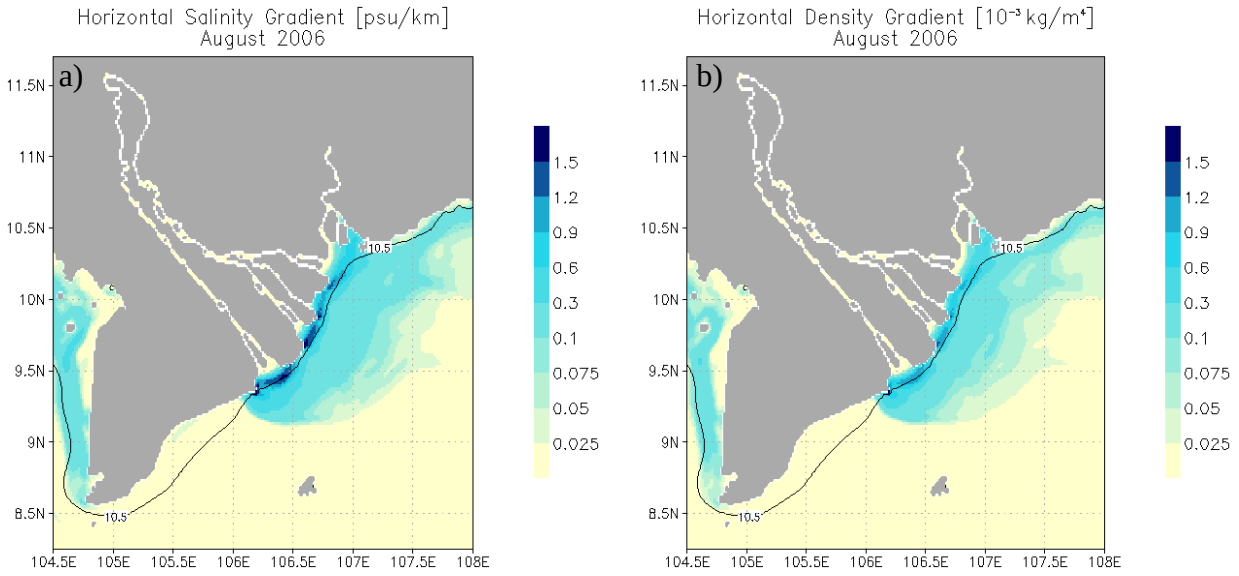

Figure 37: a) Modelled horizontal salinity gradient [psu/km] and b) modelled horizontal density gradient [10^{-3} kg/m^4] at the surface in the Mekong ROFI during the high-flow season (August 2006). The values show an average over one spring-neap cycle. In the blanked areas values could not be calculated due to the model discretization.

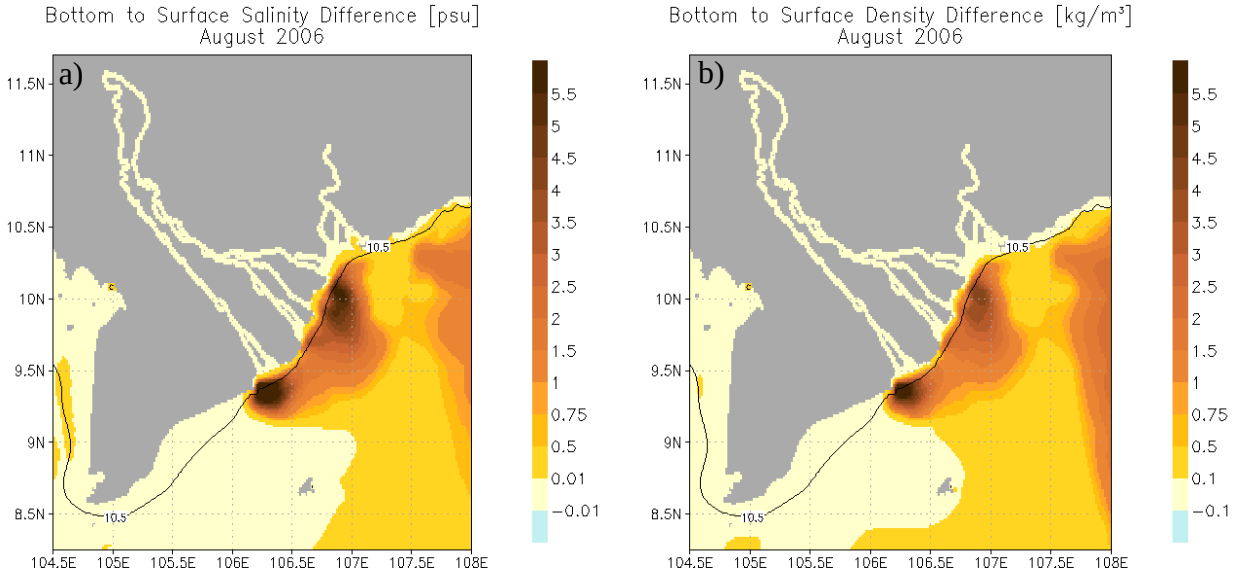

Figure 38: a) Modelled bottom to surface salinity difference [psu] and b) modelled bottom to surface density difference [kg/m³] in the Mekong ROFI during the high-flow season (August 2006). The values show an average over one spring-neap cycle. Positive values indicate a stably stratified water column and values around 0 a mixed water column.

Considering the vertical salinity difference (Figure 38) the most stable stratification can be found in the MPR offshore of the Tranh De branch and, additionally to the situation during the

winter monsoon, in the MPR to the south of the Dai branch (5.5 psu). As the positive value indicates that the salinity at the surface is lower than the salinity at the bottom, the water column is stably stratified. Generally during the summer monsoon, the vertical salinity difference is low in the coastal region and increases in the MPR of the NROFI. Hence, both during January and August the water column of the NROFI is mixed in the shallow area and stratified in the adjacent deeper area. Further offshore in the shelf region, the vertical salinity difference is low in the part adjacent to the MPR but increases again until the eastern boundary of the investigation area. The vertical difference in salinity at the eastern boundary shown in Figure 38a is formed by the gradient of the river influenced water and the deeper maximum salinity water originating from the West Philippine Sea (HEIN, 2007).

Although discharge in summer is greater than in winter, the strongest vertical gradient is located only slightly further offshore compared to January. However, the extension of the region where a vertical gradient can be observed is more extended in August and the values are considerably elevated. In contrast to the situation during the winter monsoon, no stratification is observed in the SROFI.

5.3 APPLICATION OF THE ONE-DIMENSIONAL EQUATION FOR THE POTENTIAL ENERGY ANOMALY (φ_{1D}) TO THE MEKONG ROFI

To quantify the stability of the water column, the use of the simple one-dimensional equation of the potential energy anomaly (SIMPSON et al., 1981) is an appropriate method. The formulation is in wide use for estuarine circulation studies (e.g., SIMPSON et al., 1990; RIPPETH and SIMPSON, 1996; HOLT and UMLAUF, 2008).

The results are shown on a seasonal as well as on a tidal time scale. To eliminate the effect of a varying bathymetry, all results are normalized by the depth of the water column so that the results refer to a standardized water depth of 1 m.

For the interpretation on the tidal time scale in the investigation area five representative stations (Figure 39) have been chosen. To get a representative value for these stations an areal average of a cell of 0.1° × 0.1° has been calculated. The centre of the grid cells are labelled CC, Me, MeE, Ba and BaN.

The different regional characteristics referring to the investigation period in August and January are as follows (from south to north):

- CC: The station 9.0° N/106.05° E ± 0.05 is situated in the SROFI off the river mouths. This station represents the southward directed coastal current of the Mekong River during the NE monsoon. In January the time of NE monsoon corresponds to the low-flow season. During the SW monsoon which corresponds in August to the high-flow season this station lies outside the river plume as the southward directed coastal current is not apparent at the respective monsoon phase.

- Ba, BaN: The stations 9.25° N/106.2° E ± 0.05 (region Ba) and 9.35° N/106.3° E ± 0.05 (region BaN) represent the area just off the Bassac River mouths and to the south of the Bassac River mouths. Both stations are part of the MPR of the NROFI. During the high-flow season (SW monsoon) as well as during the low-flow season (NE monsoon) these stations are situated inside the Mekong River plume.
- MeE: The station 9.9° N/107.2° E ± 0.05 extends offshore of the Ham Luong branch. It is situated in the NROFI (transition region between MPR and shelf). During the NE monsoon (low river discharge), this station lies in the outermost reaches of the river plume. During the SW monsoon (high river discharge), this station lies inside the river plume.
- Me: The station 10.0° N/106.9° E ± 0.05 is situated south of the Tieu and Dai branches in the MPR of the NROFI and represents the freshwater input by these branches.

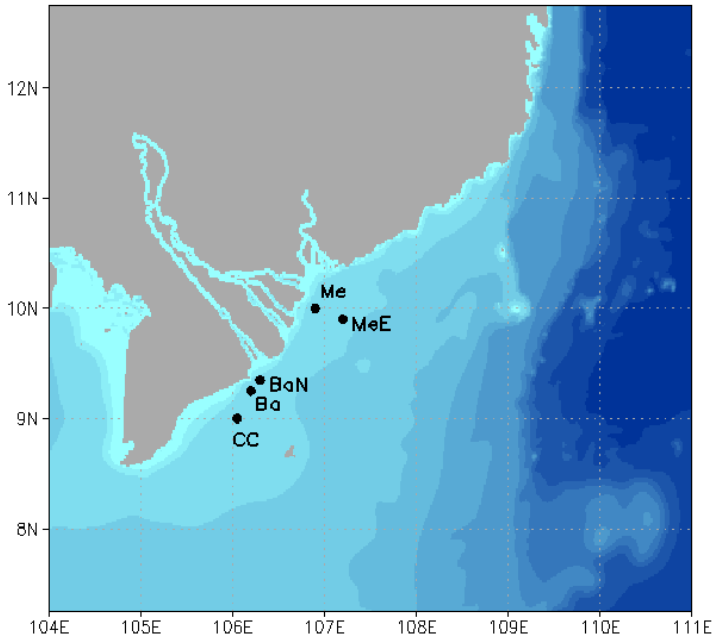

Figure 39: Representative stations in the Mekong ROFI for the investigations on the tidal time scale. Bathymetry [m] is based on the ETOPO2 (http://www.ngdc.noaa.gov/mgg/global/etopo2.html) and GEBCO (http://www.gebco.net/data_and_products/gridded_bathymetry_data) dataset.

Figure 40 shows φ_{1D} in the Mekong ROFI during the high-flow as well as during the low-flow season. φ_{1D} indicates the work required to mix the water column instantaneously. The results for August 2006 (Figure 40a) as well as for January 2007 (Figure 40b) are depicted as a temporal average over one spring-neap cycle (14.8 days).

It is obvious that in August 2006 the time averaged values are between 0 J/m³, which indicates vertically mixed conditions and > 3.3 J/m³, which indicates stratified conditions. The averaged values in January 2007 oscillate between 0 J/m³ and > 0.33 J/m³. Generally, averaged values in August are higher than averaged values in January, i.e., the water column is stronger stratified during the high-flow season (summer) than during the low-flow season (winter).

In August, the Mekong River plume is clearly visible. The two pronounced areas of strongest stratification exist near the Mekong River mouths: one is located between the Tieu and Hau branch, the second is situated between the Din An and Tranh De branch. The extension of the Mekong River plume in summer is to the NE/E. There is a great similarity with Figure 38a and b which show the mean surface to bottom salinity and the mean surface to bottom density difference, respectively.

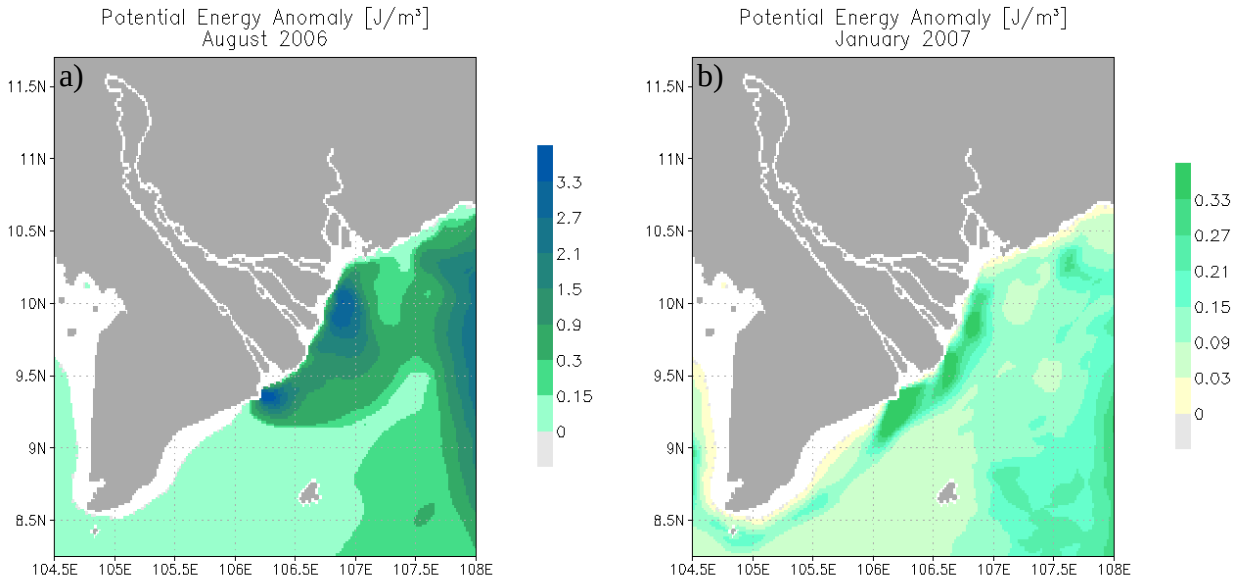

Figure 40: φ_{1D} [J/m³] in the Mekong ROFI a) during the high-flow season (August 2006) and b) during the low-flow season (January 2007). The values show an average over one spring-neap cycle. In the blanked areas values could not be calculated due to the model discretization. Positive values indicate a stably stratified water column and values around 0 J/m³ a mixed water column. Note, the scale is different between figure a and figure b.

In January, the extension of the Mekong River plume is confined to the coast. The direction is towards SW. Four areas of relatively high stratification are mapped, representing the different branches of the Mekong River. Particularly for the coastal region and the MPR there is a great similarity with Figure 34 (mean surface to bottom salinity and mean surface to bottom density difference). In August as well as in January, the shallow water area close to the shoreline is well mixed, since wind mixing and tidal mixing are more effective in the shallow parts of the shelf sea.

Figure 41 shows φ_{1D} calculated with an artificially constant but representative temperature

(T = 28.5 °C) when determining the density via the equation of state, i.e., only the effect of salinity and pressure on stratification is considered. During the high-flow season the situation in the Mekong ROFI is the same as in the previous picture (Figure 40), i.e., the freshwater input by the Mekong River has a greater influence on stratification than surface heat fluxes. Differences between these two figures can be observed in the further offshore parts adjacent to the Mekong ROFI. Here, the values of φ_{1D} are lower compared to the values depicted in the previous figure, i.e., the additional influence of temperature on the stratification is pictured. An impact of upwelling and therefore a steep gradient in the seasonal thermocline in this region has been observed by HEIN (2007).

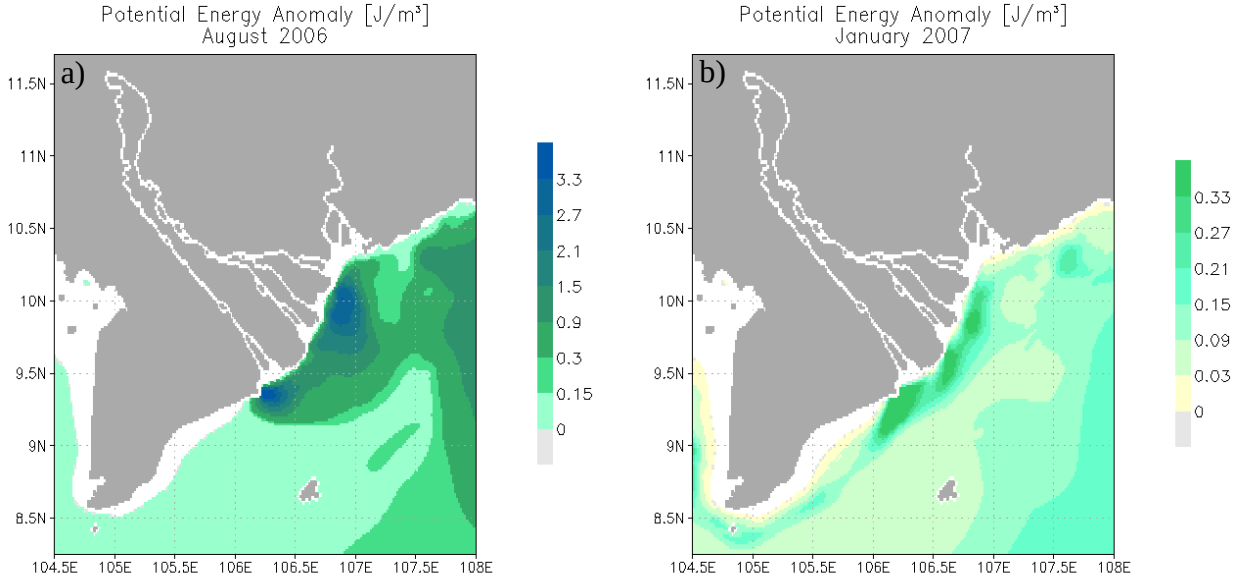

Figure 41: φ_{1D} [J/m³] in the Mekong ROFI a) in August 2006 and b) in January 2007. The values show an average over one spring-neap cycle. φ_{1D} has been calculated with an artificially constant temperature (T = 28.5 °C) when determining the density via the equation of state. In the blanked areas values could not be calculated due to the model discretization. Positive values indicate a stably stratified water column and values around 0 J/m³ a mixed water column. Note, the scale is different between figure a and figure b.

Considering the values of φ_{1D} for the low-flow season shown in Figure 41b, in the coastal area and in the MPR of the N/SROFI the situation is the same as in the previous picture. Thus, like during the high-flow season, for these areas the influence of temperature on stratification is low, whereas the influence of salinity on stratification is evident. In the shelf area the influence of temperature on density and thus on stratification is significant, which are related again to upwelling processes as they were found by HEIN (2007). However, a change in stratification due to coastal upwelling and moreover mixing processes between freshwater and uplifted water at the shelf break, are a broad field to investigate, which owes the respect to future research.To describe the stratification of the water column throughout the tidal cycle during the two monsoon phases, Figure 42 and Figure 43 are analyzed in the following.

In the region BaN in August at higher high water φ_{1D} reaches a local minimum. However, the water column is still weakly stratified. At lower low water, the water column is strongly stratified. φ_{1D} shows a local maximum. These dynamics are mostly also represented by the regions Me and MeE. However, at higher high water the water column is mixed in the region MeE. In region Me some irregularities can be observed for the first period. Region Ba shows a different characteristic. However, for this region it is difficult to determine the instant of time of local maximum and minimum, as it is rather a time period. In the region Ba the trend is that maximum stratification occurs in the period between higher low water and the ebb tide after lower high water whereas minimum stratification occurs around lower low water until flood tide after lower low water. Region CC does not show any change in stratification. The water column is mixed and remains mixed throughout the entire tidal cycle.

A pronounced spring-neap cycle is represented by the results of φ_{1D} in the region BaN. Highest stratification is reached at higher low water around neap tide whereas lowest stratification is reached at higher high water around spring tide. The region Ba shows a reversed picture, since at neap tide no pronounced stratification occurs whereas at spring tide at higher low water stratification is at its maximum. At the other regions no pronounced relationship can be observed.

Also in January there exists a relationship between the tidal phases and the degree of stratification in the region BaN. At lower low water the stratification is highest as is also the case in August. However, in contrast to the situation in August at higher high water the water column is completely mixed. Hence, no weak stratification remains. The same dynamics can be observed in the regions CC and Me. Region Ba shows some irregularities for the first period, but then the same characteristics as mentioned before. However, the water column is not completely mixed at higher high water. In the region MeE the water column is mixed and remains mixed throughout the entire tidal cycle.

The correlation between the degree of stratification and the neap-spring cycle is also represented in January in the region BaN. However, this is not as obvious as in August since stratification is generally lower in winter than in summer due to the reduced river discharge. In contrast to the situation during the summer monsoon also region Ba shows the above mentioned dynamic. At the other region no clear relationship exists.

Regions which are primarily stratified or mixed have been identified. The evolution of the potential energy anomaly over the tidal cycle at different stations has also been shown. The physical processes which determine the magnitude of stratification cannot be specified by φ_{1D}. To do so, in the next section the rate of change in stratification will be quantified by using φ_{t3D}. This allows for estimation of the individual physical processes influencing stratification and destratification of the water column.

High-flow season

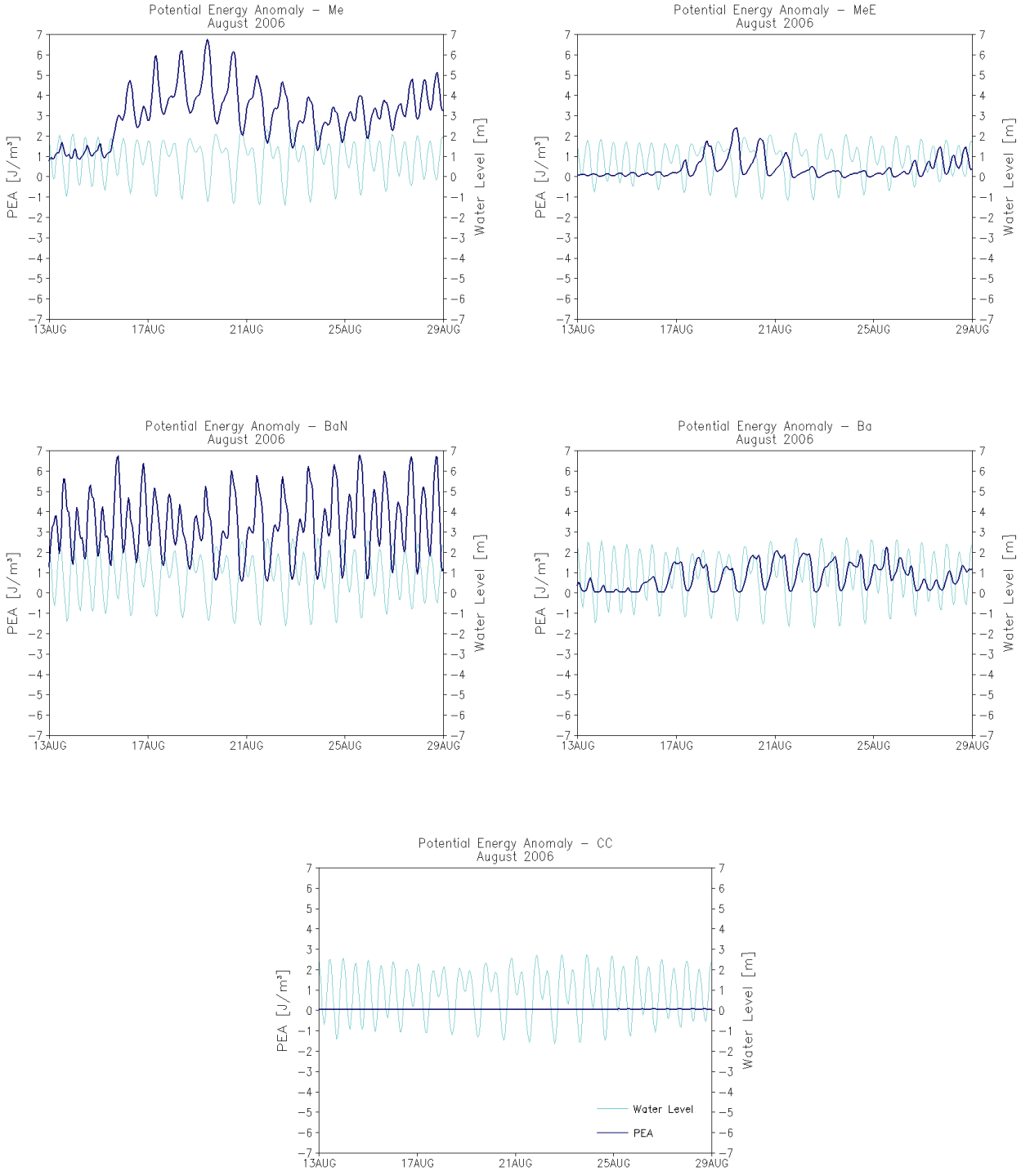

Figure 42: Time series of φ_{1D} [J/m³] (dark blue line) and water level [m] (light blue line) at the investigation stations in the Mekong ROFI for the high-flow season (August 2006). For a better visualization of the results the water level is shown with an offset of 1 m. φ_{1D} has been calculated with an artificially constant temperature (T = 28.5 °C) when determining the density via the equation of state. Positive values of φ_{1D} indicate a stably stratified water column, values of 0 J/m³ a mixed water column and negative values an unstably stratified water column.

Low-flow season

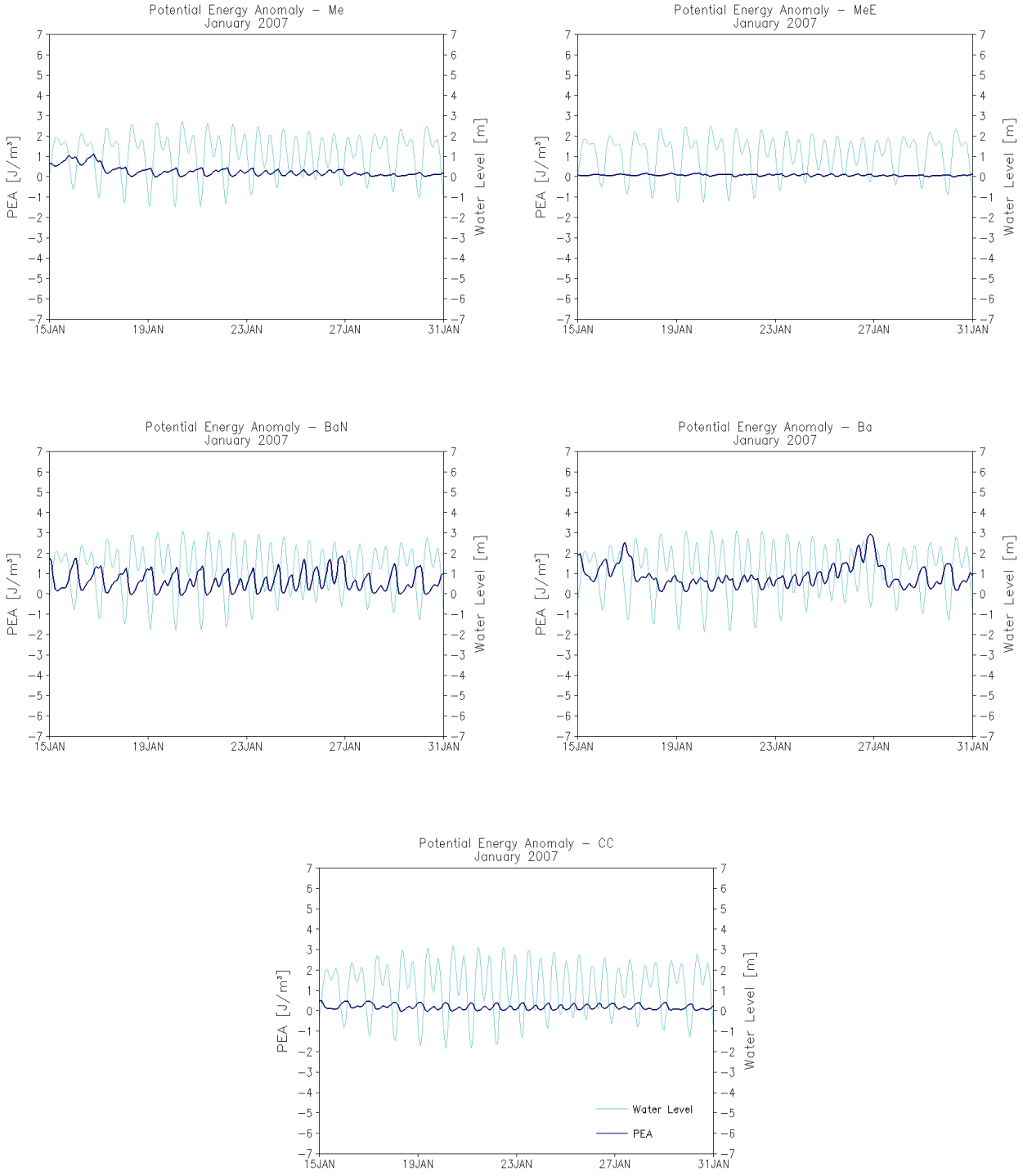

Figure 43: Time series of φ_{1D} [J/m³] (dark blue line) and water level [m] (light blue line) at the investigation stations in the Mekong ROFI for the low-flow season (January 2007). For a better visualization of the results the water level is shown with an offset of 1 m. φ_{1D} has been calculated with an artificially constant temperature (T = 28.5 °C) when determining the density via the equation of state. Positive values of φ_{1D} indicate a stably stratified water column, values of 0 J/m³ a mixed water column and negative values an unstably stratified water column.

5.4 APPLICATION OF THE THREE-DIMENSIONAL DYNAMIC EQUATION FOR THE POTENTIAL ENERGY ANOMALY (φ_{t3D}) TO THE MEKONG ROFI

River discharge, wind stress and tides force temporally and locally distinct physical processes that change the potential energy of the water column and thus the stratification. As mentioned above, these three forcing mechanisms play an important role in the Mekong ROFI. Both river discharge and wind stress underlie a strong seasonal variability, whereas tidal forces change on an intra-seasonal time scale.

In the next sections the physical processes which act to stratify and/or destratify the water column on different time scales will be identified for the Mekong ROFI. They are determined by means of the three-dimensional dynamic equation for PEA (equation 3.13), on a seasonal scale (section 5.4.1) as well as on a tidal cycle (section 5.4.2). The results are normalized by the depth of the water column. Unlike the above shown φ_{1D}, φ_{t3D} represents the time rate of change of PEA. The three-dimensional dynamic equation for PEA comprises barotropic as well as baroclinic terms.

Figure 44 shows the two barotropic terms of equation 3.13 averaged over one spring-neap cycle. These terms take the influence of depth (BT_D) and surface elevation change (BT_S) on φ_{t3D} into account. The figures illustrate that the barotropic terms are relatively small and only locally of importance. Therefore, the barotropic terms are not analyzed in more detail further on. Furthermore, the interest of this study is focused on the baroclinic processes that contribute to stratification and/or destratification in the Mekong ROFI.

In the following, φ_{t3D} is approximated by the sum of the six baroclinic terms and is denoted by φ^{*}_{t3D}. There are four horizontal terms like the horizontal advection term, the tidal straining term, the non-mean straining term, the shear dispersion term, and two vertical terms like the vertical mixing term and the vertical advection term. With this decomposition it is possible to quantify the different stratifying and destratifying processes in the Mekong ROFI.

Figure 45 shows the averaged φ^{*}_{t3D} over one spring-neap cycle for the two different seasons (high-flow and low-flow season). The density used in equation 3.13 has been calculated via the equation of state for sea water (FOFONOFF and MILLARD, 1983) and is considered as a function of temperature, salinity and pressure. Figure 46 depicts the same quantity using the density as a function of only salinity and pressure. The temperature is held artificially constant at 28.5 °C.

It can be seen from Figure 45 that during the period of high river discharge as well as during the period of low river discharge the freshwater input contributes mostly to stratify the water column. Nevertheless, there are various patches where destratification processes prevail. In August a major patch is situated just off the Din An and Tranh De branch. Other smaller patches lie off the other river mouths. There is also a larger destratification patch in the inner plume region in August. In January only one major patch exists which indicates destratification. It is situated to the south of the Tranh De branch.

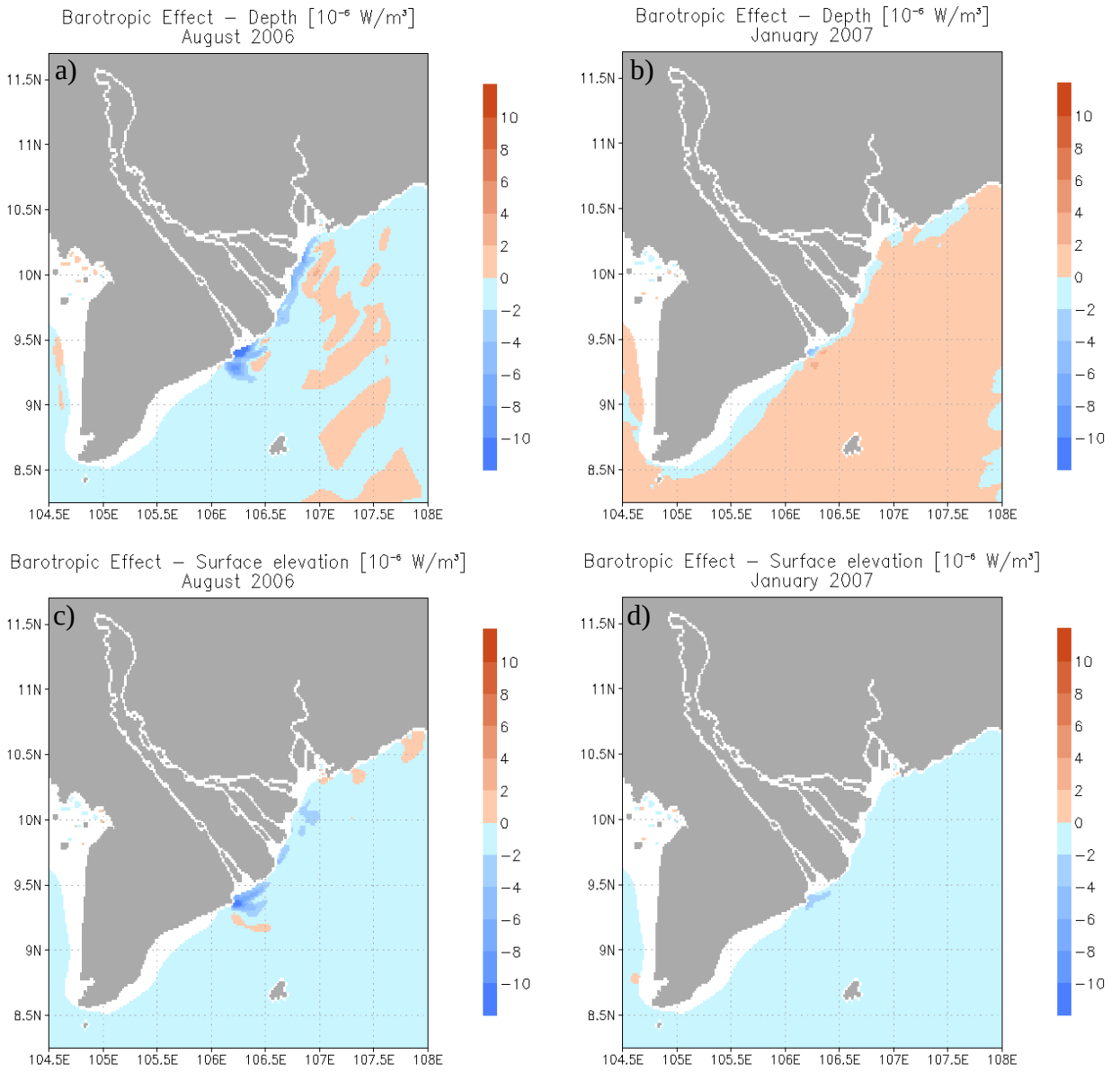

Figure 44: Barotropic effect due to depth [10^{-6} W/m³] in the Mekong ROFI a) during the high-flow season (August 2006) as well as b) during the low-flow season (January 2007) and barotropic effect due to surface elevation [10^{-6} W/m³] c) during the high-flow season (August 2006) as well as d) during the low-flow season (January 2007). The values show an average over one spring-neap cycle and have been extracted from the three-dimensional dynamic PEA equation. In the blanked areas values could not be calculated due to the model discretization. Positive values indicate stratification and negative values destratification.

Comparing Figure 45 and Figure 46 the differences are small. Only off the Mekong River plume some differences are noticeable where stratification has a thermal component. Hence, stratification in the Mekong River plume is mainly influenced by salinity. Thus, in the following the investigations will be focused on the influence of the freshwater buoyancy input on stratification.

If the results of φ_{1D} (equation 3.3) and of φ_{t3D} (equation 3.13) are combined it is possible

1) on the one hand to identify regions which are stratified or mixed (Figure 41)

STRATIFIED REGIONS:

MPR of the NROFI during the summer monsoon

MPR of the NROFI as well as SROFI during the winter monsoon

shelf edge

MIXED REGIONS:

shelf region of the SROFI

coastal regions

2) on the other hand to quantify the rate of change in stratification (Figure 46)

REGIONS WITH ELEVATED RATE OF CHANGE IN STRATIFICATION:

MPR of the NROFI during the summer monsoon

MPR of the NROFI as well as SROFI during the winter monsoon.

Thus, altogether baroclinically dynamic active regions, i.e., regions with a high rate of change in potential energy can be depicted. Based on this the Mekong River plume can be identified as baroclinically dynamic active region which extend to the NE during the SW monsoon (August) and to the SW during the NE monsoon (January) and which is strongly stratified during both seasons.

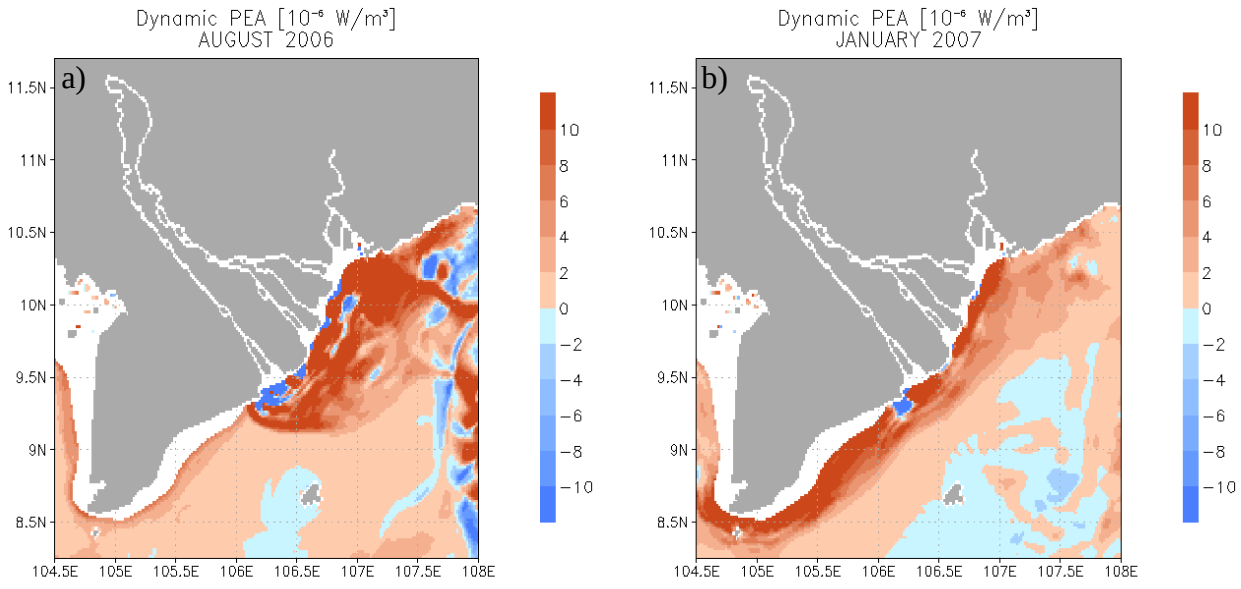

Figure 45: φ^{*}_{t3D} [10^{-6} W/m³] in the Mekong ROFI a) during the high-flow season (August 2006) and b) during the low-flow season (January 2007). The values show an average over one spring-neap cycle. In the blanked areas values could not be calculated due to the model discretization. Positive values indicate stratification and negative values destratification.

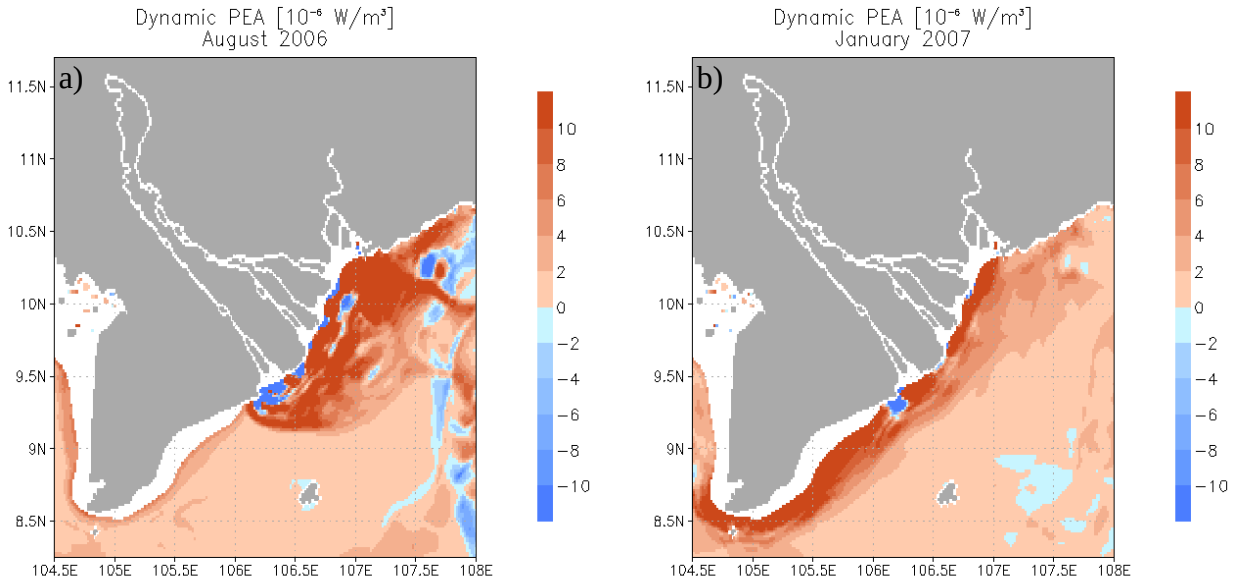

Figure 46: φ^*_{t3D} [10^{-6} W/m³] in the Mekong ROFI a) during the high-flow season (August 2006) and b) during the low-flow season (January 2007). φ^*_{t3D} has been calculated with an artificially constant temperature (T = 28.5 °C) when determining the density via the equation of state. The values show an average over one spring-neap cycle. In the blanked areas values could not be calculated due to the model discretization. Positive values indicate stratification and negative values destratification.

Figure 47 and Figure 48 show φ^*_{t3D} throughout a spring-neap cycle in August 2006 and January 2007 which represent high and low run-off conditions, respectively. The time series are depicted for the regions defined in Figure 39.

In the Figure 47 and Figure 48 it is depicted that in nearly all regions processes of stratification and destratification alternate periodically in the Mekong ROFI. Generally the range of φ^*_{t3D} is greater in the high-flow season than in the low-flow season. During the high-flow season the Mekong River discharge is severalfold higher than during the low-flow season. Therefore, in the ROFI the maximum stratification as shown by φ_{1D} (Figure 42 and Figure 43) is higher during the high-flow season which allows a higher dynamic in stratification.

That the range of φ^*_{t3D} is greater in the high-flow season than in the low-flow season is true for all stations except for the southernmost region CC. In this region the stratified southward directed coastal current is apparent only during the NE monsoon, i.e., the low-flow season but not during the SW monsoon, i.e., the high-flow season.

The maximal range of φ^*_{t3D} is reached during the period of high river discharge in the region BaN. The values oscillate between -750×10^{-6} W/m³ and $+600\times10^{-6}$ W/m³. But also in the region Me a large range can be observed during this season. During the period of low river discharge the maximal range is also reflected by the region BaN.

High-flow season

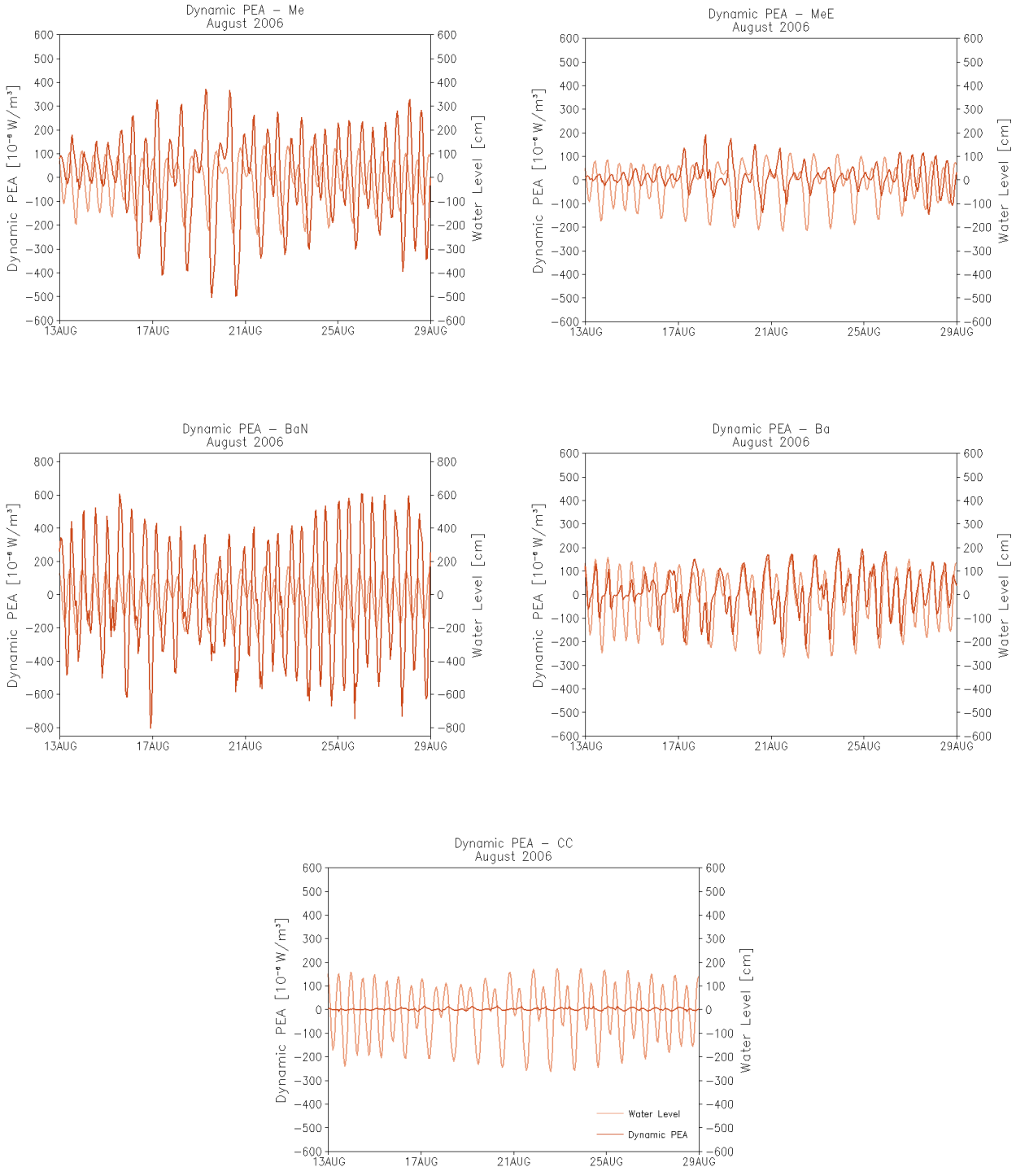

Figure 47: Time series of φ^*_{t3D} [10^{-6} W/m³] (dark red line) and water level [cm] (light red line) at the investigation stations in the Mekong ROFI for the high-flow season (August 2006). φ^*_{t3D} has been calculated with an artificially constant temperature (T = 28.5 °C) when determining the density via the equation of state. Positive values of φ^*_{t3D} indicate stratification and negative values destratification. Please note the scale of region BaN is different.

Low-flow season

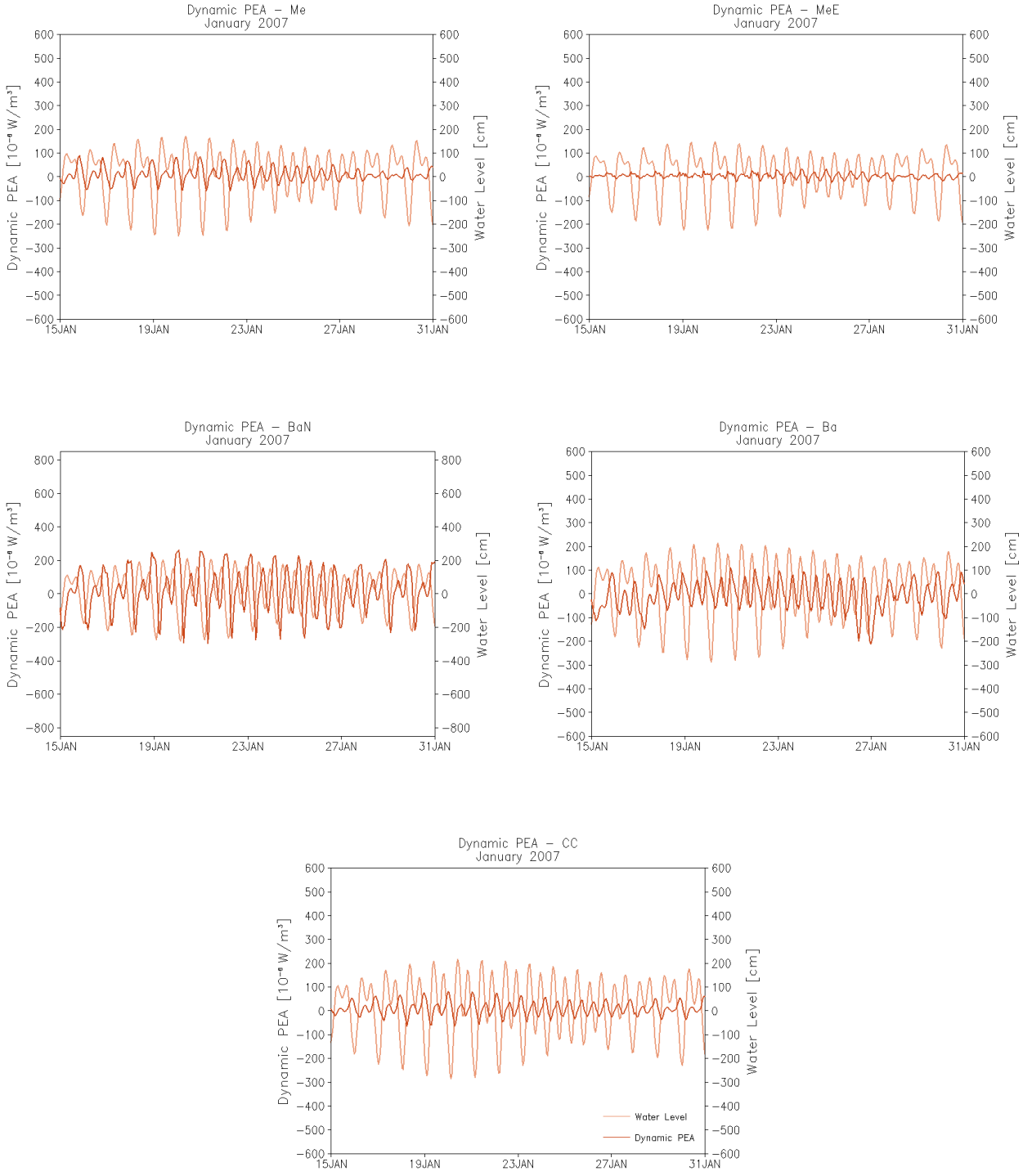

Figure 48: Time series of φ^*_{t3D} [10^{-6} W/m³] (dark red line) and water level [cm] (light red line) at the investigation stations in the Mekong ROFI for the low-flow season (January 2007). φ^*_{t3D} has been calculated with an artificially constant temperature (T = 28.5 °C) when determining the density via the equation of state. Positive values of φ^*_{t3D} indicate stratification and negative values destratification. Please note the scale of region BaN is different.

The minimum range of φ^*_{t3D} is reached in the region CC during the period of high river discharge with a value around 0 W/m³, i.e., the physical regime remains constant over time with respect to changes in stratification. The constant value around 0 W/m³ together with a value of φ_{1D} around 0 J/m³ (Figure 42) in the region CC indicates that the plume is absent during this time period.

Comparing the values of φ^*_{t3D} for the regions near the Bassac River mouth (Ba and BaN), significant differences can be noticed during both seasons. Obviously, although the distance is rather short, φ^*_{t3D} decreases conspicuously from north to south, i.e., with distance to the freshwater source.

Analyzing the dynamics within the tidal cycle it is evident that during the low-flow season (January) in the majority of the regions around higher high water and lower low water φ^*_{t3D} is about 0 W/m³, thus there is no change in stratification of the water column. Close to the time of high and low water, slack water occurs, i.e., no appreciable current flows which drives horizontal and/or vertical exchange processes. An exception shows the region MeE. Here, φ^*_{t3D} is always about 0 W/m³.

For specification in Figure 49a a 25 h time series of the region Ba during the low-flow season is depicted. During ebb tide φ^*_{t3D} is positive, i.e., stratification of the water column occurs. Around half time of ebb tide, i.e., almost at maximum ebb current, φ^*_{t3D} shows a maximum (strongest increase in stratification). Afterwards, during the second half of ebb tide, stratification processes continue with decreasing strength until low water. In contrast, during flood tide destratification of the water column is evident (negative values of φ^*_{t3D} occur) whereas around half time of flood tide, i.e., at maximum flood current, φ^*_{t3D} shows a minimum (strongest decrease in stratification). Afterwards, during the second half of flood tide, destratification continues until high water but on a decreasing level.

During the period of high river discharge the direct relationship between the tidal phases and stratification is mostly apparent in the region MeE, Me and BaN. The other regions show either no change in stratification (region CC) or a significant different relationship between the tidal cycle and the change in stratification (region Ba) (Figure 47). For exemplification in Figure 49b a 25 h time series of the region MeE during the high-flow season is depicted. The figure shows the same dynamic for φ^*_{t3D} as mentioned above for the region Ba during the low-flow season.

The distinct relationship between the tidal cycle and the change in stratification, as observed for the region Ba during the high-flow season, supports the evidence of other forces than tidal motions which are important to explain the change in stratification in the Mekong ROFI. In order to get an idea of these forces, the governing processes which act as stratifying and/or destratifying agent will be determined in the next section. The different terms of the equation for φ^*_{t3D} (mean straining, horizontal advection, non-mean straining, shear dispersion, mixing and up/downwelling; equation 3.13) are quantified to investigate the importance of the respective physical processes.

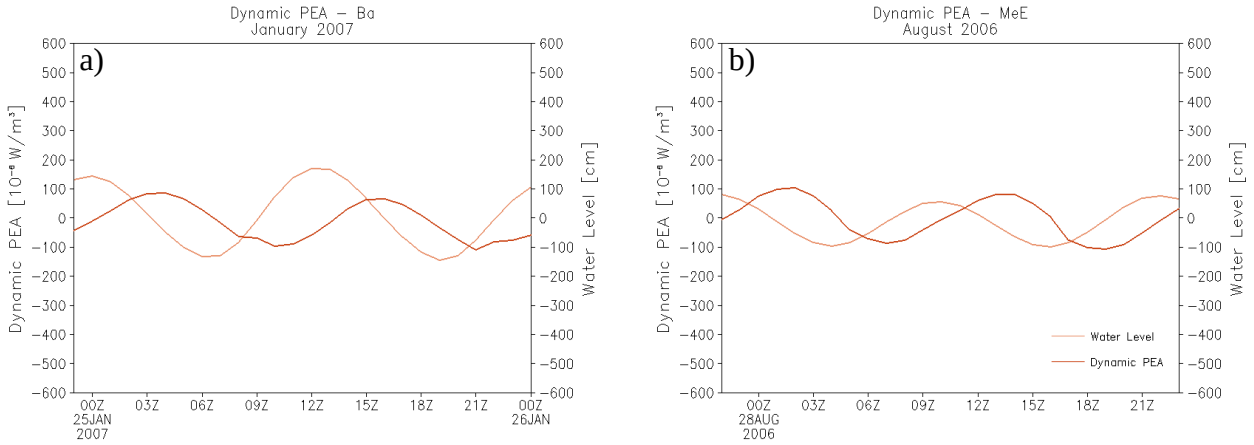

Figure 49: 25h time series of φ^*_{t3D} [10^{-6} W/m³] (dark red line) and water level [cm] (light red line) at the stations a) Ba during the low-flow season (January 2007) and b) MeE during the high-flow season (August 2006). φ^*_{t3D} has been calculated with an artificially constant temperature (T = 28.5 °C) when determining the density via the equation of state. Positive values of φ^*_{t3D} indicate stratification and negative values destratification.

5.4.1 PHYSICAL PROCESSES IN THE MEKONG ROFI ON A SEASONAL TIME SCALE

In this section the seasonality of the physical processes determined by the equation for φ^*_{t3D} is analyzed in the case of the Mekong ROFI. A temporal average over one spring-neap cycle will be determined for the two seasons (high-flow and low-flow season). The spatial distribution of the individual baroclinic terms during the high-flow season – represented by the results of August 2006 – is compared to the situation during the low-flow season – represented by the result of January 2007.

During the high-flow season the situation in the Mekong ROFI is as follows (Figure 50):

The mean straining term and the mixing term show a homogenous spatial distribution with elevated values throughout the whole plume region. Mean straining acts to stratify the water column, whereas mixing acts to destratify the water column. The shear dispersion term and the non-mean straining term hold values in a similar order of magnitude, but the spatial distribution of these terms is more heterogeneous. Non-mean straining generally acts to stratify the water column in the coastal area of the NROFI and in the shelf region. Hence, in these regions the velocity anomaly is in direction of decreasing $\tilde{\rho}$, i.e., $\tilde{u}\frac{\partial\tilde{\rho}}{\partial x}<0$ and thus the water column is stabilized ($\varphi^*_{t3D}>0$). However, shear dispersion acts to destratify the water column in the coastal area of the NROFI and in the shelf region. In the MPR non-mean straining acts to destratify the water column. In these regions the velocity anomaly is in direction of increasing $\tilde{\rho}$, so that $\tilde{u}\frac{\partial\tilde{\rho}}{\partial x}>0$ and thus the water column is de-stabilized ($\varphi^*_{t3D}<0$). In the MPR shear dispersion acts to stratify the water column. Just like mean straining and mixing, non-mean straining and shear dispersion act as counterparts.

High-flow season

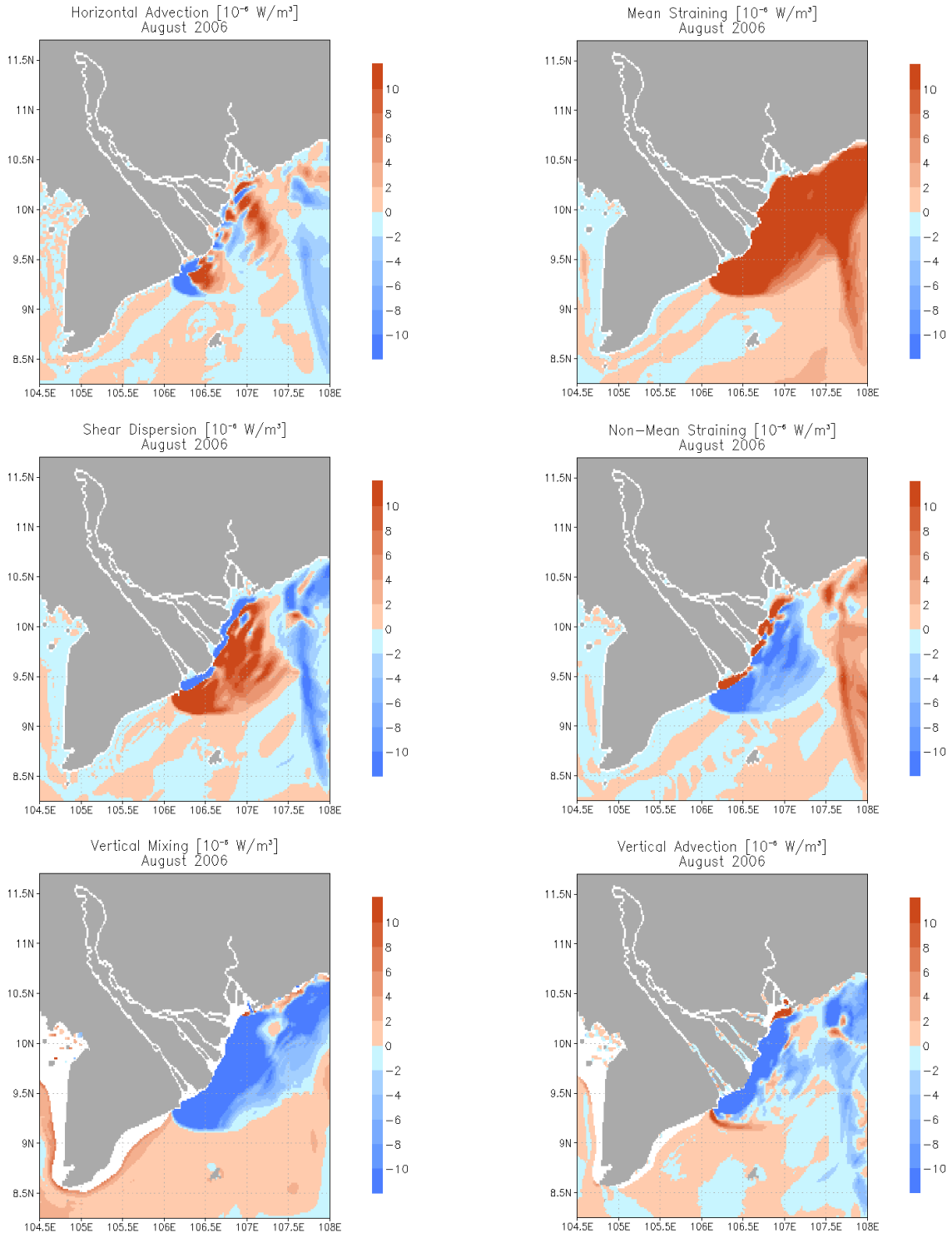

Figure 50: Baroclinic terms [10^{-6} W/m³] extracted from the three-dimensional dynamic PEA equation in the Mekong ROFI during the high-flow season (August 2006). The terms of φ^{*}_{t3D} have been calculated with an artificially constant temperature (T = 28.5 °C) when determining the density via the equation of state. The values show an average over one spring-neap cycle. In the blanked areas values could not be calculated due to the model discretization. Positive values indicate stratification and negative values destratification.

Low-flow season

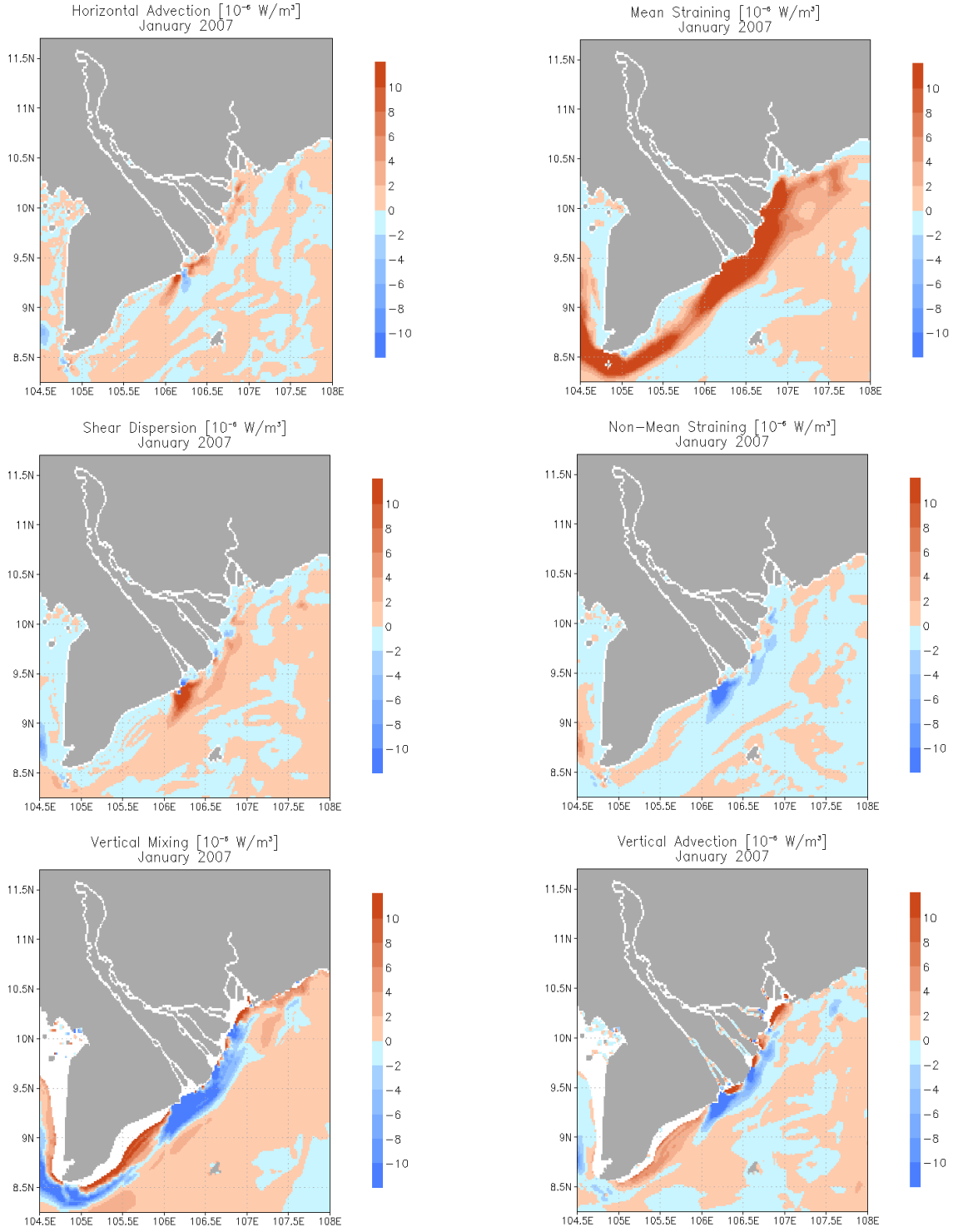

Figure 51: Baroclinic terms [10^{-6} W/m³] extracted from the three-dimensional dynamic PEA equation in the Mekong ROFI during the low-flow season (January 2007). The terms of φ^{*}_{t3D} have been calculated with an artificially constant temperature (T = 28.5 °C) when determining the density via the equation of state. The values show an average over one spring-neap cycle. In the blanked areas values could not be calculated due to the model discretization. Positive values indicate stratification and negative values destratification.

In comparison to these four processes, horizontal and vertical advection act locally bounded. The horizontal advection term shows a highly heterogeneous picture, indicating a complex horizontal circulation. The coastal region of the NROFI depicts the advection of a mixed water column giving evidence that during the high-flow season well mixed estuarine water enters the Mekong ROFI. In the MPR of the NROFI horizontal advection of stratified as well as of mixed water columns takes place. This process is the only one that indicates the different river plumes of the individual branches. Altogether, at first glance the picture seems to be chaotic but on second glance structures can be identified.

Vertical advection generally acts to change the potential energy of a water column due to the elevation of the centre of mass without changing the vertical density gradient. Input of potential energy (hence a negative φ^*_{t3D}) due to upwelling is well documented in the region of the river plume and agrees well with a) the upwelling favourable wind during the summer monsoon (HORDOIR et al., 2006), and b) upwelling due to a secondary circulation which is induced by the plume-rotation. The flow around a bend induced by plume-rotation can be seen in relation to the flow in a curving open channel or a natural riverbend. The flow around a bend produces a transverse circulation. It results from the local imbalance between the vertical varying centrifugal acceleration and the cross-plume pressure gradient. The bottom flow is slowed by friction and thus is weaker than the depth averaged axial flow. The imbalance leads to a near bottom flow in the direction of the inside of the bend. The unconstrained surface currents are stronger than the depth averaged axial flow and lead to an outward directed near surface flow. On the outside of the bend a downward flow develops (downwelling). On the inside of the bend an upward flow can be observed (upwelling) (ELSTON, 2005).

Additional downwelling in the southern frontal region of the river plume can be observed, documented by a positive φ^*_{t3D}. This process is well described by O'DONNELL (1998) who studied downwelling at the Connecticut River plume front by means of observations.

The figures that represent the contribution of the different baroclinic terms to φ^*_{t3D} during the low-flow season (Figure 51) differ greatly from those pictures that represent the high-flow season (Figure 50).

The most obvious seasonal difference is the spatial distribution. In August the terms affecting the evolution of stratification show high values in a region extending to the E/NE. This region shows a large offshore extension. In contrast, in January the terms show high values in a region extending to the SW. This region is constrained to the coast. A great similarity exists to the pictures of the bottom to surface salinity as well as density difference (Figure 34 and Figure 38), i.e., generally the regions which display a high difference in the bottom to surface salinity (density) agree with the regions showing the largest values for the baroclinic terms.

During the period of low river discharge (Figure 51), mean straining plays again a dominant role in stratifying the water column. The mixing term has a similar order of magnitude and contributes to destratify the water column like during the high-flow season. Only near the

shoreline reversed ratios can be observed. Here, the mixing term shows positive contributions to φ^*_{t3D} which implies the destruction of a density inversion, i.e., of an unstable stratification (HOFMEISTER et al., 2009). The formation of the density inversion is related to downwelling, like it is documented in the distribution of the vertical advective terms.

Downwelling in the Mekong ROFI may occur due to a downwelling favourable wind during the winter monsoon (HORDOIR et al., 2006). They stated that during the NE monsoon the wind tends to create an Ekman transport towards the coast which induces downwelling in the coastal area of the Mekong ROFI. Also frictional effects in the bottom boundary layer of the coastal current can increase the downwelling. In this case downwelling is a result of the local imbalance between the influence of the Coriolis parameter or the vertical varying centrifugal acceleration and the cross-plume pressure gradient. In analogy to the high-flow season on the inside of the rotating coastal current upwelling due to the secondary circulation can be observed (ELSTON, 2005).

Horizontal advection, shear dispersion and non-mean straining show a restricted spatial distribution. These processes act mainly close to the river mouth. As supposed, the shear dispersion term and the non-mean straining term show an inverse picture. The regions just off the Mekong River mouth depict the advection of a stratified water column giving evidence to shelf water intrusion into the Mekong Estuary. Altogether, the extension of the Mekong River Plume is reflected by the three-dimensional dynamic potential energy anomaly. The subsequent characteristics have been found:

1. A clear seasonal characteristic mainly caused by the variations in wind and run-off has been depicted.
2. Mean straining plays a major role in stratifying the water column and mixing in destratifying the water column. These characteristics are independent of the magnitude of river discharge. Nevertheless, there exists an exception for the mixing term during the low-flow season. In the region to the SE of the Peninsula the mixing term shows positive contributions to φ^*_{t3D} which indicates an unstable stratification (HOFMEISTER et al., 2009).
3. Non-mean straining and shear dispersion contribute to φ^*_{t3D} predominantly during the high-flow season. During the low-flow season these processes act only locally restricted. Both processes act directly opposed.
4. Upwelling is documented in great part of the Mekong ROFI. But locally bounded downwelling occurs as well. Vertical advection can occur due to wind stress and/or due to the imbalance between the centrifugal force and the cross-plume pressure gradient. As the largest values of the vertical advection term can be found in the vicinity of the Mekong River mouth, it can be assumed that the main process forcing up/downwelling is secondary circulation due to plume-rotation.
5. The horizontal advection terms show a spatially heterogeneous picture which discloses strong influence of small-scale non-deterministic circulations. Advection

of stratified as well as of destratified water columns takes place. Near the river mouth the horizontal advection term indicates that during summer mixed estuarine water enters the Mekong ROFI. During winter horizontal advection of a stratified water column is evident. This can be related to the fact that salt water intrusion into the Mekong Estuary takes place.

5.4.2 PHYSICAL PROCESSES IN THE MEKONG ROFI ON A TIDAL TIME SCALE

In this section the change in stratification caused by the six baroclinic processes within a spring-neap cycle will be considered. For this purpose, representative for the whole Mekong ROFI five different regions have been chosen. The same regions as described in the previous section will be considered (Figure 39).

The evolution of the six baroclinic terms throughout the tidal cycle will be analyzed for both investigation periods. In the following this evolution is depicted by the first two figures of each region for each season (Figure 52/53; Figure 55/56; Figure 58/59; Figure 61/62; Figure 64/65). Thereby, these time series are set into relation with φ_{1D} (Figure 42 and Figure 43).

Additionally, the proportion of the individual baroclinic terms in φ^*_{t3D} is depicted in the third figure of each region for each season (Figure 54; Figure 57; Figure 60; Figure 63; Figure 66) whereby the calculation for the mean straining term, for example, is as follows.

$$\begin{aligned}\varphi^*_{t3D\_sum} = &| MS_x | + | MS_y | + | ADV_x | + | ADV_y | + | NS_x | + | NS_y | \\ &+ | DIS_x | + | DIS_y | + | MIX_z | + | UD_z |\end{aligned} \tag{5.1}$$

$$MS_{prop} = \frac{| MS_x | + | MS_y |}{\varphi^*_{t3D\_sum}} \tag{5.2}$$

with $MS_{x/y}$ mean straining, $DIS_{x/y}$ shear dispersion, $ADV_{x/y}$ horizontal advection, $NS_{x/y}$ non-mean straining, MIX_z vertical mixing, UD_z vertical advection. The proportion of the other baroclinic terms in φ^*_{t3D} is calculated analogous.

Figure 52 shows the evolution of the six baroclinic terms in the region Me throughout a spring-neap cycle during the high-flow season. All terms show negative and positive values except the mean straining term which has positive values throughout the whole time period, i.e., this term always contributes to stratify the water column. The other terms – depending on the tidal cycle – act to stratify and/or destratify the water column. The values of all baroclinic terms oscillate notably throughout the tidal cycle.

Figure 54 shows the proportion of the baroclinic terms in φ^*_{t3D}, i.e., it can be deduced which are the most important processes in the region Me. However, it is obvious that the contribution of the different processes to φ^*_{t3D} changes within a tidal cycle as well as within a spring-neap cycle. To get a rough overview of the temporal and spatial variability of the physical processes in the

ROFI, the depicted intratidal oscillations in the proportions are given less importance but the general changes in the proportions are considered.

In the region Me during the high-flow season at the beginning of the depicted time period the mean straining term contributes most to φ^*_{t3D} (Figure 54). Also the vertical terms show high contributions to φ^*_{t3D}. As can be seen by φ_{1D} in Figure 42 at this time the water column is slightly stratified.

The situation changes after a few days. φ_{1D} increases strongly. During this time period the physical processes of the region are dominated by up/downwelling (Figure 54). The contribution of the shear dispersion term to φ^*_{t3D} is strongly elevated. The contributions of the non-mean straining term and the horizontal advection term to φ^*_{t3D} are increased as well. In contrast, values of the mixing term are decreased. The contribution of the mean straining term to φ^*_{t3D} diminishes as well but is still high (Figure 54).

During the low-flow season the water column changes between mixed (φ_{1D} = 0 J/m³) and slightly stratified (0 J/m³ < φ_{1D} < 1 J/m³) conditions (Figure 43). The result gives evidence of a decreased freshwater input from the upper Mekong River branches during this season. Mean straining is the main player as can be concluded from Figure 54, but also the vertical advection term and the mixing term show increased values. The other processes can be neglected. Figure 53 illustrates that the values of the mean straining term and the two vertical terms change between negative and positive values throughout the tidal cycle, i.e., depending on the tidal cycle the terms act to stratify or to destratify the water column.

High-flow season

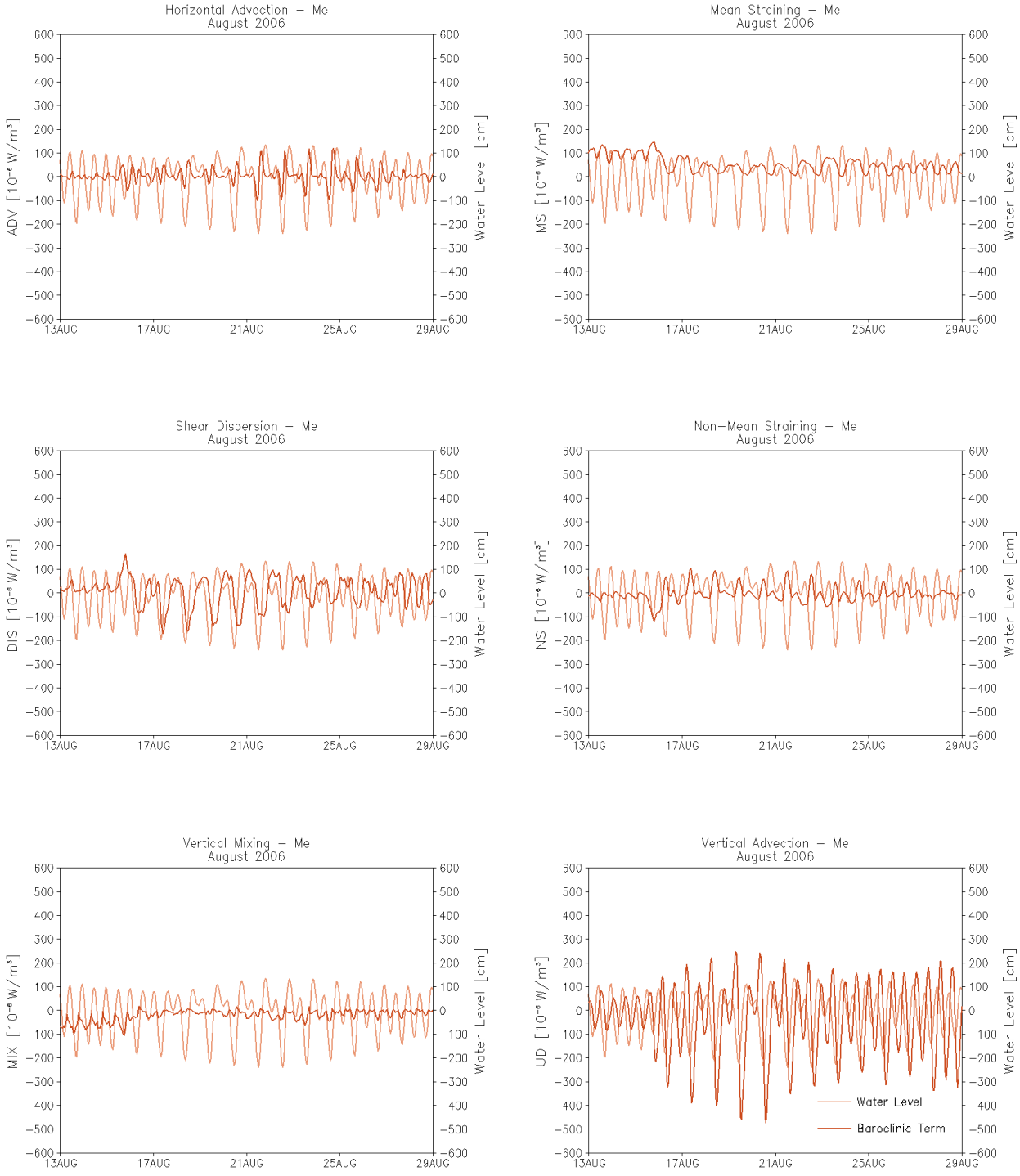

Figure 52: Time series of the baroclinic terms [10^{-6} W/m³] (dark red line) extracted from the three-dimensional dynamic PEA equation and water level [cm] (light red line) at the station 10.0° N/106.9° E (Me) for the high-flow season (August 2006). The terms in the three-dimensional dynamic PEA equation have been calculated with an artificially constant temperature (T = 28.5 °C) when determining the density via the equation of state. Positive values indicate stratification and negative values destratification.

Low-flow season

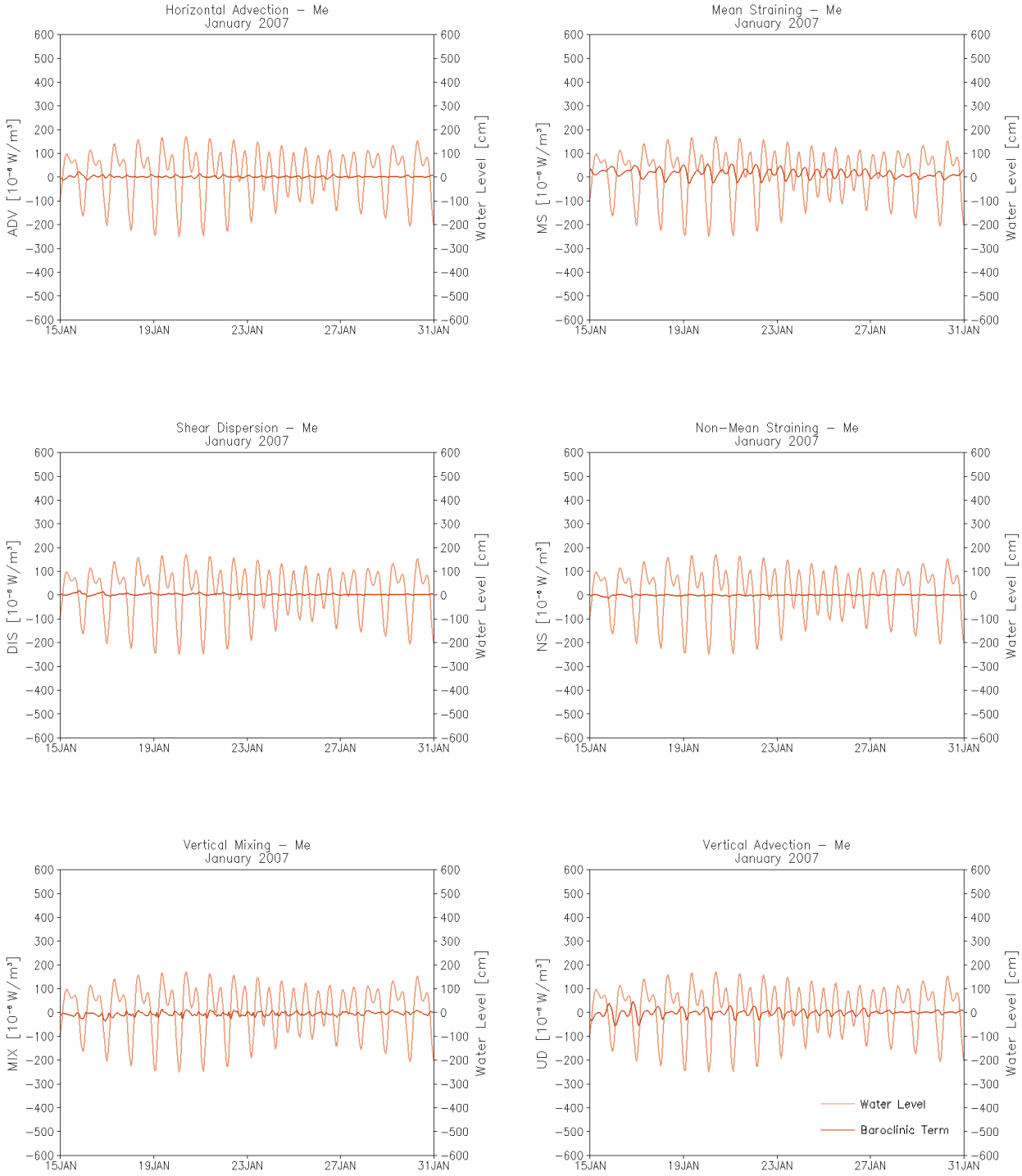

Figure 53: Time series of the baroclinic terms [10^{-6} W/m³] (dark red line) extracted from the three-dimensional dynamic PEA equation and water level [cm] (light red line) at the station 10.0° N/106.9° E (Me) for the low-flow season (January 2007). The terms in the three-dimensional dynamic PEA equation have been calculated with an artificially constant temperature (T = 28.5 °C) when determining the density via the equation of state. Positive values indicate stratification and negative values destratification.

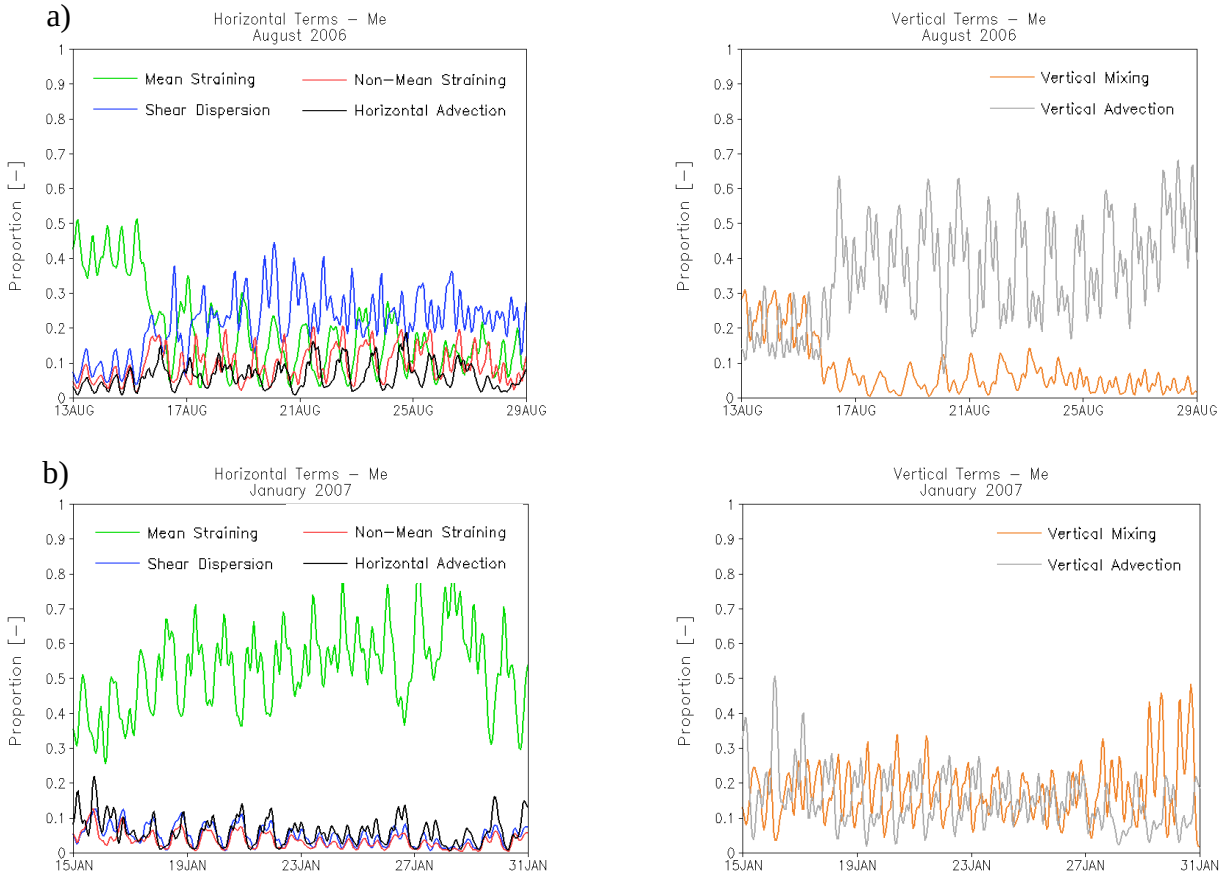

Figure 54: Time series of the proportion of the baroclinic terms in φ^*_{t3D} [-] at the station 10.0° N/106.9° E (Me) a) for the high-flow season (August 2006) and b) for the low-flow season (January 2007). The terms in the three-dimensional dynamic PEA equation have been calculated with an artificially constant temperature (T = 28.5 °C) when determining the density via the equation of state. The data is smoothed by a moving average.

In the region MeE during the high-flow season during the first four days the water column is almost mixed (Figure 42). Then for the next six days depending on the tidal cycle stratification and destratification periods alternate. Afterwards, the water column is almost mixed again, before at the end of the mapped spring-neap cycle oscillating stratified and mixed conditions prevail again.

Considering the physical processes acting during this time, the above described temporal variability is displayed in Figure 55 and Figure 57 as well. During the first four days, the regime is dominated by mean straining and to a lower extent by mixing (Figure 57). The values of these terms oscillate between negative and positive values depending on the tidal cycle (Figure 55), i.e., they act to stratify as well as to destratify the water column.

Then, a regime shift takes place as the dominance of the mean straining and the mixing term is interrupted. Horizontal processes are then dominated by horizontal advection and shear dispersion processes besides mean straining. However, also the non-mean straining term shows elevated values. It can be deduced that during this time period a river front passes the region, resulting in the temporary high proportion of the advection term to φ^*_{t3D} (Figure 57) and a large stratification input (Figure 42). Thereby, during these days the river plume front passes the area MeE several times due to tidal action which is demonstrated in the oscillating values of the advection term (Figure 55). The other terms show an oscillation between negative and positive values as well so that depending on the tidal cycle the processes force stratification or destratification of the water column.

Subsequently again, almost mixed conditions can be observed. At this time period the mean straining and the mixing term show a high proportion in φ^*_{t3D} (Figure 55 and Figure 57). At the end of the depicted time period a river plume front passes once more (decrease of mean straining and mixing, increase in horizontal advection, shear dispersion and non-mean straining).

During the period of low river discharge the water column is mixed and remains mixed (Figure 43). The values of all baroclinic terms are closed to 0 W/m³. Only mean straining and mixing show some slightly higher values during the tidal cycle (Figure 56). As Figure 57 depicts the relative contribution of the terms to φ^*_{t3D}, these slightly higher values of these two terms results in a high relative contribution.

High-flow season

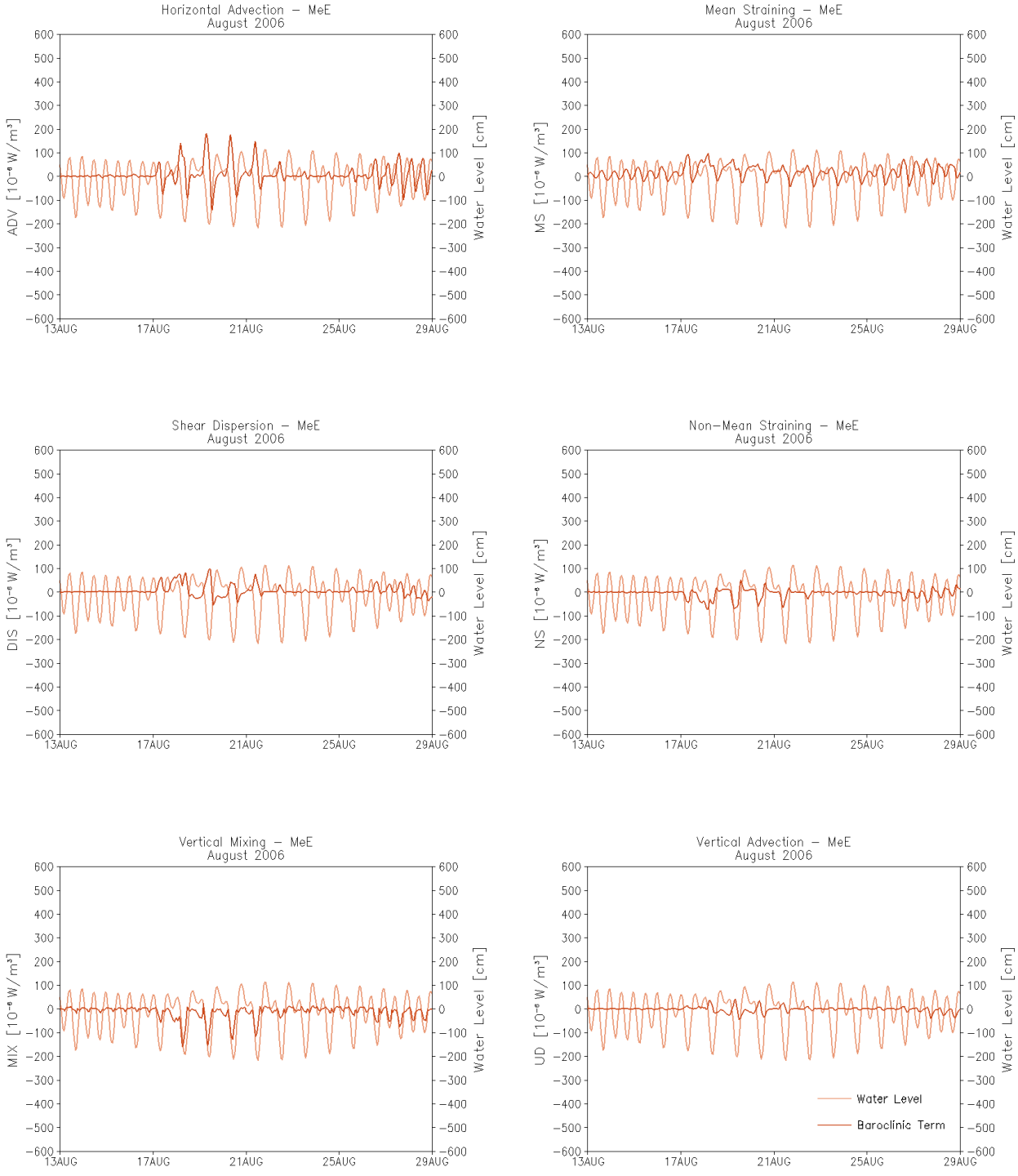

Figure 55: Time series of the baroclinic terms [10^{-6} W/m³] (dark red line) extracted from the three-dimensional dynamic PEA equation and water level [cm] (light red line) at the station 9.9° N/107.2° E (MeE) for the high-flow season (August 2006). The terms in the three-dimensional dynamic PEA equation have been calculated with an artificially constant temperature (T = 28.5 °C) when determining the density via the equation of state. Positive values indicate stratification and negative values destratification.

Low-flow season

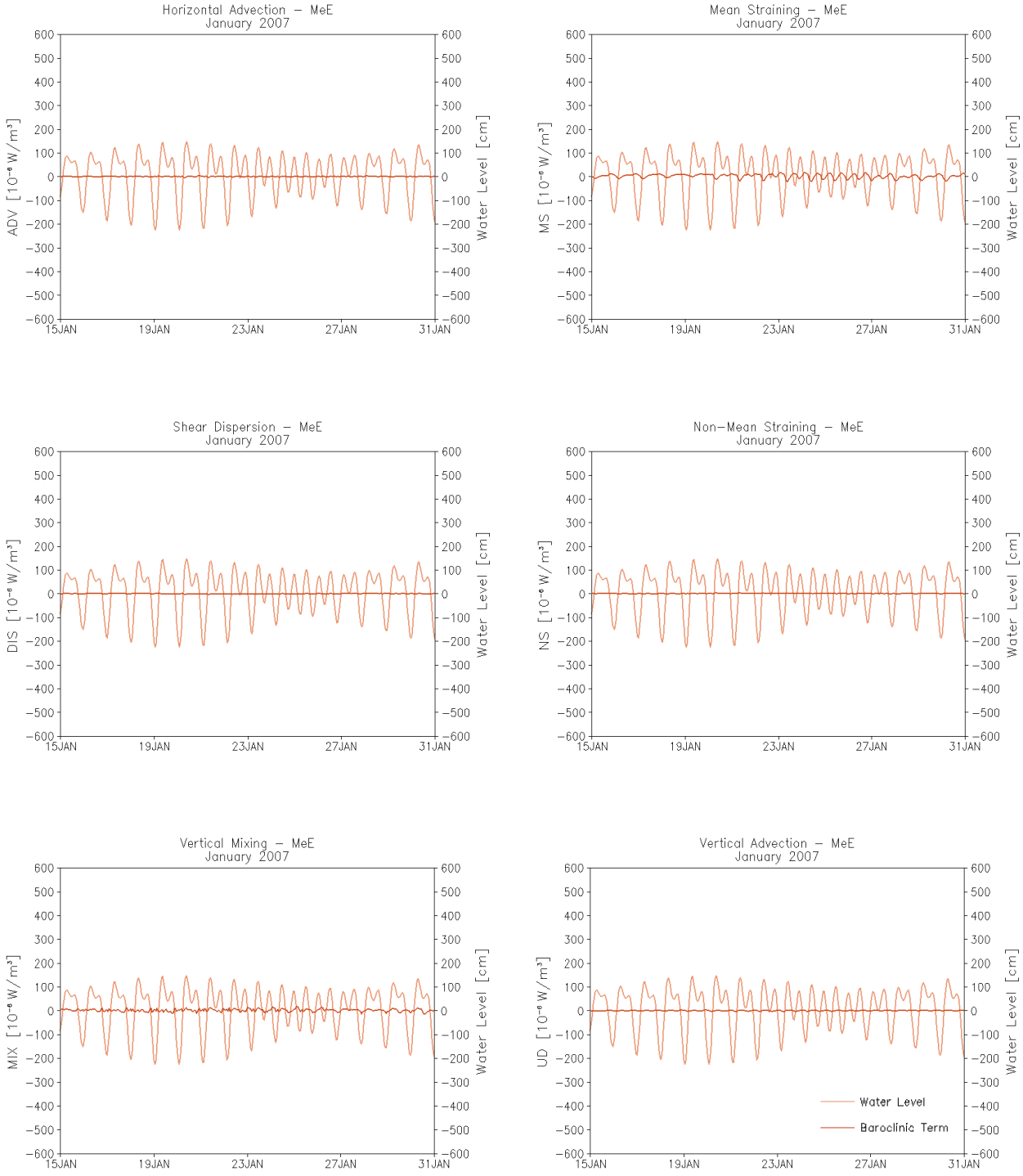

Figure 56: Time series of the baroclinic terms [10^{-6} W/m³] (dark red line) extracted from the three-dimensional dynamic PEA equation and water level [cm] (light red line) at the station 9.9° N/107.2° E (MeE) for the low-flow season (January 2007). The terms in the three-dimensional dynamic PEA equation have been calculated with an artificially constant temperature (T = 28.5 °C) when determining the density via the equation of state. Positive values indicate stratification and negative values destratification.

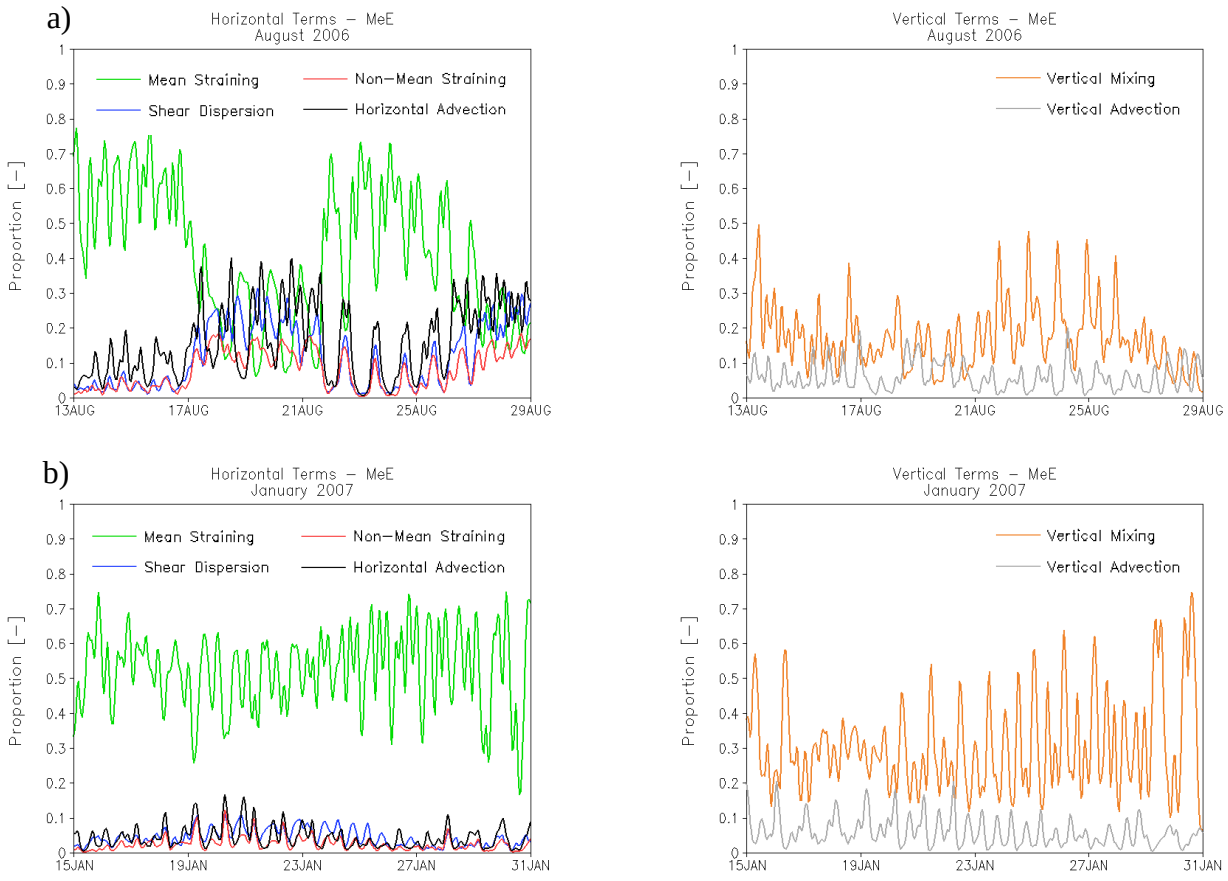

Figure 57: Time series of the proportion of the baroclinic terms in φ^*_{t3D} [-] at the station 9.9° N/107.2° E (MeE) a) for the high-flow season (August 2006) and b) for the low-flow season (January 2007). The terms in the three-dimensional dynamic PEA equation have been calculated with an artificially constant temperature (T = 28.5 °C) when determining the density via the equation of state. The data is smoothed by a moving average.

The situation in the Bassac region is as follows (Figure 58 to Figure 63):

During the high-flow season in the region BaN the main physical process that acts here is vertical advection (Figure 60). Also the mean straining contributes strongly to φ^*_{t3D}. The other baroclinic terms (mixing, shear dispersion, non-mean straining and horizontal advection) contribute less to φ^*_{t3D}, but they are also important processes in the region just off the Bassac River mouth.

Apart from the values of the mixing and the mean straining term, the values of the other terms oscillate strongly between negative and positive values (Figure 58). The mixing term shows generally negative values, i.e., the process acts to destratify the water column, whereas the mean straining term shows positive values, i.e., it acts to stratify the water column. The water column is stratified throughout the whole time period (Figure 42). However, as a consequence of the interaction of the distinct processes the regime changes periodically between slightly stratified and stratified conditions.

During the period of low river discharge the regime switches periodically between mixed and stratified conditions (Figure 43). The main physical process is mean straining, but also for the mixing term high proportion in φ^*_{t3D} can be observed. The vertical advection term shows only temporarily high proportion in φ^*_{t3D} (Figure 60). All terms show negative and positive values throughout the tidal cycle (Figure 59), i.e., depending on the tidal cycle the processes act to stratify or to destratify the water column. However, in general the mixing term and the non-mean straining term show negative values, i.e., these processes act to destratify the water column whereas the shear dispersion term shows mainly positive values, i.e., it acts to stratify the water column.

An interesting point is that during the period of high river discharge mean straining always contributes to water column stratification (Figure 58). During the period of low river discharge this is not the case. The straining process contributes to stratify but also to destratify the water column (Figure 59). Mean straining is divided into estuarine circulation and tidal straining (BURCHARD and HOFMEISTER, 2008). Tidal straining is not dependant on the seasonal freshwater input. In contrast, the estuarine circulation is. During August in comparison to January more freshwater enters the ROFI which establishes stronger horizontal density gradients. These gradients drive a more pronounced estuarine circulation which superimposes the tidal straining. Thus, at this location during both seasons both processes occur, but in August mean straining forces a stabilization of stratification due to a strongly developed estuarine circulation.

High-flow season

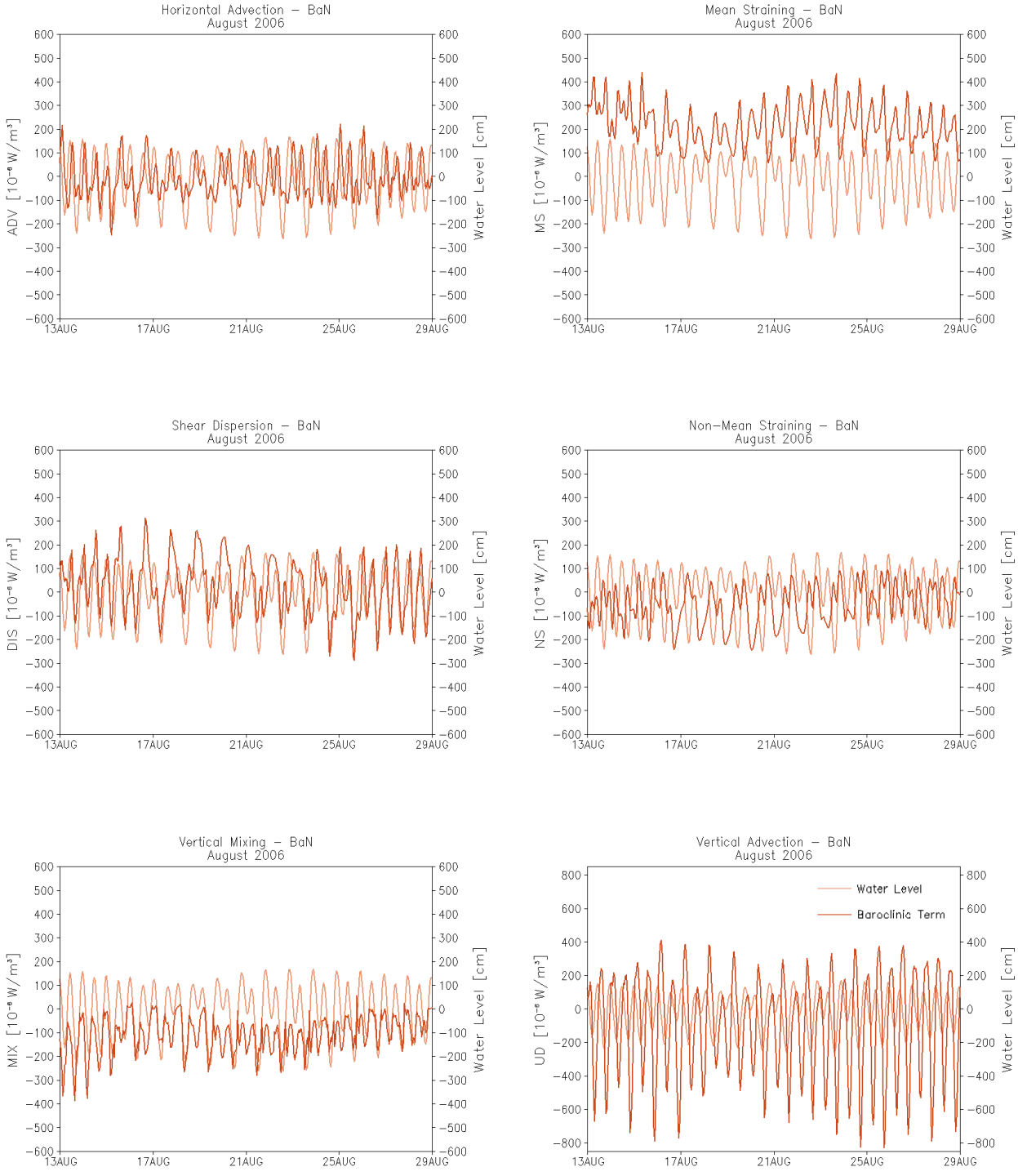

Figure 58: Time series of the baroclinic terms [10^{-6} W/m³] (dark red line) extracted from the three-dimensional dynamic PEA equation and water level [cm] (light red line) at the station 9.35° N/106.3° E (BaN) for the high-flow season (August 2006). The terms in the three-dimensional dynamic PEA equation have been calculated with an artificially constant temperature (T = 28.5 °C) when determining the density via the equation of state. Positive values indicate stratification and negative values destratification. Please note the scale of the vertical advection term is different.

Low-flow season

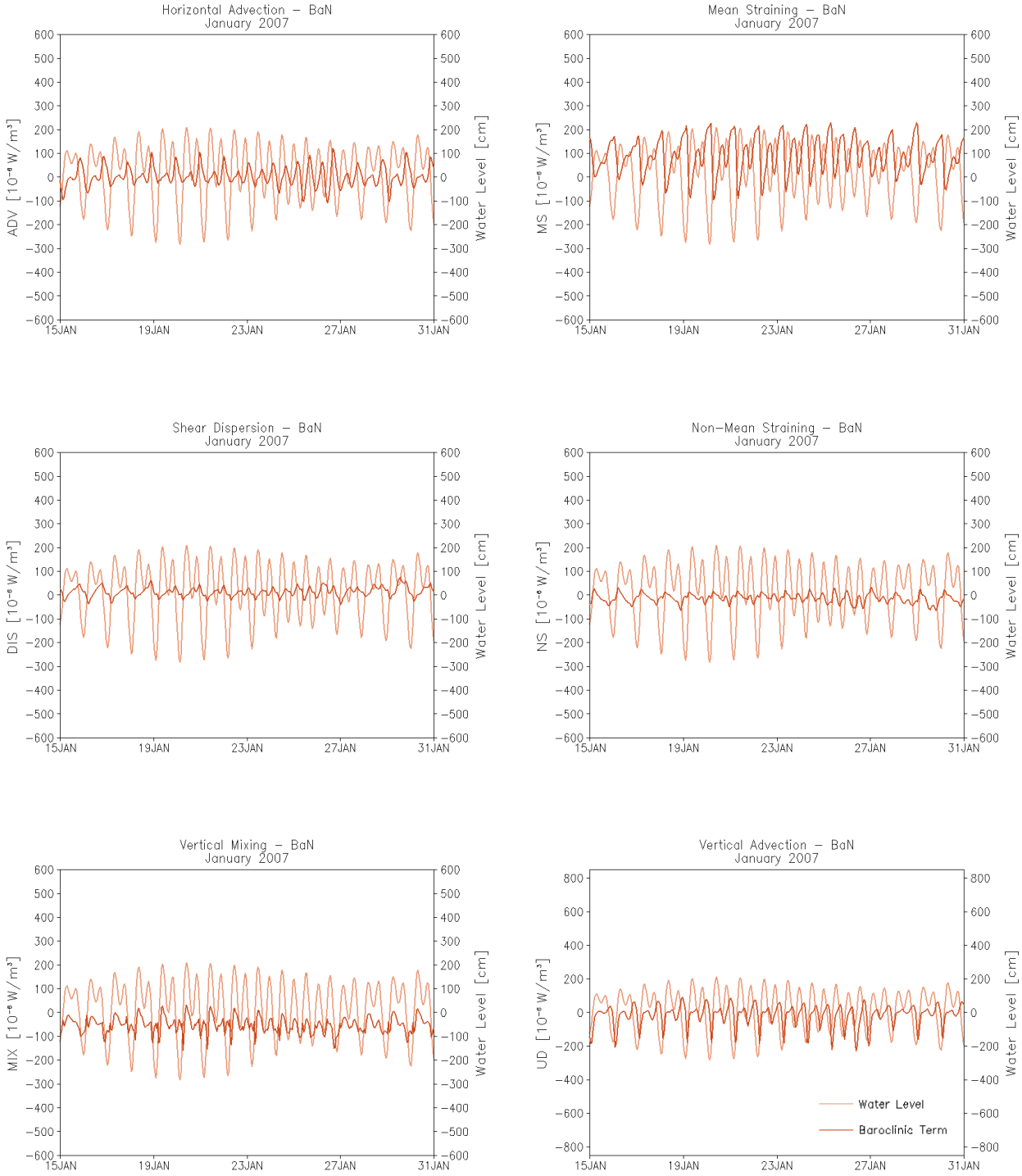

Figure 59: Time series of the baroclinic terms [10^{-6} W/m³] (dark red line) extracted from the three-dimensional dynamic PEA equation and water level [cm] (light red line) at the station 9.35° N/106.3° E (BaN) for the low-flow season (January 2007). The terms in the three-dimensional dynamic PEA equation have been calculated with an artificially constant temperature (T = 28.5 °C) when determining the density via the equation of state. Positive values indicate stratification and negative values destratification. Please note the scale of the vertical advection term is different.

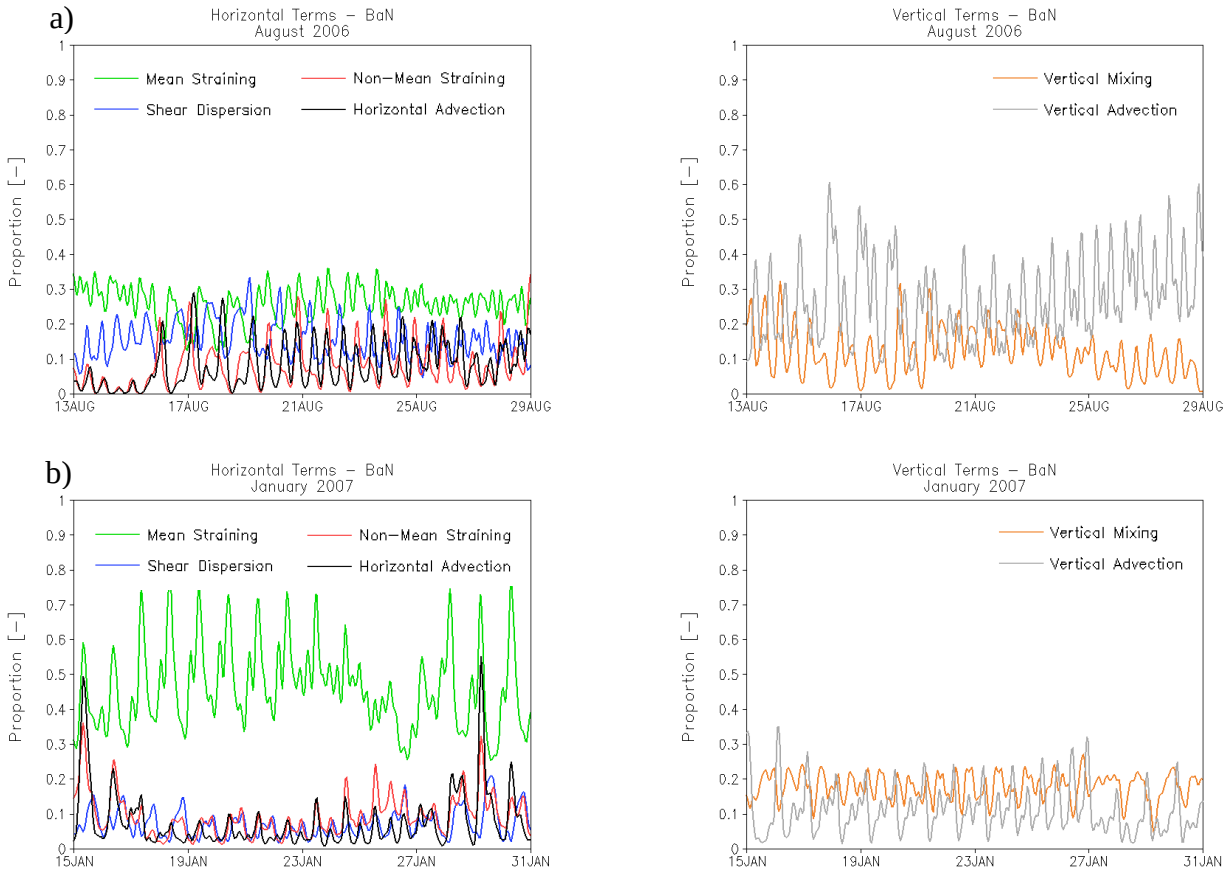

Figure 60: Time series of the proportion of the baroclinic terms in φ^{*}_{t3D} [-] at the station 9.35° N/106.3° E (BaN) a) for the high-flow season (August 2006) and b) for the low-flow season (January 2007). The terms in the three-dimensional dynamic PEA equation have been calculated with an artificially constant temperature (T = 28.5 °C) when determining the density via the equation of state. The data is smoothed by a moving average.

Further to the south of the Bassac River mouth in the region Ba during the high-flow season all baroclinic terms show positive as well as negative values throughout the tidal cycle (Figure 61). Depending on the tidal cycle the processes act to stratify or to destratify the water column. However, mean straining and shear dispersion act mainly to stratify the water column and non-mean straining acts mainly - like the mixing term - to destratify the water column.

In this region the situation during the first days differs from the situation during the remaining time period. During the first days mixing and vertical advection show elevated values (Figure 63). All horizontal processes show a contribution to φ^*_{t3D} in the same range. After three days the proportion of the vertical terms in φ^*_{t3D} decreases, whereas the contribution of the horizontal advection term to φ^*_{t3D} increases.

As opposed to the region BaN the water column changes periodically between stratified and mixed conditions (Figure 42). This gives evidence to the fact that in contrast to the area BaN this region is situated closer to the boundary of the plume where the influence of the buoyancy freshwater input is reduced and stirring can cause a complete mixing of the water.

It is interesting that in contrast to the area BaN in this area mean straining does not basically act to stratify the water column (Figure 61). This suggests that although the freshwater input in August is very high, in this area the estuarine circulation - and the resulting stratification input - is less important. The area Ba lies further at the boundary of the plume than the area BaN.

During the low-flow season, in the region Ba the water column oscillates between stratified and mixed conditions (Figure 43). The φ^*_{t3D} signal is dominated by mean straining and depending on the tidal cycle by up/downwelling as well as mixing (Figure 63). The mean straining term is mainly greater than 0 W/m³, i.e., it acts to stratify the water column which gives evidence of an estuarine circulation (Figure 62). This effect is overlaid by tidal straining which acts in both directions as it can be recognized by the oscillation between negative and positive values.

High-flow season

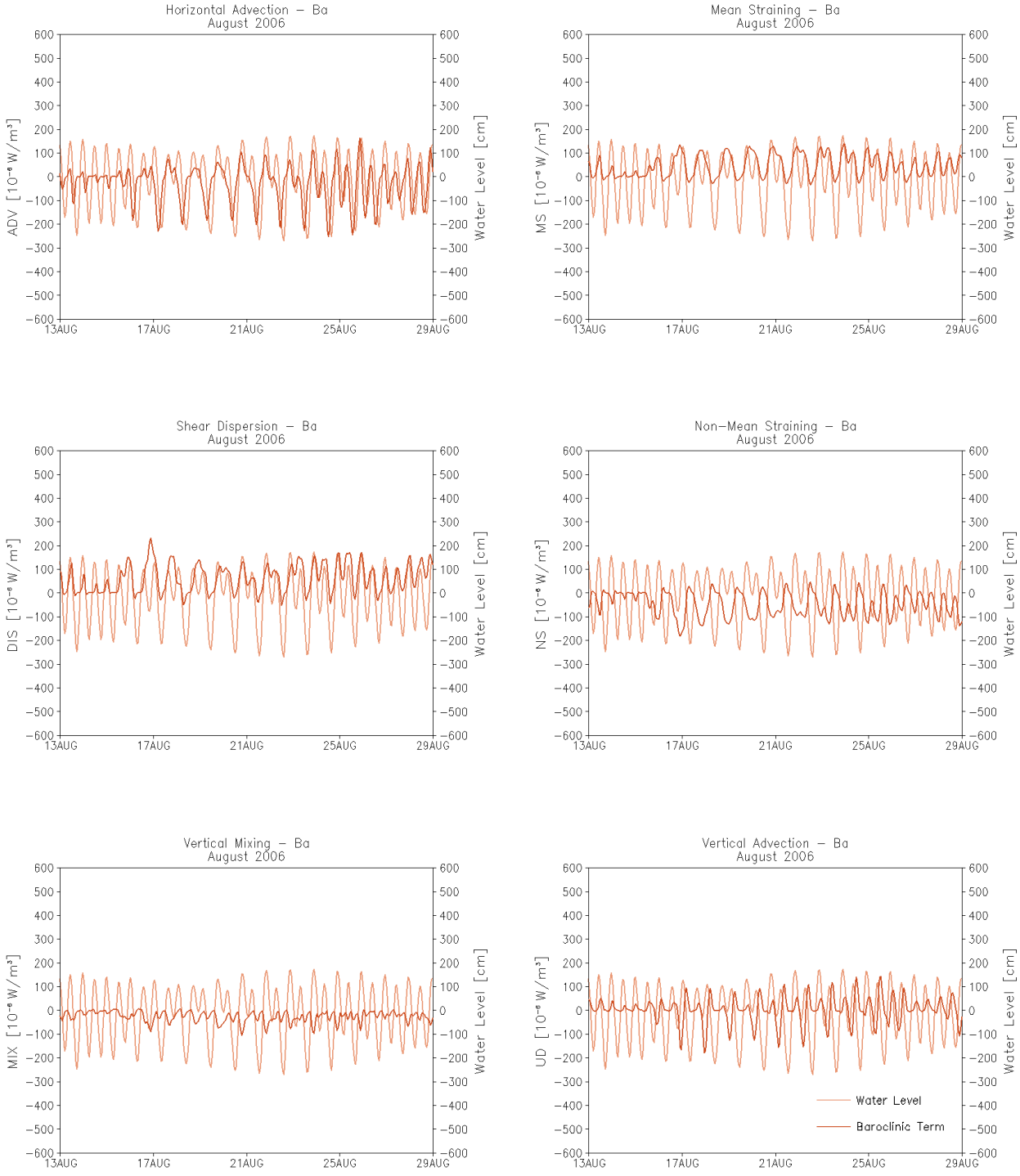

Figure 61: Time series of the baroclinic terms [10^{-6} W/m³] (dark red line) extracted from the three-dimensional dynamic PEA equation and water level [cm] (light red line) at the station 9.25° N/106.2° E (Ba) for the high-flow season (August 2006). The terms in the three-dimensional dynamic PEA equation have been calculated with an artificially constant temperature (T = 28.5 °C) when determining the density via the equation of state. Positive values indicate stratification and negative values destratification.

Low-flow season

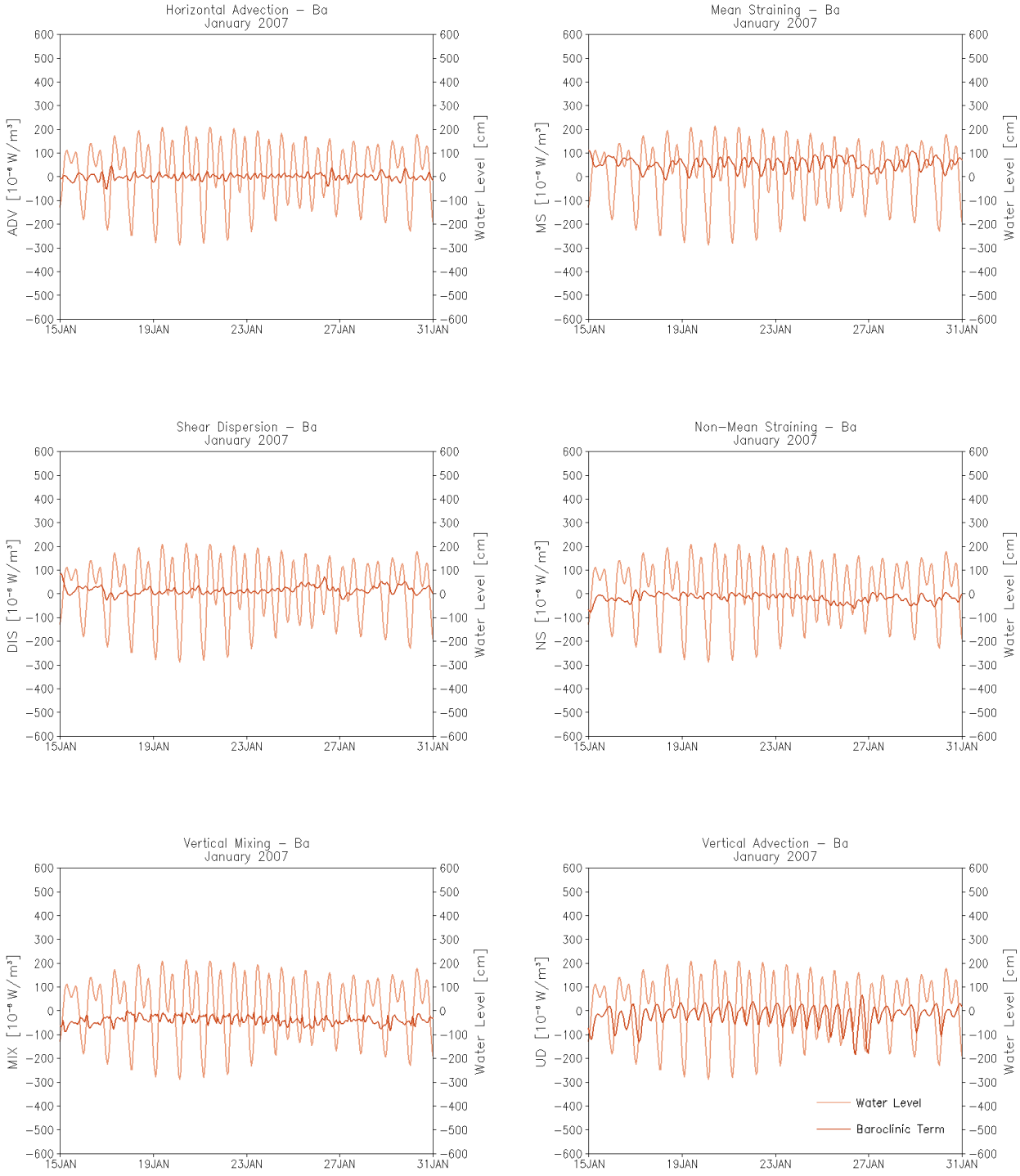

Figure 62: Time series of the baroclinic terms [10^{-6} W/m³] (dark red line) extracted from the three-dimensional dynamic PEA equation and water level [cm] (light red line) at the station 9.25° N/106.2° E (Ba) for the low-flow season (January 2007). The terms in the three-dimensional dynamic PEA equation have been calculated with an artificially constant temperature (T = 28.5 °C) when determining the density via the equation of state. Positive values indicate stratification and negative values destratification.

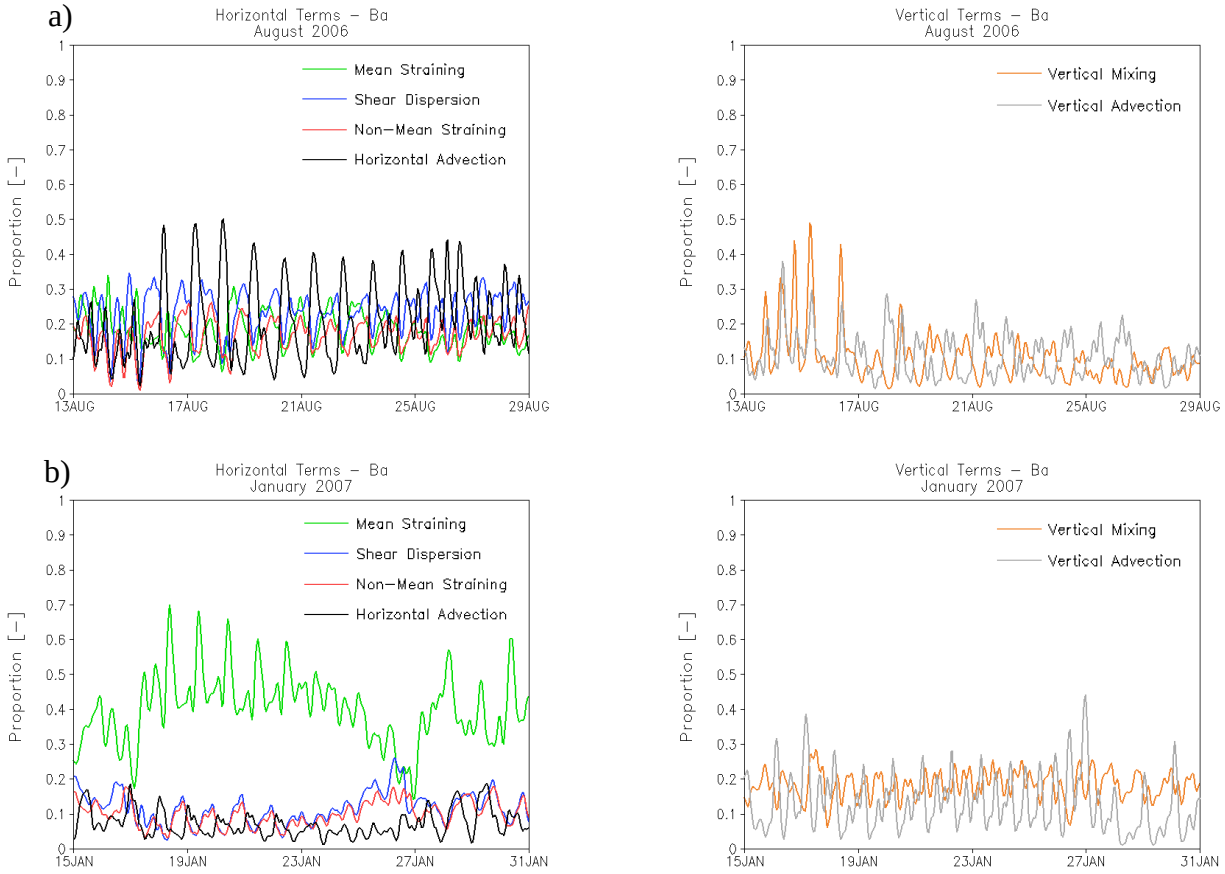

Figure 63: Time series of the proportion of the baroclinic terms in φ^*_{t3D} [-] at the station 9.25°N/106.2°E (Ba) a) for the high-flow season (August 2006) and b) for the low-flow season (January 2007). The terms in the three-dimensional dynamic PEA equation have been calculated with an artificially constant temperature (T = 28.5 °C) when determining the density via the equation of state. The data is smoothed by a moving average.

Figure 64 shows the time series for the area CC during the period of high river discharge, whereas Figure 65 depicts the situation during low river discharge. The area is representative for the southward directed baroclinic current during the winter monsoon. During the summer monsoon the plume is directed toward E/NE so that during this season there is no influence of the freshwater buoyancy input in this region.

Generally during the period of high river discharge all baroclinic terms have a value close to 0 W/m³ (Figure 64), i.e., the degree of stratification of the water column does not change notably with time. As can be concluded from Figure 42 the water column is mixed and remains mixed. Although the baroclinic terms show values close to 0 W/m³, in relation to the other terms the vertical terms contribute most to φ^*_{t3D} (Figure 66a).

During the period of low river discharge the most important baroclinic process contributing to φ^*_{t3D} is mean straining (Figure 66). Mixing and vertical advection play a minor role. The other baroclinic terms do not have a remarkable influence on the change in stratification of the water column in this region.

During this season mean straining acts periodically in both directions – in stratifying and destratifying the water column (Figure 65). The same is true for the vertical processes. The water column changes between mixed and slightly stratified conditions (Figure 43).

In section 5.3 it has been mentioned that during the low-flow season a strong relationship exists between the tidal phases and the stratification of the water column (local maximum at lower low water and local minimum at higher high water) for the majority of the regions (Figure 43). Summarizing the Figure 52 to Figure 66 it can be deduced that during the low-flow season mean straining is the dominant process in all regions except in the region MeE where no change in stratification occurs. Mean straining is caused by estuarine circulation and tidal straining (BURCHARD and HOFMEISTER, 2008).

However, during the period of high river discharge the relationship (local maximum at lower low water and local minimum at higher high water) between the tidal phases and the stratification of the water column is only apparent in the region MeE, Me and BaN. The region Ba shows a different relationship between the tidal cycle and the change in stratification whereas the region CC shows no change in stratification. Figure 52 to Figure 66 depicts that during the high-flow season the absolute dominance of mean straining – like it is the case during the low-flow season – is only temporary true for the region MeE. If considering solely the horizontal processes, in the region BaN the horizontal governing process is mean straining as well. In the region Me the main horizontal physical process acting is shear dispersion. However, in total vertical advection dominates both regions (BaN and Me). In the region Ba horizontal advective processes play a major role. Stratification by advection is not induced by a vertical velocity shear but it can be interpreted as the transport of a stratified water column into the region Ba.

High-flow season

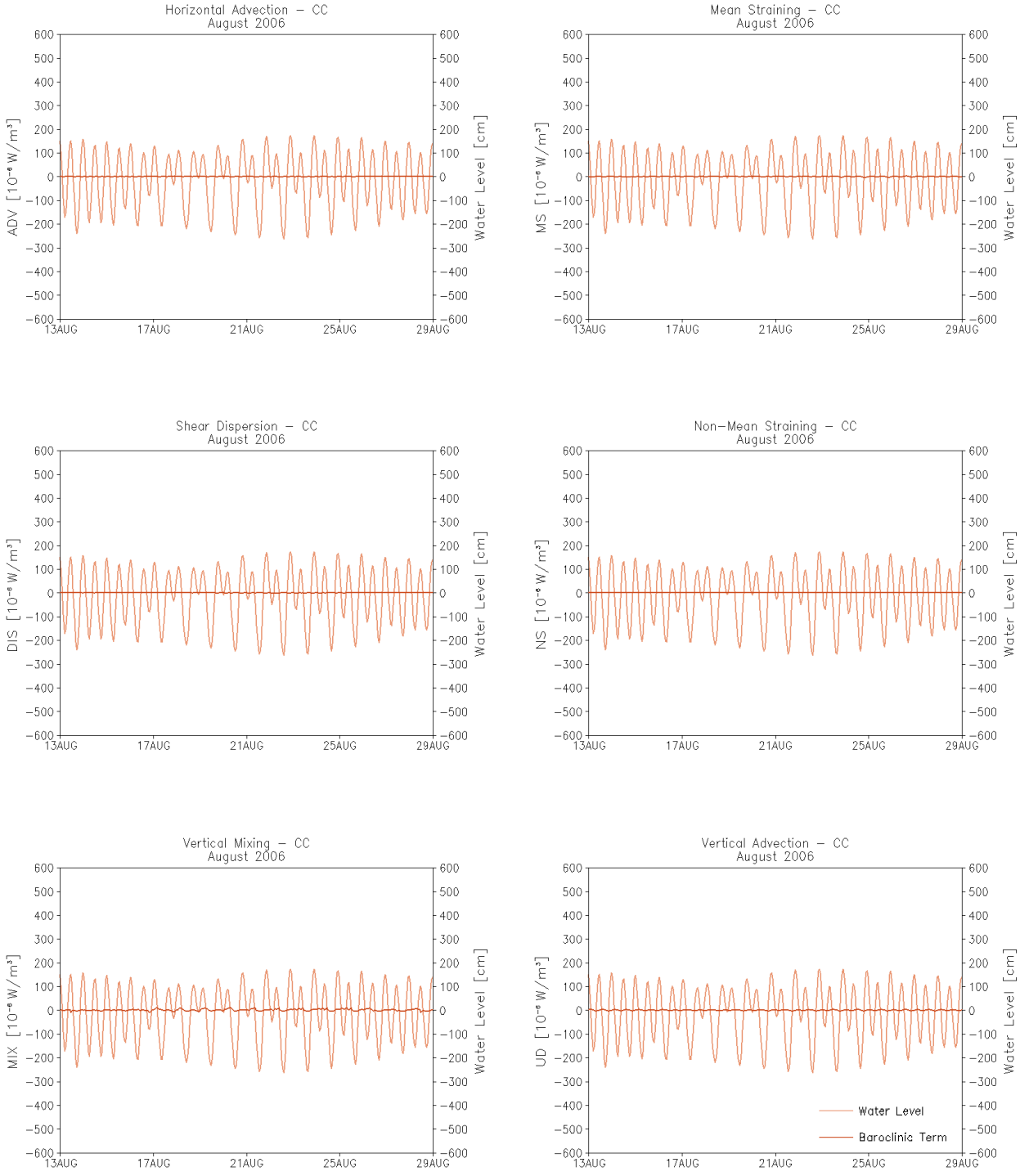

Figure 64: Time series of the baroclinic terms [10^{-6} W/m³] (dark red line) extracted from the three-dimensional dynamic PEA equation and water level [cm] (light red line) at the station 9.0° N/106.05° E (CC) for the high-flow season (August 2006). The terms in the three-dimensional dynamic PEA equation have been calculated with an artificially constant temperature (T = 28.5 °C) when determining the density via the equation of state. Positive values indicate stratification and negative values destratification.

Low-flow season

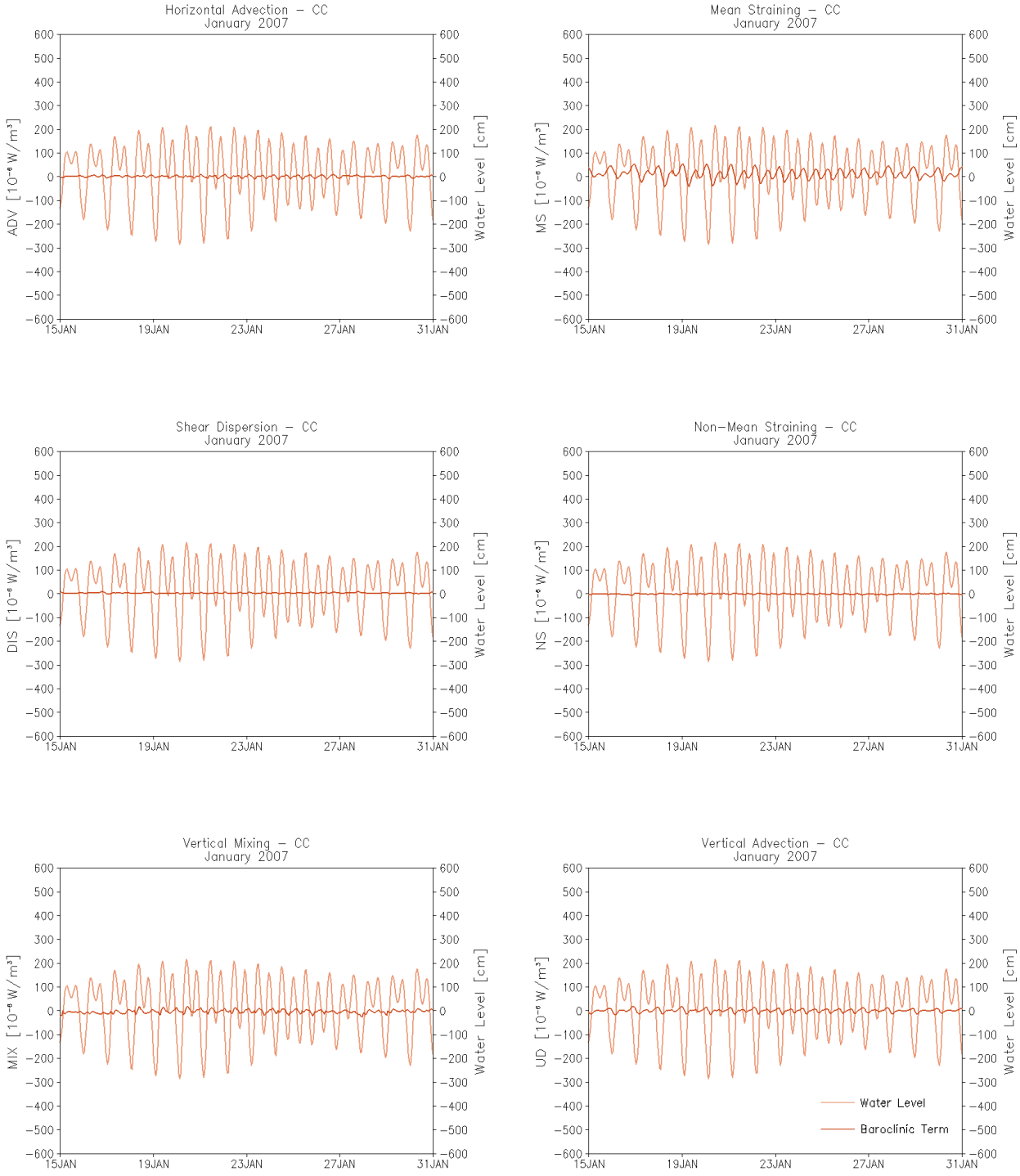

Figure 65: Time series of the baroclinic terms [10^{-6} W/m³] (dark red line) extracted from the three-dimensional dynamic PEA equation and water level [cm] (light red line) at the station 9.0° N/106.05° E (CC) for the low-flow season (January 2007). The terms in the three-dimensional dynamic PEA equation have been calculated with an artificially constant temperature (T = 28.5 °C) when determining the density via the equation of state. Positive values indicate stratification and negative values destratification.

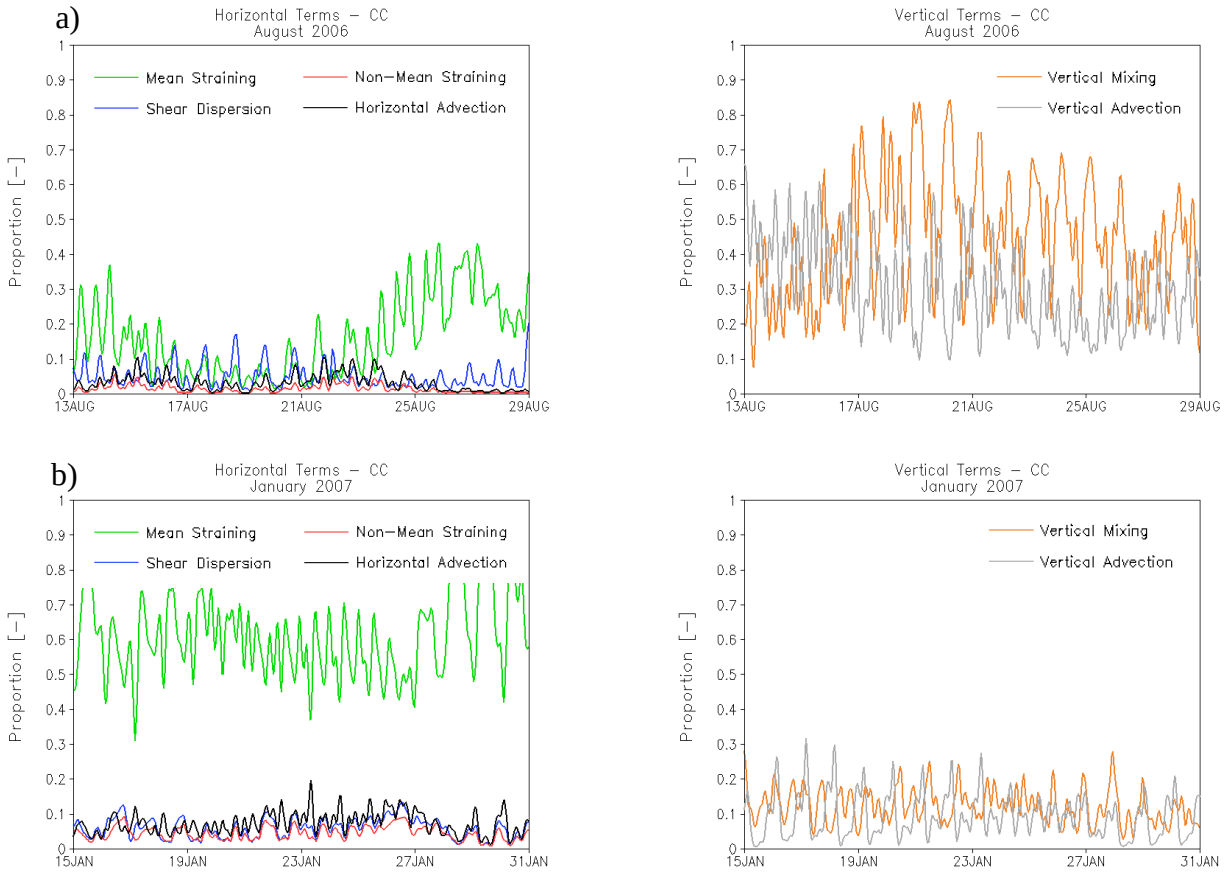

Figure 66: Time series of the proportion of the baroclinic terms in φ^*_{t3D} [-] at the station 9.0° N/106.05° E (CC) a) for the high-flow season (August 2006) and b) for the low-flow season (January 2007). The terms in the three-dimensional dynamic PEA equation have been calculated with an artificially constant temperature (T = 28.5 °C) when determining the density via the equation of state. The data is smoothed by a moving average.

CHAPTER 6

DISCUSSION

In this study, the main physical processes being responsible for the spreading of the freshwater plume in the Mekong ROFI are determined. A synthesis of these processes changing the stratification of the water column during the different seasons is the basis for applied regional studies of the impact of climate change, sediment management and ecology. Both time scales are comparatively examined.

In order to get an idea about the particularities of the tropical Mekong ROFI, the results of the three-dimensional dynamic equation for potential energy anomaly in the Mekong ROFI are considered in context to those in other regions.

6.1 CIRCULATION AND PLUME EXTENSION DURING THE LOW-FLOW SEASON AND THE HIGH-FLOW SEASON

CURRENTS

During the winter monsoon during the second half of January the results show a pronounced baroclinic coastal current which is created by the input of low-density water from the Mekong River. The current is weak in the region off the upper river mouth, but develops to a strong baroclinic current in the region to the south of the Tranh De branch. The main current flows off the shallow coastal area to the SE of Zhongnan Peninsula. The surface currents head towards SW (Figure 31a).

Also HORDOIR et al. (2006) found a baroclinic current which stays off the shallow coastal area. The authors stated that the baroclinic current is mainly created by the four southernmost mouths of the Mekong River. They explained the weakness of the baroclinic current in the region adjacent to the upper Mekong River mouths by the shallow bottom extending far offshore. During the NE monsoon in March and at the end of October the flow heads towards SW.

HORDOIR et al. (2006) show the hydrodynamics during the onset of the winter monsoon at the end of October as well as during the decay of the monsoon in March. Because of the larger river discharge at the end of October, the baroclinic current is more pronounced and the velocities are around 0.3 m/s. These surface velocities are larger than in March (0.1 m/s). Figure 31c shows

that the surface velocities of the baroclinic current in January are about 0.2 m/s. This seems reasonable as the discharge decreases from October until April. It is also obvious from Figure 31a that the basin-wide circulation follows roughly the shelf edge which is directed to the S/SW. GAN and QU (2008) showed the existence of a coastal jet flowing along the shelf edge in southward direction during winter. Hence, during winter the baroclinic circulation in the Mekong ROFI is separated from the basin-wide circulation.

On the contrary during the summer monsoon the baroclinic circulation and the basin-wide circulation converge in the region off the Mekong River. The currents of the basin-wide circulation head mainly towards NE which is the direction of wind stress. The currents of the plume in the vicinity of the river mouths are directed towards E/SE. However, the further offshore parts of the plume show currents heading towards E/NE (Figure 35a).

GAN and QU (2008) also found a northeastward coastal jet east of Zhongnan Peninsula that separates from the coast at about 12° N. The jet is driven mainly by the southwestly monsoonal wind stress over the shelf in the southern part of the SCS and the western intensification. HORDOIR et al. (2006) also stated that during the SW monsoon during the first days of October outside the river plume area the surface currents follow the wind stress direction, i.e., they are directed towards NE. Inside the river plume area the currents head mainly towards SE which is opposed to the situation shown in Figure 35a. The difference can be explained by the fact that the month of October is a transition period between the two monsoon phases so that the circulation is relatively unstable and changes often in strength and direction. The summer circulation is not fully developed so that the currents do not flow in direction of wind stress. However, in August, which is the investigation period of this study, the NE monsoon is fully developed. Relatively high wind stress and the steady basin-wide circulation yield the typical summer circulation with a plume heading towards NE (Figure 35a).

Considering the surface current velocities in Figure 35c it is shown that during the summer monsoon they are strong in the whole model area, except in the coastal area of the SROFI. HORDOIR et al. (2006) also found strong currents in the river plume and small currents in the coastal region of the SROFI. However, they also simulated small currents in the shelf region of the SROFI. The difference can be related to the distinct simulation periods as well. HORDOIR et al. (2006) considered the month of October which is a transition period between the two monsoon phases, whereas the month of August represent a typical summer monsoon situation.

SALINITY AND TEMPERATURE

During the NE monsoon in January the freshwater plume extends to the SW (Figure 32a). The surface to bottom salinity difference is high in the MPR of the NROFI and lower in the MPR of the SORFI. Both regions are stratified due to the freshwater buoyancy input. On the contrary, in the coastal area and in the shelf region the surface to bottom salinity difference is small, i.e., the water column is mixed.

This vertical salinity distribution is also represented in the study of HORDOIR et al. (2006): During the NE monsoon in March a vertical salinity gradient is evident in the MPR of the NROFI (their figure 6). In the SROFI the water column is completely mixed in the shallow coastal area and slightly stratified in the baroclinic current (their figure 7). The authors concluded that as the area is rather shallow, stratification is destroyed by vertical mixing.

However, during the NE monsoon at the end of October the plume is wider and stratification in both, the coastal area and the MPR of the SROFI, is higher than in March (their figure 10 and 11). Unlike the study of HORDOIR et al. (2006) this study shows that in the coastal area of the SROFI a vertical salinity gradient is absent (Figure 34a). The lower stratification in the coastal region of the SROFI in January is a consequence of the lower freshwater input during January compared to October. From October until April the discharge decreases considerably (Figure 13).

During the SW monsoon in August the plume heads toward NE, i.e., contrary to the direction of Kelvin wave propagation (Figure 36a). Although the Coriolis force causes a south-/southwestward deflection of the Mekong River plume, the prevailing flow direction is towards NE. The inherently south-/southwestward deflected current is balanced by the seasonal prevailing northeastward monsoon winds and by the current of the basin-wide circulation and consequently heads towards NE in the shelf region. The smaller Coriolis parameter in the tropics (near the equator) may influence the reversal of the plume (NIKIEMA et al., 2007). Thus a smaller opposing force, like e.g. wind stress, is needed to reverse the river plume.

GARCIA BERDEAL et al. (2002) studied the influence of wind stress and ambient flow on the plume direction of the Columbia River. They observed that the direction of the Columbia River plume changes with the seasons like it is the case for the Mekong River plume. During winter the Columbia River plume heads usually towards N which is the direction of Kelvin wave propagation. The prevailing wind and the coastal current are also directed northward. During summer the Columbia River plume heads towards SW, which is contrary to the direction of Kelvin wave propagation. The prevailing winds and coastal currents are to the S.

Figure 36a shows that the plume during the SW monsoon is broader than during the winter monsoon. The figures of HORDOIR et al. (2006) show that during the first days in October a strongly stratified river plume broadly extends over the shelf (their figure 8 and 9). However, their figure 8 shows a much more extended plume than the Figure 36a. The difference can be explained by the different periods which are considered. As mentioned above during October, which is their investigation period, the monsoon starts to change and so does the circulation whereas during August, which is the investigation period of this study, the SW monsoon is fully developed. The basin-wide circulation with currents heading towards NE constrains the plume to the coast (GAN and QU, 2008).

Considering the modelled temperature during the summer monsoon the values are between 28 °C and 29 °C in the offshore part of the investigation area (Figure 36b). However, in the

coastal area where the water is shallow the temperature is raised (> 29 °C). XIE et al. (2003) shows the temperature distribution by AVHRR SST climatology for August (their figure 3). Here, the temperature in the region of the investigation area is also between 28 and 29 °C. However, the elevated temperatures in the coastal area are not represented by the satellite data.

During the winter monsoon the temperatures are between 27 °C in the coastal area and 24 °C in the furthest offshore part of the investigation area (Figure 32b). Thus, there is a strong horizontal temperature gradient from the coast to the shelf edge. This gradient can be explained by the separation of the southward coastal jet from the coast of central Vietnam at around 11.5° N. Further to the south the jet follows the shelf edge (GAN and QU, 2008) and the Mekong ROFI is not influenced by the relative cold water which is transported by the jet from the Northern SCS towards the south. Additionally, the separation of the jet is related to upwelling of cold water (HEIN, 2007).

6.2 STRATIFICATION IN THE MEKONG ROFI ON THE SEASONAL AND ON THE TIDAL TIME SCALE

By means of the one-dimensional equation for the potential energy anomaly the stability of the water column has been quantified. φ_{1D} reflects the work required to mix a water column instantaneously.

Considering the results on a seasonal time scale during both monsoon phases the area of strongest stratification can be found in the MPR (Figure 40 and Figure 41). The surface to bottom salinity difference shows the same picture (Figure 34 and Figure 38). The influence of temperature on the stability of the water column can be neglected in the MPR (Figure 40 and Figure 41). However, at the shelf edge the influence of temperature is evident which can be related to upwelling processes (HEIN, 2007).

Considering the results on a tidal time scale during the high-flow season in the regions BaN, Me and MeE maximum stratification occurs close to the time of lower low water, whereas a minimum occurs close to the time of higher high water. The study of SIMPSON (1997) showed a similar dynamic in the Liverpool Bay. In the Liverpool Bay the tides are dominated by a standing wave. In general, the tides can also be dominated by a progressive Kelvin wave like it is the case in the Rhine ROFI for example. Then, minimum (maximum) stratification is observed at low (high) water.

It can be concluded that at the region BaN, Me and MeE the tides are rather dominated by a standing wave (maximum stratification at lower low water, minimum stratification at higher high water) like it is the case in the Liverpool Bay than by a progressive wave. At the Region Ba the instant of time of the local maximum and minimum is hard to determine. Maximum stratification occurs around higher low water until the ebb tide after lower high water and a local minimum occurs around lower low water until flood tide after lower low water. Here, the tides seem to be dominated neither by a standing wave nor by a progressive wave. However, the

results of section 5.4.2 show that in the region Ba horizontal advective processes play a major role. An analysis of the tidal induced dynamic is difficult due to a superposition of different processes.

However, comparing the occurrence of stratification within a tidal cycle with the measured dynamics of the mooring station during the field trip in April 2007 (Figure 26), it seems that the results are contradictory. At this location (9.26° N, 106.31° E) minimum stratification has been observed at low water and maximum stratification at high water. These characteristics correspond to a system which is rather influenced by a progressive Kelvin wave than by a standing wave.

The apparent inconsistency can be clarified when regarding the study of ZU et al. (2008). In his figure 2b it is depicted that in the region of the NROFI, where the regions BaN, Me and MeE rather form part of, the tidal ellipses of the M_2 tide are rather perpendicular to the coast which argues for a standing wave. Further to the south, i.e., in the SROFI, where the mooring station of the field trip rather is located, the form of the tidal ellipses changes, showing the influence of a coast-parallel component. Region Ba is situated in between these two areas which may explain why the relation between the tidal cycle and stratification is more complex – additionally to the superposition of several physical processes.

Regarding the occurrence of stratification throughout a spring-neap cycle, in the Liverpool Bay ROFI maximum stratification is observed 2–3 days after neap. At spring tide the water column is completely mixed (SHARPLES and SIMPSON, 1995). Regarding Figure 47 and Figure 48 these characteristics are also visible for the region BaN during both monsoon seasons and for the region Ba during the winter monsoon. At the time around neap tide φ_{1D} shows maximal values and around spring tide minimal ones.

However, during the summer monsoon Ba shows a different relationship between the tidal cycle and the change in stratification which in a first approximation appears to be random. The random behaviour of stratification and destratification is caused by horizontal advection (Figure 61 and Figure 63). During the period of dominant diurnal tide the flow direction is constant over a longer time period than during the period of dominant semidiurnal tide. Thus, during the period of dominant diurnal tide the displacement of a water column caused by horizontal advection is increased. During this period also φ_{1D} is highest which results from the advection of more stratified water than at times of dominant semidiurnal tide. At the other regions (CC, MeE and Me) no pronounced relationship exists.

HANSEN AND RATTRAY (1966) classified estuaries in different types of stratified systems/salt-wedge type, partially stratified systems and well-mixed systems. If we apply and simplify the classification for the ROFI we can remark that

1) during the high-flow season the Mekong ROFI is a stratified system because the water column is stratified during the whole tidal period in the regions closest to the river mouth (Me and BaN) and

2) during the low-flow season the Mekong ROFI is a partially stratified system because the system switches between mixed and stratified conditions in these regions.

6.3 DOMINANT PHYSICAL PROCESSES IN THE MEKONG

In the following sections the dominant physical processes for each time scale are revealed to discover the differences between the scales. The dominant processes which act in the different regions of the Mekong ROFI are sketched for each time scale.

6.3.1 SYNTHESIS FOR THE SEASONAL TIME SCALE

To assess the physical processes that dominate the different regions of the Mekong ROFI on a seasonal time scale, the long-term contributions of the six individual baroclinic terms to φ^*_{t3D} are investigated.

For example, the calculation for the mean straining term is as follows.

$$MS_{mean} = \left| \frac{1}{n} \sum_{t=1}^{t=t\max} (MS_x(t)) \right| + \left| \frac{1}{n} \sum_{t=1}^{t=t\max} (MS_y(t)) \right| \tag{6.1}$$

$$\begin{aligned} \varphi^*_{t3D\_mean} = & \left| \frac{1}{n} \sum_{t=1}^{t=t\max} (MS_x(t)) \right| + \left| \frac{1}{n} \sum_{t=1}^{t=t\max} (MS_y(t)) \right| + \left| \frac{1}{n} \sum_{t=1}^{t=t\max} (NS_x(t)) \right| \\ & + \left| \frac{1}{n} \sum_{t=1}^{t=t\max} (NS_y(t)) \right| + \left| \frac{1}{n} \sum_{t=1}^{t=t\max} (ADV_x(t)) \right| + \left| \frac{1}{n} \sum_{t=1}^{t=t\max} (ADV_y(t)) \right| \\ & + \left| \frac{1}{n} \sum_{t=1}^{t=t\max} (DIS_x(t)) \right| + \left| \frac{1}{n} \sum_{t=1}^{t=t\max} (DIS_y(t)) \right| + \left| \frac{1}{n} \sum_{t=1}^{t=t\max} (MIX_z(t)) \right| \\ & + \left| \frac{1}{n} \sum_{t=1}^{t=t\max} (UD_z(t)) \right| \end{aligned} \tag{6.2}$$

$$MS_{season} = \frac{MS_{mean}}{\varphi^*_{t3D\_mean}} \tag{6.3}$$

with $MS_{x/y}$ the mean straining term, $DIS_{x/y}$ shear dispersion, $ADV_{x/y}$ horizontal advection, $NS_{x/y}$ non-mean straining, MIX_z vertical mixing, UD_z.vertical advection, t time step and n number of values. The calculation of the other terms is done analogously.

The calculation of $\varphi^*_{t3D\ -mean}$ is done with the absolute values of the individual terms which can be positive or negative so that they can cancel each other. The absolute value of φ^*_{t3D} can be lower than the absolute value of the individual terms.

Figure 50 and Figure 51 show if a process acts to stratify or to destratify the water column in the long-term. However, it is not possible to disclose the relative proportion of the different terms in φ^*_{t3D} and thus the governing processes for the different regions of the Mekong ROFI. This is possible by means of equation 6.1 to 6.3.

Figure 67 shows the situation during the high-flow season. In the MPR and in the coastal region of the NROFI the proportion of the mean straining term in φ^*_{t3D} is mainly > 30 %. If the mean straining term is averaged over one spring-neap cycle, it can be deduced that the process acts to stratify the water column during the high-flow season (Figure 50). However, during a spring-neap cycle it is also possible that the process acts to destratify the water column (Figure 55 and Figure 61). Mean straining is caused by both estuarine circulation and tidal straining.

Considering the mixing term in the MPR and in the coastal region of the NROFI it generally shows a proportion of about 10–30 % in φ^*_{t3D}. However, in the coastal region of the SROFI the proportion of the mixing term in φ^*_{t3D} increases to values > 30 %. Vertical mixing acts as a destratifying agent in the MPR. Surprisingly, in the coastal region the mixing term shows positive contributions to φ^*_{t3D} which gives evidence of an unstable stratification (Figure 50). HORDOIR et al. (2006) stated that in the Mekong ROFI there is a strong interaction between the bottom friction and the river plume. Therefore tidal mixing – due to the interaction of tidal dynamics with the bottom (friction) – influences the stratification of the plume.

The shear dispersion term also plays a main role in great parts of the MPR. Here, the proportion of the shear dispersion term in φ^*_{t3D} is about 10–30 %. However, in the region off the river mouths and to the north of the MPR the proportion is < 10 %. In the MPR shear dispersion mainly acts to stratify the water column. However, off the river mouth and to the north of the MPR the water column is destratified due to shear dispersion (Figure 50).

The non-mean straining term shows a similar pattern to that of the shear dispersion term and large part of the MPR shows a proportion in φ^*_{t3D} of about 10–30 %. Non-mean straining acts opposite to shear dispersion so that it is a destratifying agent in the MPR and a stratifying agent in the region off the river mouths and to the north of the MPR (Figure 50).

Horizontal advection and vertical advection play only locally a role with a proportion of about 10–30 %. The horizontal advection term shows elevated values near the S/SE boundary of the river plume. In this region advection of a stratified as well as of a mixed water column takes place. In the coastal region of the NROFI horizontal advection of a mixed water column takes place (Figure 50). The vertical advection term holds values of about 10–30 % off the river mouths (Figure 67) where upwelling occurs (Figure 50). Also in the MPR upwelling happens. But in this region the vertical advection term plays only a minor role as its proportion in φ^*_{t3D} is < 10 %. HORDOIR et al. (2006) show that during the SW monsoon the wind tends to create an Ekman transport away from the coast (upwelling).

Figure 69 summarizes these findings as a synthesis of the dominant processes.

Additional to the stratification and destratification processes in the ROFI at the shelf edge also the different baroclinic processes are present. CHEN (2005) investigated the distribution of the JEBAR (Joint Effect of Baroclinicity and Relief) term on the East-Chinese Shelf. He found that extreme values are located at the shelf break. However, these findings lie behind the scope of this study but should be the subject of further investigations.

Figure 68 shows the situation in the Mekong ROFI during the low-flow season. It is obvious that the dominant processes in most part of the ROFI are mean straining and mixing like during the high-flow season. Almost in the whole ROFI the proportion of the mean straining term is > 30 %. The mixing term shows only locally restricted to some smaller parts of the coastal region of the SROFI and of the Northern NROFI a proportion > 30 % in φ^*_{t3D}. Generally, its proportion is about 10–30 %. HORDOIR et al. (2006) stated that vertical mixing plays a major role in the Mekong ROFI during the winter monsoon. Due to the shallow bottom, stratification is destroyed by vertical mixing in the baroclinic coastal current.

Like during the high-flow season, mean straining acts to stratify the water column and mixing mainly acts to destratify the water column. An exception is discovered in the coastal region of the SROFI where a positive mixing term indicates an unstably stratified water column (Figure 51).

The other four baroclinic terms show a proportion < 10 % for the major part of the ROFI. However, locally there are some patches which show higher values. For instance, near the river plume front the proportion of the shear dispersion term in φ^*_{t3D} is about 10–30 %. The same can be observed for the proportion of the non-mean straining term in φ^*_{t3D}. In the area of the river plume front shear dispersion acts to stratify the water column and non-mean straining to destratify the water column (Figure 51).

In the coastal region of the ROFI the proportion of the vertical advection term in φ^*_{t3D} is about 10–30 %. Here, downwelling takes place (Figure 51). HORDOIR et al. (2006) pointed out that during the NE monsoon the wind tends to create an Ekman transport towards the coast so that downwelling occurs. However, in the MPR of the ROFI upwelling can be observed which can be related to upwelling due to the secondary circulation (ELSTON, 2005). Although the proportion of the horizontal advection term is generally low (< 10 %), Figure 51 shows that a stratified water column is advected into the region off the river mouths. Figure 70 summarizes these findings as a synthesis of the dominant processes.

High-flow season

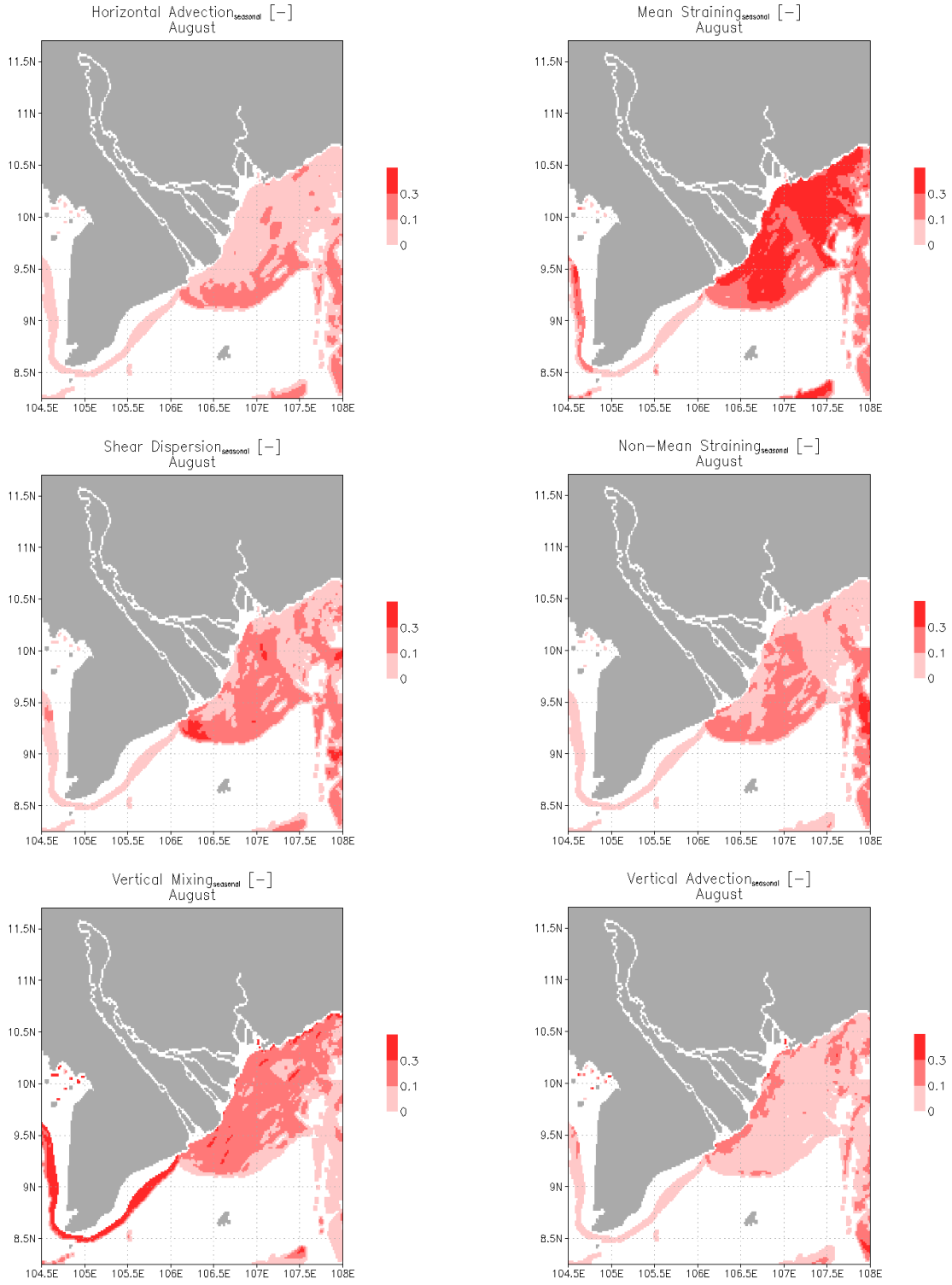

Figure 67: Seasonal relative proportions of the baroclinic terms [-] in φ^*_{t3D} in the Mekong ROFI during the high-flow season (August 2006). The values have been calculated with an artificially constant temperature (T = 28.5 °C) when determining the density via the equation of state. In the blanked areas values had not been calculated due to a low value of φ^*_{t3D}; the condition for the blanked areas is that the absolute value of the mean φ^*_{t3D} is $< 3\times10^{-6}$ W/m³.

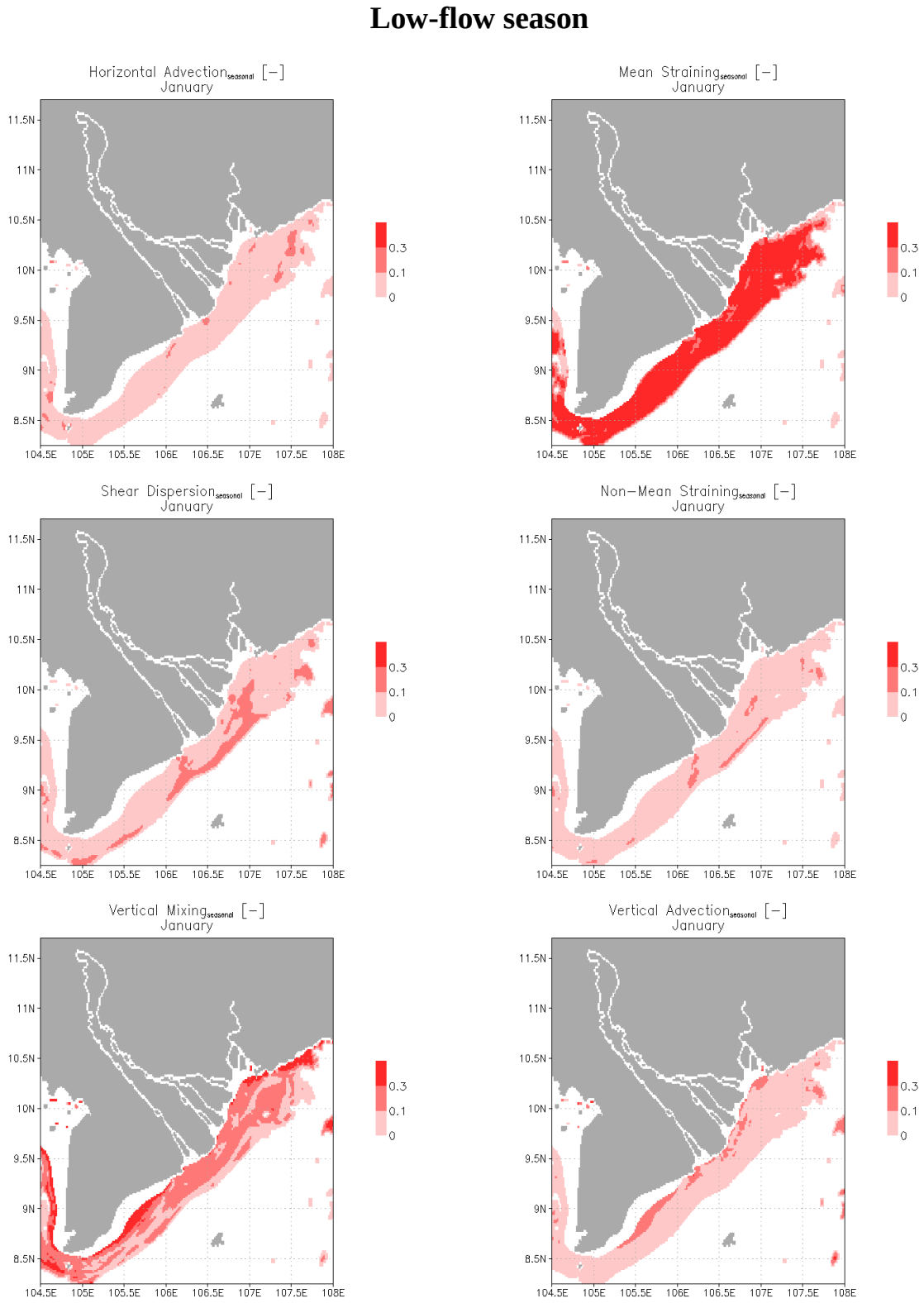

Figure 68: Seasonal relative proportions of the baroclinic terms [-] in φ^*_{t3D} [-] in the Mekong ROFI during the low-flow season (January 2007). The values have been calculated with an artificially constant temperature (T = 28.5 °C) when determining the density via the equation of state. Ihe blanked areas values had not been calculated due to a low value of φ^*_{t3D}; the condition for the blanked areas is that the absolute value of the mean φ^*_{t3D} is $< 3\times10^{-6}$ W/m³.

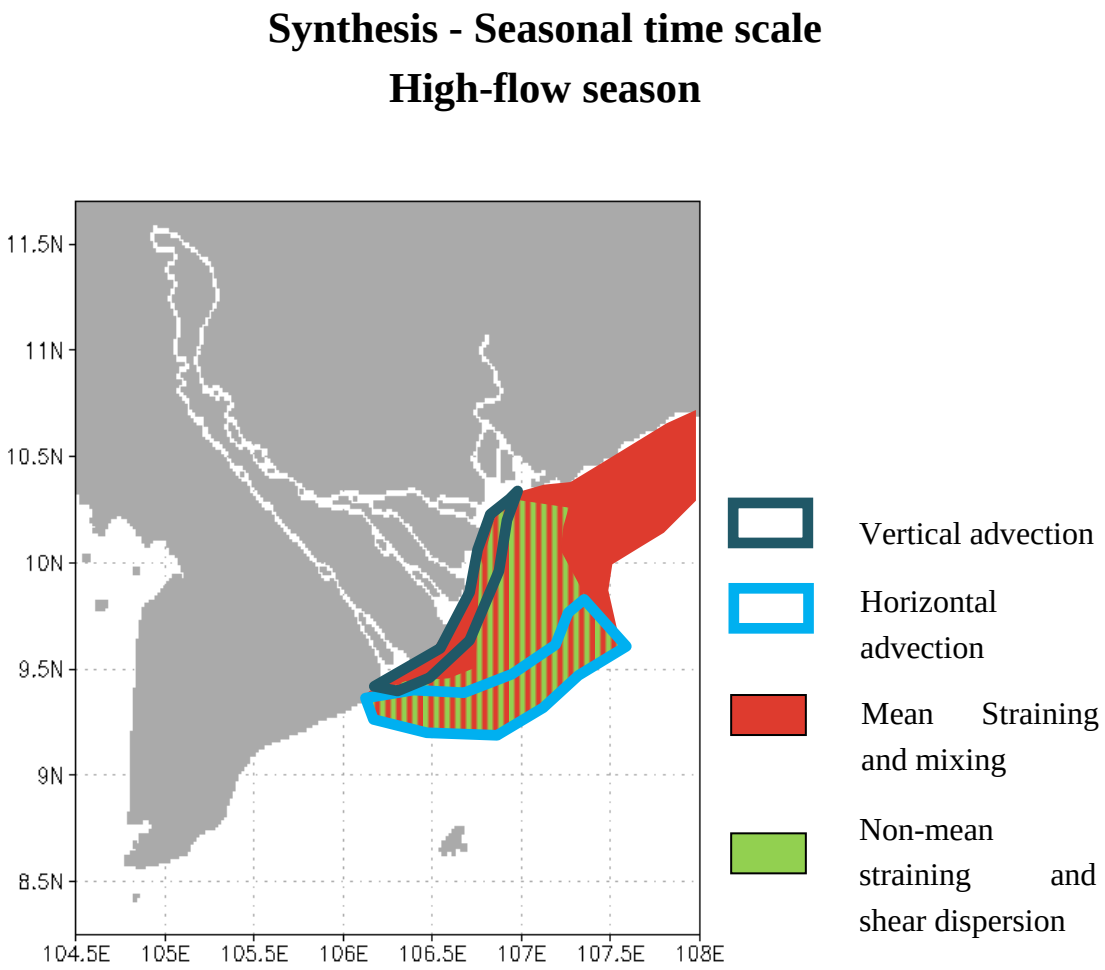

Figure 69: Synthesis of the dominant physical processes in the Mekong ROFI during the high-flow season (August 2006): seasonal time scale.

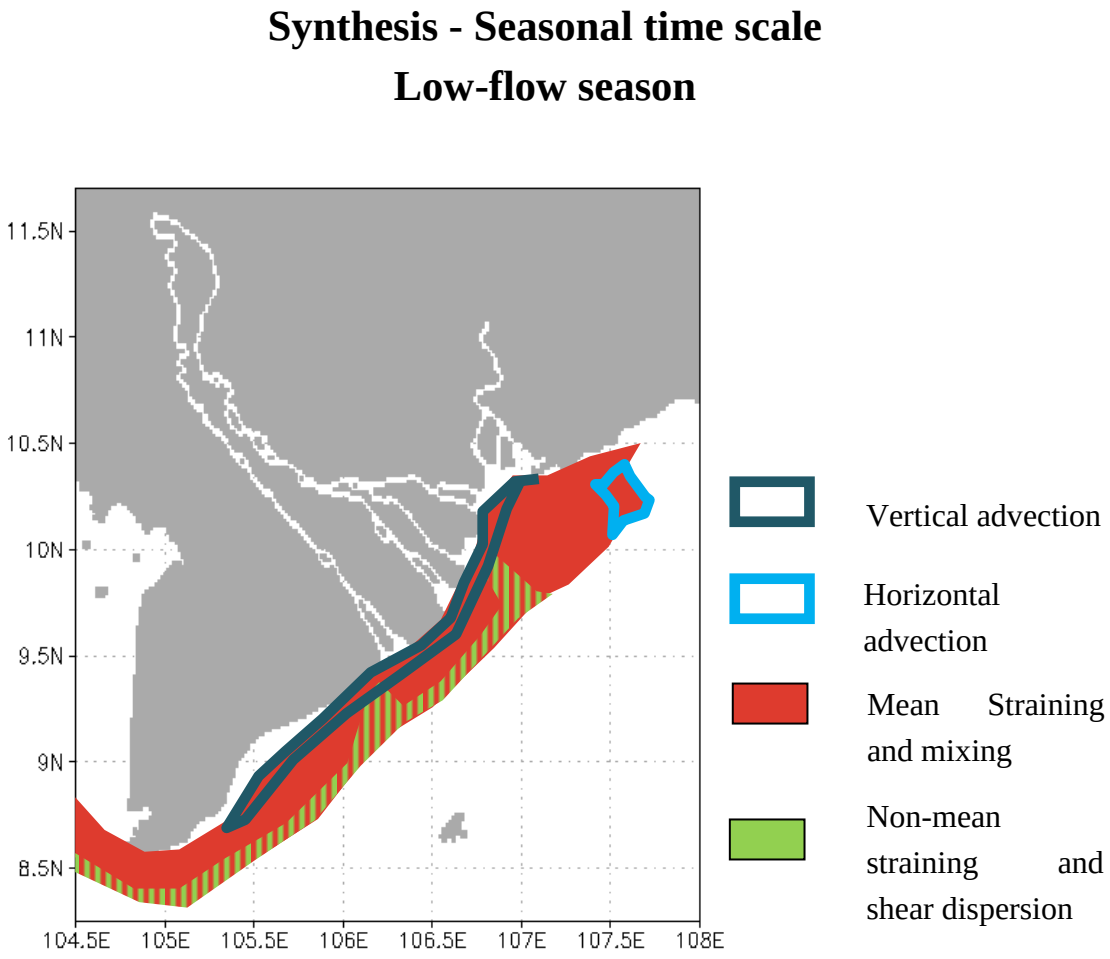

Figure 70: Synthesis of the dominant physical processes in the Mekong ROFI during the low-flow season (January 2007): seasonal time scale.

6.3.2 SYNTHESIS FOR THE TIDAL TIME SCALE

In this section for the different regions in the Mekong ROFI the dominant processes that act on the stratification of the water column on a tidal time scale are investigated. Therefore, the integrated variability of the different terms is determined for a tidal cycle. In this study, the integrated variability is defined by the deviation of the individual term at time step t from its mean value over a tidal cycle. The higher the deviation from the mean value, the higher the amplitude of the term and so is the influence of the respective process to changes in the potential energy of the water column during a tidal cycle. Although other forces (e.g., wind stress) contribute to this variability, the main driver is the tide. Thus, in the following this variability is referred to as tidally induced variability.

As an example the calculation for the mean straining term (MS_x and MS_y) is shown (equation 6.4 to 6.6).

$$MS_{\mathrm{var}} = \frac{1}{n}\sum_{t=1}^{t=t\max} \left| \; (MS_x(t) - \frac{1}{n}\sum_{t=1}^{t=t\max} MS_x(t) \; \right| + \frac{1}{n}\sum_{t=1}^{t=t\max} \left| \; (MS_y(t) - \frac{1}{n}\sum_{t=1}^{t=t\max} MS_y(t) \; \right| \tag{6.4}$$

$$\varphi^{*}_{t3D\_\mathrm{var}} = MS_{\mathrm{var}} + ADV_{\mathrm{var}} + DIS_{\mathrm{var}} + NS_{\mathrm{var}} + MIX_{\mathrm{var}} + UD_{\mathrm{var}} \tag{6.5}$$

$$MS_{tidal} = \frac{MS_{\mathrm{var}}}{\varphi^{*}_{t3D\_\mathrm{var}}} \tag{6.6}$$

with $MS_{x/y}$ the mean straining term, $DIS_{x/y}$ shear dispersion, $ADV_{x/y}$ horizontal advection, $NS_{x/y}$ non-mean straining, MIX_z vertical mixing, UD_z.vertical advection, t time step and n number of values. The other terms are calculated analogously.

Figure 71 shows the relative proportion of the tidally induced variability of the individual terms in the total tidally induced variability ($\varphi^{*}_{t3D\_\mathrm{var}}$) during the high-flow season in the investigation area. In the MPR all terms show only a local dominance. The horizontal advection term shows the highest values in some parts of the inner plume. In the coastal region of the NROFI/SROFI as well as in the Northern NROFI the values of ADV_{tidal} are decreased (< 0.1).

Shear dispersion contributes to $\varphi^{*}_{t3D\_\mathrm{var}}$ mainly in the region of the outer plume (> 20 %) whereas in the Northern NROFI and in the coastal region of the SROFI the contribution is lower (< 10 %). The non-mean straining term also displays the highest proportion in $\varphi^{*}_{t3D\_\mathrm{var}}$ in the region of the outer plume (> 0.1). In the coastal region and in the Northern NROFI non-mean straining generally contributes less to $\varphi^{*}_{t3D\_\mathrm{var}}$ (< 10 %).

The mixing term shows the highest values in the whole coastal region extending from the SROFI to the Northern NROFI (> 0.2). But also in the MPR the values are generally elevated. Like the mixing term, the vertical advection term contributes to $\varphi^{*}_{t3D\_\mathrm{var}}$ mainly in the coastal region of the NROFI/SROFI with values of > 20 %. Additionally, the relative proportion is high in some parts of the inner plume and at the shelf edge.

The mean straining term depicts the largest values in the region of the Northern NROFI and locally in a region extending from the Din An branch to the river plume front (> 0.2). Figure 73 shows a synthesis of the dominant processes on a tidal time scale during the high-flow season.

Comparing Figure 71 (tidal time scale) with Figure 67 (seasonal time scale) the difference between the distinct time scales can be detected. The solely dominance of the mean straining and mixing term – as it is the case on a seasonal time scale – cannot be observed on a tidal time scale. From Figure 71 it is obvious that on a tidal time scale mean straining acts mainly in the Northern NROFI. In the other parts of the Mekong ROFI it acts only on a decreased level. Regarding the mixing term, on a seasonal time scale the process acts primarily in the coastal region and on a decreased level throughout the whole plume. Also on a tidal time scale mixing acts particularly in the coastal region and on a decreased level in the region of the inner plume. Considering the horizontal and vertical advection terms on a tidal time scale these terms hold higher relative values than on a seasonal time scale indicating a higher influence on changing the potential energy in the Mekong ROFI on a tidal time scale. Shear dispersion and non-mean straining show a similar pattern on a tidal time scale as well as on a seasonal time scale.

To explain the higher relevance of the advection terms on the tidal time scale, the study of OONISHI (1977) gives some indications. In his study he distinguishes the constant flow and the tidal flow as typical flows in a coastal current system. The tidal flow is defined by the currents that have a semidiurnal or diurnal period. The constant flow has commonly time scales longer than the tidal period and mainly reflects the effects of wind stress, density variations, tidal residuals and remote currents on the flow.

In this section we consider density structures which are advected by the tidal flow over an absolute distance, i.e., the tidal excursion length, during a spring-neap cycle. Within each tidal cycle the density structure is moved forward and backward. The summarised absolute distance over a spring-neap cycle is therefore relatively high. In contrast, on the seasonal scale we regard density structures transported by the constant flow and its total distance covered over a spring-neap cycle. On this longer time scale the forward and backward movement of the frontal structure by the tidal flow is generally almost averaged out. Only the constant flow forced by wind stress, density variations, tidal residuals and remote currents advects the frontal structure. Thus, generally the instantaneous advection by the tidal flow is stronger than the advection by the constant flow. Transferring this to the results of the Mekong ROFI it explains why the horizontal advection terms hold higher relative values on the tidal time scale than on a seasonal time scale. Since through the continuity equation horizontal and vertical advection are inevitably linked, high values of the horizontal advection terms on the tidal time scale generally also causes high values of the vertical advection terms.

Figure 72 shows the relative proportion of the tidally induced variability of the individual terms in the tidally induced variability of φ^*_{t3D} during the low-flow season.

The highest relative proportion can be observed by the mean straining term throughout the

whole plume region (> 0.2). This is also true for the mixing term. Only in the coastal region to the south of the different river branches the values of both terms are decreased (< 0.2).

Horizontal advection plays a major role in the outer plume region (> 0.1). A similar pattern can be seen in Figure 72 for the shear dispersion term as well as for the non-mean straining term. For these terms the highest relative proportion in $\varphi^{*}_{t3D\_\mathrm{var}}$ can also be denoted in the outer plume region with values > 0.1. The vertical advection term shows a reversed picture to these latter terms as it holds the highest values in the coastal region (> 0.2) as well as in the adjacent inner plume region (> 0.1), but lower values in the frontal region (< 0.1). Figure 74 shows a synthesis of the dominant processes on a tidal time scale during the low-flow season.

Comparing Figure 68 (seasonal time scale) and Figure 72 (tidal time scale) it can be deduced that during the low-flow season on a tidal time scale mean straining and mixing are the main process changing the potential energy anomaly in the Mekong ROFI. The dominance of the mean straining and mixing terms could also be observed on a seasonal time scale, although the values of the mixing term are smaller. Both, the horizontal and vertical advection term represent a higher influence in changing the potential energy anomaly on time scales of a tidal cycle than on a seasonal time scale. An explanation has been given above. Shear dispersion and non-mean straining processes are again of equal importance on both time scales.

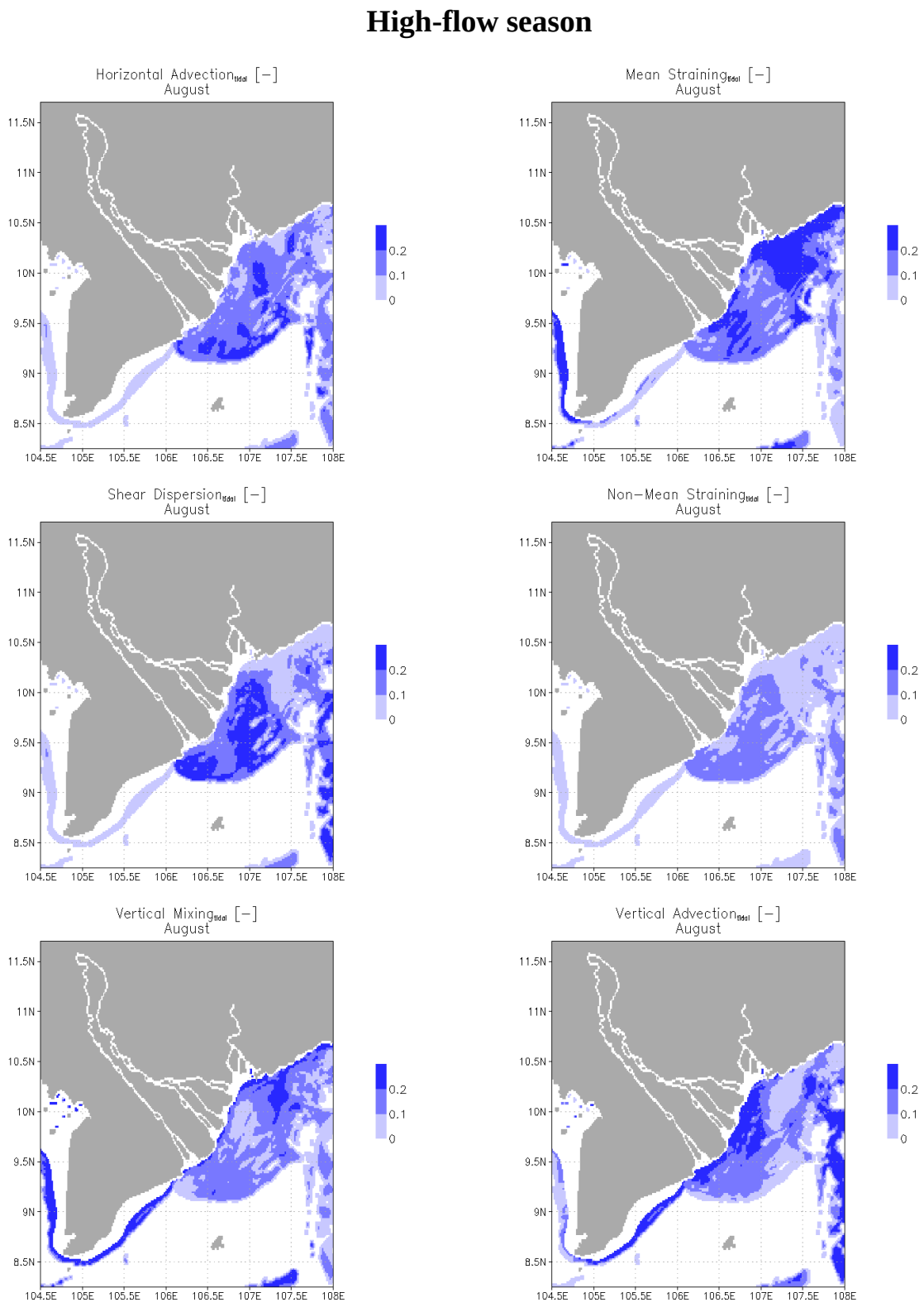

Figure 71: Tidally induced variability of the baroclinic terms [-] in the Mekong ROFI during the high-flow season (August 2006). The values have been calculated with an artificially constant temperature (T = 28.5 °C) when determining the density via the equation of state. In the blanked areas values had not been calculated due to a low value of φ^*_{t3D}; the condition for the blanked areas is that the absolute value of mean φ^*_{t3D} is < 3×10^{-6} W/m³.

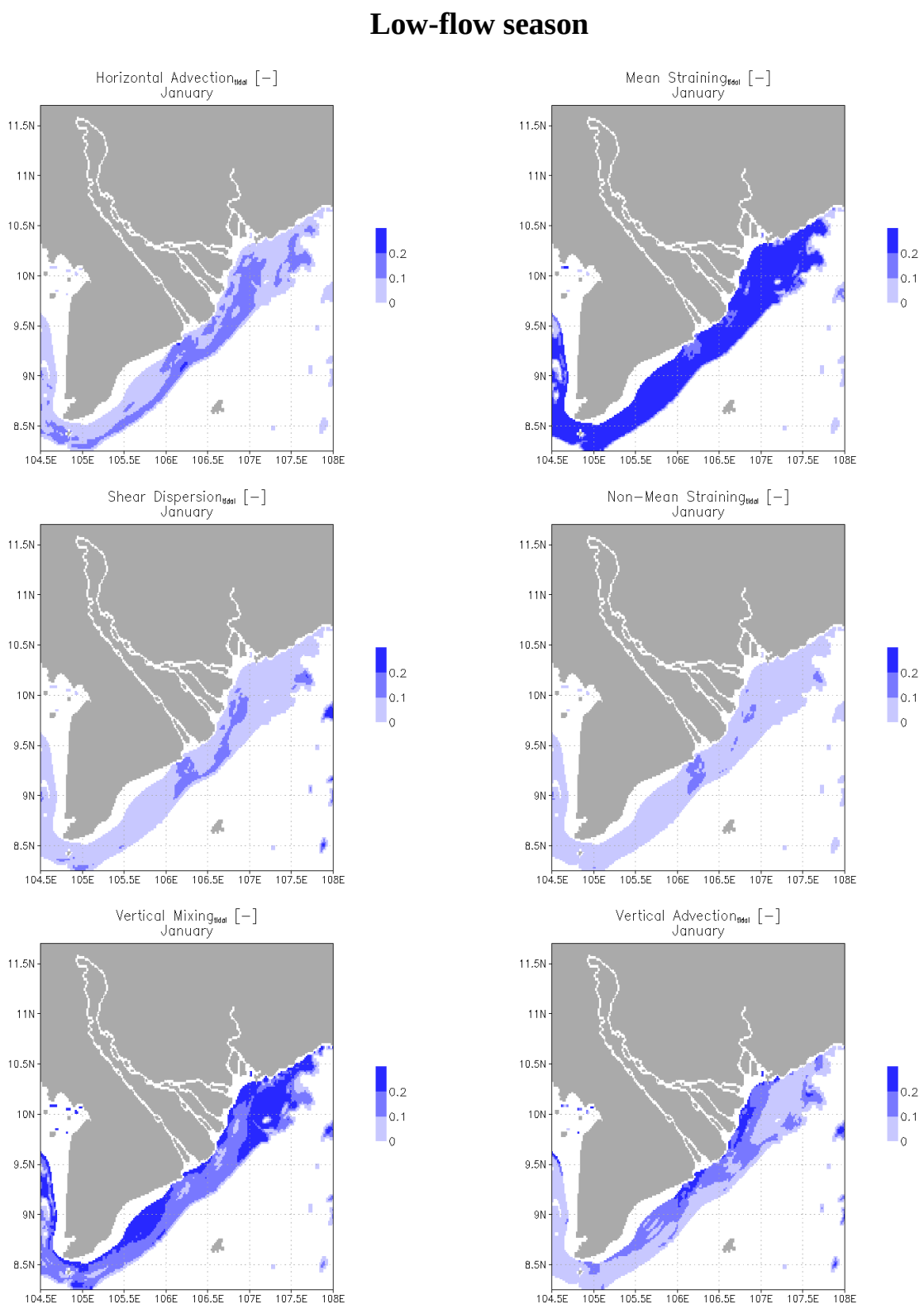

Figure 72: Tidally induced variability of the baroclinic terms [-] in the Mekong ROFI during the low-flow season (January 2007). The values have been calculated with an artificially constant temperature (T = 28.5 °C) when determining the density via the equation of state. In the blanked areas values had not been calculated due to a low value of φ^*_{t3D}; the condition for the blanked areas is that the absolute value of mean φ^*_{t3D} is < 3×10^{-6} W/m³.

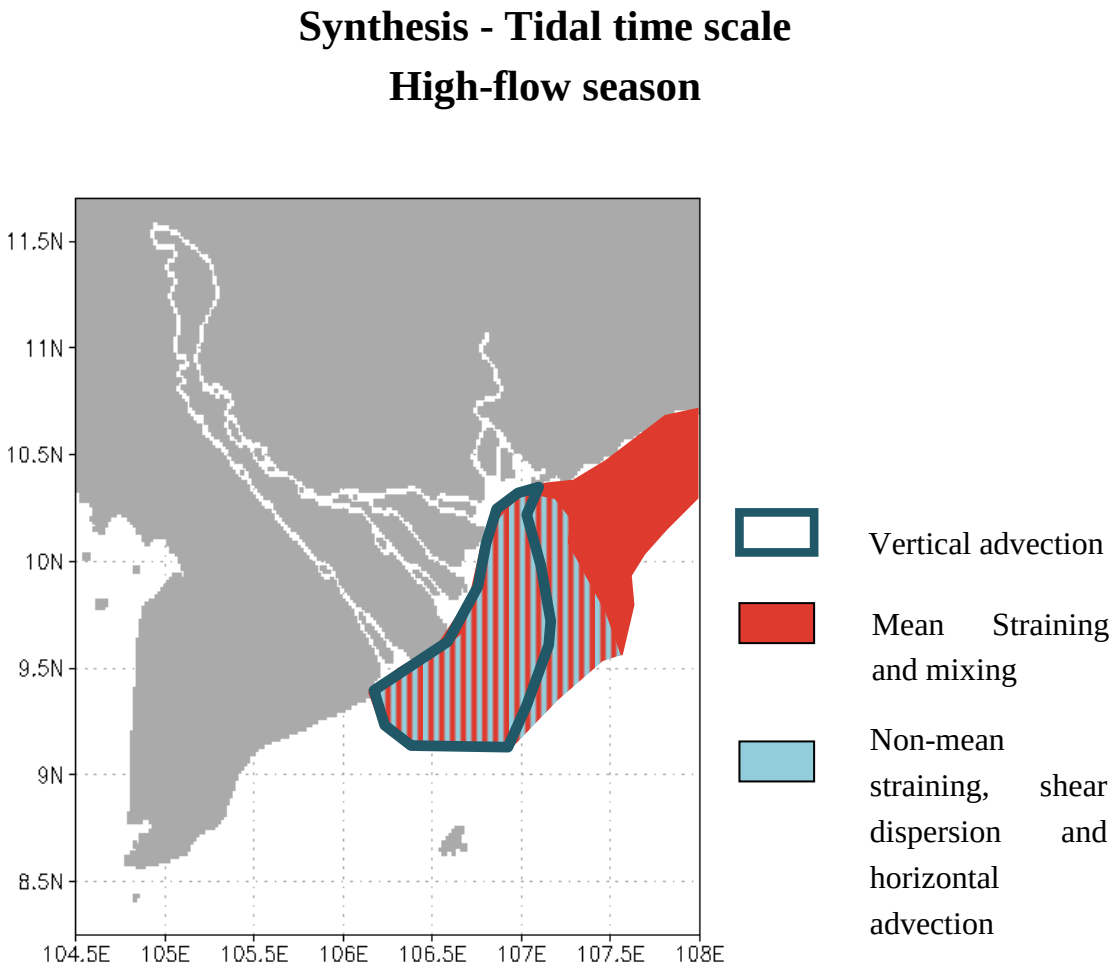

Figure 73: Synthesis of the dominant physical processes in the Mekong ROFI during the high-flow season (August 2006): tidal time scale.

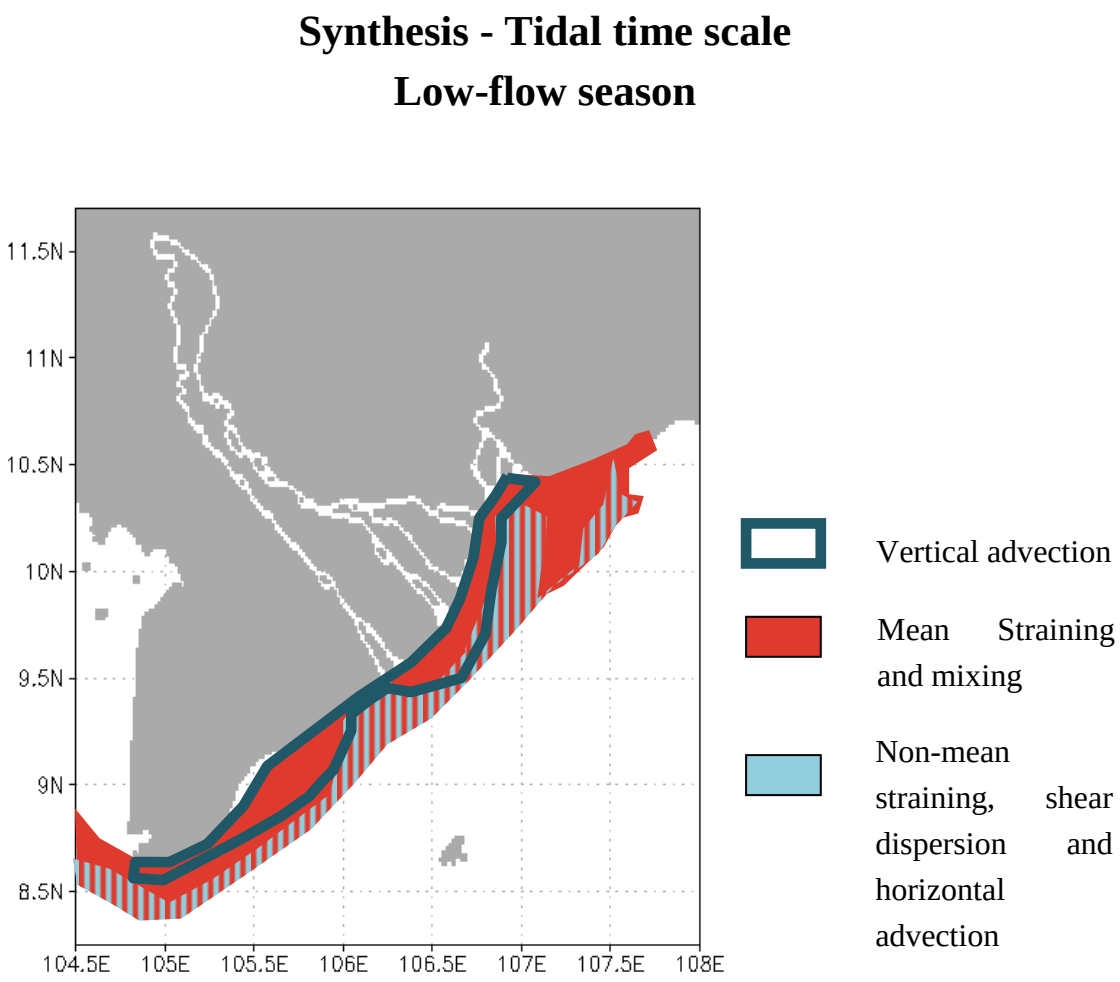

Figure 74: Synthesis of the dominant physical processes in the Mekong ROFI during the low-flow season (January 2007): tidal time scale.

6.4 POTENTIAL ENERGY ANOMALY IN OTHER REGIONS

To date, there have been three leading studies in which the three-dimensional dynamic equation for potential energy anomaly is used as a tool to analyze the model results in terms of prevailing stratification and mixing processes (BURCHARD and HOFMEISTER, 2008; DE BOER et al., 2008; HOFMEISTER et al., 2009). In the following the results of these three studies will be summarized and compared to the results of the Mekong ROFI to discover the similarities and differences between the physical systems of different coastal regions.

BURCHARD and HOFMEISTER (2008) carried out a one-dimensional SIPS (strain-induced periodic stratification) study as well as a two-dimensional estuarine circulation study for an idealized model area. First, the one-dimensional case will be considered. In this model, a rectilinear tide is prescribed. Both, the wind stress and the density gradient are supposed to be constant and to act in the direction of flow. Earth rotation is neglected. Zero density fluxes through surface and bottom were assumed. The water depth is constant (10 m).

The results of the one-dimensional SIPS study demonstrate that over a tidal cycle the water column switches between stratified and mixed conditions. Around high water the water column is completely mixed (φ_{1D} = 0 J/m³). At this time neither straining nor mixing takes place. During ebb tide the mean straining term increases which indicates that less dense water is sheared over denser water. The term is not fully balanced by the mixing term such as φ_{1D} increases. At the end of ebb tide mixing processes stop, but mean straining processes are still taking place resulting in a maximum increase of φ_{1D}. Around low water mean straining processes are still acting but are decreasing in strength. Mixing starts again. During flood tide the mean straining term further decreases such as at full flood tide both mean straining and mixing act to destratify the water column. The result is a maximum decrease of φ_{1D}.

Figure 75 represents a time series of the area BaN during the low-flow season. To compare the results of this study with the results of the SIPS study, BaN has been chosen as the horizontal processes are dominated by mean straining and the vertical processes by mixing like it is the case in the SIPS study. Considering Figure 75 it can be noticed that over a tidal cycle φ_{1D} shows the same dynamic, i.e., a stratified water column around low water and a mixed water column around high water.

During the whole tidal cycle at the area BaN mean straining and mixing counteracts as mean straining always acts to stratify the water column and mixing acts to destratify the water column. This is similar to the results of the SIPS study during ebb tide. However, during full flood tide the SIPS study presents that mean straining acts to destratify the water column. Mean straining is divided into estuarine circulation and tidal straining (BURCHARD and HOFMEISTER, 2008). The difference can be explained by the fact that in the one-dimensional case the estuarine circulation is less effective.

Analysing the dynamics over a tidal cycle in more detail, in the Mekong ROFI at high water no

straining but mixing on a low level takes place. This is different to the situation in the SIPS study where at high water neither mixing nor straining acts. During ebb tide and low water the dynamics in both studies are comparable: As less dense water is sheared over denser water, the value of the mean straining term increases. The stratification input is not balanced by mixing that acts to erode the stratification so that φ_{1D} increases. The processes proceed until around low water where φ_{1D} reaches a maximum.

During flood tide φ_{1D} decreases in both studies which is that the water column destratifies. In the Mekong ROFI the decrease of φ_{1D} can be explained by mixing which is not balanced by mean straining. However, in the SIPS study, the water column is destratified not only because of mixing but also due to reversed straining.

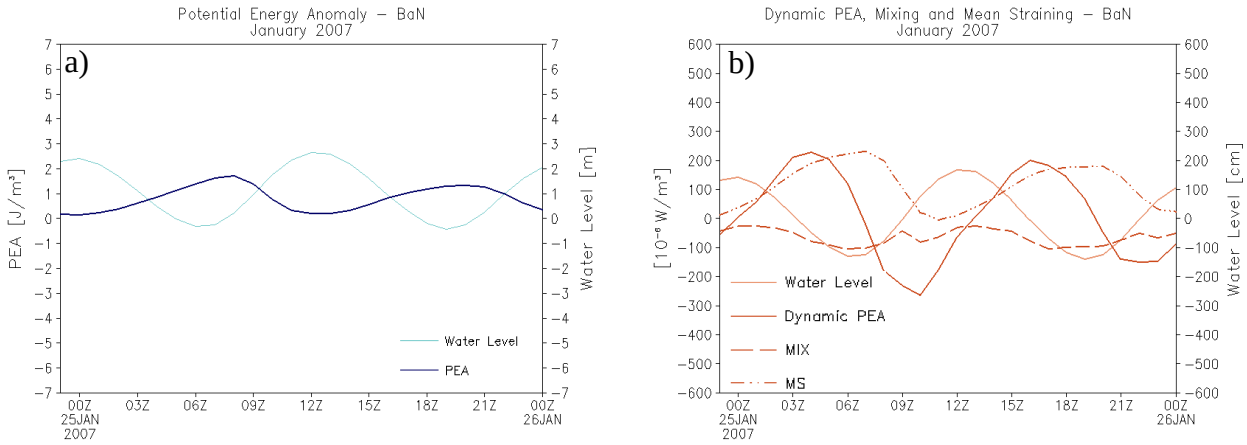

Figure 75: a) Time series of φ_{1D} [J/m³] (dark blue line) and water level [m] (light blue line) at the station 9.35° N/106.3° E (BaN) during the low-flow season (January 2007). For a better visualization of the results water level is shown with an offset of 1 m. The values of φ_{1D} have been calculated with an artificially constant temperature (T = 28.5 °C) when determining the density via the equation of state. Positive values of φ_{1D} indicate a stably stratified water column, values of 0 J/m³ a mixed water column and negative values an unstably stratified water column. b) Time series of the baroclinic terms and φ^*_{t3D} [10^{-6} W/m³] as well as water level [cm] at the station 9.35° N/106.3° E (BaN) in January 2007. The terms in the three-dimensional dynamic equation for potential energy anomaly have been calculated with an artificially constant temperature (T = 28.5 °C) when determining the density via the equation of state. Positive values of φ^*_{t3D} indicate stratification and negative values destratification. Dark red solid line is φ^*_{t3D}, dark red long dash is the vertical mixing term, dark red dash dot dot is the mean straining term and light red solid line is water level.

Considering φ^*_{t3D} in Figure 75, it can be deduced that in the Mekong ROFI other processes than mixing and mean straining are also acting on the (de)stratification of the water column as the sum of both terms does not represent φ^*_{t3D}. Thus, although at the area BaN mean straining and mixing are the dominant processes, the dynamics in the Mekong ROFI are much more complex than they can be described by a one-dimensional model. In the case of the one-dimensional simulation, the influence of earth rotation and the regional differences (e.g., tidal ellipses, the

varying bathymetry) cannot be reflected.

Considering the two-dimensional study of BURCHARD and HOFMEISTER (2008) the effect of horizontal advection, non-mean straining and vertical advection can be investigated. For this study an idealized estuary is considered as well. Earth rotation is neglected. The salinity gradient decreases linearly over the estuary. Meteorological forcing is not accounted for. The tide is idealized by a semi-diurnal sinosodial curve with a sea surface amplitude elevation of 1 m.

Two positions were analyzed by the authors. Position A is situated 62 km and Position B 20 km off the river mouth. At position A the water column is fully destabilized during flood whereas at position B the water column is stably stratified during the whole time period. Due to the distance to the Mekong mouths and the fact that during flood the water column is mixed, station A will be set in comparison to the region MeE during the high-flow season (Figure 55 and Figure 57). Station B is situated in the vicinity of the river mouth and thus this station will be contrasted with the regions Me (Figure 52 and Figure 54) and BaN (Figure 58 and Figure 60) during the high-flow season. The water column of these two areas remains stratified during the whole tidal cycle.

The two-dimensional study of BURCHARD and HOFMEISTER (2008) shows that at position A only mean straining and vertical mixing play a significant role, as for the case of the one-dimensional investigation. After low water φ_{1D} has a maximum which is eroded by mean straining and mixing. At full flood φ_{1D} is negative which indicates an unstably stratified water column. The positive mixing term is completely balanced by the negative mean straining term. At slack water after flood, φ_{1D} has a local maximum.

In the Mekong ROFI at the region MeE a general dominance of vertical mixing and mean straining can be observed as well (Figure 55 and Figure 57). However, the dynamic is interrupted by the passage of a front. During the passage, the mean straining term and the mixing term decrease whereas the advection term, shear dispersion term and non-mean straining term increase.

Regarding Figure 42 φ_{1D} generally has a local maximum around lower low water like it is the case in the two-dimensional study around low water. However, contrary to the results of the two-dimensional study around higher high water a local minimum is observed. At high water the study of BURCHARD and HOFMEISTER (2008) shows a local maximum. The difference can be explained taking the mean straining term into account. The mean straining term reflects the estuarine circulation and the tidal straining. In the study of BURCHARD and HOFMEISTER (2008) around high water the mean straining term has a local maximum which the authors have been related to the estuarine circulation. In the Mekong ROFI at the area MeE around higher high water the mean straining term has values close to 0 W/m³, i.e., there is no input of stratification by this term.

At ebb tide in the Mekong ROFI the mean straining term is positive indicating an input of stratification. Mixing also takes place and counteracts the mean straining process. These

dynamics are also shown by the two-dimensional study of BURCHARD and HOFMEISTER (2008). However, in the Mekong ROFI the input of stratification by mean straining is higher than the erosion of stratification by mixing, so that during ebb tide in total the water column is stratified. The processes continue during whole ebb tide so that at low water a local maximum in stratification is reached. This is the same for the two-dimensional study.

At flood tide in the Mekong ROFI mixing decreases (values are around 0 W/m³ or slightly positive) and mean straining acts to destratify the water column. Adding both processes, in total a destratification of the water column takes place until at high water the water column is completely mixed. The study of BURCHARD and HOFMEISTER (2008) generally indicates a negative value for the mean straining term for flood tide as well. However, the mixing term shows clearly positive values which can be related to an unstably stratified water column, i.e., φ_{1D} has negative values.

At position B, which is situated closer to the coast than position A, the study of BURCHARD and HOFMEISTER (2008) displays that horizontal advection, vertical advection and mean straining are the dominant processes. At low water φ_{1D} has a minimum because the frontal region is situated furthest off-coast of location B and main part of the water column consists of freshwater from the river. After the onset of flood the stratification is stabilized due to horizontal advection. Mean straining is acting opposed to it. With increasing flood current, the halocline is raised due to vertical advection. At slack tide after flood φ_{1D} shows a maximum. The stratification input is mainly attributed to mean straining. Horizontal advection acts again opposed to it.

Comparing the processes at position B (BURCHARD and HOFMEISTER, 2008) to the processes of the region Me in the Mekong ROFI it is evident that in the Mekong ROFI the physical processes are dominated by vertical advection, mean straining and shear dispersion. Horizontal advection and non-mean straining also play a role in the Mekong ROFI during a tidal cycle (Figure 52). At position B the horizontal advection term, the mean straining tem as well as the vertical advection term show high values. The non-mean straining term shows lower values which may be related to the lower complexity (e.g. 2D study) of their idealized model.

Regarding Figure 52 the non-mean straining term shows a local maximum at slack tide in the Mekong ROFI. At this time the direction of the currents changes, i.e., from ebb tide to flood tide or vice versa. Then the curvature radius of the tidal ellipses is maximal which is reflected by rotating currents. The tides at the area Me are dominated by a standing wave. The tidal ellipses at this area are narrow (ZU et al., 2008), i.e., the rotation of the currents at slack tide is maximal. In the two-dimensional study of BURCHARD and HOFMEISTER (2008) the tidal ellipses are rectilinear and the current velocity switches simply the sign. It can be deduced that in the area Me the non-mean straining term is maximal when the currents rotate.

However, the dynamic of φ_{1D} at the area Me is reversed to the dynamic of φ_{1D} at location B. In the Mekong ROFI at low water φ_{1D} shows a local maximum whereas at high water it shows a local minimum. At the region Me the tides are rather dominated by a standing wave (maximum

stratification at lower low water, minimum stratification at higher high water (SIMPSON, 1997)) than by a progressive wave. During ebb tide an input of stratification due to mean straining takes place. Considering the vertical advection term it can be deduced that downwelling occurs (positive value). The shear dispersion term has mainly positive values during ebb tide. Then, around low water the mean straining term shows the largest value whereas the vertical advection term and the shear dispersion term have values around 0 W/m³. This yields a local maximum in φ_{1D}.

During flood tide the mean straining term is still positive but decreased. The shear dispersion term shows mainly negative values. The halocline is raised due to upwelling (negative value). Around high water the vertical advection term shows values around 0 W/m³. The mean straining term shows a local minimum which can reach values around 0 W/m³. The shear dispersion term has also a local minimum. Thus, φ_{1D} has a local minimum.

The same dynamics can be observed when considering the area BaN. At this area a dominance of mean straining and vertical advection is illustrated. These terms act in the same way as mentioned above for the area Me.

DE BOER et al. (2008) apply the three-dimensional dynamic equation for the potential energy anomaly to the results of an idealised model simulation of the Rhine River Plume to analyze the physical processes affecting stratification. In their study, the effect of tides and river discharge (2500 m³/s) are considered, wind forcing is neglected. A 20 m deep rectangular basin is supposed. A simulation of 36 h has been realized. These authors present an illustration (their figure 8) that shows the dominant terms affecting stratification in the Rhine ROFI. The figure is based on covariance results of three semi-diurnal tidal cycles: In the following the time-invariant results of the Rhine ROFI will be compared with the long-term results of the Mekong ROFI (Figure 67 to Figure 70).

DE BOER et al. (2008) demonstrate that in the Rhine ROFI in the vicinity of the river mouth, in the coastal region and at the offshore edge of the river plume vertical advection and non-mean straining occur. However, consulting their figure 3 it can be concluded that vertical advection mainly acts in the region of the river mouth. In the Mekong ROFI vertical advection mainly takes place in the coastal region off the river mouths as well. However, as during the low-flow season the Mekong River plume is directed to the SW, vertical advection is also important in the coastal region of the SROFI. During this season the winds of the NE monsoon create an Ekman transport towards the coast which induces downwelling in the coastal area of the Mekong ROFI (HORDOIR et al., 2006). Like in the Rhine ROFI, at the offshore edge of the Mekong River plume some smaller patches where vertical advection occurs can be found.

In both ROFIs non-mean straining dominates the offshore edge of the plume. The shear dispersion term shows the same regional distribution like the non-mean straining term, both in the Mekong ROFI and in the Rhine ROFI.

In the Rhine ROFI in the rear area of the river plume mean straining and horizontal advection is

important. This is also true for the front region of the plume. In the inner region of the downstream coastal current only the mean straining term dominates. Considering the Mekong ROFI during both seasons horizontal advection also dominates in the rear area of the bulge but not in the front part. In the long term horizontal advection is highest where the basin-wide current meets the plume, i.e. in the case of the Mekong ROFI in the rear part. In contrast, in the publication of DE BOER et al. (2008) the values of the horizontal advection term are elevated when the tidal currents intersect the plume. During the low-flow season in the Mekong ROFI both the plume region and the coastal current are dominated by mean straining. During the high-flow season – as the coastal current is absent during this season – the process acts only in the plume region.

Contrary to the results of this study, it is obvious that in the Rhine ROFI tidal mixing is only locally of importance in the region of the river mouth (their figure 3). The results of this study show that in the Mekong ROFI during both seasons the whole plume region apart from the offshore edge is dominated by the mixing process with the highest values in some parts of the coastal area. Vertical mixing has a great importance in the Mekong ROFI (HORDOIR et al., 2006). The model approach of the Rhine ROFI does not account for wind forcing and topography. This may explain the higher mixing values in the Mekong ROFI.

The third and most recent study was outlined by HOFMEISTER et al. (2009). They investigated the stratifying and destratifying processes in the Limfjord in Denmark. A three-dimensional high-resolution numerical model study was presented for the year 2003. The physical regime of that region switches periodically from stratified to mixed conditions. Due to the authors in the central Limfjord changes in stratification can be explained by a complex interaction of differential advection, heating and turbulent mixing. The study is more focused on regional aspects than the both former studies. However, the system of the Limfjord is very different from that of the Mekong ROFI, therefore a comparison of both systems seems to be critical. The differences in the boundary conditions (Mekong: dominant river discharge; Limfjord: diffuse freshwater supply) of these two systems suggest the need of a detailed study for each single region to disclose the regional characteristic physical processes.

CHAPTER 7

CONCLUSIONS

In Vietnam, the fishery sector is of great importance since 80 % of households in coastal communities get their income from this sector. Moreover, one-third of animal protein in the Vietnamese diet is delivered from small-scale fishing. Some important fishing grounds are located off the Mekong River mouth (POMEROY et al., 2009; STREAM, 2000). Thus, understanding the physical processes in this area which directly or indirectly have an effect on the marine ecosystem is of high significance.

The physical processes in a ROFI are determined by the buoyancy input as freshwater, as well as by the stirring effect of wind, waves and tides. Competition between these mechanisms estabilishes the level of stratification of the water column. Depending on whether the water column is mixed or stratified, the vertical flux of water properties like heat, salt, momentum and of water substances like nutrients, sediments can be elevated or reduced (SIMPSON et al., 1990).

Due to the high annual freshwater input, the Mekong ROFI is an excellent example for investigations on (de)stratifying processes. In this study, the hydrodynamic conditions of the Mekong ROFI and their seasonal variability were calculated by means of the three-dimensional baroclinic model HAMSOM (BACKHAUS, 1982, 1985). For validation, different datasets were used. The datasets consist of altimeter data (SSH and SST), in-situ measurements conducted during two field studies (salinity), discharge measurements and data from predictions (tidal elevations). A comparison of the hydrodynamic model results with these data show a good agreement between the datasets. However, some inaccuracies in the model results could be detected whereby an essential shortcoming is the low resolution of forcing data.

The in-situ salinity data collected during both monsoon seasons show the horizontal and vertical salinity gradients in the Mekong ROFI. Hereby, the complexity of frontal structures in this region and the stratifying influence of the freshwater input are apparent. Sharp gradients dominate the region. The data of a 25 h mooring station indicate the rapid and strongly local changes in stratification during a tidal cycle. Herewith, also the general deficiencies of a numeric model are revealed, i.e., the numeric diffusion and the deficiency to represent fluctuations and small scale processes. Even though the transport equation is solved with second

order accuracy, these challenges remain. However, overall it can be concluded that although there are uncertainties and deficiencies in the model results, the results are sufficiently accurate for analysing the local and temporal variability of the processes of stratification and destratification in the Mekong ROFI.

From the validated hydrographic parameters, it can be deduced that the changing boundary conditions, i.e., monsoon wind and river discharge, implicate a clear seasonal variability in the density distribution as well as in the flow field of the Mekong ROFI. This seasonality is especially reflected by the plume behavior as during the summer monsoon the direction of the Mekong River plume differs from the plume direction during the winter monsoon, i.e., during summer the plume shows a behavior which contrasts with the general, idealized plume picture.

To investigate the level of stratification in the Mekong ROFI, the one-dimensional equation for the potential energy anomaly (SIMPSON et al., 1981) is applied to the hydrodynamic model results. Here, it has been shown that due to the higher freshwater input the Mekong River plume is stronger stratified during the high-flow season (summer) than during the low-flow season (winter). Moreover, during the high-flow season close to the river mouth the stratification of the water column is evident during the whole tidal period. Thus, it can be deduced that during this season the Mekong ROFI is a stratified system. In contrast during the low-flow season the Mekong ROFI is a partially stratified system as the system switches between mixed and stratified conditions.

The study demonstrates the limitation of the one-dimensional equation, as it is not possible to identify the physical processes acting during the different seasons to stratify or mix the water column. Thus, the three-dimensional dynamic equation for the potential energy anomaly (BURCHARD and HOFMEISTER, 2008; DE BOER et al., 2008) has been consulted.

On seasonal time scales, there are of course similarities between both monsoon phases. The mixing and the mean straining term dominate nearly the whole Mekong ROFI, whereby mean straining acts to stratify the water column and mixing acts predominantly as destratifying agent. From the positive mean straining term it can be concluded that on the long-term the estuarine circulation and the asymmetric tidal straining are crucial processes in the Mekong ROFI. The high values of the vertical mixing term shows the great importance of wind stress and tidal forces on the physical dynamics in the Mekong ROFI.

The major difference between the two monsoon phases is that during the summer monsoon also the other four physical processes (shear dispersion, non-mean straining, horizontal and vertical advection) play – although generally locally restricted – an important role. Therefore, it can be concluded that during summer the driving mechanisms, i.e., the density-driven circulation, the classical plume advection into the direction of the coastal trapped Kelvin wave and the summer-monsoon induced circulation, superimpose in a different manner than during the winter monsoon. This implicates the higher complexity of processes in the Mekong ROFI during the summer monsoon.

Moreover, not only the strength of the physical processes is different between the two monsoon phases, but also the long-term evolution. This is especially reflected by the horizontal and vertical advection terms. During the summer monsoon close to the river mouth the horizontal advection term is negative which gives evidence that well-mixed estuarine water enters the Mekong ROFI. In contrast during the winter monsoon shelf water intrusion into the Mekong Estuary is taking place which is indicated by a positive horizontal advection term. Thus, for the assessment of salinity intrusion into the Mekong Estuary which is important for climate change studies or studies about the management of agriculture as well as hydropower dams both seasons have to be discussed separately.

The vertical advection term shows that during the summer monsoon in the Mekong River plume upwelling occurs, whereas during the winter monsoon also downwelling occurs. The change of the wind direction during the monsoon phases and additionally – in restricted areas – the secondary circulation induced by the plume-rotation can be considered for explanation. The upwelling related to the river plume dynamics has an effect on the nutrient availability in the ROFI as it can bring nutrients from deeper areas to the surface. This is an important process for the marine ecosystem.

The results of the tidal time scale implicate that the physical processes had to be considered independently for each monsoon phase. Even on this time scale the seasonal differences reflected by the boundary conditions cause distinct physical processes for the respective monsoon phase. During the low-flow season the main physical processes in the Mekong River plume are mean straining and mixing. However, also horizontal and vertical advection are important processes. During the high-flow season there is no single process which plays a dominant role in the Mekong ROFI. In distinct regions of the ROFI different processes are of importance showing the complexity of the summer circulation like mentioned above.

The dominant physical processes on the tidal time scale differ from the main processes on the seasonal time scale. The major difference between the time scales is evident when considering the horizontal and vertical advection terms. On a tidal time scale these terms hold higher values than on a seasonal time scale. This is due to the stronger instantaneous advection of density structures by the tidal flow, i.e., the higher tidal excursion length, because of the forward and backward movement during the tidal cycle. In general the advection by the constant flow forced by wind stress, density variations, tidal residuals and remote currents is lower (seasonal scale).

As the different values of the advection terms show, a transfer of the results from one time scale to another should be avoided in a system where the boundary conditions change on different time scales. Applicability is given when considering the sediment dynamics in the Mekong ROFI. The advection has a direct effect on the transport distance of the sediments discharged by the Mekong River. To conclude from the sediment transports measured on the tidal time scale to the littoral drift on the seasonal time scale, as it has been done by WOLANSKI et al. (1996, 1998), has to be seen as critical.

Altogether, the broad range of the determined physical processes with its complex spatial and temporal variations reflects that the Mekong ROFI is a highly dynamic system which is strongly influenced by tides, monsoon winds and river discharge. This complexity should be kept in mind by related disciplines.

CHAPTER 8

OUTLOOK

The reversal of the Mekong River plume is an interesting phenomenon as it conflicts with the theory that the flow propagates parallel to the coast in the direction of Kelvin wave propagation. For the Mekong ROFI this is the case during the winter monsoon. However, during the summer monsoon the flow is directed against the direction of Kelvin wave propagation. To date, the processes which force the reversal of the Mekong River plume have not been sufficiently proven by scientists. However, it is a need for further studies to investigate the forces which counteract the Kelvin wave propagation so that the plume direction is changed from SW to NE. A possibility to study this point could be by means of model experiments. Thus, it could be analyzed which forces cause the reversal of the plume, i.e., if it is only a wind-driven effect or if the reversal is forced only by the remote currents or if both mechanisms act in combination on the flow.

Considering the study of HORDOIR et al. (2006) a first guess can be done. Due to their model domain, which does not include the shelf break and its boundary conditions, only the wind-driven effect is pictured. Hence, the boundary current at the shelf break which flows during winter southward and during summer northward is not represented by their model. Their results of the first days of October show that although the mean wind stress direction is from SW, the plume is not fully reversed. Thus the interaction of both wind stress direction and the direction of the remote shelf break current seems likely to have an effect on the reversal of the Mekong River plume.

Another interesting point to investigate is the effect of the hydropower dams on the Mekong River discharge and thus on the physical processes in the ROFI. The Mekong River Commission shows an overview of proposed and completed dams along the mainstream of the Mekong River (http://www.mrcmekong.org/topics/sustainable-hydropower/). Altogether 19 dams are proposed or completed whereas 8 are situated in the Upper Mekong Basin which drains parts of China and 11 in the Lower Mekong Basin which drains parts of Lao PDR, Myanmar, Thailand, Cambodia and Vietnam. According to LU and SIEW (2006) and KUMMU and VARIS (2007) the total storage capacity of the Chinese dams is planned to be over 40 km³. The mean annual discharge of the

Mekong River is 475 km³ (MRC, 2005).

LU and SIEW (2006) studied the impact of the Manwan dam, which was the first dam in operation, on the water discharge and the sediment flux in the Lower Mekong River. The Manwan dam has a storage capacity of around 1 km³ which is a relatively small volume compared to the total storage capacity of all Chinese dams. The authors stated that after the construction of the Manwan dam the Mekong River discharge has not decreased significantly at Pakse (Cambodia) which is the most downstream station. However, the mean monthly sediment concentration has decreased at all stations of the Mekong Estuary, but only the decrease in Can Tho is significant.

KUMMU and VARIS (2007) discussed the possible hydrological impacts of the eight reservoirs in China on the Lower Mekong and reveal that the flow during the dry season is increased, whereas the flow during the wet season is decreased. ADAMSON (2001) studied the potential impact of the Chinese hydropower dams on the flow regime of the Lower Mekong by means of two scenarios – 10 % as well as 20 % regulation in China. It has to be mentioned that the contribution of the upper Mekong, the so called Yunnan component, to the hydrology of the Lower Mekong is much higher in the dry season than in the wet season. Therefore, the mean flow in the dry season could increase by 20 % in the furthest downstream parts of the Mekong River. During March and April the flow could be elevated by 50 %.

In contrast to the situation in the dry season during the wet season these impacts are weakened significantly as the relative contribution of the Yunnan component to flood flows diminishes downstream. In Cambodia the mean discharge between May and October is estimated to decrease by around 5%. Thus, the studies show that the amplitude of the seasonal cycle of discharge could be decreased. Subsequently, the buoyancy input to the estuary by the river is changed which could have an effect on the level of stratification and the underlying physical processes in the ROFI. If more (less) freshwater from the Mekong River enters the SCS during the dry (wet) season, the horizontal density gradients are increased (decreased) which drive the estuarine circulation. Thus, as the estuarine circulation is reflected by mean straining, this process should be elevated in the dry season and reduced in the wet season. However, also a shift in the other physical processes, which were discussed in this study, is likely.

As due to the hydropower dams the sediment flux changes as well according to KUMMU and VARIS (2007) and LU and SIEW (2006), a modified sediment dynamic is possible. For instance, a higher discharge during the winter monsoon could transport more sediment into the Gulf of Thailand.

HEIN (2007) shows an influence of stratification on the upwelling off the Vietnamese coast by the Mekong River discharge during summer. According to his study upwelling at the coast is reduced as stratification in the area is increased due to the transport of Mekong water to the upwelling area.

In this study, the three-dimensional dynamic potential energy anomaly has been calculated for

both seasons only over a spring-neap cycle. To detect a long-term variability of the physical processes, i.e., interannual to decadal variability, changes of φ^{*}_{t3D} have to be investigated on longer time periods. Thus, it could be possible to show the effect of El Niño and climate change on the physical processes forcing stratification in the Mekong ROFI.

EASTHAM et al. (2008) investigate the possible climate change in the Mekong Basin by 2030. The authors stated that in the part of the Mekong which drains Southern Vietnam the annual runoff is increased. However, during the dry season the flow is decreased. As this is opposing the expected effect of hydropower dams, the climate change effect on the mean straining term should also be considered for instance, if forecasts are performed. WANG et al. (2006) investigate the interannual variability of the SCS associated with El Niño. When an El Niño occurs in the Pacific, the winter northeast monsoon wind over the SCS is weakened. The wind stress change will have an additional effect on the (de)stratifying processes.

Generally, the Mekong ROFI with its physical inherent variability, its ecosystem but also with its anthropogenic interference is an interesting region which offers many research aspects for future studies.

ACKNOWLEDGEMENTS

At this point I would like to thank all those who support me to compose this work:

Dr. Thomas Pohlmann for the scientific support, the helpful suggestion and useful comments as well as Prof. Dr. Sündermann.

Dr. Hartmut Hein for the scientific support as well as myriad of discussions, the tireless encouragement, his understanding and the nice time in Vietnam.

The staff of the Institute of Oceanography in Nha Trang and the crew of the research vessel for their support and assistance in Vietnam.

The members of the cruises for passing a very good time in Vietnam.

Dr. Kristina Fiedler and Prof. Dr. Petra Döll for providing the modelled Mekong River discharge data.

Kieran O'Driscoll to correct the English.

All the colleagues of the Institute of Oceanography in Hamburg for the technical and scientific support.

Levin Hein to pass on me many times and to be the sunshine day by day.

This work was funded by the Deutsche Forschungsgemeinschaft.

LIST OF ABBREVIATIONS

ADCP: Acoustic Doppler Current Profiler

ADV_X+ADV_Y: Horizontal advection term of φ_{t3D}

AVHRR: Advanced Very-High Resolution Radiometer

AVISO: Archiving, Validation and Interpretation of Satellite Oceanographic data

BT_D: Barotropic effects like the influence of depth of φ_{t3D}

BT_S: Barotropic effects due to surface elevation change of φ_{t3D}

CNES: Centre National d'Etudes Spatiales

COHERENS: COupled Hydrodynamical Ecological model for REgioNal Shelf seas

CTD: Conductivity, Temperature, and Depth Sensor

$DIFF_X$+$DIFF_Y$: Horizontal diffusion of φ_{t3D}

DIS_X+DIS_Y: Shear dispersion term of φ_{t3D}

ETOPO2: Global Gridded 2-minute Database available from National Geophysical Data Center, National Oceanic and Atmospheric Administration, U.S. Department of Commerce

GEBCO: General Bathymetric Chart of the Oceans

HAMSOM: HAMburg Shelf Ocean Model

MIX_Z: Vertical mixing term of φ_{t3D}

MODAS: Modular Ocean Data Assimilation System

MOODS: US Navy's Master Oceanographic Observation Data Set

MPR: Main Plume region

MS_X+MS_Y: Mean straining term of φ_{t3D}

NCAR: National Center for Atmospheric Research

NCEP: National Centers for Environmental Prediction

NROFI: Northern Mekong ROFI

NS_X+NS_Y: Non-mean straining term of φ_{t3D}

OTPS: Oregon State University Tidal Prediction Software

OTIS: Oregon State University Tidal Inversion Software

PEA: Potential Energy Anomaly (in general)

PSU: Practical Salinity Units

ROFI: Region Of Freshwater Influence

SCS: South China Sea

SIPS: Strain-Induced Periodic Stratification

SROFI: Southern Mekong ROFI

SSH: Sea Surface Height

SSALTO/DUACS: Segment Sol multimissions d'ALTimétrie, d'Orbitographie et de localisation précise/Data Unification and Altimeter Combination System

SST: Sea Surface Temperature

UD_Z: up/downwelling term of φ_{t3D}

WGHM: WaterGAP Global Hydrology Model

LIST OF SYMBOLS

g: gravitational acceleration [m/s²]

h: location of bed [m]

H: depth [m]

K_z vertical eddy diffusivity [m²/s]

$K_{x,y}$ are the horizontal eddy diffusivities [m²/s]

Q(x,y,z,t): sources and sinks term

$\overline{Q}$: depth integrated sources and sinks term

R: centre of mass of a water column

u, v: horizontal velocities in x,y-direction [m/s]

$\bar{u}$, $\bar{v}$: depth averaged velocities in x,y-direction [m/s]

$\tilde{v} = v - \bar{v}$: deviation of v from the depth mean value [m/s]

$\tilde{u} = u - \bar{u}$: deviation of u from the depth mean value [m/s]

V: Volume [m³]

w: vertical velocity [m/s]

x, y: horizontal coordinates [m]

z: vertical coordinate [m]

φ_{1D} : one-dimensional potential energy anomaly [J/m³]

φ_{t1D} : one-dimensional dynamic potential energy anomaly [J/m³]

φ_{t3D} : three-dimensional dynamic potential energy anomaly [10^{-6} W/m³]

φ^{*}_{t3D} : three-dimensional baroclinic dynamic potential energy anomaly [10^{-6} W/m³]

η : free surface [m]

ρ : density [kg/m³]

$\overline{\rho}$: depth averaged density [kg/m³]

$\tilde{\rho}_{\eta}$: perturbation density at the free surface [kg/m³]

$\tilde{\rho} = \rho - \overline{\rho}$: deviation of ρ from the depth mean value [kg/m³]

$\langle\ \rho' u'\ \rangle$, $\langle\ \rho' v'\ \rangle$, $\langle\ \rho' w'\ \rangle$: turbulent fluxes of mass in the x, y, z direction [kg/(m² s)]

$\langle \rho' w' \rangle|_s$, $\langle \rho' w' \rangle|_b$: surface and bottom density flux [kg/(m² s)]

LIST OF FIGURES

REFERENCES

ADAMSON, P. T. (2001): Hydrological perspectives of the Lower Mekong. *International Water Power and Dam Construction* 53(3): 16-21.

ANTONOV, J. I., R. A. LOCARNINI, T. P. BOYER, A. V. MISHONOV and H. E. GARCIA (2006): World Ocean Atlas 2005, Volume 2: Salinity. *In*: S. Levitus (Ed.). NOAA Atlas NESDIS 62. U.S. Government Printing Office, Washington D. C. 182pp.

ARAKAWA, A. and V. R. LAMB (1977): Computational design of the basic dynamical processes of the UCLA general circulation model. *Methods in Computational Physics* 17: 173-265.

BACKHAUS, J. O. (1982): A semi-implict scheme for the shallow water equations for application to shelf sea modelling. *Continental Shelf Research* 2(4): 243-254, doi: 10.1016/0278-4343(82)90020-6.

BACKHAUS, J. O. (1985): A three-dimensional model for the simulation of shelf sea dynamics. *Deutsche Hydrographische Zeitschrift* 38(4): 165-187, doi: 10.1007/BF02328975.

BARRON, C. N. and A. B. KARA (2006): Satellite-based daily SSTs over the global ocean. *Geophysical Research Letters* 33(L15603): 4pp, doi: 10.1029/2006GL026356.

BEARDSLEY, R. C., T. F. DUDA, J. F. LYNCH, J. D. IRISH, S. R. RAMP, C.-S. CHIU, T.-Y. TANG, Y.-J. YANG and G. FANG (2004): Barotropic tide in the northeast South China Sea. *Journal of Oceanic Engineering* 29(4): 1075-1086, doi: 10.1109/JOE.2004.833226.

BORIS, J. P. and D. L. BOOK (1973): Flux-corrected transport. I. SHASTA, a fluid transport algorithm that works. *Journal of Computational Physics* 11(1): 38-69, doi: 10.1016/0021-9991(73)90147-2.

BOYER, T. P., M. E. CONKRIGHT, S. LEVITUS, C. STEPHENS, T. O' BRIEN, D. JOHNSON and R. GELFELD (1998a): NOAA Atlas NESDIS 21, World Ocean Database 1998 Volume 4: Temporal Distribution of Conductivity/Salinity-Temperature-Depth (Pressure) Stations. U.S. Government Printing Office, Washington D.C. 160pp.

BOYER, T. P., M. E. CONKRIGHT, S. LEVITUS, D. JOHNSON, J. ANTONOV, T. O' BRIEN, C. STEPHENS and R. GELFELD (1998b): NOAA Atlas NESDIS 22, World Ocean Database 1998 Volume 5: Temporal Distribution of Station Data Temperature and Salinity Profiles. U.S. Government Printing Office, Washington D.C. 108pp.

BURCHARD, H. and R. HOFMEISTER (2008): A dynamic equation for the potential energy anomaly for analysing mixing and stratification in estuaries and coastal seas. *Estuarine, Coastal and Shelf Science* 77(4): 679-687, doi: 10.1016/j.ecss.2007.10.025.

CHAO, S.-Y., P.-T. SHAW and S. Y. WU (1996a): Deep water ventilation in the South China Sea.

Deep-Sea Research I 43(4): 445-466, doi: 10.1016/0967-0637(96)00025-8.

CHAO, S.-Y., P.-T. SHAW and S. Y. WU (1996b): El Niño modulation of the South China Sea circulation. *Progress in Oceanography* 38(1): 51-93, doi: 10.1016/S0079-6611(96)00010-9.

CHEN, X. (2005): Analysis of the circulation on the East-Chinese Shelf and the adjacent Pacific Ocean. Ph.D. dissertation. Universität Hamburg. 185pp.

CHU, P. C. and C. P. CHANG (1997): South China Sea warm pool in boreal spring. *Advances in Atmospheric Sciences* 14(2): 195-206, doi: 10.1007/s00376-997-0019-8.

CHU, P. C., H.-C. TSENG, C. P. CHANG and J. M. CHEN (1997): South China Sea warm pool detected in spring from the Navy's Master Oceanographic Observational Data Set (MOODS). *Journal of Geophysical Research* 102(C7): 15761-15771, doi: 10.1029/97JC00628.

CHU, P. C., N. L. EDMONS and C. FAN (1999): Dynamical mechanisms for the South China Sea seasonal circulation and thermohaline variabilities. *Journal of Physical Oceanography* 29(11): 2971-2989, doi: 10.1175/1520-0485(1999)029<2971:DMFTSC>2.0.CO;2.

DAI, A. and K. E. TRENBERTH (2002): Estimates of freshwater discharge from continents: Latitudinal and seasonal variations. *Journal of Hydrometeorology* 3(6): 660-687, doi: 10.1175/1525-7541(2002)003<0660:EOFDFC>2.0.CO;2.

DE BOER, G. J., J. D. PIETRZAK and J. C. WINTERWERP (2008): Using the potential energy anomaly equation to investigate tidal straining and advection of stratification in a region of freshwater influence. *Ocean Modelling* 22(1-2): 1-11, doi: 10.1016/j.ocemod.2007.12.003.

DIBARBOURE, G., O. LAURET, F. MERTZ and V. ROSMORDUC (2008): SSALTO/DUACS User Handbook: (M)SLA and (M)ADT Near-Real Time and Delayed Time Products. 1.9. Aviso Altimetry, Ramonville St. Agne, France. 39pp.

DING, Y. and T. N. KRISHNAMURTI (1987): Heat budget of the Siberian High and the winter monsoon. *Monthly Weather Review* 115(10): 2428-2449, doi: 10.1175/1520-0493(1987)115<2428:HBOTSH>2.0.CO;2.

DING, Y., C. LI and Y. LIU (2004): Overview of the South China Sea monsoon experiment. *Advances in Atmospheric Sciences* 21(3): 343-360.

DIPPNER, J. W., K. V. NGUYEN, H. HEIN, T. OHDE and N. LOICK (2007): Monsoon-induced upwelling off the Vietnamese coast. *Ocean Dynamics* 57(1): 46-62, doi: 10.1007/s10236-006-0091-0.

DÖLL, P., F. KASPAR and B. LEHNER (2003): A global hydrological model for deriving water availability indicators: model tuning and validation. *Journal of Hydrology* 270(1-2): 105-134, doi: 10.1016/S0022-1694(02)00283-4.

EASTHAM, J., F. MPELASOKA, M. MAINUDDIN, C. TICEHURST, P. DYCE, G. HODGSON, R. ALI and M. KIRBY (2008): Mekong River Basin Water Resources Assessment: Impacts of Climate Change. CSIRO: Water for a Healthy Country National Research Flagship.

EGBERT, G. D., A. F. BENNETT and M. G. G. FOREMAN (1994): TOPEX/POSEIDON tides estimated using a global inverse model. *Journal of Geophysical Research* 99(C12): 24821-24852, doi: 10.1029/94JC01894.

EGBERT, G. D. and S. Y. EROFEEVA (2002): Efficient inverse modeling of barotropic ocean tides. *Journal of Atmospheric and Oceanic Technology* 19(2): 183-204, doi: 10.1175/1520-0426(2002)019<0183:EIMOBO>2.0.CO;2.

ELSTON, S. A. (2005): Secondary circulation in a sinuous coastal plain estuary. Ph.D. dissertation. Georgia Institute of Technology. 294pp.

FISHER, N. R., J. H. SIMPSON and M. J. HOWARTH (2002): Turbulent dissipation in the Rhine ROFI forced by tidal flow and wind stress. *Journal of Sea Research* 48(4): 249-258, doi: 10.1016/S1385-1101(02)00194-6.

FOFONOFF, N. P. and R. C. MILLARD (1983): Algorithms for computation of fundamental properties of sea water. *In*: UNESCO technical papers in marine science. Vol. 44. UNESCO Division of Marine Science, Paris. 58 pp.

FOX, D. N., W. J. TEAGUE, C. N. BARRON, M. R. CARNES and C. M. LEE (2002): The Modular Ocean Data Assimilation System (MODAS). *Journal of Atmospheric and Oceanic Technology* 19(2): 240-252, doi: 10.1175/1520-0426(2002)019<0240:TMODAS>2.0.CO;2.

FUNG, I. Y., D. E. HARRISON and A. A. LACIS (1984): On the variability of the net longwave radiation at the ocean surface. *Reviews of Geophysics and Space Physics* 22(2): 177-193, doi: 10.1029/RG022i002p00177.

GAN, J., H. LI, E. N. CURCHITSER and D. B. HAIDVOGEL (2006): Modeling South China Sea circulation: Response to seasonal forcing regimes. *Journal of Geophysical Research* 111(C06034): 20pp, doi: 10.1029/2005JC003298.

GAN, J. and T. QU (2008): Coastal jet separation and associated flow variability in the southwest South China Sea. *Deep-Sea Research I* 55(1): 1-19, doi: 10.1016/j.dsr.2007.09.008.

GARCIA BERDEAL, I., B. M. HICKEY and M. KAWASE (2002): Influence of wind stress and ambient flow on a high discharge river plume. *Journal of Geophysical Research* 107(3130): 24pp, doi: 10.1029/2001JC000932.

GRIFFITHS, R. W. and P. F. LINDEN (1982): Laboratory experiments on fronts. Part I: Density-driven boundary currents. *Geophysical and Astrophysical Fluid Dynamics* 19(3-4): 159-187, doi: 10.1080/03091928208208954.

HANSEN, D. V. and M. RATTRAY (1966): New dimensions in estuary classification. *Limnology and Oceanography* 11(3): 319-326, doi: 10.4319/lo.1966.11.3.0319.

HARMS, I. H., U. HÜBNER, J. O. BACKHAUS, M. KULAKOV, V. STANOVOY, O. V. STEPANETS, L. A. KODINA and R. SCHLITZER (2003): Salt intrusions in Siberian river estuaries: Observations and model experiments in Ob and Yenisei. *In*: R. Stein, K. Fahl, D. K. Fütterer, E. M. Galimov

and O. V. Stepanets (Ed.). Siberian River runoff in the Kara Sea: Characterisation, quantification, variability and environmental significance. Proceedings in Marine Sciences. Vol. 6: p. 27-46. Elsevier, Amsterdam.

HEIN, H. (2007): Vietnam Upwelling - Analysis of the upwellling and related processes in the coastal area off South Vietnam. Ph.D. dissertation. Universität Hamburg. 163pp.

HEIN, H., B. KARFELD and T. POHLMANN (2007): Mekong Water Dispersion: Measurements and consequences for the hydrodynamical modelling. *Journal of Water Resources and Environmental Engineering* (Special Issue, August 2007): 21-28.

HEIN, H., B. HEIN and T. POHLMANN (submitted): Recent sediment dynamics in the Mekong ROFI. *Global and Planetary Change*.

HILL, A. E. (1998): Buoyancy effects in coastal and shelf seas. *In*: K. H. Brink and A. R. Robinson (Ed.). The Sea. P. 21-62. John Wiley and Sons, New York.

HOFMEISTER, R., H. BURCHARD and K. BOLDING (2009): A three-dimensional model study on processes of stratification and de-stratification in the Limfjord. *Continental Shelf Research* 29(11-12): 1515-1524, doi: 10.1016/j.csr.2009.04.004.

HOLT, J. and L. UMLAUF (2008): Modelling the tidal mixing fronts and seasonal stratification of the Northwest European Continental shelf. *Continental Shelf Research* 28(7): 887-903, doi: 10.1016/j.csr.2008.01.012.

HORDOIR, R., K. D. NGUYEN and J. POLCHER (2006): Simulating tropical river plumes, a set of parametrizations based on macroscale data: A test case in the Mekong Delta region. *Journal of Geophysical Research* 111(C09036): 18pp, doi:10.1029/2005JC003392.

HU, J., H. KAWAMURA, H. HONG and Y. QI (2000): A review on the currents in the South China Sea: Seasonal circulation, South China Sea Warm Current and Kuroshio Intrusion. *Journal of Oceanography* 56(6): 607-624, doi: 10.1023/A:1011117531252.

HUANG, D., J. SU and J. O. BACKHAUS (1999): Modelling the seasonal thermal stratification and baroclinic circulation in the Bohai Sea. *Continental Shelf Research* 19(11): 1485-1505, doi: 10.1016/S0278-4343(99)00026-6.

HUNGSPREUGS, M., W. UTOOMPRURKPORN, A. SNIDVONGS and S. RATANACHONGKIAT (1998): A comparative study of trace metal contamination in the Mekong Delta and the Chao Phraya Estuary. *International Workshop on the Mekong Delta, 23-27 February 1998, Chiang Rai, Thailand*: 150-168.

HUYNH, S. (2002): Hydrodynamic study of Ha Long Bay. Bachelor thesis. University of Western Australia. 81pp.

HWANG, C. and S.-A. CHEN (2000): Circulations and eddies over the South China Sea derived from TOPEX/Poseidon altimetry. *Journal of Geophysical Research* 105(C10): 23943-23965, doi:10.1029/2000JC900092.

ISOBE, A. and T. NAMBA (2001): The circulation in the upper and intermediate layers of the South China Sea. *Journal of Oceanography* 57(1): 93-104, doi: 10.1023/A:1011130905369.

KALNAY, E., M. KANAMITSU, R. KISTLER, W. COLLINS, D. DEAVEN, L. GANDIN, M. IREDELL, S. SAHA, G. WHITE, J. WOOLLEN, Y. ZHU, A. LEETMAA, R. REYNOLDS, M. CHELLIAH, W. EBISUZAKI, W. HIGGINS, J. JANOWIAK, K. C. MO, C. ROPELEWSKI, J. D. WANG, R. JENNE and D. JOSEPH (1996): The NCEP/NCAR 40-Year Reanalysis Project. *Bulletin of the American Meteorological Society* 77(3): 437-471, doi: 10.1175/1520-0477(1996)077<0437:TNYRP>2.0.CO;2.

KARA, A. B. and C. N. BARRON (2007): Fine-resolution satellite-based daily sea-surface temperature over the global ocean. *Journal of Geophysical Research* 112(C05041): 16pp, doi:10.1029/2006JC004021.

KEMPE, S. and P. KRAHE (2005): Water and biogeochemical fluxes in the river Rhine catchment. *Erdkunde* 59: 216-250.

KITE, G. (2001): Modelling the Mekong: Hydrological simulation for environmental impact studies. *Journal of Hydrology* 253(1-4): 1-13, doi: 10.1016/S0022-1694(01)00396-1.

KOCHERGIN, V. P. (1987): Three-dimensional prognostic models. *In*: N. S. Heaps (Ed.). Three-dimensional coastal ocean models, Coastal and Estuarine Sciences. 4: p. 201-208. American Geophysical Union, Washington D.C. doi: 10.1029/CO004p0201.

KONDO, J. (1975): Air-sea bulk transfer coefficients in diabatic conditions. *Boundary-Layer Meteorology* 9(1): 91-112, doi: 10.1007/BF00232256.

KUMMU, M. and O. VARIS (2007): Sediment-related impacts due to upstream reservoir trapping, the Lower Mekong River. *Geomorphology* 85(3-4): 275-293, doi: 10.1016/j.geomorph.2006.03.024.

KUO, N.-J., Q. ZHENG and C.-R. HO (2000): Satellite observation of upwelling along the western coast of the South China Sea. *Remote Sensing of Environment* 74(3): 463-470, doi: 10.1016/S0034-4257(00)00138-3.

KUO, N.-J., Q. ZHENG and C.-R. HO (2004): Response of Vietnam coastal upwelling to the 1997-1998 ENSO event observed by multisensor data. *Remote Sensing of Environment* 89(1): 106-115, doi: 10.1016/j.rse.2003.10.009.

LAP NGUYEN, V., T. K. O. TA and M. TATEISHI (2000): Late Holocene depositional environments and coastal evolution of the Mekong River Delta, Southern Vietnam. *Journal of Asian Earth Sciences* 18(4): 427-439, doi: 10.1016/S1367-9120(99)00076-0.

LAX, P. D. and B. WENDROFF (1960): Systems of conservation laws. *Communications on Pure and Applied Mathematics* 13(2): 217-237, doi: 10.1007/0-387-28148-7_18.

LAX, P. D. and B. WENDROFF (1964): Difference schemes for hyperbolic equations with high order of accuracy. *Communications on Pure and Applied Mathematics* 17(3): 381-398, doi:

10.1002/cpa.3160170311.

LE SOUËF, K. (2006): Estuarine processes in the Blackwood River Estuary. Bachelor thesis. University of Western Australia. 109pp.

LEONARD, B. P. (1979): A stable and accurate convective modelling procedure based on quadratic upstream interpolation. *Computer Methods in Applied Mechanics and Engineering* 19(1): 59-98, doi: 10.1016/0045-7825(79)90034-3.

LEONARD, B. P. (1991): The ULTIMATE conservative difference scheme applied to unsteady one-dimensional advection. *Computer Methods in Applied Mechanics and Engineering* 88(1): 17-74, doi: 10.1016/0045-7825(91)90232-U.

LIHAN, T., S.-I. SAITOH, T. IIDA, T. HIRAWAKE and K. IIDA (2008): Satellite-measured temporal and spatial variability of the Tokachi River Plume. *Estuarine, Coastal and Shelf Science* 78(2): 237-249, doi: 10.1016/j.ecss.2007.12.001.

LIM, Y. K., K. Y. KIM and H. S. LEE (2002): Temporal and spatial evolution of the Asian summer monsoon in the seasonal cycle of synoptic fields. *Journal of Climate* 15(24): 3630-3644, doi: 10.1175/1520-0442(2002)015<3630:TASEOT>2.0.CO;2.

LIN, J. and A. Y. KUO (2001): Secondary turbidity maximum in a partially mixed microtidal estuary. *Estuaries* 24(5): 707-720, doi: 10.2307/1352879.

LINDEN, P. F. and J. E. SIMPSON (1988): Modulated mixing and frontogenesis in shallow seas and estuaries. *Continental Shelf Research* 8(10): 1107-1127, doi: 10.1016/0278-4343(88)90015-5.

LIU, W. T. and X. XIE (1999): Spacebased observations of the seasonal changes of South Asian monsoons and oceanic responses. *Geophysical Research Letters* 26(10): 1473-1476, doi:10.1029/1999GL900289.

LOCARNINI, R. A., A. V. MISHONOV, J. ANTONOV, T. P. BOYER and H. E. GARVCIA (2006): World Ocean Atlas 2005, Volume 1: Temperature. *In*: S. Levitus (Ed.). NOAA Atlas NESDIS 61. U.S. Government Printing Office, Washington D. C. 182pp.

LU, X. X. and R. Y. SIEW (2006): Water discharge and sediment flux changes over the past decades in the Lower Mekong River: possible impacts of the Chinese dams. *Hydrology and Earth Syststem Sciences* 10(2): 181-195, doi: 10.5194/hess-10-181-2006.

LUYTEN, P. J., J. E. JONES, R. PROCTOR, A. TABOR, P. TETT. and K. WILD-ALLEN (1999): COHERENS - A Coupled Hydrodynamical-Ecological Model for Regional and Shelf Seas: User Documentation. MUMM Report, Management Unit of the Mathematical Models of the North Sea. 914pp.

MAYER, B., P. E. DAMM, T. POHLMANN and S. RIZAL (2010): What is driving the ITF? An illumination of the Indonesian throughflow with a numerical nested model system. *Dynamics of Atmospheres and Oceans* 50(2): 301-312, doi: 10.1016/j.dynatmoce.2010.03.002.

MELLOR, G. L. and T. YAMADA (1974): A hierarchy of turbulence closure models for planetary boundary layers. *Journal of Atmospheric Science* 31(7): 1791-1806, doi: 10.1175/1520-0469(1974)031<1791:AHOTCM>2.0.CO;2.

MELLOR, G. L. and P. A. DURBIN (1975): The structure and dynamics of the ocen surface mixed layer. *Journal of Physical Oceanography* 5(4): 718-728, doi: 10.1175/1520-0485(1975)005<0718:TSADOT>2.0.CO;2.

METZGER, E. J. and H. E. HURLBURT (1996): Coupled dynamics of the South China Sea, the Sulu Sea, and the Pacific Ocean. *Journal of Geophysical Research* 101(C5): 12331-12352, doi:10.1029/95JC03861.

METZGER, E. J. (2003): Upper ocean sensitivity to wind forcing in the South China Sea. *Journal of Oceanography* 59(6): 783-798, doi: 10.1023/B:JOCE.0000009570.41358.c5.

MILLIMAN, J. D. and R. MEI-E (1995): River flux to the sea: Impact of human intervention on river systems and adjacent coastal areas. *In*: D. Eisma (Ed.). Climate Change: Impact on coastal habitation. P. 57-84. Lewis Publications, Boca Raton.

MRC (2004): Lower Mekong Hydrologic Yearbooks: Yearbook 2003-2004. CD-ROM. MRC, Vientiane, Lao PRD.

MRC (2005): Overview of the hydrology of the Mekong Basin. MRC, Vientiane, Lao PRD. 82pp.

MÜNCHOW, A. and R. W. GARVINE (1993): Buoyancy and wind forcing of a coastal current. *Journal of Marine Research* 51(2): 293-322, doi: 10.1357/0022240933223747.

NGUYEN, A. D. and H. H. G. SAVENIJE (2006): Salt intrusion in multi-channel estuaries: A case study in the Mekong Delta, Vietnam. *Hydrology and Earth Syststem Sciences* 10(5): 743-754, doi: 10.5194/hess-10-743-2006.

NGUYEN, A. D., H. H. G. SAVENIJE, D. N. PHAM and D. T. TANG (2007): Using salt intrusion measurements to determine the freshwater discharge distribution over the branches of a multi-channel estuary: The Mekong Delta case. *Estuarine, Coastal and Shelf Science* 77(3): 433-445, doi: 10.1016/j.ecss.2007.10.010.

NGUYEN, K. D., S. GUILLOU and N. V. PHAM (1998): A 3-D numerical study of the tidal circulation in the Mekong Delta Coastal Zones, Vietnam. *International Workshop on the Mekong Delta, 23-27 February 1998, Chiang Rai, Thailand*: 57-71.

NIKIEMA, O., J.-L. DEVENON and M. BAKLOUTI (2007): Numerical modeling of the Amazon River plume. *Continental Shelf Research* 27(7): 873-899, doi: 10.1016/j.csr.2006.12.004.

O'DONNELL, J. (1998): Convergence and downwelling at a river plume front. *Journal of Physical Oceanography* 28(7): 1481-1495, doi: 10.1175/1520-0485(1998)028<1481:CADAAR>2.0.CO;2.

OONISHI, Y. (1977): A numerical study on the tidal residual flow. *Journal of Oceanography*

33(4): 207-218, doi: 10.1007/BF02109693.

ORLANSKI, I. (1976): A simple boundary condition for unbounded hyperbolic flows. *Journal of Computational Physics* 21(3): 251-269, doi: 10.1016/0021-9991(76)90023-1.

PEDERSEN, L. B. and L. P. PRAHM (1974): A method for numerical solution of the advection equation. *Tellus* 26(5): 594-602, doi: 10.1111/j.2153-3490.1974.tb01637.x.

PEDLOSKY, J. (1987): Geophysical Fluid Dynamics. 2nd edition. Springer-Verlag, New York. 710pp.

PLATE, E. J. (2007): Early warning and flood forecasting for large rivers with the lower Mekong as example. *Journal of Hydro-environment Research* 1(2): 80-94, doi: 10.1016/j.jher.2007.10.002.

POHLMANN, T. (1987): A three dimensional circulation model of the South China Sea. *In*: J. C. J. Nihoul and B. M. Jamart (Ed.). Three-dimensional models of marine and estuarine dynamics. Elsevier Oceanography Series. Vol. 45: p. 245-268. Elsevier, Amsterdam. doi: 10.1016/S0422-9894(08)70451-3.

POHLMANN, T. (1991): Untersuchung hydro- und thermodynamischer Prozesse in der Nordsee mit einem dreidimensionalen numerischen Modell. *Berichte aus dem Zentrum für Meeres- und Klimaforschung der Universität Hamburg* 23: 116pp.

POHLMANN, T. (1996a): Predicting the thermocline in a circulation model of the North Sea - Part I: model description, calibration and verification. *Continental Shelf Research* 16(2): 131-146, doi: 10.1016/0278-4343(95)90885-S.

POHLMANN, T. (1996b): Calculation the annual cycle of the vertical eddy viscosity in the North Sea with a three-dimensional baroclinic shelf sea circulation model. *Continental Shelf Research* 16(2): 147-161, doi: 10.1016/0278-4343(94)E0037-M.

POHLMANN, T. (1996c): Calculating the development of the thermal vertical stratification in the North Sea with a three-dimensional baroclinic circulation model. *Continental Shelf Research* 16(2): 163-194, doi: 10.1016/0278-4343(95)00018-V.

POHLMANN, T. (1996d): Simulating the heat storage in the North Sea with a three-dimensional circulation model. *Continental Shelf Research* 16(2): 195-213, doi: 10.1016/0278-4343(95)00032-V.

POHLMANN, T. (2006): A meso-scale model of the central and southern North Sea: Consequences of an improved resolution. *Continental Shelf Research* 26(19): 2367-2385, doi: 10.1016/j.csr.2006.06.011.

POMEROY, R., K. A. THI NGUYEN and H. X. THONG (2009): Small-scale marine fisheries policy in Vietnam. *Marine Policy* 33(2): 419-428, doi: 10.1016/j.marpol.2008.10.001.

PRITCHARD, D. W. (1967): What is an estuary: Physical viewpoint. *In*: G. H. Lauff (Ed.). Estuaries. Vol. 83: p. 3-5. American Association for the Advancement of Science Publication,

Washington D.C.

PUTRI, M. R. and T. POHLMANN (2009): Hydrodynamic and transport model of the Siak Estuary. *Asian Journal of Water, Environment and Pollution* 6(1): 67-80.

RIPPETH, T. P. and J. H. SIMPSON (1996): The frequency and duration of episodes of complete vertical mixing in the Clyde Sea. *Continental Shelf Research* 16(7): 933-947, doi: 10.1016/0278-4343(95)00022-4.

ROE, P. L. (1986): Characteristic-based schemes for the Euler equations. *Annual Review of Fluid Mechanics* 18: 337-365, doi: 10.1146/annurev.fl.18.010186.002005.

ROJANA-ANAWAT, P., S. PRADIT, N. SUKRAMONGKOL and S. SIRIRAKSOPHON (2001): Temperature, salinity, dissolved oxygen and water masses of Vietnamese waters. Proceedings of the SEAFDEC Seminar on Fishery Resources in the South China Sea, Area IV: Vietnamese Waters: 346-355.

RONG, Z., Y. LIU, H. ZONG and Y. CHENG (2007): Interannual sea level variability in the South China Sea and its response to ENSO. *Global and Planetary Change* 55(4): 257-272, doi: 10.1016/j.gloplacha.2006.08.001.

SARACENO, M., P. T. STRUB and P. M. KOSRO (2008): Estimates of sea surface height and near-surface alongshore coastal currents from combinations of altimeters and tide gauges. *Journal of Geophysical Research* 113(C11013): 20pp, doi:10.1029/2008JC004756.

SCHRUM, C. (1994): Numerische Simulation thermodynamischer Prozesse in der Deutschen Bucht. *Berichte aus dem Zentrum für Meeres- und Klimaforschung: Ozeanographie* 15: 175pp.

SCHRUM, C. (1997): Thermohaline stratification and instabilities at tidal mixing fronts: Results of an eddy resolving model for the German Bight. *Continental Shelf Research* 17(6): 689-716, doi: 10.1016/S0278-4343(96)00051-9.

SHARPLES, J. and J. H. SIMPSON (1995): Semi-diurnal and longer period stability cycles in the Liverpool Bay ROFI. *Continental Shelf Research* 15(2-3): 295-314, doi: 10.1016/0278-4343(94)E0003-5.

SHAW, P.-T. and S.-Y. CHAO (1994): Surface circulation in the South China Sea. *Deep Sea Research Part I: Oceanographic Research Papers* 41(11-12): 1663-1683, doi: 10.1016/0967-0637(94)90067-1.

SHAW, P.-T., S.-Y. CHAO and L.-L. FU (1999): Sea surface height variations in the South China Sea from satellite altimetry. *Oceanologica Acta* 22(1): 1-17, doi: 10.1016/S0399-1784(99)80028-0.

SIGNORET, M., M. A. MONREAL-GÓMEZ, J. ALDECO and D. A. SALAS-DE-LEÓN (2006): Hydrography, oxygen saturation, suspended particulate matter, and chlorophyll-a fluorescence in an oceanic region under freshwater influence. *Estuarine, Coastal and Shelf Science* 69(1-2): 153-164, doi: 10.1016/j.ecss.2006.04.011.

SIMIONATO, C. G., V. L. MECCIA, W. C. DRAGANI and M. N. NUÑES (2006): On the use of the NCEP/NCAR surface winds for modeling barotropic circulation in the Río de la Plata Estuary. *Estuarine, Coastal and Shelf Science* 70(1-2): 195-206, doi: 10.1016/j.ecss.2006.05.047.

SIMPSON, J. E. (1987): Gravity currents: In the environment and the laboratory. 1st edition. Ellis Horwood, Chichester. 244pp.

SIMPSON, J. H. and J. R. HUNTER (1974): Fronts in the Irish Sea. *Nature* 250: 404-406, doi:10.1038/250404a0.

SIMPSON, J. H., C. M. ALLEN and N. C. G. MORRIS (1978): Fronts on the Continental Shelf. *Journal of Geophysical Research* 83(C9): 4607-4614, doi: 10.1029/JC083iC09p04607.

SIMPSON, J. H., D. J. CRISP and C. HEARN (1981): The shelf-sea fronts: Implications of their existence and behavior. *Philosophical Transactions of the Royal Society of London. Series A, Mathematical, Physical and Engineering Sciences* 302(1472): 531-546, doi: 10.1098/rsta.1981.0181.

SIMPSON, J. H., J. BROWN, J. MATTHEWS and G. ALLEN (1990): Tidal straining, density currents, and stirring in the control of estuarine stratification. *Estuaries and Coasts* 13(2): 125-132, doi: 10.2307/1351581.

SIMPSON, J. H. (1997): Physical processes in the ROFI regime. *Journal of Marine Systems* 12(1-4): 3-15, doi: 10.1016/S0924-7963(96)00085-1.

SIMPSON, J. H. and A. SNIDVONGS (1998): The influence of monsoonal river discharge on tropical shelf seas: The Gulf of Thailand as a case for study. *International Workshop on the Mekong Delta, 23-27 February 1998, Chiang Rai, Thailand*: 86-99.

SMAGORINSKY, J. (1993): Some historical remarks on the use of non-linear viscosities. *In*: B. Galperin and S. A. Orszag (Ed.). Large Eddy Simulation of complex engineering and geophysical flows - Proceedings of an international workshop in Large Eddy Simulation. P. 1-34. Cambridge University Press, Cambridge.

SOUZA, A. J. and I. D. JAMES (1996): A two-dimensional (x-z) model of tidal straining in the Rhine ROFI. *Continental Shelf Research* 16(7): 949-966, doi: 10.1016/0278-4343(95)00033-X.

STREAM (2000): Poverty and aquatic resources in Vietnam: an assessment of the role and potential of aquatic resource management in poor people's livelihoods. Support to Regional Aquatic Resources Management (STREAM), Bangkok, Thailand. 37pp.

TA, T. K. O., V. L. NGUYEN, M. TATEISHI, I. KOBAYASHI, Y. SAITO and T. NAKAMURA (2002a): Sediment facies and late Holocene progradation of the Mekong River Delta in Bentre Province, southern Vietnam: an example of evolution from a tide-dominated to a tide- and wave-dominated delta. *Sedimentary Geology* 152(3-4): 313-325, doi: 10.1016/S0037-0738(02)00098-2.

TA, T. K. O., V. L. NGUYEN, M. TATEISHI, I. KOBAYASHI, S. TANABE and Y. SAITO (2002b):

Holocene delta evolution and sediment discharge of the Mekong River, southern Vietnam. *Quarternary Science Reviews* 21(16-17): 1807-1819, doi: 10.1016/S0277-3791(02)00007-0.

TANABE, S., T. K. O. TA, V. L. NGUYEN, M. TATEISHI, I. KOBAYASHI and Y. SAITO (2003): Delta evolution model inferred from the holocene Mekong Delta, southern Vietnam. *In*: F. H. Sidi, D. Nummedal, P. Imbert, H. Darman and H. W. Posamentier (Ed.). Tropical deltas of Southeast Asia - Sedimentology, stratigraphy, and petroleum geology. SEPM Special Publication. Vol. 76: p. 175-188. Tulsa, Oklahoma, USA.

TANG, D. L., H. KAWAMURA, P. SHI, W. TAKAHASHI, L. GUAN, T. SHIMADA, F. SAKAIDA and O. ISOGUCHI (2006): Seasonal phytoplankton blooms associated with monsoonal influences and coastal environments in the sea areas either side of the Indochina Peninsula. *Journal of Geophysical Research* 111(G01010): 9pp, doi:10.1029/2005JG000050.

WANG, C., W. WANG, D. WANG and Q. WANG (2006): Interannual variability of the South China Sea associated with El Niño. *Journal of Geophysical Research* 111(C03023): 19pp, doi: 10.1029/2005JC003333.

WANG, W. and C. WANG (2006): Formation and decay of the spring warm pool in the South China Sea. *Geophysical Research Letters* 33(L02615): 4pp, doi: 10.1029/2005GL025097.

WEI, H., Y. HE, Q. LI, Z. LIU and H. WANG (2007): Summer hypoxia adjacent to the Changjiang Estuary. *Journal of Marine Systems* 67(3-4): 292-303, doi: 10.1016/j.jmarsys.2006.04.014.

WIESNER, M. and PARTICIPANTS (2006): Cruise report RV Sonne 187 Vietnam. Land-Ocean-Atmosphere interactions in the coastal zone of Vietnam. Berichte - Reports Institut für Geowissenschaften, 23, Universität Kiel. 99pp.

WILLIAMS, B. J. (2006): Hydrobiological Modelling. University of Newcastle, NSW, Australia. 680pp.

WISEMAN, W. J., N. N. RABALAIS, R. E. TURNER, S. P. DINNEL and A. MACNAUGHTON (1997): Seasonal and interannual variability within the Louisiana coastal current: Stratification and hypoxia. *Journal of Marine Science* 12(1-4): 237-248, doi: 10.1016/S0924-7963(96)00100-5.

WOLANSKI, E., N. H. NGUYEN, T. D. LE, H. N. NGUYEN and N. T. NGUYEN (1996): Fine-sediment dynamics in the Mekong River Estuary, Vietnam. *Estuarine, Coastal and Shelf Science* 43(5): 565-582, doi: 10.1006/ecss.1996.0088.

WOLANSKI, E., N. H. NHAN and S. SPAGNOL (1998): Sediment dynamics during low flow conditions in the Mekong River Estuary, Vietnam. *Journal of Coastal Research* 14(2): 472-482.

WU, C.-R., P.-T. SHAW and S.-Y. CHAO (1998): Seasonal and interannual variations in the velocity field of the South China Sea. *Journal of Oceanography* 54(4): 361-372, doi: 10.1007/BF02742620.

WU, C.-R. and T. L. CHIANG (2007): Mesoscale eddies in the northern South China Sea. *Deep-Sea Research Part II: Tropical Studies in Oceanography* 54(14-15): 1575-1588, doi:

10.1016/j.dsr2.2007.05.008.

WYRTKI, K. (1961): Physical oceanography of the Southeast Asian Water. *In*: NAGA Report Volume 2. Scientific results of marine investigations of the South China Sea and Gulf of Thailand 1959-1961. eScholarship Repository, Scripps Institution of Oceanography, University of California, San Diego. 195pp.

XIE, S.-P., Q. XIE, D. WANG and W. T. LIU (2003): Summer upwelling in the South China Sea and its role in regional climate variations. *Journal of Geophysical Research* 108(3261): 13pp, doi: 10.1029/2003JC001867.

XU, H., S.-P. XIE, Y. WANG, W. ZHUANG and D. WANG (2007): Orographic effects on the South China Sea summer climate. Assimilation of remote sensing and in situ data in modern numerical weather and environmental prediction models, San Diego, California, USA, X. Zou, D. Barker and F.-X. Le Dimet (Ed.). Proceedings of SPIE. 6685: 66850K-66850K-12. doi: 10.1117/12.730375.

YOSHIMURA, C., M. C. ZHOU, A. S. KIEM, K. FUKAMI, H. A. P. HAPUARACHCHI, H. ISHIDAIRA and K. TAKEUCHI (2009): 2020s scenario analysis of nutrient load in the Mekong River Basin using a distributed hydrological model. *Science of the Total Environment* 407(20): 5356-5366, doi: 10.1016/j.scitotenv.2009.06.026.

ZU, T., J. GAN and S. Y. EROFEEVA (2008): Numerical study of the tide and tidal dynamics in the South China Sea. *Deep-Sea Research Part I: Oceanographic Research Papers* 55(2): 137-154, doi: 10.1016/j.dsr.2007.10.007.